The Use Of Gravimetric & Chromatographic Analysis To Study Surface Properties Of Powders

Ketan Lalit Vora
BSC (Hons) MRPharmS

2005

A thesis submitted in partial fulfilment of the requirements of the Faculty of Medicine, University of London, for the award of the Degree of Doctor of Philosophy

The School of Pharmacy
University of London
29-39 Brunswick Square
London WC1N 1AX

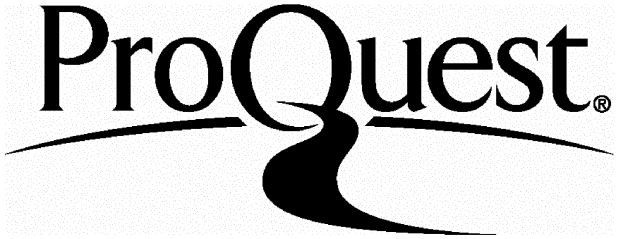

ABSTRACT OF THESIS

Pharmaceutical processing can affect the crystallinity of drug substances, leading to batch-to-batch variation and changes in the physicochemical behaviour of the final dosage form. The study of the effects of such processing is important to allow the control of manufacturing procedures in order to ensure the consistent quality of the finished product. The aims were to investigate and measure the changes in the surface properties of four compounds when subjected to pharmaceutical processing. The work also highlights the difficulties associated with the study of hydrates due to their water loss either by accident or intent when equilibrated prior to experimental analysis.

Characterisation studies using a gravimetric approach coupled with near infrared spectroscopy showed the discovery of a new crystal transition for theophylline during hydration of the dehydrate lattice. A crystallisation type transition at 40-50% relative humidity occurred during rehydration. This suggested a probable "ghost hydrate structure" for the dehydrate packing. The sorption of water, during rehydration, allowed the structure to have sufficient mobility to transform back into the anhydrous form prior to hydrate formation. Such a technique can show real-time events of solid-state transitions for sophisticated powdered solids, and can thus help formulators monitor changes during manufacture of a product.

Gravimetric analysis of compounds using a novel approach of probing the surface with solvents other than water provided useful data. It was possible to follow changes in non-micronised and micronised calcium mupirocin. Due to the hydrophilic nature of the compound it interacted with the polar probes to a greater extent. Once micronised the sample showed stronger wettability to all the probes probably due to amorphous regions, greater surface energy and/or larger surface areas created during micronisation. Interestingly, tests on the micronised sample after one year showed some recovery suggesting that increased surface area was not the only cause of the greater wetting but possibly also changes in the surface energy. Changes on the dihydrate form were not

measurable due to the inability to retain the hydrate when water vapour was absent from the system. The method proved unsuitable for the other compounds due to minimal wetting or poor equilibration. This technique has allowed process-induced batch variability to be measured where conventional techniques such as x-ray diffractometry and solution calorimetry have failed.

Chromatographic analysis of the surface of the compounds has proved successful especially where the gravimetric approach has shown limitations. Differences in surface energetics of both micronised and non-micronised forms of calcium mupirocin and nabumetone were attainable. Over time the surface energy of the samples recovered, suggesting the formation of a thermodynamically unstable surface state immediately after micronisation. Measurements of the hydrated forms (calcium mupirocin and theophylline) were possible chromatographically. Water into/onto the drugs reduced the dispersive and acidic components of the surface. Also the dehydrated form of theophylline showed very high surface energy values, corroborating the recognised instability of the lattice. Batch-to-batch variability between Sigma and Fluka forms of theophylline and magnesium stearate have also been highlighted by the differences in their respective surface energy values. Chromatography allows the determination of small changes in surface characteristics and has provided a new approach to successfully comparing hydrates for the first time.

Gravimetric and chromatographic techniques have provided an alternative method to investigate process induced batch variability. Understanding the way surfaces interact with probes of varying polarity can help allow the selection of the appropriate solvent during processing in order to prevent undesirable changes to the original compound.

Sorted!.....Ain't It?

ACKNOWLEDGEMENTS

Foremost, I would like to thank my supervisors Professor Graham Buckton and Mr David Clapham, from the School of Pharmacy and GlaxoSmithKline (GSK) respectively for allowing me to explore my own ideas and providing invaluable help and guidance throughout the PhD. I would also like to thank Dr Simon Gaisford for his help in correcting and editing this thesis. The funding by the Engineering and Physical Sciences Research Council (EPSRC) and GSK cannot also be forgotten.

I would also like to express my gratitude to Keith Barnes for always being available to help fix and set-up instruments on innumerable occasions no matter how small or large the tasks were. Thanks should also be given to Dave McCarthy who conducted all the microscopy work.

I would also like to acknowledge some of my fellow colleagues including Abi, Ashish, Ameet, Amina, Brijesh, Claire, Dima, Emma, John, Laurent, Matt and Viraj who have provided insightful discussions, encouragement and direction throughout this PhD. I would like to also thank all of my friends at the university for making the three years fun and providing support as well as listening to the odd moans when things went wrong.

Finally, I would like to thank my family (Lalit, Pratibha, Hiten and Rakhi) for their continued help and support throughout the course of this PhD. My friends outside of university have to also be acknowledged for the escapism from the PhD that they gave me.

CONTENTS

LIST OF FIGURES

Introduction

Methods

Results – Characterisation Of The Compounds Under Investigation

Results – Investigating The Interaction Of Powder Surfaces With Solvents Of Different Polarities Using Dynamic Vapour Sorption

Results & Discussion – The Use Of Inverse Gas Chromatography To Investigate The Surface Energetics Of Powder Surfaces

LIST OF TABLES

Introduction

Methods

Results & Discussion – Characterisation Of The Compounds Under Investigation

Results & Discussion – The Use Of Inverse Gas Chromatography To Investigate The Surface Energetics Of Powder Surfaces

ABBREVIATIONS & SYMBOLS

a	Surface Area Of A Probe Molecule ($m^2 g^{-1}$)
a	Freundlich Constant
A	Ampere
a_m	Molecular Cross-Sectional Area
AIDS	Acquired Immune Deficiency Syndrome
AN	Gutmann Acceptor Number (kcal mol^{-1})
AN*	Modified Gutmann Acceptor Number (kcal mol^{-1})
ANOVA	One-Way Analysis Of Variance
API	Active Pharmaceutical Ingredient
BC	Before Christ
BET	Brunauer, Emmett & Teller
BNF	British National Formulary
BOC	British Oxygen Company
C	BET Adsorption Energy Constant
ca	Approximately
cal	Calories
cc	Cubic centimetre
cos θ	Cosine Of Contact Angle
Cp	Heat Capacity ($J K^{-1} mol^{-1}$)
d	Change in
der.	Derivative
DN	Gutmann Donor Number (kcal mol^{-1})
DSC	Differential Scanning Calorimetry
DVS	Dynamic Vapour Sorption
F	Flow Rate ($mL min^{-1}$)
F	Force (N)
FID	Flame Ionisation Detector
g	Gram
G	Dry Mass Of Sample (g)
G	Gibb's Free Energy For Sorption ($kJ mol^{-1}$)
GMP	Good Manufacturing Practice
GSK	GlaxoSmithKline
h	Hour
H	Enthalpy ($kJ mol^{-1}$)
H(v)	van't Hoff's Enthalphy ($kJ mol^{-1}$)
HDSC	Hyper Differential Scanning Calorimetry (HyperDSC)
HTS	High Throughput Screening
IGC	Inverse Gas Chromatography
IUPAC	International Union Of Pure And Applied Chemistry
J	Joule
J	Compression Factor
K	Kelvin
K	Equilibrium Constant
K'	Constant
K^A	Acidic Component
K^D	Basic Component
KF	Karl Fischer
kV	Kilovolt
ln	Natural Log
L	Litre
m	Metre
min	Minute
mol	Moles
n	Freundlich Constant
N	Avogadro's Number = 6.02205 x 10^{23} (mol^{-1})
NCE	New Chemical Entity
NIR	Near Infrared Spectroscopy
NSAID	Non-Steroidal Anti-Inflammatory Drug
o/w	Oil In Water
p	Perimeter (m)
P	Pressure ($N m^{-2}$)
Pa	Pascal ($N m^{-2}$)
Po	Saturation Vapour Pressure ($N m^{-2}$)

P/Po	Partial Pressure
P_i/P_o	Ratio Of Inlet To Outlet Pressure
PMMA	Poly Methyl Methacrylate
P_{sg}	Vapour Pressure Of Adsorbate (N m^{-2})
Psi	Pounds Per Square Inch
q	Heat (J)
Q	Heat Adsorbed (J)
R	Gas Constant = 8.314 (J K^{-1} mol^{-1})
R^2	Correlation Coefficient Value
RH	Relative Humidity (%)
RMM	Relative Molecular Mass
s	Second
S	Entropy (J mol^{-1} K^{-1})
Sa	Adsorbent Surface Area (m^2 g^{-1})
S.D.	Standard Deviation
SEM	Scanning Electron Microscopy
SMS	Surface Management Systems
SNV	Standard Normal Variance
SolCal	Solution Calorimetry
t	Time (s)
t_r	Retention Time (s)
t_o	Reference Elution Time (s)
t_n	Net Retention Time (s)
T	Temperature (K)
T_b	Boiling Point (°C)
T_g	Glass Transition Temperature (K)
T_K	Kauzmann Temperature (K)
T_m	Melting Temperature (K)
TAM	Thermal Activity Monitor
TCD	Thermal Conductivity Detector
TGA	Thermogravimetric Analysis
U	Internal Energy
US	United States
UV	Ultraviolet
V	Volume (m^3)
Vads	Volume Adsorbed (m^3)
Vm	Monolayer Coverage (m^3)
V_N	Net Retention Volume (m^3)
vs	Versus
v/v	Volume Per Volume
w	Weight (g)
w	Work Done
W	Watt
W_{adh}	Work Of Adhesion (mJ m^{-2})
w/o	Water In Oil
w/o/w	Water In Oil In Water
XRPD	X-Ray Powder Diffractometry
°C	Degrees Celsius
°	Degree
$	Dollar
Δ	Change In
ΔG_A^0	Total Free Energy Of Adsorption (kJ mol^{-1})
ΔG_A^{SP}	Specific Free Energy Of Adsorption (kJ mol^{-1})
ΔH^D_{VAP}	Dispersive Component Of The Heat Of Vaporisation (kJ mol^{-1})
%	Percentage
π	Standard Surface Pressure (N m^{-2})
θ	Bragg Angle
γ^D_S	Solid Surface Energy (mJ m^{-2})
γ^D_L	Liquid Surface Energy (mJ m^{-2})
γ_{LV}	Surface Tension (Liquid/Vapour Interface) (mJ m^{-2})

Other notations:

k (kilo) – 10^3; **d** (deci) 10^{-1}; **c** (centi) 10^{-2}; **m** (milli) 10^{-3}; **μ** (micro) 10^{-6}; **n** (nano) 10^{-9}.

1. INTRODUCTION

During product development a pharmaceutical company must consider many factors from conception of drug candidate to formulation of the final product. Any process or even variation in process can alter the final form of the compound favourably or disadvantageously. The solid-state phase transformation of the active ingredient in a dosage form can dramatically alter the pharmaceutical properties of the preparation such as the bioavailability (Halebalian & McCrone, 1969). If such problems are not minimised the development of a product may have to be stopped or possibly even the removal of a drug from the market. This can equate to a loss of time, effort and money. It can cost over US$800 million to convert a discovery compound to a commercial product, with development spanning approximately 15 years and only 1 in 500 discovery compounds reaching the market (DiMasi *et al.*, 2003).

It is important to highlight some case studies that have come to prominence in the pharmaceutical world, where process-induced phase transitions have manifested during the formulation of an active pharmaceutical ingredient (API). Gardner *et al.* (2004) have discussed two examples of pharmaceutical drugs – ritonavir (Norvir®) and alendronate (Fosamax®). After the launch of ritonavir, for the treatment of AIDS, it was found that the API marketed transferred to a more thermodynamically stable polymorph that did not provide as good a therapeutic response. The product had to be removed from the market until a full investigation had been conducted. Consequently a lot of time and money was spent to resolve the problem. Secondly, the drug alendronate was marketed and patented in the trihydrate form. However, since the discovery of a stable monohydrate form a second pharmaceutical company has attempted to patent this form of the drug. It will attempt to then market the drug in direct competition with Fosamax® and thus impinge on its company's profits. It is essential to understand and define the phase transitions that can take place for a material. These include crystallisation, polymorphism, hydration, solvation and amorphous character, and the factors that can affect such transitions.

1.1 Crystalline Solids

Crystalline implies a packing of molecules in which the structural units, termed unit cells, are repeated regularly and indefinitely in three dimensions in space (Vippagunta & Brittain, 2001). The majority of compounds exist in one or more crystalline forms. Every crystal can be classified individually. One such classification can be found in the International Tables for Crystallography (Hahn, 1987). Here the crystal is assigned to one of the 230 possible space groups, their symmetries and the symmetries of their diffraction patterns.

Many drugs can exist in more than one crystalline form. This is known as '*polymorphism*', and each crystalline form is termed a '*polymorph*'. The polymorphs of a drug have the same chemical composition but differ during crystallisation when the drug's packing arrangements and/or conformations are different from one another. As a result polymorphs will possess differing physical and chemical properties.

Pseudopolymorphs are crystalline solid adducts containing solvent molecules within the crystal structure, in either stoichiometric or nonstoichiometric proportions, giving rise to unique differences in the physical and pharmaceutical properties of the drug (Vippagunta & Brittain, 2001). Pseudopolymorphs are also known as '*solvates*'. If the solvate within the crystal structure is water, then the solvate is referred to as a '*hydrate*'.

The effects of pharmaceutical processes during the development of a drug can affect the final crystalline form of the drug in the dosage form. This in turn can lead to the end product not possessing the desired effect and different batches possibly having different properties. Processes such as grinding, milling, drying, compaction, oven drying and wet granulation could accelerate phase transitions in solids. Therefore it is important to choose the most stable polymorph of a drug and to control the crystal form during processing, to avoid such variations. Furthermore this will save time and cost during the development of the drug.

1.2 Amorphous Solids

An amorphous solid is best described by the following diagram [Fig. 1.1]:

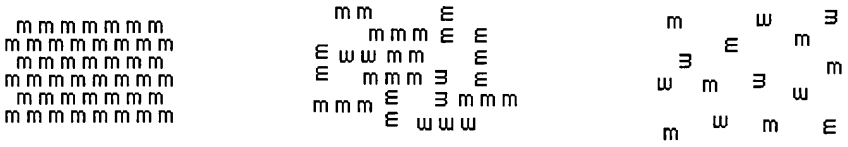

Crystalline Solid **Amorphous Solid** **Gas**

Fig. 1.1: Schematic representation of the structure of an amorphous solid compared to a crystalline solid and a gas (Yu, 2001).

Amorphous solids possess molecular arrangements like a crystal. However this arrangement is short-ranged, unlike a crystal where there is long-range order of molecular packing. Also the molecules in an amorphous solid are not arranged as randomly as they would be in the gaseous phase. Other important attributes to an amorphous solid are:

- May have greater apparent solubility and dissolution rate than its respective crystal form.
- They have higher energy, entropy and free energy than the corresponding crystal. Therefore they are usually less stable physico-chemically than the corresponding crystal.
- Due to their instability they can undergo structural relaxation.
- Amorphous forms of drugs and excipients can be produced during processing and on storage they can revert to the thermodynamically stable crystalline forms (Buckton & Lane, 2000). Examples of processes that can cause amorphous solids to form are lyophilisation and spray drying.
- Possess residual crystallinity, polymorphic states and regions of different density.

A crystalline solid may contain regions of amorphous nature. These areas are sometimes known as '*reactive hot-spots*'. This is because they are generally

thermodynamically unstable (at a higher energy state than the crystalline form). Due to the amorphous nature the solid can absorb water to a greater extent than its respective crystalline form. Therefore amorphous regions can be subject to physical and/or chemical degradation. Amorphous compounds are of scientific interest due to the advantage of greater dissolution over their respective crystalline phase for delivering pharmaceutical agents (Hancock & Parks, 2000).

1.3 Glass Transition Temperature (T_g)

A material's glass transition temperature (T_g) is the temperature below which molecules have very little mobility. Materials are rigid and brittle below their T_g and can undergo plastic deformation above it.

The chemical and physical properties of a solid state can be altered due to the effects of moisture. Processes such as lyophilisation, spray drying, granulation and also prolonged exposure to the atmosphere containing water vapour can alter the properties of a drug.

The interaction between water and crystalline solids proceeds in three main ways:

1) Adsorption of water vapour to the solid-air interface.
2) Dissolution of the solid in water absorbed from the air (deliquescence).
3) Hydrate formation.

Water has a greater impact on amorphous solids than crystalline solids of the same drug, as it is usually able to interact in the solid. This is in contrast to crystalline solids where water exerts its effects via adsorption of monolayers to the solid surface. As a result the degree of water uptake depends on the surface area available. However uptake of water in amorphous solids is greatly determined by the total mass of the amorphous solid.

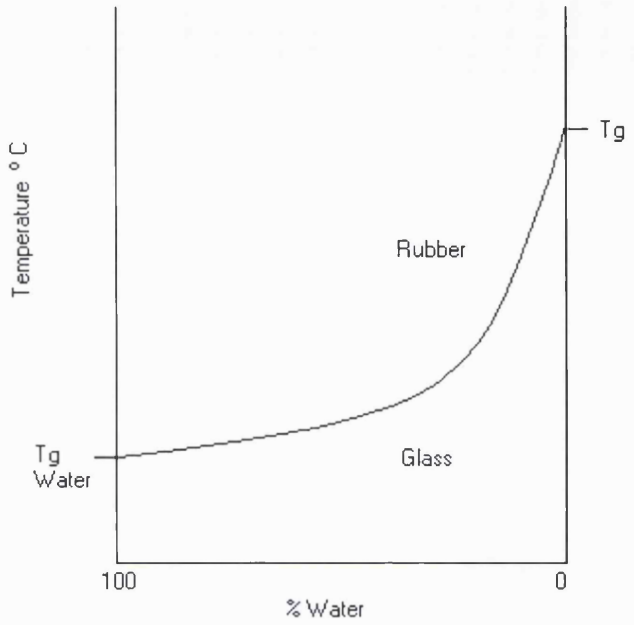

Fig. 1.2: Solute-water state diagram, which illustrates the effect of water plasticisation and its effects on T_g (Ahlneck & Zografi, 1990).

Water dissolved in an amorphous solid, can act as a plasticiser to increase greatly the free volume of the solid by reducing hydrogen bonding between adjoining molecules of the solid, with a corresponding reduction in its glass transition temperature, T_g (Ahlneck & Zografi, 1990). Fig. 1.2 provides a schematic representation of this change for a typical amorphous solid.

Below T_g the molecules are bound tighter i.e. glass-like. On the other hand above T_g the molecules are freer to move around, showing rubbery characteristics. If the experimental temperature (T) is higher than the T_g, then crystallisation should occur. Before crystallisation occurs the substance will undergo structural collapse. The rate at which crystallisation proceeds will depend on how far below T_g is from T. T_g can be lowered by adding a plasticiser such as water [Fig. 1.2] to induce crystallisation.

1.3.1 The Glassy State Theory

When a material cools from its melt changes occur with respect to the volume and enthalpy of the material [Fig. 1.3]. These changes are dependent on the rate

of cooling. If a material is imagined in its liquid state, the molecules will be randomly orientated and thus movement will also correlate in a random manner throughout the liquid.

Slow cooling:

If the material (in the liquid form) was cooled slowly, the liquid would undergo volume reduction as the mobility of the molecules would have decreased. Similarly, it will reduce in enthalpy too. At a specific temperature, or narrow temperature range, the liquid will crystallise and there will be a dramatic loss of volume due to contraction. The molecules arrange into ordered crystal lattices and thus its molecular mobility and volume occupied decreases. Further cooling will result in the material reducing in volume at a very slow rate, much slower than when the liquid phase was cooling. If the sample is reheated, it will melt (T_m) at the same temperature at which the crystalline state was formed.

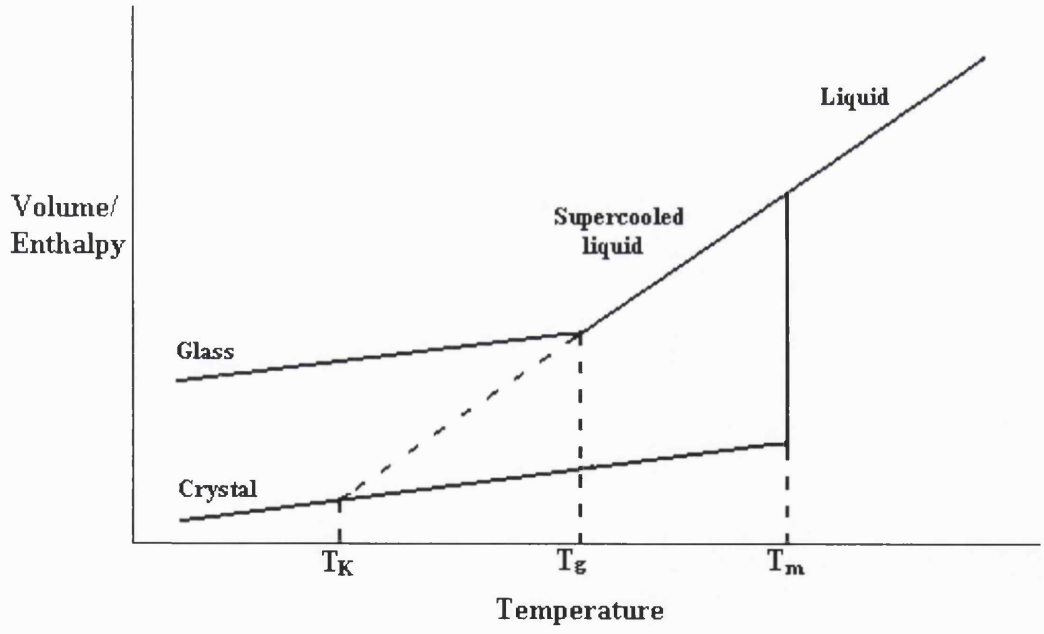

Fig. 1.3: Schematic depiction of the variation of volume/enthalpy with changing temperature (Hancock & Zografi, 1997).

Rapid cooling:

If the material is rapidly cooled from the liquid state, the molecules within the system will not have sufficient time to arrange themselves into an ordered lattice. Instead the molecules will remain in a randomly orientated manner even though their mobility has decreased. The material carries on the same contraction curve seen for the liquid and cools at a temperature below the crystallisation temperature. It can be postulated (Kauzmann paradox) that if the cooling were rapid enough, the curve would continue and cross the curve corresponding to the solid (T_K – Kauzmann temperature). T_K is the temperature at which the entropy of the liquid becomes the same as that of the crystal. However in practice this is not the case, as the curve deviates due to the glass transition (T_g). At the glass transition temperature there is a sudden and rapid decrease in molecular mobility. This is a direct result of the system becoming more viscous. These phenomena can be directly related to rubbers. Below the T_g the rubber is hard and brittle and above is soft and pliable. This macroscopic state change from pliable to brittle is in fact not the same as the change from a liquid to a solid. This is because the molecules in the material are randomly orientated above and below the T_g and thus in effect there is no real phase change.

Amorphous materials are thermodynamically unstable and will tend to revert to the crystalline form on storage (devitrification) (Craig *et al.*, 1999). The rate at which this occurs can be affected by the temperature it is stored at. If the temperature is above T_g, recrystallisation will proceed fairly quickly. However, if stored below T_g then recrystallisation is slower and dependent on how far below T_g the sample is stored. It has been suggested that if the sample is stored 50 °C below its T_g then the system should be fairly stable (Hancock & Zografi, 1997). The value of T_g for a sample will vary according to the time scale of the experimental method being used (Hancock *et al.*, 1995) (i.e. the rate at which it is cooled). Therefore, there is no one T_g for any material (that is not pure and dry).

1.4 Interfacial Phenomena

Interfacial phenomena describe the interaction between two surfaces in contact with each other. The term interface is defined by The Concise Oxford Dictionary as '(a) physics – a surface forming a common boundary between two regions and (b) a point where interaction occurs between two systems, processes, subjects etc'. Thus, in science this would be regarded as the interface between two surfaces that would include solid/liquid, solid/vapour, liquid/vapour or immiscible phases of the same state – solid/solid or liquid/liquid. The interfacial properties of a surface will be dependent on the states (solid, vapour or gas) of each surface. The research in this manuscript is related to the interaction between solid and vapour surfaces with gravimetric and gas chromatographic approaches. However, all the different interfaces are briefly described in the next section. A more thorough discussion can be found in the text by Buckton (1995).

1.4.1 Types Of Interfaces

1.4.1.1 Liquid/Vapour Interface

In a liquid the Van der Waals forces in the fluid environment hold the molecules together. This is in contrast to a gas where the molecules have total freedom of movement. In a liquid/vapour interface the molecules at the surface of a liquid will behave differently to those in the bulk of the liquid. A molecule in the bulk of the liquid will engage interaction forces from molecules all around it with no net force in any one direction acting upon it. However, the same molecule on the surface would show a net inward pull. This is due to the weaker pull from the gas molecules at the surface compared to the pull of the molecules in the liquid state.

The inward pull (contraction) at the surface would be directly related to the surface tension produced. The surface tension is the term used to quantify the interface between liquids and vapours. Surface tension is the net force per unit area acting on the liquid surface. It can be measured by a 'capillary rise method'.

Such a method involves placing a capillary tube into a bath of liquid. The level of the liquid will be different in the capillary tube to that in the liquid bath. This change in level is used to measure the surface tension, assuming there has been complete wetting of the glass capillary by the liquid.

Another approach of measuring the surface tension is by the 'Wilhelmy plate method'. A thin plate (perimeter about 40 mm) is lowered to the surface of a liquid and the downward force directed to the plate is measured. Surface tension is directly the force divided by the perimeter of the plate. A very important point with this method must be noted. There must be complete wetting of the plate to ensure the contact angle between the plate and the liquid is zero.

1.4.1.2 Liquid/Liquid Interface

A liquid/liquid interface involves the combination of two immiscible liquids such as oil and water. The second liquid can either spread over the primary liquid or form into a droplet depending on its spreading coefficient. An emulsion is the dispersion of two immiscible liquids, one of which is finely subdivided and uniformly distributed as droplets (the dispersed phase) throughout the other (continuous phase). Emulsions can be either oil in water (o/w), water in oil (w/o) or a multiple system such as water in oil in water (w/o/w). There are many advantages to the use of emulsions as a pharmaceutical dosage form:

- More palatable route of administration for oils, by delivering in an aqueous medium.
- Providing variable drug release rates.
- Multiple emulsions allow the incorporation of incompatible compounds.

1.4.1.3 Solid/Liquid Interface

Due to the net imbalance of forces in the surface of a solid, the solid will have a surface energy. Unlike liquids, due to the rigidity of a solid compound it may possess areas of differing surface energies. This could be a result of prior processing (such as micronisation). The surface characteristics of solids cannot

be deduced directly by using the same methods as for liquids. Techniques such as contact angle and inverse gas chromatography (IGC) are the methods of choice. The principles of IGC have been fully described in chapter 6 and as a result only contact angle will briefly be described in this chapter (section 1.6.1).

1.4.1.4 Solid/Vapour Interface

The solid/vapour interface is an important research area as data such as wettability and surface area determinations of a compound can be established. Adsorption (onto the surface) and absorption (into the bulk) of vapour molecules or even both (known as sorption) are the processes involved with such an interface. Such interactions can be measured by vapour sorption techniques such as dynamic vapour sorption (DVS) and IGC. The surface adsorption theories will be discussed in greater depth in section 1.5.

1.4.1.5 Solid/Solid Interface

Solid/solid interfaces have the difficulty of obtaining 100% contact due to the roughness of solids. Also processing of the materials can lead to this rough nature on the surface and create areas of differing surface energies. In the pharmaceutical environment solid/solid interfaces are of interest with regards to friction, lubrication and adhesion. Friction is a problem for example during tablet formulation where interaction with the machine parts could cause damage to both the tablet and the equipment. This can to some degree be minimised with the use of a lubricant. A lubricant placed between the interface of two solid surfaces can help to reduce the frictional force and subsequent shearing that could have taken place. A lubricant can be in the form of a gas, condensed liquid from a vapour, liquid or a solid. The most common liquid form of lubricant is oil and solid lubricants include soft crystals such as graphite. Adhesion of materials with the aid of a 'glue' is important within the pharmaceutical industry. Adhesion helps for film coating of materials to solid products, binders during wet granulation and drugs to carrier particles during dry powder inhalation. Similarly the breakdown of the adhesive may also be important in allowing the release of the drug at the desired location.

1.5 Surface Adsorption Theories

The history of adsorption science had been charted in a review by Dabrowski (2001). The author has tabulated the earliest experimental age of adsorption science by the Egyptians and Sumerians in 3750 BC with their use of charcoal for the reduction of copper, zinc and tin ores for manufacture of bronze, through to observed and recorded experiments of scientists such as Dewar (1904) who found selective adsorption of oxygen from its mixture with nitrogen during air uptake by charcoal. Dabrowski (2001) has further documented the development of isotherm equations such as Langmuir, Freundlich and BET (all discussed in sections 1.5.3, 1.5.4 and 1.5.5 respectively) to deal with the physical adsorption of gases and vapours.

Physisorption	**Chemisorption**
Low heat of adsorption (< 2 or 3 times latent heat of evaporation).	High heat of adsorption (> 2 or 3 times latent heat of evaporation).
Non-specific.	Highly specific.
Monolayer or multiplayer adsorption.	Monolayer adsorption only.
No dissociation of adsorbed species.	May involve dissociation.
Only significant at relatively low temperatures.	Possible over a wide range of temperatures.
Rapid, non-activated and reversible.	Activated, may be slow and irreversible.
No electron transfer expected, although polarisation of sorbate may occur.	Electron transfer leading to bond formation between sorbate and surface.

Table 1.1: Differences between physisorption and chemisorption. (Adapted from Ruthven, 1984).

Although the work presented in this thesis deals mainly with physical adsorption (physisorption), chemical adsorption (chemisorption) must also briefly be mentioned. Physisorption involves relatively weak intermolecular forces, whereas chemisorption involves the formation of chemical bonds between the

adsorbing molecule and the surface of the adsorbent. Table 1.1 highlights the differences between the two types of adsorption.

1.5.1 Thermodynamics Of Adsorption

A solid will adsorb vapour to a different degree after processing due to its changed surface energy. The adsorption of vapours promotes the reduction of the interfacial free energy at the surface. There is always a drive for any system to revert to the most stable state possible if conditions allow such transformations. As a liquid is a fluid system the surface energy of a liquid is the same throughout the surface because surface molecules are free to rearrange themselves. However the rigidity of a solid structure prevents such molecular movement to occur. As a result higher energy sites on the surface will interact with vapour to a greater extent to reduce the interfacial free energy. A basic knowledge of thermodynamics is required to understand the changes in enthalpy during adsorption. A good basis has been provided from the text by Smith (1982).

The 'First Law of Thermodynamics' states that energy can be converted from one form to another but it can neither be created nor destroyed. Thus, the sum of all the energy changes in an isolated system must equate to zero.

$$\Delta U = Q - w \qquad \text{[Equation 1.1]}$$

'ΔU' is the change in internal energy when changing from one state to another, 'Q' is the heat absorbed by the system and 'w' is the work done on the system (transfer of energy from one mechanical system to another). Under constant pressure the internal energy can be linked to the enthalpy (H) with the following relationship:

$$H = U + PV \qquad \text{[Equation 1.2]}$$

'P' is the pressure and 'V' is the volume of the system. Following from the first law, the 'Second Law of Thermodynamics' can be defined in many ways. One

such way is that any system, which is free of external influences, becomes more disordered with time. This disorder can be expressed in terms of the quantity called entropy (*S*). Entropy can be better described by considering the spontaneous melting of ice. When ice melts, the regular hydrogen-bonded structure of ice is replaced by the fluid association of water molecules in liquid water. This spontaneous change involves a transition from an ordered arrangement of particles to a less ordered arrangement. A decrease in the degree of order in a system is correlated by an increase in entropy (positive value). The change in entropy of a system is related to the enthalpy change and the Gibbs free energy (ΔG):

$$\Delta G = \Delta H - T\Delta S \qquad \text{[Equation 1.3]}$$

All spontaneous physical and chemical changes take place in the direction of a decrease in the free energy. Adsorption, also a spontaneous process, dictates that the change in the Gibbs free energy must be negative. The adsorption of a gas or vapour creates a greater degree of order to the system implying a decrease in entropy. However, a spontaneous process correlates to a positive entropy and therefore the only variable remaining is the change in enthalpy. Thus an exothermic process of adsorption produces a negative enthalpy response. The thermodynamics of adsorption could be quantified by calorimetric methods.

1.5.2 Types Of Isotherms

The IUPAC classification of adsorption isotherms has divided the isotherms into six with each having specific characteristics.

Type I

- Adsorbents are microporous.
- Langmuir type isotherm obtained when adsorption is restricted to a monolayer.

Type II

- Adsorbents are nonporous or macroporous.
- Strong fluid-solid interactions.

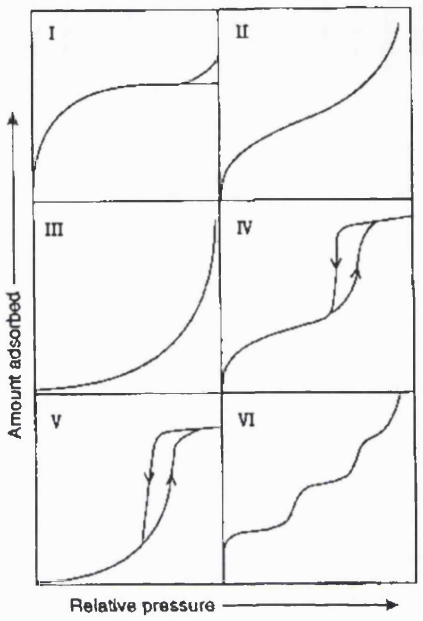

Fig. 1.4: IUPAC classification of adsorption isotherms (Sing *et al.*, 1985).

Type III

- Adsorbents are nonporous or macroporous.
- Weak fluid-solid interactions.

Type IV

- Adsorbents are mesoporous.
- Strong fluid-solid interactions.
- Hysteresis loops associated with capillary condensation in the mesopores.

Type V

- Adsorbents are mesoporous.
- Weak fluid-solid interactions.
- Hysteresis loops associated with capillary condensation in the mesopores.

Type VI

- Adsorbents are nonporous or macroporous.

- Stepwise multilayer adsorption occurs.

Pores are classified according to pore diameter (Barton *et al.*, 1999):

- Micropores = less than 2 nm
- Mesopores = 2-50 nm
- Macropores = greater than 50 nm

1.5.2.1 Adsorption Procedure

Typically for a Type II/IV isotherm [Fig. 1.5], initially the majority of gas molecules adsorb onto the sample with small increases in partial pressure [Step A-B]. Soon a monolayer is formed over the sample surface. Thereafter the volume adsorbed increases slowly with the rise in partial pressure [Step B-C]. Continual increase in pressure will then induce the filling of the mesopore structure (smallest first) with a very rapid increase in the volume adsorbed [Step C-D]. Just before saturation, vapour pressure is reached and all the pore structure is filled. The removal of gas will cause the pores to empty, largest first. This desorption process is used to characterise pore structures. Capillary condensation is generally responsible for the filling of mesopores and macropores (i.e. pores of the width >2 nm) (Sing, 2001). However this process is secondary to multilayer adsorption on pore walls and is complete if a plateau is reached at higher partial pressures. The filling of micropores is controlled by stronger interactions between the adsorbate molecules and pore walls (Barton *et al.*, 1999).

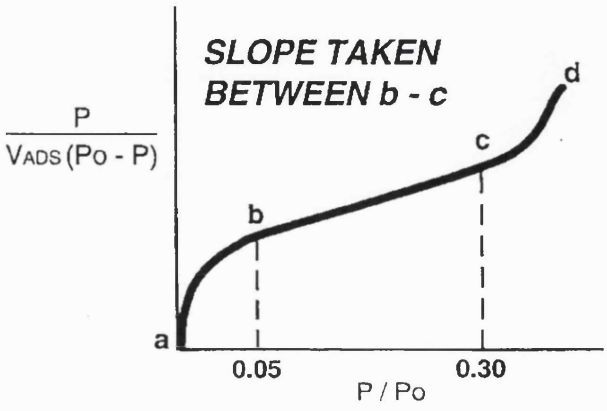

Fig. 1.5: Diagram of a typical Type II/IV adsorption isotherm.

The phenomenon of capillary condensation first involves the gas adsorbing into the pores at a low density. After a sufficient amount of gas has been supplied, it spontaneously condenses into a liquid-like state inside the pores. In some case, the adsorbed liquid may be denser than the corresponding bulk liquid, allowing large amounts to be stored inside the material.

Mathematical models have been formulated to explain the adsorption isotherms produced. There are many models reported in literature. Three such models that will be described are the Langmuir, Freundlich and BET models.

1.5.3 Langmuir Theory

The Langmuir isotherm was developed by Irving Langmuir in 1916 to describe the dependence of the surface coverage of an adsorbed gas on the pressure of the gas above the surface at a fixed temperature (Langmuir, 1916; 1918). The assumptions made with this mathematical model include:

- Adsorption sites on the surface of a material are identical and equally accessible such that adsorption is desirable over the entire surface.
- Neighbouring adsorbing molecules already adsorbed do not affect each other (minimal attraction or repulsion).
- All sites are energetically equivalent.

The Langmuir isotherm is the simplest theoretical model for monolayer adsorption. The Langmuir isotherm can be written as:

$$\frac{P}{Vads} = \frac{P}{Vm} + \frac{1}{K'Vm} \qquad \text{[Equation 1.4]}$$

'Vads' is the volume of gas adsorbed at any one time, 'Vm' is the amount of gas required to produce monolayer coverage, 'P' is the pressure of the vapour and 'K'' is a constant. The gradient is characterised by '1/Vm' and the intercept by '1/(K'Vm)'. The characteristic shape of a Langmuir isotherm is that of a Type I

isotherm [Fig. 1.4]. There is an initial rapid adsorption of the adsorbate, which then reaches a plateau with increasing partial pressure. Any further increases in the partial pressure do not cause an increase in the adsorption.

1.5.4 Freundlich Theory

The Freundlich isotherm is an equilibrium isotherm that is used very often due to its practicality. This relationship is used for a heterogeneous surface composed of different classes of adsorption sites (to which many surfaces fit). Consequently the enthalpies of adsorption vary exponentially. This is in direct contrast to the Langmuir isotherm where the enthalpy of adsorption does not alter with the surface coverage. The Freundlich equation can be linearised to form:

$$\ln \text{Vads} = \ln a + 1/n \ln P \qquad \text{[Equation 1.5]}$$

'Vads' corresponds to the amount of gas adsorbed and 'P' is the pressure of the vapour, with '*a*' and 'n' being Freundlich constants. The Y-axis intercept provides an idea of the adsorption capacity of a surface.

1.5.5 BET Theory

The BET theory was developed in 1938 by Brunauer, Emmett and Teller (Brunauer *et al.*, 1938). It is a mathematical model that makes three major assumptions:

- The evolved energy associated with a nitrogen molecule adsorbing on a sample surface and that of a nitrogen molecule adsorbing onto a previously adsorbed nitrogen molecule is different.
- The surface of the sample has uniform attraction to nitrogen molecules as it is homogenous.
- Neighbouring nitrogen molecules already adsorbed do not affect each other as the attractive forces are assumed to be vertical.

However, the BET theory is not a complete theory for all circumstances. It can only be implemented on samples that produce 'Type II' and 'Type IV' isotherms. Other isotherms show deviation from BET predictions. It may be anticipated that one of the reasons for the inadequacies of the BET theory, and other adsorption isotherm theories, is due to the failure of real systems to conform to the assumption that the surfaces are homogenous (Rudzinski & Everett, 1992).

The BET method is widely used to determine the surface area of porous materials such as theophylline (Antila & Yliruusi, 1991). Nitrogen is generally considered to be the most suitable adsorptive for surface area determination and it is usually assumed that the BET monolayer is close packed, giving $a_m(N_2)$ = 0.162 nm^2 at 77 K (a_m is the molecular cross-sectional area occupied by the adsorbate molecule in the complete monolayer) (Toth *et al.*, 1999).

The BET equation (Brunauer *et al.*, 1938) [Equation 1.6] permits calculation of monolayer capacity from an adsorption isotherm using only mass of a sample as the dependent input. Thus the surface area of a sample can be calculated.

$$\frac{P}{Vads\,(Po-P)} = \frac{C-1}{Vm\,C} \times \frac{P}{Po} + \frac{1}{Vm\,C} \qquad \text{[Equation 1.6]}$$

- Vads = Volume adsorbed
- Vm = Monolayer volume
- C = Adsorption energy constant
- P = Sample pressure
- Po = Saturation vapour pressure of adsorbate

NB: *In any one test Vm and C are constants.*

Intercept = 1/VmC

Slope = C-1/VmC

The BET equation can only be applied at coverages not greatly exceeding monolayer coverage. Unfortunately this can only truly occur on homogenous

surfaces. This is due to the fact that in heterogeneous surfaces, at which interactions between admolecules come into play, there will be a significant effect of multilayer (mostly secondary) adsorption (Rudzinski & Everett, 1992).

For a graph plotted using the BET theory, the plot should be linear to allow the derivation of C and Vm from the slope and intercept of the line. It is commonly found experimentally that for simple gases a linear graph is observed in a limited range of partial pressures, typically 0.05 to 0.35 (Rudzinski & Everett, 1992). It is evident that the location and extent of the linear region of a BET plot is dependent on the adsorption system (both adsorbent and adsorptive) and the operational temperature (Sing, 2001).

The BET equation was the mathematical model of choice for analysis of gravimetric data (chapter 5). Such a model was selected due to its successful wide use and advantages over other theories. The Type II isotherm is the most common isotherm produced, therefore the BET equation can successfully be applied to calculate the surface area from the monolayer coverage. The BET equation reduces to the Langmuir equation when a system does not adsorb more than that relating to a monolayer.

1.6 Surface Energetics

The surface energetics are an important characteristic of a material's surface that can be measured to provide valuable information regarding the wettability of any material. Early work by Fowkes (1964) has been a catalyst in the development of surface chemistry and specifically surface energetics in terms of a surface's non-polar and polar components. Two well-known methods used to determine the surface energetics of powders are contact angle and IGC. The application of IGC and the theories behind the technique have been fully discussed in chapter 6. Only contact angle will be briefly discussed within this section to provide an alternative to using IGC and to discuss the problems associated with such a technique.

1.6.1 Contact Angle

Measurement of the contact angle of a droplet on a surface is used to determine the wettability of the surface. Liquids that wet a surface (or spread) have a low contact angle (during complete wetting the angle is equal to 0°); liquids that do not wet, but rather form a bubble over the surface, have a high contact angle (180° angle suggesting no wetting). The contact angle is the angle formed at the solid/liquid/vapour interface by the drop on the solid, measured through the liquid. Contact angles can be measured by machines such as the 'Dynamic Contact Angle Analyser' that utilises the Wilhelmy plate method (as described earlier – section 1.4.1.1). It is defined as:

$$F = p\gamma_{LV}\cos\theta \qquad \text{[Equation 1.7]}$$

'*F*' is the force measured by the balance, 'p' is the perimeter of the sample at the interface, 'γ_{LV}' is the surface tension of the liquid vapour interface and 'cos θ' is the cosine of the contact angle.

The surface tensions of the partially wetting (test) liquids need to be accurately established prior to measurement of the contact angle of the samples (experiments conducted on clean glass slides alone). Three different test liquids are used of which one must be apolar and two polar. The samples are attached onto the glass slide (devoid of any dust and grease) using an adhesive. The powder should ideally be evenly distributed and full coverage should be obtained. From the results the surface energy components of the material under investigation can be calculated. The calculations have been clearly transcribed in the paper by Rillosi and Buckton (1995).

1.6.2 The Disadvantages Of The Contact Angle Approach

Although contact angle determinations can provide a useful measure of the surface characteristics of a material, there are many disadvantages to the technique. The problems associated with contact angle measurements have been

discussed extensively (Buckton, 1993; Buckton, 1995), and have been briefly detailed below.

Contact angle measurements can differ between one experiment to another if the glass slide has not been properly cleaned i.e. by heat to remove any grease or dirt on the surface. The same is applicable to the surfaces of powdered materials. Contamination from the atmosphere onto the sample surface can alter contact angle results too. The method of experimentation can also have a bearing on the results obtained. For example it has been shown that placing the sample on the glass plate using an adhesive is better than compressed plates of powder (Dove *et al.*, 1996).

The lack of homogeneity on the surface of the material is a major problem that can lead to erroneous results. The fact that it is very unlikely that a material surface is perfectly smooth will make it very difficult to measure a true contact angle as it may differ when measured on different areas of the surface. Therefore the sample as a whole may not be reflected by the measured contact angle. Another source of error for contact angle measurements is to ensure the drop of liquid is less than 10 μL to avoid deformation of the drop by gravity.

The low levels of impurities in pharmaceutical powders can have a significant impact on the surface energies of materials. Such impurities can possess their own surface characteristics or can create defects in the crystal surface. Impurities are abundant in many excipients such as magnesium stearate. These excipients are essential to provide the lubricant properties of magnesium stearate. Thus, the difficulties in controlling the impurities from batch-to-batch would add to the complication of such measurements. Finally the lack of even distribution of powder on a glass slide and possible gaps in the powder layer can lead to inaccurate contact angle measurements.

The problems discussed in measuring surface energies, via contact angles, of powders have led to alternative methods. IGC is a very convenient approach to measure surface energies of materials. Although there are also disadvantages to the technique itself, many of the problems associated with contact angle are

eliminated. Other approaches for assessing the wettability of a compound include gravimetric vapour sorption and calorimetry. Both vapour sorption and IGC are discussed in chapters 5 and 6 respectively. Calorimetric methods have been used to establish successfully the effects of milling techniques on the adsorption of water onto aspirin (Buckton *et al.*, 1988).

1.7 Batch-To-Batch Variation

Batch-to-batch variation of powders and final dosage forms is an undesirable aspect of pharmaceutical drug development. The opportunity for changes to the API and the excipients to occur are numerous during the development process. Any such changes can influence the physical, chemical and mechanical properties of a compound. The manufacture of any pharmaceutical product begins with raw materials, and the quality of these will ultimately determine the value of any finished product (Brittain, 1989). Variability is prevalent between powders from different suppliers as well as from the same supplier. Even lot-to-lot variation during formulation can lead to varying physical properties of API's and excipients.

Good manufacturing practice (GMP) can help minimise variations within a batch and from batch-to-batch. Good manufacturing practice involves careful control and validation of all aspects of the development process such as raw materials, equipment, experimental procedures and packaging. Usually it is found that the thermodynamically stable crystal form of the API is the preferred final dosage form state. However, on occasions, if an amorphous or metastable compound can be stored with great stability, then it can be utilised due to the greater dissolution that may transpire. However it is important to be aware of conditions such as temperature and humidity that can affect stability, and the time-scales and environmental factors in which thermodynamically unstable API's and excipients will revert back to their stable form.

As already mentioned, process-induced phase transitions can occur at any stage of the development phase. An example of the types of processes that take place

for an API's conversion to a solid oral dosage form has been shown on Fig. 1.6. Size reduction by processes such as milling can improve surface area and uniformity of the API, but can also create amorphous regions due to shearing of the particles. Another problem of milling is the heat generated during the process that can lead to dehydration and other polymorphic changes. Many changes that may occur take place on the surface and thus prove to be difficult to detect with numerous analytical techniques. Also increased surface energy can elevate the likelihood of interaction with excipients.

Granulation is performed to improve the physical characteristics of a compound such as lubrication, flowability, compressibility and cohesion. Wet granulation (e.g. fluid-bed mixing) can be a precursor to phase transitions as described in the review by Morris *et al.* (2001). Water or solvents used in the system can create hydrates and solvates or even induce crystallisation. Additionally during drying of the wet granular compound there could be dehydration to a metastable form and even dissociation of part of the compound. Some of the problems with wet granulation can be resolved by dry granulation. The lack of water/solvent will prevent possible formation of hydrates or solvates. Also there will be no drying process and therefore elevated temperatures are not used. However the dry compaction method, possibly with the use of a roller, can promote amorphous nature within the surface and possible dehydration due to the heat generated by the process. Finally melt granulation involves mixing the API with a complete or partial melt of the excipients. Once granulated the mixture is chilled to allow solidification and binding. When the API interacts with the melted excipient mixture it may also melt or dissolve to a certain extent. This will also help with the binding of the system. Adversely, cooling of the system could easily lead to phase transformations.

Spray drying is another technique that could be utilised during drug formulation. Spray drying can create particles that are homogenous, porous, amorphous and uniform in size and shape. However, such a process involves dissolving or dispersing the API and can therefore lead to hydrate/solvate formation. The production of amorphous character could also be a disadvantage.

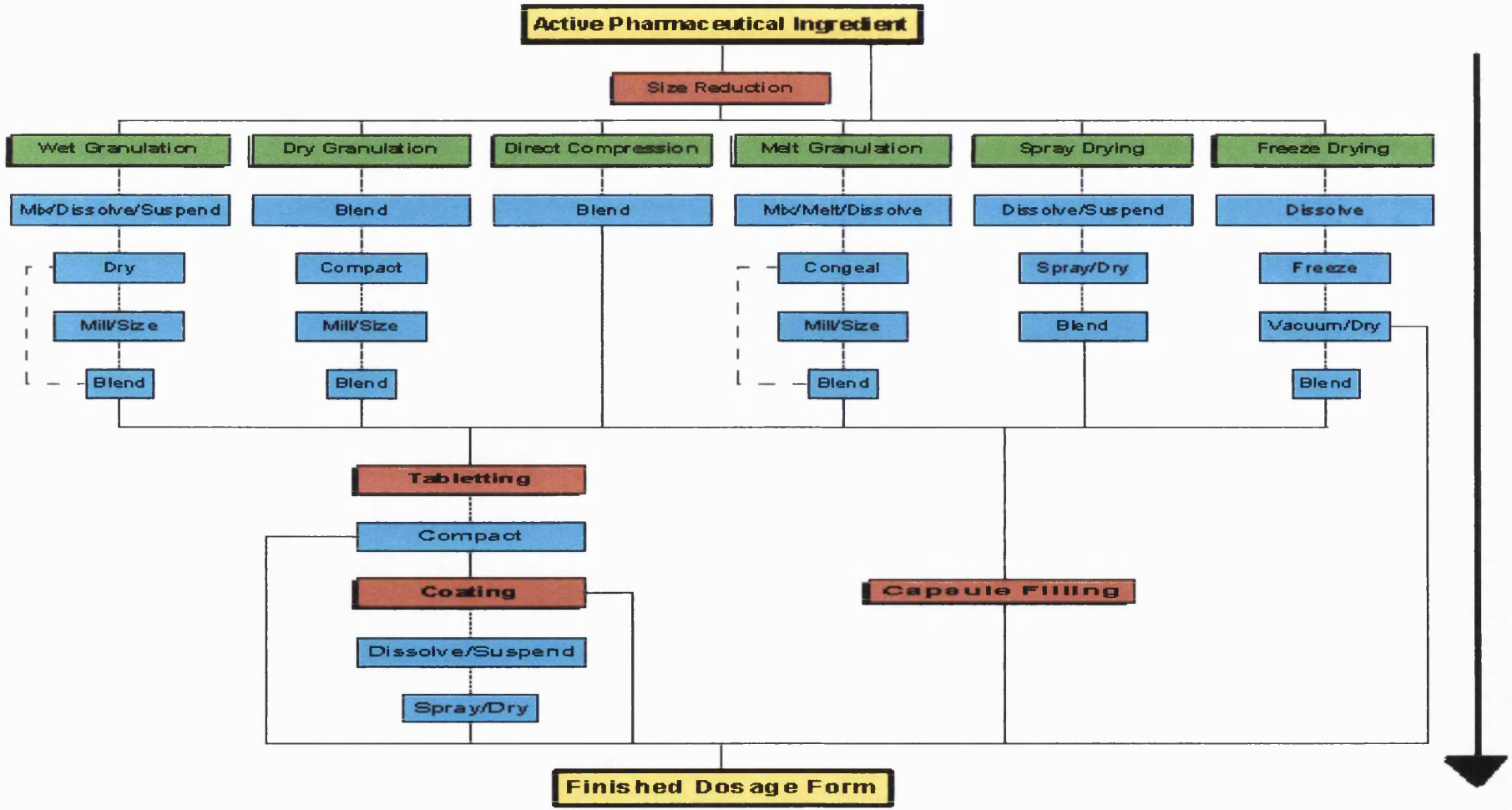

Fig. 1.6: **Processes involved during solid oral dosage form preparation – (Adapted from Zhang *et al.*, 2004).**

Freeze drying removes almost all moisture (water) from a system. It is useful in producing stable products with long shelf lives. One such famous example is Nescafe®, produced by Nestle®. Nestle® helped Brazil solve their coffee surplus by freeze-drying stores of coffee. Of course, as well as being an advantage the creation of amorphous nature could also be a disadvantage. Additionally dispersion of the API in a solvent may also lead to phase transitions.

Encapsulation of a powder should cause limited stress on the compound and therefore negate the opportunity of any phase transitions to transpire. Coating of a tablet can prove to be very advantageous. Unpleasant tastes can be masked by a drug coat, and a tablet can be made to look more aesthetically pleasing. These improvements may help with patient compliance during treatment. Also tablet coating can be utilised to provide modified-release forms of the drug by spraying the drug solution. This coat can provide immediate drug release prior to the bulk of the drug being available. However by preparing a solution spray of the drug for coating, there is a chance of hydration or solvation taking place. Table 1.2 summarises the advantages and disadvantages of some of the techniques possibly involved in the formulation of an oral dosage form.

It is important to understand and to some extent, where possible, to predict phase transformations that may manifest during processing. This is a key area, as the prevalence of variability from batch-to batch will probably relate to the intensity of processing. Other areas of research in optimisation of formulation techniques include high throughput screening (HTS) of candidate drugs to assess the phase transitions that may take place or to obtain the appropriate conditions for a candidate to be developed. Chaubal (2004) has provided a review on HTS specifically concentrating on nano-particles, and Morissette *et al.* (2004) have discussed HTS crystallisation methodologies for the identification and characterisation of diverse forms of APIs using limited amounts of compound. Another review by Koh *et al.* (2003), has discussed the current drive in pharmaceutical analysis. This includes areas of development such as HTS, combinatorial techniques of analysis, and chemometrics. Chemometrics is defined as the use of multivariate data analysis and mathematical tools to extract information from chemical data (Yu *et al.*, 2004).

Technique	Advantages	Disadvantages
Size Reduction	Improved morphology and flow, enhanced uniformity and increased surface area.	Amorphous nature created especially at the surface. Heat generated leading to polymorphic transitions i.e. dehydration.
Wet Granulation	Increased properties; flowability, cohesion, compressibility and lubrication. Versatile technique.	Crystallisation of amorphous nature. Hydration/solvation during wetting. Dehydration and possible dissociation during drying.
Dry Granulation	Increased properties; flowability, cohesion, compressibility and lubrication. Prevents hydration/solvation. Prevents dehydration and possible dissociation.	Amorphous character due to the stress applied. Heat generation could cause dehydration.
Melt Granulation	Increased properties; flowability, cohesion, compressibility and lubrication. Partial/complete melt of API serves as a binder.	Cooling can cause phase transformations.
Spray Drying	Homogenous, porous, uniform size and shape particles. Produces amorphous material.	Dissolving or dispersing of API can lead to hydration/solvation. Amorphous phase produced.
Freeze Drying	Creation of amorphous nature. Development of stable products with long shelf lives.	Amorphous phase produced. Possible hydration/solvation when dissolved or dispersed.
Encapsulation	Simple process without any stress on material.	Phase transitions very unlikely.
Coating	Taste-masking, modified release of tablet, aesthetic to help with patient compliance.	Spraying the drug solution as a coat for modified release tablets can cause phase transformations such as hydration/solvation.

Table 1.2: Summary of the advantages and disadvantages of some techniques involved during drug formulation with regards to causing phase transitions of the API and/or excipients.

Each phase transition of an API displays unique physicochemical properties that can profoundly influence the bioavailability, manufacturability, purification, stability and many other characteristics of the drug (Byrn *et al.*, 1999). Even small changes on the surface of a compound can affect the physical and chemical properties of a drug. However, any such transitions are not always easy to detect. Therefore there is always a need to invent new techniques and develop older techniques to increase the sensitivity and detection of any possible changes.

2. AIMS

The aims of the project are to:

- Characterise the compounds in terms of their crystal lattice structures (anhydrous and hydrate forms).

- Investigate the materials in terms of their batch-to-batch variability as regards to the effects of micronisation and direct batch comparisons from supplier products obtained from Sigma-Aldrich, Poole, UK (Sigma and Fluka batches).

- Study the nature and wettability of compounds and their surfaces when probed with polar and non-polar solvents to compare:

    a) Effects of micronisation.
    b) Hydrate forms of the compounds.
    c) Batch variability from supplier.

- Evaluate two vapour adsorption techniques for assessing the wettability of compounds.

3. MATERIALS & METHODS

3.1 Materials

Material	Supplier
Theophylline Anhydrous Sigma	[Lot: 80K1367] Sigma-Aldrich, Poole, UK
Theophylline Anhydrous Fluka	[Lot: 403967/1 42100] Sigma-Aldrich, Poole, UK
Calcium Mupirocin Dihydrate	[Lot: WPJ 33/5] GlaxoSmithKline, Harlow, UK
Nabumetone	[Lot: NB 2243] GlaxoSmithKline, Harlow, UK
Magnesium Stearate Sigma	[Lot: U00714] Sigma-Aldrich, Poole, UK
Magnesium Stearate Fluka	[Lot: 03190] Sigma-Aldrich, Poole, UK
Methanol HPLC grade	Fisher Chemicals, Loughborough, UK
Ethanol HPLC grade	BDH, Leicestershire, UK
Propan-2-ol HPLC grade	Fisher Chemicals, Loughborough, UK
Hexane HPLC grade	Fisher Chemicals, Loughborough, UK
Butan-1-ol HPLC grade	Fisher Chemicals, Loughborough, UK
Phosphorous Pentoxide 98%	Lancaster, Morecambe, UK
Sodium Chloride	Sigma-Aldrich, Poole, UK
Potassium Sulphate	Sigma-Aldrich, Poole, UK
Magnesium Chloride	Sigma-Aldrich, Poole, UK
Hydranal Composite 5K	Sigma-Aldrich, Poole, UK
Hydranal Ketosolver	Sigma-Aldrich, Poole, UK
N,N-Dimethylformamide	Fisher Chemicals, Loughborough, UK

Table 3.1: List of materials used during the experimental studies.

3.2 Dynamic Vapour Sorption (DVS)

Name & Model: Dynamic Vapour Sorption Analyser 1
(Surface Measurement Systems, London, UK)

The introduction and methodology of the DVS apparatus has been discussed in chapter 5 (section 5.3), which deals with the majority of the DVS experiments within this thesis.

3.3 Dynamic Vapour Sorption (DVS) – Near Infrared Spectroscopy (NIR)

Name & Model: NIRSystems 6500 spectrometer
(Foss NIR Systems, Cheshire, UK)

3.3.1 Introduction

Spectroscopy is the measurement and interpretation of electromagnetic radiation absorbed, scattered, or emitted by atoms, molecules, or other chemical species (Willard *et al.*, 1988). Changes in the energy states of the investigating compound due to absorption or emission can be directly related to the chemical entities of the compound and viewed as a spectrum. Near-infrared spectroscopy is one of the most rapidly growing analytical techniques in pharmaceutical analysis because it offers rapid, non-destructive analysis of pharmaceutical dosage forms (Guo *et al.*, 1990).

The infrared region of the electromagnetic spectrum is found between the red end of the visible spectrum (wavelength – 700 nm) to the microwave region (wavelength - 500,000 nm). The near infrared region, at which the NIR apparatus measures at, spans from a wavelength of 800 nm to 2500 nm. Essentially atom-atom bonds within molecules vibrate at specific frequencies (their potential energy). When they absorb light at a specific frequency to that at which they were vibrating, they are excited to a higher energy level (as defined

by quantum mechanics). This transition accounts for the presence of a specific frequency of radiation and hence the presence of a spectral line. The spectra can be measured by the ratio of the intensity of reflectance of radiation by the sample, or transmittance of radiation through the sample to that impinging on it.

The spectrum arises from absorption bands and overtones, and combinations of fundamental mid-infrared stretching and bending modes (Ciurczak & Drennen, 2002). The low wavelength absorptivities, which arise from C-H, O-H and N-H bonds is a primary reason for the usefulness of the technique. Fundamental transitions are so called to characterise an excitation from the ground energy state (potential – v_0) to next highest energy state (v_1). Transitions that are greater than just one energy state, from the potential, are defined as overtones (e.g. v_0 to v_2). Combination bands arise when transitions occur for two or more different bonds vibrating at similar frequencies.

3.3.2 Methodology

A fibre optic probe, created by Foss NIR Systems was connected to a NIRSystems 6500 spectrometer. The probe was positioned 3-4 mm under the sample pan of the DVS. The spectra were recorded over the infrared wavelength range of 1100-2500 nm every 15 minutes. All measurements were a mean of 32 scans over 40 seconds (resolution of 2 nm). NIR data were collated during DVS experiments. NIR data processing and analysis were carried out using Vision software (version 2.21).

The standard NIR spectra can be affected by the sample geometry. A general offset of the baseline across the spectral region can be observed due to the changes of particle size. However by mathematically subjecting the data to standard normal variance (SNV) and second derivative treatments this variance of sample geometry can be minimised. Also the second derivative of a spectrum helps enhance the differences in intensity and wavelength positions to allow structural differences in the materials to be interpreted. SNV and other normalisation techniques for NIR spectra have been discussed in a review by Blanco *et al.* (1998). With this method a peak of negative displacement in the

second derivative spectrum corresponds directly to a positively displaced peak in the original spectrum. All experiments were run in triplicate and only with theophylline.

3.3.3 Calibration

Calibration was conducted before each experiment using a reference signal obtained from a ceramic tile.

3.4 Inverse Gas Chromatography (IGC)

Name & Model: Inverse Gas Chromatograph Analyser
(Surface Measurement Systems, London, UK)

The fundamentals of IGC and the methodologies undertaken have been described in chapter 6 (section 6.3), which has solely been devoted to IGC work.

3.5 Isothermal Microcalorimetry

Name & Model: *Thermometric LKB 2277 Thermal Activity Monitor (TAM)*
(Thermometric, Jarfalla, Sweden)

3.5.1 Introduction

Chemical and biological reactions can be monitored by the TAM apparatus. Both exothermic (heat-producing) and endothermic (heat-absorbing) reactions are measured by the system. Other information that can be obtained include;

- Rate of basic chemical reactions.
- Extent of basic chemical reactions.
- Changes of phase.
- Changes of structure.
- Metabolism of living systems.

The TAM equipment is very sensitive and can measure thermal events to fractions of a microwatt. The TAM operates by utilising the basic principle of thermal equilibrium within a system, such that any heat produced diffuses away. This process can be termed as 'Heat Flow' or 'Heat Leakage' [Fig. 3.1]. Optimal thermal stability can be achieved by creating a heat sink, using a 25-litre water thermostat (distilled water), surrounding the reaction measuring vessel.

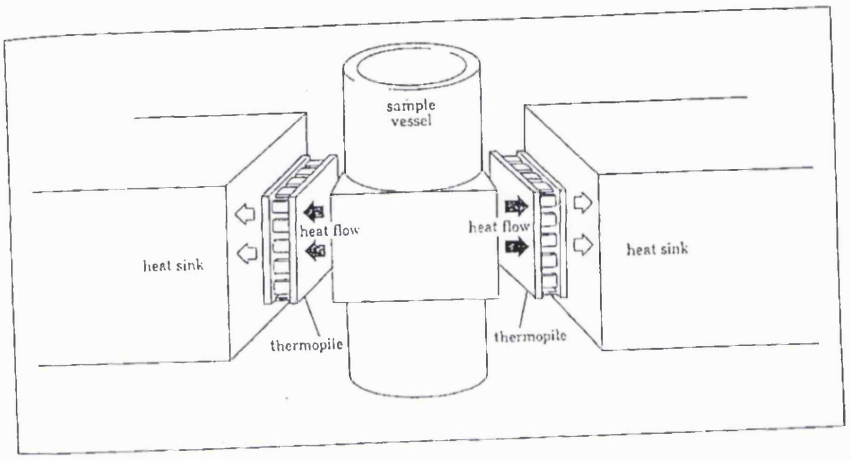

Fig. 3.1: The heat flow principle.

Experiments can be conducted within a temperature range of 5-80 °C and up to four individual measuring vessels can be used at any one time. The vessels are maintained at a constant temperature with a variance of +/- 2 x 10^{-4} °C. The heat energy that is generated is channelled through 'Peltier elements' before escaping to the heat sink. Peltier elements are extremely sensitive thermopile blankets acting as thermoelectric generators using the 'Seebeck effect'. They are made up of numerous semiconductor junctions aligned in series in the form of a sandwich. They are extremely sensitive detectors and convert heat energy into a voltage signal proportional to the heat flow. This is represented as a measure of the thermal energy produced by the sample per unit time.

Results are quantified by electrical calibration where known power values are passed through built-in precision resistors.

The TAM machine allows conduction of four types of isothermal microcalorimetry experiments (the data presented deals only with perfusion and solution calorimetry):

1) Ampoule
2) Perfusion
3) Titration
4) Solution

3.5.2 Perfusion Calorimetry - Methodology

Calcium mupirocin was the only drug to be investigated using this method. A sample of approximately 30 mg was weighed directly into the perfusion ampoule. The ampoule was secured to the lid of the perfusion unit [Fig. 3.2] and sealed. Before conducting an experiment the water/solvent in the humidifying wells was removed and replaced with 0.5 mL of new water/solvent.

The unit was then lowered carefully (into side A) and slowly into the standby position with the use of the positioning ring and clamp screw. The unit was gradually lowered and clamped in a stepwise manner. A normal steel ampoule and lowering hook was used for the reference side. After about 30 minutes the unit was lowered to the measuring position. This process was done slowly and without any frictional disturbances, to prevent other experiments within the TAM machine recording such disturbances.

The nitrogen line was attached to the unit with the gas flow at an inert level (0% RH). Condensation in the nitrogen line could occur when high relative humidities are used. This was avoided by setting the flow switch temperature to 40 °C. The RH within the system was controlled by 'mass flow controllers' to provide an accurate flow of wet and dry gas (nitrogen), which were passed through two humidifier wells.

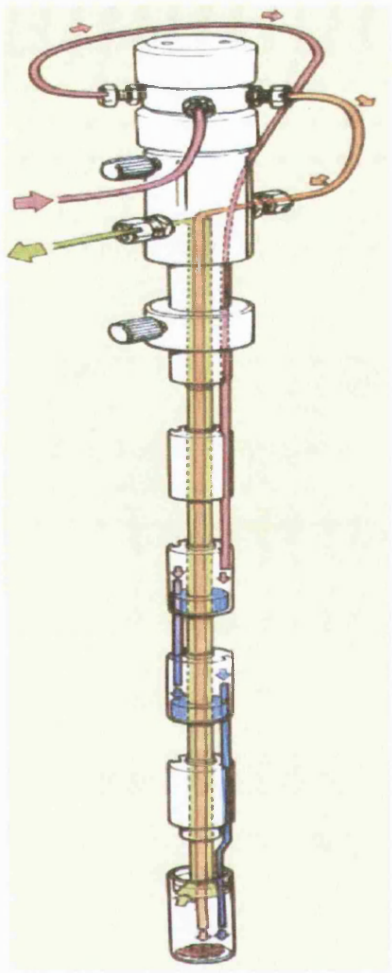

Fig. 3.2: Schematic diagram of the perfusion unit.

The main method used was similar to that of the DVS work. A step method was created where the sample remained initially at 0% RH during calibration. Then the samples were exposed to increments of 5% RH up to 35% RH and back down to 0% RH (again in 5% decrements), with each step lasting 3 h. For some experiments with water another step method was utilised, simply consisting of a 0%, 35% and back down to 0% RH stages. (Note that the term relative humidity is replaced by partial pressures when discussing solvents other than water). The solvents used were water, methanol, ethanol and propan-2-ol. Hexane could not be used as it damages the O-rings within the unit. All experiments were performed in triplicate with the water bath being maintained at 25 °C.

3.5.3 Perfusion Calorimetry - Calibration

The amplifier range was selected for calibration. This was dependent on the energy response expected and could range in μW from 3, 10, 30, 100, 300, 1000 or 3000. The choice was dependent on ensuring the whole response was measured whilst attempting to gain the greatest accuracy by choosing the lowest setting possible. Settings of 300, 1000 and 3000 μW were used.

After loading of the perfusion unit and subsequent settling of the baseline, calibration was conducted during the initial 0% RH stage of the experiment (perfusion unit in side A and reference ampoule in side B). Therefore calibration was performed with every experiment. A baseline was deemed to have been achieved at the experimental position when it read 0 μW (+/- 0.1 μW). If the reading was not correct, it was adjusted via the zero control.

Next the 'electrical calibration' option was selected to power the channel to the desired amplifier range. Once the signal had reached a plateau it was checked to see if it was within the displayed range. If not, the fine gain on the amplifier panel was adjusted to the set value. When the calibration was completed, the electrical signal was switched off. Once the signal had returned back to zero and a baseline achieved, the value was checked to ensure it was 0 μW +/- 0.1 μW. Once more any variances were adjusted by the zero control. Finally calibration was complete and the experiment was manually changed to the next RH stage.

The RH generated by the perfusion unit was checked using salt solutions. In a similar manner to DVS calibration salt solutions of sodium chloride (75.3%) and magnesium chloride (32.8%) at 25 °C (Nyqvist, 1983) were the standards chosen. The salt solutions were placed in both the sample and reference ampoules. The nitrogen cylinder was turned off and the perfusion unit allowed to equilibrate in the TAM. This would prevent the dry flow of nitrogen into the ampoules. Once a baseline was achieved and zeroed, the value of the expected RH (of the salt solution) was keyed into the software and the nitrogen flow opened. The signal was allowed to stabalise. If the signal was below 0 μW power output (opposite procedure taken if signal was above 0 μW) the RH was manually increased until

the plot crossed the Y-axis at zero, in 1% RH increments. The RH was increased and decreased in a similar manner 3 times to work out the average RH at which it crossed the Y-axis. This would be the actual RH value required (on the perfusion setting) to provide the relative humidity that the salt solution produced. This was conducted for both salt solutions and if there was a major difference between the values obtained against the true RH of the salt solutions, the manufacturers would have to be contacted.

3.5.4 Solution Calorimetry (SolCal) – Methodology

Solution calorimetry allows the heat of solution of any particular solute (solid/liquid), in a solvent it can dissolve in, to be calculated. Detection of minute physico-chemical changes of a material can be measured as every process involves the uptake or loss of heat. The principle of a solution calorimeter is straightforward. A liquid reactant was held in a Dewar. Another reactant, either a liquid or a solid, was put in a small glass cell and immersed in the first liquid. Mixing was achieved by rotating the cell with a mechanical rotor (this also held the glass ampoule). After the system came to thermal equilibrium, the reaction was started by pressing a push rod in the centre of the rotating cell to release the reactant inside (sapphire breaking tip cutting through the glass ampoule). The heat released or absorbed in the reaction caused the temperature of the system to rise or drop. The reaction was allowed to go to completion and the temperature change was recorded.

The solution calorimeter is an adiabatic calorimeter (no heat flow between the system and the surroundings). The reaction vessel used was a 100 mL pyrex glass vessel containing a thermistor and heater. The vessel, when connected to the holder, contained the electrical component called the 'Wheatstone bridge'. This heated the solution in the vessel, controlled the stirrer and monitored the temperature of the vessel. Thus the heat produced was measured by the thermistor due to the resistance being related to the temperature in the vessel.

Approximately 100 mg of calcium mupirocin/nabumetone was used for each experiment. Methanol was the solvent of choice to dissolve the calcium

mupirocin and N,N-dimethylformamide (DMF) was used for nabumetone experiments. The samples were accurately weighed once filled into the ampoules. The ampoules were plugged with a silicon bung and sealed using molten bees' wax. The ampoules were attached to the stirrer prior to experimentation. The unit was then lowered into the TAM at the equilibration position. When the standard deviation of the temperature was below 10 μK, the SolCal was lowered to the experimental position. Once the standard deviation of temperature re-stabalised (below 10 μK), electrical calibration was initiated. After calibration the glass ampoule was broken and the heat change detected. Finally a second electrical calibration was performed. Solcal was performed in triplicate on non-micronised and micronised calcium mupirocin.

3.5.5 Solution Calorimetry - Calibration

Heat changes between the calorimeter and the environment along with those involved with stirring would affect the final heat of response. These were mathematically adjusted by the software with the use of the baseline temperatures obtained during calibrations. The electrical calibrations also allowed the system to possess thermal data from which to base the calculations for the reaction process. Test calibrations were also conducted monthly with tris dissolved in 0.1M hydrochloric acid to use as a reference heat of solution value.

3.6 X-Ray Powder Diffractometry (XRPD)

Name & Model: PW 3710 X-Ray Diffractometer
(Philips, Cambridge, UK)

3.6.1 Introduction

The XRPD tube contains a copper anode. This anode is bombarded with electrons under high potential to produce x-rays. The x-rays then pass out of the tube via a beryllium window. The x-ray beam produced is focused by a series of divergence slits within the goniometer on to the flat surface of the sample.

The rays diffracted at Bragg angle θ, by suitably orientated crystallites within the sample all converge approximately to a single line, where a receiving slit is placed. The x-ray beam passes through the receiving slit onto a second parallel slit system, a scatter slit and a monochromator. Finally the beam reaches the detector where the signal provides an output of intensity vs. scan angle 2θ.

The degree of crystallinity of a sample can be described by the diffraction pattern it produces:

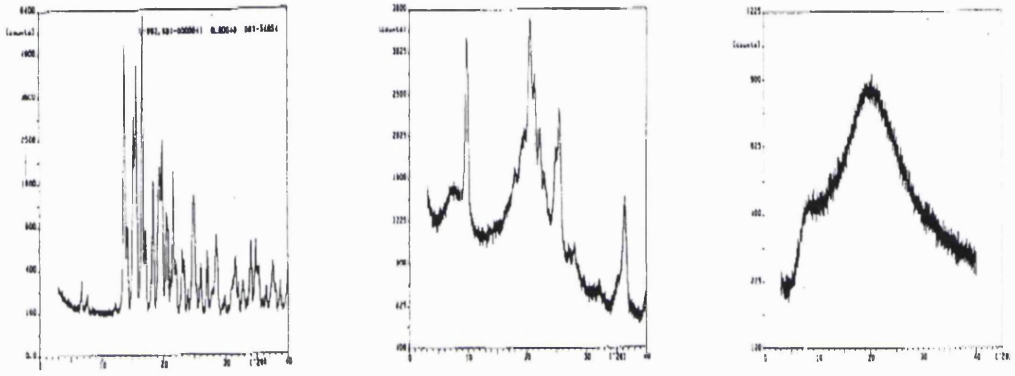

[A] [B] [C]

Fig. 3.3: Typical XRPD patterns of [A] crystalline, [B] partially amorphous and [C] amorphous samples.

The sample is said to be crystalline if the baseline is flat between 3° and 40° 2θ and the peaks are sharp and well defined [Fig. 3.3A]. The sample is said to be a mixture of crystalline and amorphous nature if the baseline rises to a broad hump at about 20° 2θ before decreasing again, and has superimposed peaks [Fig. 3.3B]. A smooth hump without any peaks would indicate the material to be amorphous [Fig. 3.3C].

3.6.2 Methodology

Powders for testing should preferably have a particle size of <50 μm. Large particles may give rise to preferred orientation and poor adhesion in the sample holder. This can lead to contamination within the machine. The sample was carefully filled into the 27 mm diameter cavity of the sample holder. The baseplate of the sample holder was gently tapped on the bench top to allow the

powder to settle. Excess powder was removed and the cavity levelled using a glass block.

Samples were measured at 45 kV and 30 mA. The start angle (2θ) was 5° and end angle was 40°. The scan speed was 0.05° 2θ/s. Experiments were run in triplicate on all samples.

3.6.3 Calibration

Calibration of the machine was conducted every month. A standard silicon compact in a sample holder was used to maintain the integrity of the results obtained. Linearity checks were made to confirm that the measured peaks for the standard conformed to within the limits stated by the manufacturer.

3.7 Thermogravimetric Analysis (TGA)

Name & Model: TGA 2950 Thermogravimetric Analyser
(TA Instruments, Surrey, UK)

3.7.1 Introduction

The TGA instrument measures weight changes of a sample as it is being exposed to increasing temperature changes. The TGA consists of a null position balance which is kept horizontal by an optically controlled meter movement. An equal amount of light is blocked from reaching two photodiodes by a small flag positioned on top of the balance arm.

The position of the balance arm and flag moves in response to any weight changes in the sample pan. This movement will result in an unequal amount of light reaching the two photodiodes. Bringing the balance arm back to the null position rectifies the resulting imbalance. This is accomplished automatically by the control circuitry due to a change in the current. The current difference is directly proportional to the change in mass and is thus recorded as a weight signal.

The employment of the null position principle allows the sample to remain in the same position within the furnace. This in turn permits the temperature to be accurately controlled, as the temperature might vary throughout the furnace. The TGA is <+/- 0.1% accurate and has a resolution of 0.1 μg.

The furnace contains a unit of low mass alumina that can be heated up to 1000 °C. Nitrogen gas (60 cc/min) was used to prevent contamination of the furnace by sweeping away any evolved gases or decomposition products out of the furnace. Also the balance assemblies were kept clean with a smaller flow of nitrogen gas (40 cc/min) to prevent decomposition material from the sample contaminating the balance. The machine contains a compressed air supply to help cool the furnace between each run. A water reservoir within the system gives the heater something to work against so that accurate heating rates can be achieved.

3.7.2 Methodology

All TGA experiments were run, using open aluminium pans, at a ramp rate of 10 °C/min. Three runs each were conducted for all measurements. The end temperatures that the experiments were run to were sample dependent:

- Theophylline – 300 °C
- Calcium Mupirocin – 150 °C
- Nabumetone – 100 °C
- Magnesium Stearate – 150 °C

The sample masses used were also dependent on each compound. The mass of sample used for each run was +/- 1 mg to obtain more consistent results. This was because the surface area of the sample can affect the rate of weight loss.

3.7.3 Calibration

The equipment was calibrated every month. There were two types of calibration:

a) Weight calibration
b) Temperature calibration

The weight was calibrated using 100 mg and 1 g standards. The temperature was calibrated using indium as a reference (melting point of 156.60 °C). As well as calibrating monthly, calibration was also initiated when the power was cut or the thermocouple moved.

3.8 Differential Scanning Calorimetry (DSC)

Name & Model: DSC 7
(Perkin Elmer, Buckinghamshire, UK)

3.8.1 Introduction

A differential scanning calorimeter (DSC) measures the amount of energy (heat) absorbed or released by a sample as it is heated or cooled. There are many processes that can be detected by DSC by the enthalpic reaction that is produced [Table 3.2]. The DSC 7 and the Pyris 1 operate with a power compensation design. There are individual sample and reference micro-furnaces so that a 'thermal-null' system is operated. The micro-furnaces provide very fast heating/cooling rates and rapid temperature equilibrium. The thermal-null system works with the aid of two separate control loops that precisely control the temperature of the sample and reference furnaces. The 'average temperature control loop' provides power to both furnaces at the pre-determined rate and temperature range, ensuring that both furnaces are always at the same temperature. The 'differential temperature control loop' measures any differences in the temperature that occurs between both furnaces. If a material in the sample furnace gives out or takes up energy, the temperature of the two furnaces will be different. The platinum resistance thermometer sensing any temperature changes retains thermal null, in the form of a power adjustment by the differential temperature control loop to bring the two furnaces back to the same temperature. The amount of energy that is provided or removed from the

system is directly proportional to the energy change of the system. As a result a direct measurement of energy and thus ΔH can be made.

Process	Exotherm	Endotherm
Solid-Solid Transition	Yes	Yes
Crystallisation	Yes	
Melting		Yes
Vaporisation		Yes
Sublimation		Yes
Adsorption	Yes	
Desorption		Yes
Desolvation (Drying)		Yes
Decomposition	Yes	Yes
Solid-Solid Reaction	Yes	Yes
Solid-Liquid Reaction	Yes	Yes
Solid-Gas Reaction	Yes	Yes
Curing	Yes	
Polymerisation	Yes	
Catalytic Reactions	Yes	
Glass Transition (T_g)	Change in baseline	----------

Table 3.2: Types of reactions and their observed behaviour in the DSC.

The data are plotted as temperature versus power. The heat flow is shown in units of watts (W) and is found by the heat 'q' supplied per unit time 't'. The heating rate is the temperature increase 'T' per unit time 't'. Therefore;

$$\frac{\text{Heat}}{\text{Time}} = \frac{dq}{dt} = \text{Heat flow} \qquad \text{[Equation 3.1]}$$

$$\frac{\text{Temperature rise}}{\text{Time}} = \frac{dT}{dt} = \text{Heating rate} \quad \text{[Equation 3.2]}$$

If the heat flow is divided by the heating rate, an equation representing the heat capacity (Cp) is produced. This can also be extracted from a DSC plot.

$$\frac{dq}{dT} = Cp = \text{Heat capacity} \quad \text{[Equation 3.3]}$$

3.8.2 Methodology

For all experiments a ramp rate of no greater than 10 °C/min was utilised. Samples were weighed onto aluminium pans (Perkin Elmer) and were non-hermetically sealed. The temperatures that's the four compounds under investigation were scanned up to were:

- Theophylline – 300 °C
- Calcium Mupirocin – 150 °C
- Nabumetone – 100 °C
- Magnesium stearate – 150 °C

Smaller sample weights result in smaller peaks, improved resolution and decreased sensitivity. Large lumps in the sample cause poor contact with the sample pan, therefore poor thermal contact, poor resolution and increased likelihood of sample noise. Slow heating/cooling rates result in improved resolution, thermal events are allowed to occur, sensitivity to small changes reduced and slow analysis times. All experiments were conducted a minimum of three times.

3.8.3 Calibration

Calibrations were conducted using IUPAC standards. The metals used were indium (156.60 °C) and zinc (419.47 °C). Calibrations were performed before each set of experiments. The conditions of the calibration were set up exactly the same as to be used for the samples. This ensured accurate data were produced. (Note - Onset temperature of an event should always be the recorded value as sample size does not affect the result as long as other parameters are kept constant). The furnace was also calibrated periodically. The high temperatures reached during furnace calibration allowed the furnace to be cleaned of any decomposed materials from other experiments. Also the lids of the furnace were cleaned using a bunsen burner to ensure all decomposed materials had been removed.

3.8.4 HyperDSC (HDSC)

Name & Model: Pyris 1
(Perkin Elmer, Buckinghamshire, UK)

HDSC is a relatively new technique devised by Pijpers *et al.*, 2002. It allows the ability to study the transitions of systems by applying much higher controlled cooling and heating rates. Rates up to 500 °C/min can be used unlike conventional DSC where lower than 10 °C/min rates are usually utilised. There are many advantages to HDSC:

- Very high throughput of samples as such high heating/cooling rates are used.
- Heat capacity data are more easily obtained since instrumental drift is negligible during such rapid measurements.
- Low sample masses used (milligrams or even micrograms). Conventionally low sample sizes would result in a loss of sensitivity however this is compensated by the increase in sensitivity with the application of a higher rate.

- HDSC allows the examination of the compound as near to as it already is ('snapshot' of sample). For example a slow scan rate may cause the sample to change and therefore produce other responses, which the original sample did not possess.
- Effects of decomposition are displaced to higher temperature allowing events near to decomposition to be studied more easily.
- Easier to observe a T_g for a sample as the change in baseline is more pronounced and the duration of T_g is longer.

Experiments were conducted on calcium mupirocin and nabumetone at scan rates of 100, 200 and 300 °C/min. Calibration was performed in the same manner as stated in section 3.8.3, and all experiments were performed in triplicate.

3.9 Scanning Electron Microscopy (SEM)

Name & Model: Philips SEM XL20
(Philips, Eindhoven, Netherlands)

3.9.1 Introduction

SEM differs from conventional light microscopes by not employing a series of glass lenses to bend light waves in order to create a magnified image. The magnified image is produced by using electrons instead of light waves. The advantage of SEM is that images can be seen at a much greater magnification than can be achieved with a light microscope.

3.9.2 Methodology

The sample is mounted onto adhesive carbon discs attached to SEM stubs and coated with gold by sputtering for 4 min at 30 mA. The voltage used to obtain the micrographs are shown on the individual SEMs. Once the sample is ready it is placed inside the microscope's vacuum column through an airtight door. Once the air is pumped out of the column, an electron gun emits a beam of high-energy electrons. This beam of electrons would normally travel in all directions.

However, the beam is focused to a very fine point by proceeding through a series of magnetic lenses. A schematic of the SEM equipment is shown in Fig. 3.4.

The sample is scanned row by row with the aid of scanning coils to focus the beam back and fourth. When the electron beam hits each spot on the sample, secondary electrons are knocked loose from the surface. These secondary electrons are counted by a detector, and the signals sent to an amplifier. Finally the image is formed by the number of electrons emitted from each spot on the sample.

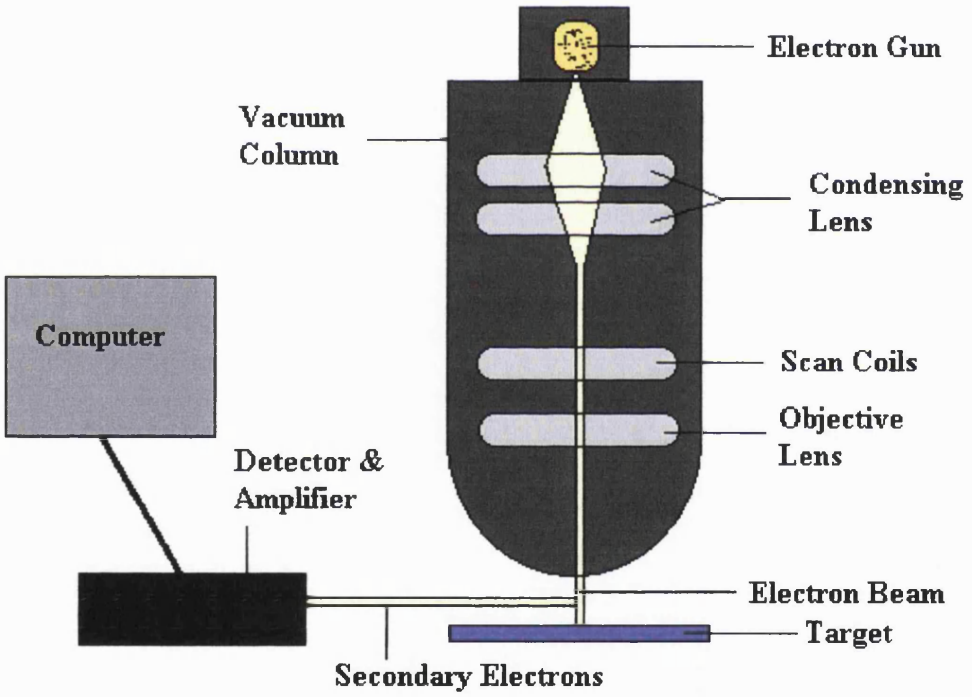

Fig. 3.4: Schematic diagram of the SEM apparatus.

3.9.3 Calibration

No calibration as such was required for the machine.

3.10 Particle Size Analysis

Name & Model: Sympatec HELOS-System
(Sympatec GmbH, Clausthal-Zellerfeld, Germany)

3.10.1 Introduction

The Sympatec system uses the principle of an equivalent sphere for its measurements. This is a sphere that is equal to the real particle in terms of the physical parameter being measured. The measurement taken is area based. Thus the equivalent sphere is the sphere, which would produce the same scattering intensities as the particle (sphere of equal area). The Fraunhofer theory is the method of choice for practical applications as opposed to the Mie theory. The Mie theory requires spherical particles with smooth surfaces and a knowledge of their optical parameters, and also it cannot cope with mixtures of different components. The Fraunhofer theory also assumes all particles are of spherical shape. Without refractive index values of the particles and medium the Mie calculations have no more validity than the Fraunhofer approximation.

3.10.2 Methodology

A helium-neon laser was utilised for measurements. When the light from the laser emits in the path of a particle it scatters. Smaller particles scatter at large angles and larger particles at small angles. The scattered light data were transformed to a distribution of particle size information using the Fraunhofer theory. An appropriate measurement lens was chosen for each drug dependent upon the size range of the particles observed via optical microscopy. Choosing the appropriate lens allowed greater accuracy of the measurements. A pressure profile was obtained initially (for each drug) and the results compared to microscopy. Ideally a plateau in the distribution is seen (i.e. a point when the aggregates are dispersed to allow the sizing of the primary particles). Further increments of the pressure would relate to the fracture of the primary particles. All analysis of particle size data must be treated with care due to possible

misleading conclusions obtained for sizing any particle that is not spherical in shape. All experiments were conducted in triplicate.

3.10.3 Calibration

A system check was conducted according to the manufacturer guidelines every month.

3.11 Karl Fischer (KF)

Name & Model: 701 KF Titrino
(Metrohm, Buckingham, UK)

3.11.1 Introduction

Water analysis by this titration method was developed in 1935 by Karl Fischer. He formulated the standard equation (by mixing a reagent containing pyridine, sulphur dioxide and iodine):

$$2H_2O + SO_2 + 2Py + I_2 \longrightarrow H_2SO_4 + 2HI{*}Py \qquad \text{[Equation 3.4]}$$

Due to the presence of a strong odour, the pyridine was replaced by a solvent (methanol) and a base imidazole (the imidazole also increased the speed of the reaction and provided a more stable end point). Thus a two step equation was formed by Eugen Scholz in the 1980's.

$$SO_2 + MeOH + B \longleftrightarrow MeSO_3^- + HB^+ \qquad \text{[Equation 3.5a]}$$

$$MeSO_3^- + H_2O + I_2 + 2B \longrightarrow MeSO_4^- + 2HB+ + 2I^- \qquad \text{[Equation 3.5b]}$$

However side reactions occurred such as the generation of water from ketones reacting with methanol. Therefore new reagents (halogenated alcohols) were developed to prevent such adverse reactions. Volumetric KF determinations are made by the use of a platinum electrode within the apparatus. This electrode detects the presence of water and thus electronically instructs the release of the

reagent. On reaching the end point the concentration of iodine is calculated to provide a value for the percentage of water in the original sample.

3.11.2 Methodology

The 701 KF Titrino was used to corroborate the TGA data for theophylline as only water content would be measured with this method. Due to the presence of ketones within the theophylline structure the solvents used were Composite 5K and Ketosolver. Tests were conducted on anhydrous (from supplier), hydrated and dehydrated (prepared in the DVS or desiccators – see section 3.12) forms of theophylline. All water determination experiments were run in triplicate.

3.11.3 Calibration

Calibration was conducted by using Hydranal water standards from Sigma-Aldrich.

3.12 Salt Solutions

Saturated salt solutions can be used to maintain specified relative humidities in closed chambers for stability studies (Nyqvist, 1983). The salt solutions potassium sulphate and sodium chloride were prepared to provide a relative humidity of 97% and 75% respectively within a desiccator at 25 °C. The salt solutions were prepared by mixing each salt in distilled water at 60 °C for 30 hours. A 0% RH desiccator was created by using phosphorous pentoxide powder. No prior preparation was required as with the salt solutions.

Samples were stored in all the desiccators to provide different environments:

- Anhydrous theophylline samples were stored in the 0% desiccator to prevent any moisture gain. Samples of anhydrous theophylline were placed in the 97% RH desiccator to form the monohydrate. Finally hydrate samples were removed from the 97% RH desiccator and returned to the 0% RH desiccator to form dehydrated theophylline.

- Samples of calcium mupirocin were stored in the 0% RH and 97% RH desiccators respectively to lose the hydrate and then reform it.

- Nabumetone was placed in the 0% RH desiccator for drying and the 97% RH desiccator to observe if any moisture was collected within the compound.

- Magnesium stearate was stored in the 0%, 75% and 97% RH desiccators to attempt to remove the hydrates (0% RH) and reform them (75% RH and 97% RH).

Samples for each of the compounds were removed and tested by other equipment to help with the characterisation studies.

3.13 Nitrogen BET Specific Surface Area Analysis

Name & Model: Gemini 2360 Surface Area Analyser
(Micromeritics, Dunstable, UK)

3.13.1 Introduction

The Gemini apparatus measures the surface properties of solids in terms of their specific surface area (m^2/g). The monolayer capacity is measured using the BET equation (see section 1.5.5). Nitrogen molecules were used as the adsorbate as it is an inert gas that should not interact with the sample under investigation. Samples were initially prepared by outgassing. Outgassing (under vacuum) removed any adsorbed gases and moisture from the sample surface. To outgas the sample was heated by the furnace. However, care must be taken not to set the temperature too high that the sample begins to decompose.

The adsorption (condensation) of gas onto the surface of the outgassed sample was conducted at known partial pressures. The quantity of adsorbate gas was

incrementally increased at a constant temperature. Once the pressure in the tube had equilibrated, at each partial pressure, that pressure value was recorded. The volume of gas adsorbed was measured as a function of the relative pressure produced by the non-adsorbed molecules. The relative pressure is a ratio of the pressure in the sample tube to the saturation vapour pressure of the adsorbate gas (pressure at which the adsorbate gas liquefies). A plot of partial pressure versus volume of gas adsorbed can be created (isotherm) from which the monolayer concentration can be worked out and therefore the specific surface area.

3.13.2 Methodology

The methodology undertaken was dependent upon the sample investigated. Out-gassing of samples was only conducted if the sample would not undergo any adverse effects.

- Calcium Mupirocin – 40 °C overnight.
- Nabumetone – 40 °C overnight.
- Theophylline – 40 °C overnight
- Magnesium Stearate – None

Magnesium stearate was not out-gassed as it was very difficult to remove the contaminants and bound moisture from the sample without changing the structure of the excipient. Therefore it was best to compare the two batches of magnesium stearate without any pre-preparation. Calcium mupirocin was out-gassed and therefore the specific surface area values obtained were of the dehydrated form. If the sample had not been out-gassed then it would be fair to assume lower values of specific surface area would have been obtained.

Multi-point analysis was carried out with all the samples to provide accurate readings. However, this was not possible with magnesium stearate due to poor correlation over a multi-point region. As a result only single-point determination was carried out for comparative purposes. This is not the ideal method as the confidence in the data is not great and as such is only used for comparative purposes.

3.13.3 Calibration

Calibration was carried out on the equipment at 6 monthly intervals using 0.5-0.6 mg of the carbon black reference material supplied by Micromeritics. The sample was outgassed for 10 minutes at room temperature followed by one hour at 300 °C under vacuum. The weight of the sample was recorded after outgassing. Using nitrogen as the adsorbate, a multi-point BET calculation was conducted over 0.05-0.3 P/Po. After analysis the sample was brought back to room temperature and re-weighed. If the difference between the before and after weight measurements was greater than 5%, the analysis was discarded. The surface area of the sample was calculated and the minimum acceptable correlation coefficient value (R^2) was 0.995. The nominal surface area was 24 m^2/g and the results compared to ensure it was within the expected limits of the manufacturer.

3.14 Micronisation

Name & Model: GEM-T Microniser WN1376
(Christison Scientific Equipment Ltd., Gateshead, UK)

The GEM-T microniser employs the principles of the venturi effect. Size reduction of particles occurs through particle impact and attrition.

The grind pressure (from the O Jet) should be lower than the drive pressure (P Jet) to prevent drug flow back. The pressure from the jets allows the bombardment of particles (impact chamber). During bombardment the particle size reduces. This reduction in particle size allows the motion of these smaller particles towards the discharge chamber. When the particles have been reduced to a specific size they will be able to exit via the discharge chamber into the collection pot. Dry air was used to provide a drive pressure of 80 Psi and a grind pressure of 60 Psi.

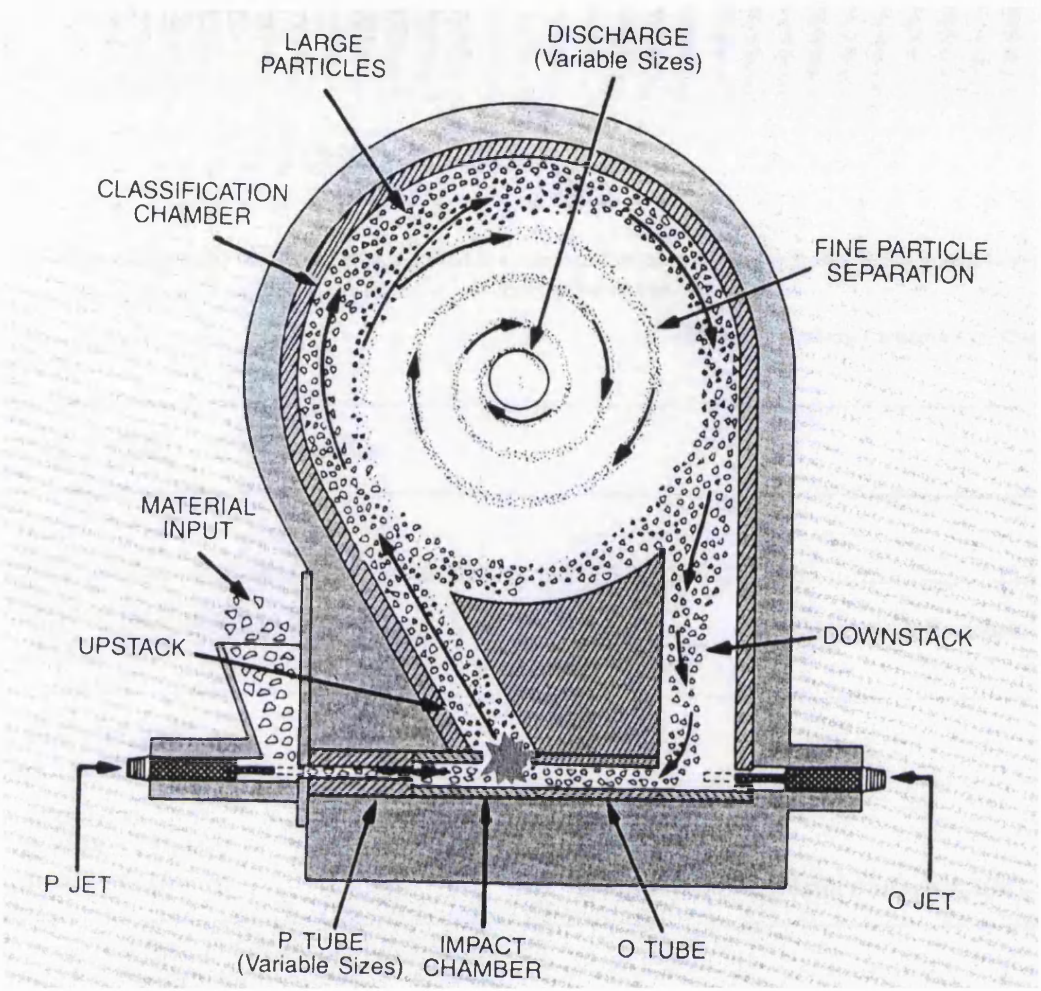

Fig 3.5: Internal diagram of the GEM-T microniser.

3.15 Statistics

3.15.1 Student's *t*-Test

A Student's *t*-test was carried out when analysis between two groups was required to assess whether there was a significant difference or not. A paired sampled Student's *t*-test was used. This was the *t*-test of choice as mostly samples from the same batch were analysed against each other. The independent sampled Student *t*-test was utilised when samples from different batches were compared. Such a *t*-test required the knowledge of whether or not the variances between the two groups were equal or different. The variance was calculated by the homogeneity of variances test (*F*-test or Levene statistic). The analysis of

both the Student's *t*-test and *F*-test for variances were determined using Microsoft Excel.

3.15.2 One-Way Analysis Of Variance (ANOVA)

Significance analyses between multiple groups were carried out using ANOVA, where the significant difference of one factor (one-way) between groups was required. Student's *t*-test cannot be used to compare multiple groups due to the increased likelihood of a Type I or Type II error. A Type I error occurs when the null hypothesis is wrongly rejected (i.e. when it is thought a significant difference between groups exists). A Type II error is thus the opposite of a Type I error - the error of accepting the null hypothesis. ANOVA calculates the variability within a group against the variability between groups. ANOVA was performed using SPSS for Windows.

For all statistical analyses a significant difference was accepted if the *p* value was below 0.05.

4. RESULTS & DISCUSSION

Characterisation Of The Compounds Under Investigation

It was important to characterise the four compounds under investigation before being able to make judgments and interpretations of the DVS (chapter 5) and IGC (chapter 6) work that followed. The two main drugs of interest were theophylline and calcium mupirocin. Nabumetone and the excipient magnesium stearate were also investigated. This allowed more thorough conclusions to be made of the DVS and IGC techniques, as studies on a hydrophobic drug (nabumetone) and a variable batch-to-batch excipient (magnesium stearate) added to the findings by showing advantages and disadvantages to the two techniques.

During the course of the characterisation studies important findings have been further investigated and discussed within this chapter. Some of the studies have also been published such as the discovery of a new crystal transition for theophylline (Vora *et al.*, 2004).

4.1 Aims

The aims were to characterise the four compounds in terms of their different forms and their batch-to-batch variability. The techniques employed within this chapter would help to highlight batch-to-batch variability originating from the suppliers (Sigma-Aldrich, Poole, UK) in terms of Sigma and Fluka batches of the two compounds (theophylline and magnesium stearate). With calcium mupirocin and nabumetone, non-micronised and micronised batches of the drugs were compared. Techniques would therefore be utilised to understand the differences and similarities of the compounds.

Studies would also be performed to determine the different hydrate forms of the compounds and the ease at which they could be formed and removed. This would help provide information on the conditions required to maintain or lose the hydrates for the powder surface investigations using DVS and IGC. Although DVS work will specifically be presented in chapter 5, standard DVS experiments (using water vapour) would also be performed within this chapter to understand the conditions at which the hydrates are formed and lost and the ease of these processes.

4.2 Theophylline

4.2.1 Introduction

The BNF (2000) states that theophylline is a bronchodilator used for reversible airways obstruction. Theophylline is metabolised in the liver. The half-life of the drug depends on a number of factors. The half-life could be increased due to cirrhosis, old age and drugs such as cimetidine, or reduced by smoking, alcoholism and drugs such as phenytoin.

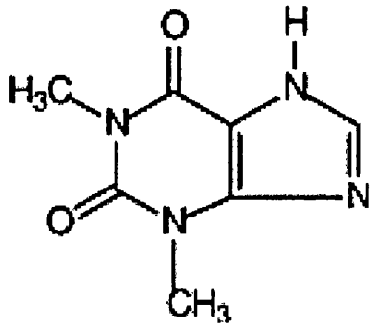

Fig. 4.1: Molecular diagram of theophylline.

Theophylline has a very narrow therapeutic margin. A plasma-theophylline concentration of between 1-20 mg/L is usually required for satisfactory bronchodilation. Thus, knowing the half-life of the drug is important in being able to sustain drug levels within the therapeutic margin. The dosage of the drug can be altered to account for variations in the half-life caused by the above

factors. However, changes of the drug (i.e. to different polymorphs) during manufacture and processing can alter the properties of the drug such as absorption, excretion and metabolism. If the change in polymorph has not been noticed it can therefore affect the concentration of the drug in the plasma. The levels could be too low or too high, leading to disastrous effects to the patient.

Theophylline is a drug that exists in three different forms; anhydrate, monohydrate and a metastable dehydrate (Suzuki *et al.*, 1989). It has been reported that anhydrous theophylline will convert to the monohydrate form at greater than 80% relative humidity (RH) (Fokkens & Blaey, 1984; Rodriguez-Hernando *et al.*, 1992; Serajuddin, 1986; Lehto & Laine, 2000; Zhu *et al.*, 1996). The hydrate will subsequently dehydrate at RH below 20% (Fokkens & Blaey, 1984; Suihko *et al.*, 1997; Yoshihashi *et al.*, 1998). The differences between the anhydrous, hydrate and dehydrate forms have been identified by use of X-ray diffraction (Suzuki *et al.*, 1989; Phadnis & Suryanarayanan, 1997), differential scanning calorimetry and infra-red spectroscopy (Suzuki *et al.*, 1989), and more recently NIR spectroscopy as a stand alone technique (Rasanen *et al.*, 2001).

It is important to control, monitor and understand the phase transformations of particles during processing and storage. Changes that may occur could lead to variations in physical and chemical properties such as the bioavailability and efficacy of a pharmaceutical product. Processes including grinding, milling, drying, compaction, oven drying and wet granulation could accelerate phase transitions in solids. Hydration and dehydration can alter the product performance of drugs (Herman *et al.*, 1989; Otsuka *et al.*, 1991). Agbada and York (1994) established that particle size, crystal defects, sample weight and surface characteristics can alter the mechanism and activation energy of dehydration. Temperature (Shefter & Kmack, 1967; Duddu *et al.*, 1995) and humidity (Ledwidge & Corrigan, 1997) can play an important role in the rate of dehydration. Consequently it can be understood that many variables have to be assessed and controlled during the manufacture of any pharmaceutical drug.

4.2.2 The Anhydrate, Hydrate & Dehydrate Comparison

TGA data of the original anhydrous batch of theophylline showed no mass loss up to 180 °C [Fig. 4.2]. Beyond this temperature (from 180 °C to 270 °C) there was an approximate 9% mass loss. This mass loss was not believed to be attributed to hydrate water and probably a result of some part of the theophylline molecule dissociating and melting from the compound. However, when the believed hydrate form (prepared in the DVS and 97% RH desiccator) was tested an approximate 9% mass loss was observed before 100 °C [Fig. 4.3] – monohydrate theophylline contains 9.08% moisture.

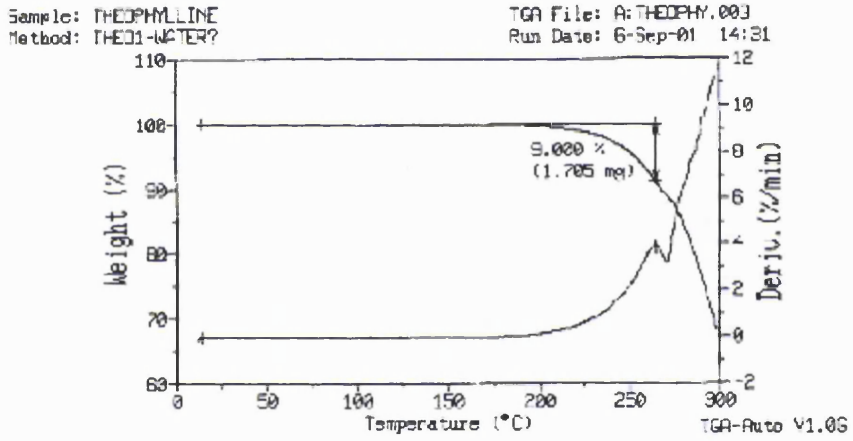

Fig. 4.2: TGA graph of anhydrous theophylline.

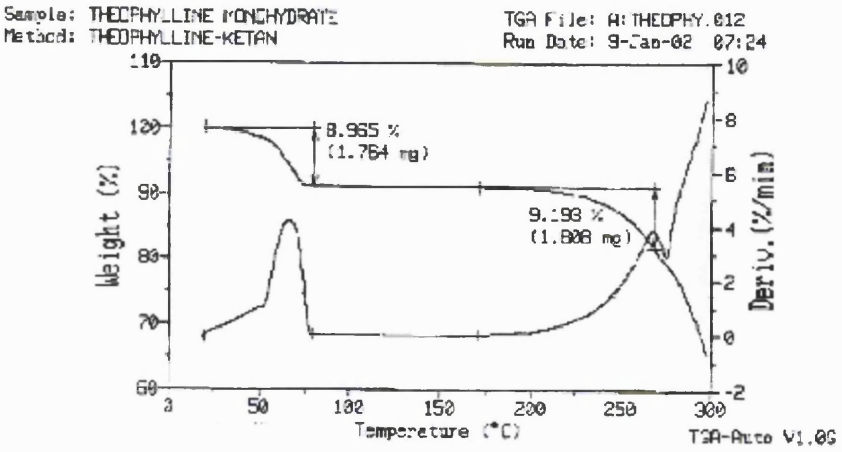

Fig. 4.3: TGA graph of theophylline monohydrate.

Further TGA analysis on the dehydrated form of theophylline (prepared in the DVS or 0% RH desiccator) produced graphs exactly the same as that seen in Fig. 4.2.

It was important to confirm the accuracy of the assumption, that between 180-270 °C, the mass loss observed was due to the loss of some part of the theophylline molecule rather than moisture. Karl Fischer (KF) analysis was the method of choice as this technique would only measure the moisture content of a sample [Table 4.1]. KF analysis has substantiated the hypothesis that the approximate 9% mass losses after 180 °C were not due to water loss from within the drug molecule.

Run	Anhydrous (%)	Monohydrate (%)	Dehydrate (%)
1	0	9.31	0
2	0	9.98	0
3	0.08	8.88	0
Average	0.027	9.39	0
Standard Deviation	0.046	0.55	0

Table 4.1: KF analysis showing the percentage water loss from the three crystal lattices of theophylline.

DVS results showed [Fig. 4.4] that at 0% RH a steady baseline was established for the anhydrous theophylline sample. When the humidity of the system was raised to 95%, there was a lag phase and then the sample began to gain mass rapidly. The lag phase was a property of the drug and is indicative of a critical RH requirement for hydrate formation (prior to this only adsorption of moisture onto the surface occurs). The mass increase started to tail off after 820 min at 95% RH. At this point the mass had increased by 9% (the mass gain for the formation of theophylline monohydrate). When the 5% RH stage was initiated the mass of the sample dropped steeply. This mass loss took place within 700 min and returned to the original dry weight, indicating that the theophylline

monohydrate converted to dehydrated theophylline. There was no further mass loss when the humidity in the system was reduced to 0%.

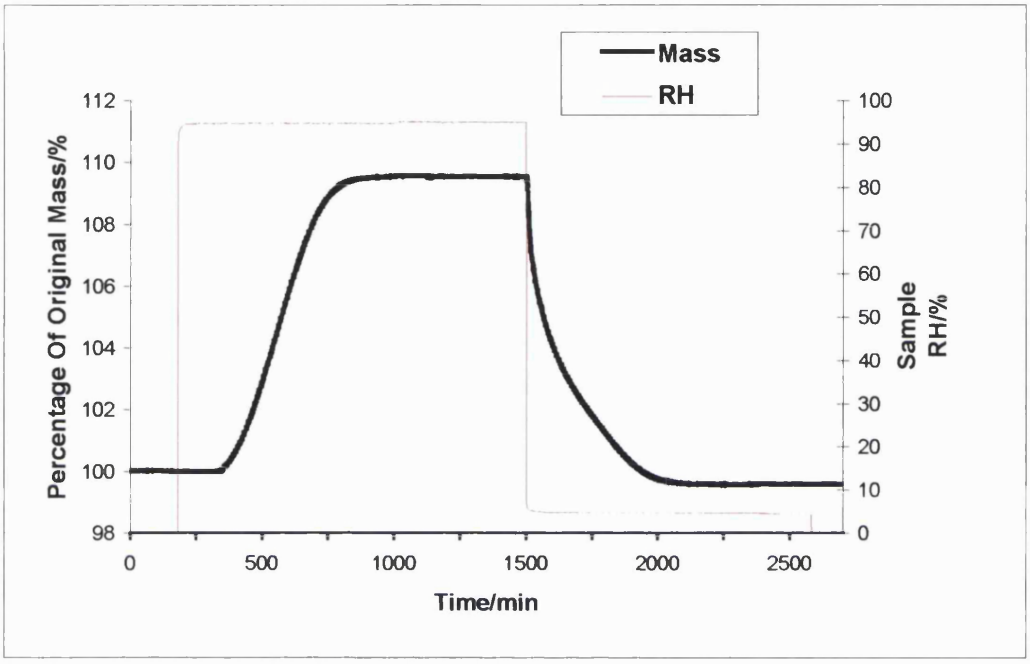

Fig. 4.4: Water sorption for the formation of the hydrate from anhydrous theophylline, by exposure to 95% RH. (0% RH for 3 h, 95% RH for 22 h, 5% RH for 18 h and finally 0% RH for 3 h).

In Fig. 4.5a the second derivative NIR spectra of theophylline are presented for a sample that had been exposed to the initial 3 hours of drying (anhydrous), and then also at the end of the 95% RH stage (hydrate). There were many new peaks and shifts when the hydrate was produced, but the most notable were the peaks at approximately 1478 nm corresponding to the first overtone –OH and 1972 nm relating to an –OH deformation combination band that were prominent in the hydrate spectra. A peak at approximately 1440 nm was seen in the anhydrate spectrum, but was lost when the hydrate was formed. Other significant differences between the spectra of the anhydrous and hydrate forms included the peaks at 1660 nm and 2260 nm, which were seen as single peaks for the hydrate but as double peaks in the anhydrous lattice. Also the peaks at 1725 nm and

2344 nm were not seen on the anhydrous spectra. The remainder of the peaks, not discussed, were present in both the anhydrous and hydrate spectra.

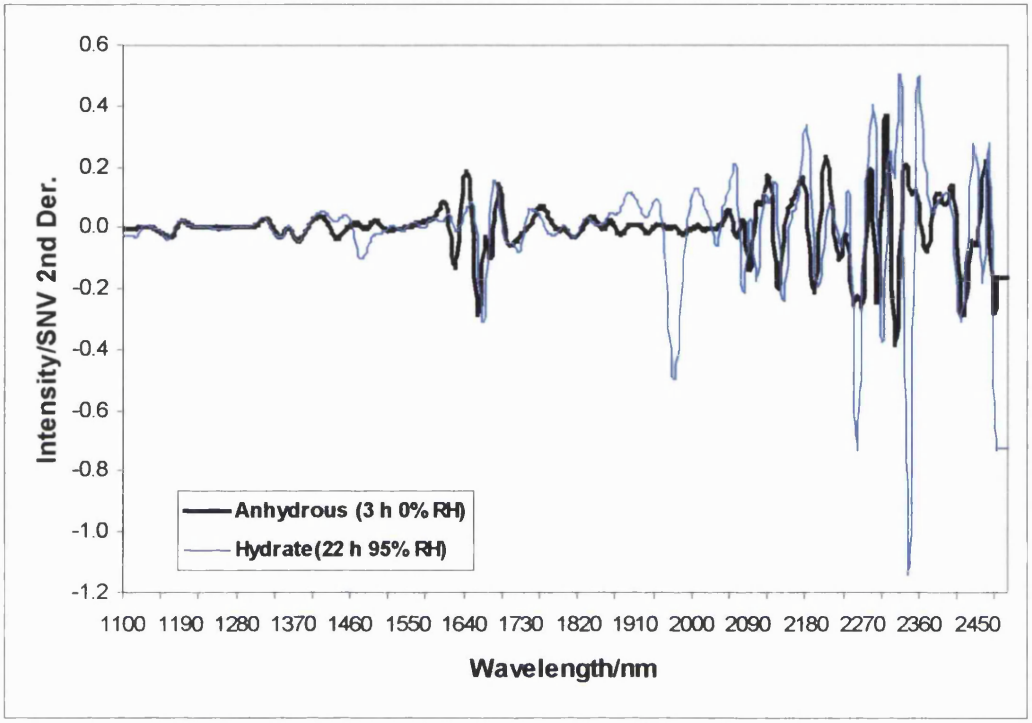

Fig. 4.5a: NIR data comparing anhydrous and hydrated theophylline.

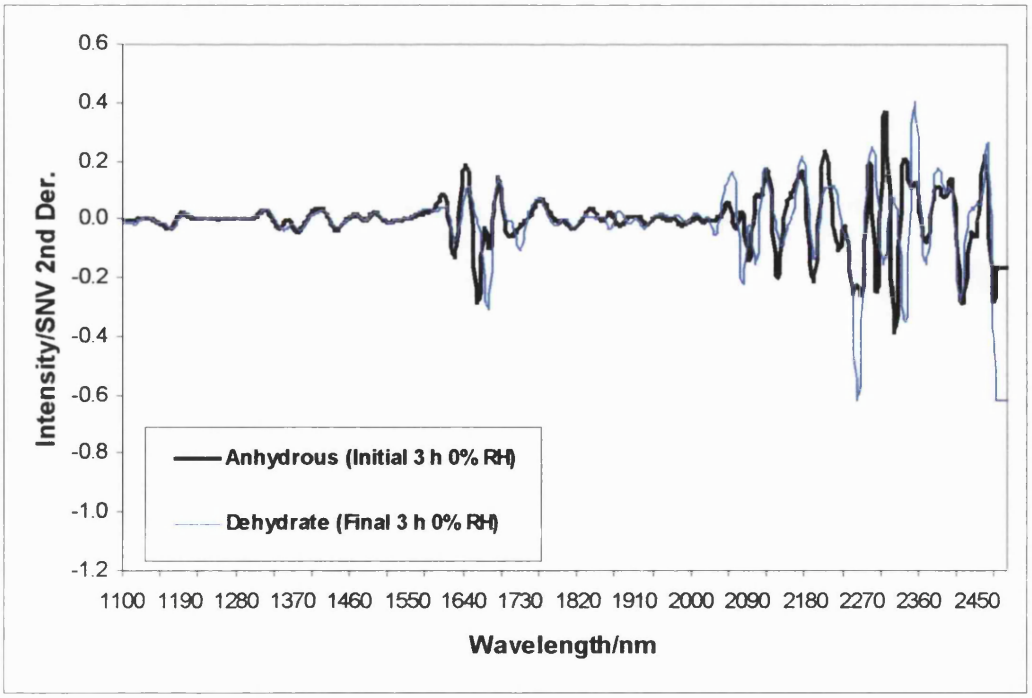

Fig. 4.5b: NIR data comparing anhydrous and dehydrated theophylline.

In Fig. 4.5b the 2nd derivative spectra for anhydrous theophylline (at the end of the initial 3 hours of drying) and for dehydrated theophylline (at the end of the final 0% RH stage) are shown. Both the spectra lacked the characteristic –OH deformation of the monohydrate at approximately 1972 nm. However, the spectrum for the dehydrate did contain some peaks that were found on the hydrate spectrum and which were not present on the original anhydrous spectrum. These were at approximately 1660 nm, 1725 nm, 2260 nm and 2344 nm. In the anhydrous spectrum the peaks at 1660 nm and 2260 nm regions were double peaks, whereas only single peaks were seen for both the hydrate and dehydrate spectra. The peak at 1725 nm for the dehydrate was distinctly different from that seen for the hydrate [Fig. 4.5a].

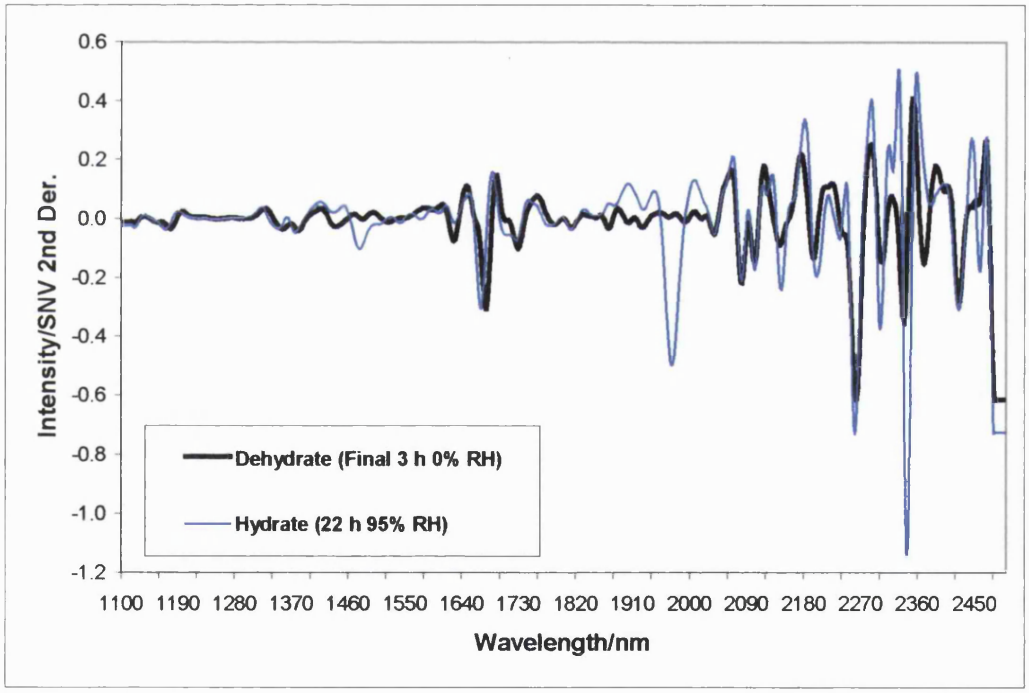

Fig. 4.5c: NIR data comparing hydrated and dehydrated theophylline.

In Fig. 4.5c the spectrum of the hydrate is compared with that for the sample which had been dehydrated at 0% RH for 3 hours. The spectrum of the dehydrated sample did not show the sharp peak at 1972 nm or at 1478 nm, but the dehydrate did show similar peaks to the hydrate at approximately 1660 nm, 1725 nm, 2260 nm and 2344 nm. A summary of the similarities and differences of the spectra obtained for the three lattice structures is presented in Table 4.2.

It can be concluded that although dehydrated theophylline contained no water it still differed from anhydrous theophylline, and showed many similarities to the structure of monohydrate theophylline.

Main Peaks/nm	Anhydrous	Hydrate	Dehydrate
1440	Yes	No	Yes
1478	No	Yes	No
1660	Double peak	Single peak	Single peak
1710	Yes	No	No
1725	No	Yes	Yes
1972	No	Yes	No
2260	Double peak	Single peak	Single peak
2322	Yes	No	No
2344	No	Yes	Yes

Table 4.2: Summary table of the presence of major peaks in the three theophylline lattices from the NIR data.

The differences in crystal lattice structures observed with the use of NIR have been corroborated using XRPD [Fig. 4.6]. The diffraction patterns of anhydrous, monohydrate and dehydrated theophylline were exactly the same as those reported by Phadnis and Suryanarayanan (1997). The dehydrated theophylline XRPD pattern, in keeping with the NIR responses, also contained peaks that were a combination of those found in the hydrate and anhydrous diffraction patterns.

The x-ray powder diffraction pattern for anhydrous theophylline [Fig. 4.6a] showed an initial sharp peak at 7.195° 2θ and then a very intense peak (high

count) at 12.675° 2θ, after which there was another sharp peak at 14.425° 2θ and a lower intensity peak at 17.805° 2θ. The diffraction pattern of the sample was exactly the same as that from Phadnis and Suryanarayanan (1997).

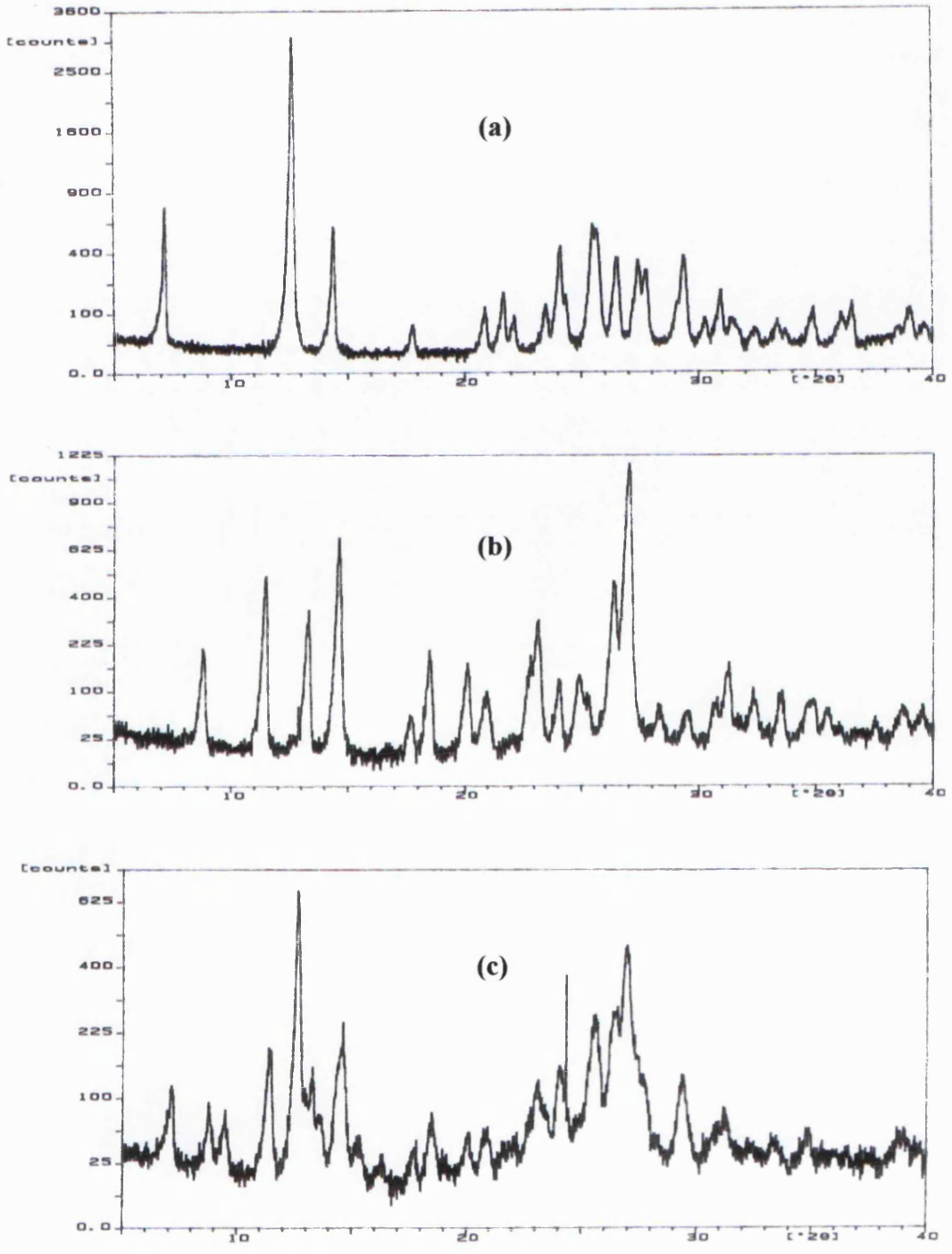

Fig. 4.6: XRPD patterns of (a) anhydrous theophylline, (b) monohydrate theophylline and (c) dehydrated theophylline.

Unlike anhydrous theophylline [Fig. 4.6a] there were four distinct peaks before 15° 2θ in the diffraction pattern for theophylline monohydrate [Fig. 4.6b]. These were at 8.830, 11.480, 13.310 and 14.645° 2θ. None of these four peaks were observed in the anhydrous theophylline pattern. The anhydrous sample produced a single peak at 17.805° 2θ, however the pattern from the hydrated sample showed a similar peak at 17.720° 2θ and an additional peak at 18.505° 2θ.

Furthermore, there were only 2 peaks at 20.100° 2θ and 20.930° 2θ in the monohydrate pattern, unlike the pattern produced from the anhydrous sample where three peaks were seen within the same range (20.905, 21.695 and 22.150° 2θ). As can be seen by comparing the two diffraction patterns there were also some other small differences in the set of peaks between 20-32° 2θ. All this showed that the samples were both not the same, and that the pattern produced from the suspected hydrate corroborated well with the XRPD of the hydrate found by Phadnis and Suryanarayanan (1997).

The XRPD diffraction pattern obtained from the dehydrated theophylline sample [Fig. 4.6c] showed similarities and variances from the patterns of the anhydrous and monohydrate theophylline samples. Firstly there were nine distinct peaks by 15° 2θ. There were four peaks in the hydrate pattern and only three peaks for the anhydrous pattern. The peaks seemed to be a combination of those found in the hydrate and anhydrous diffraction patterns. The peaks at 7.180, 12.645 and 14.335° 2θ were seen in the anhydrous x-ray pattern. The peaks found at 8.780, 11.450, 13.310, and 14.605° 2θ were also similar to those seen in the monohydrate pattern.

The broad band of peaks between 20-32° 2θ were not as well defined as they were in the diffraction patterns of the anhydrous and hydrate theophylline. However, the diffraction pattern produced did match well with the XRPD pattern again produced by Phadnis and Suryanarayanan (1997), to show that the sample was dehydrated theophylline.

4.2.3 Relationship Between Mass Change And NIR Peak Intensity

In the absence of NIR data it is left to rely on the rates of mass gain and mass loss to determine whether the hydrate is forming or being lost. However it is preferable to be able to check what is happening to the sample directly. In Fig. 4.7 the change in intensity of the key peaks related to the formation of the hydrate are plotted on the same time axis as mass change data (the mass change and NIR data were measured simultaneously on the same sample).

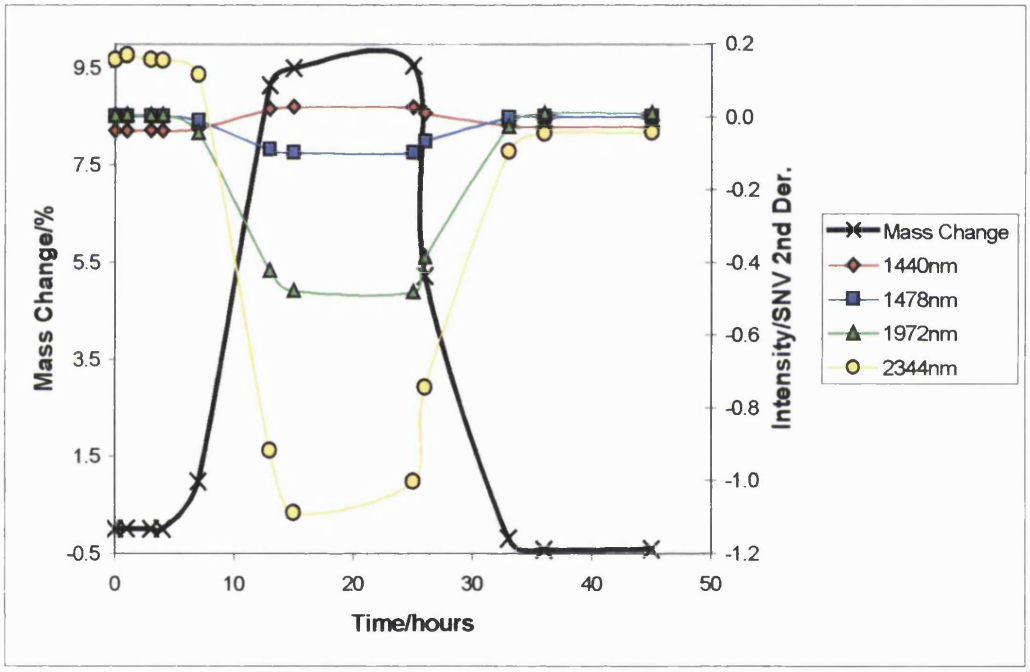

Fig. 4.7: A comparison of NIR peak intensities and mass change during the formation and loss of the hydrate.

It can be seen that the intensity (a negative peak in second derivative) mirrors the change of mass. In Fig. 4.8 the major hydrate peak (that at 1972 nm) is plotted as a function of mass change and it can be seen that there is a direct linear relationship for the formation of the hydrate, showing an exact match between mass change and structural change. However when the mass was lost there was significant hysteresis, with a lag in the rate of change of the spectroscopic intensity. This was the case for other peaks as well and shows that the theophylline retained something of the hydrate structure even though the water

was being removed. This was in keeping with the notion of the dehydrate having a structure that retains aspects of the hydrate packing (with the water missing).

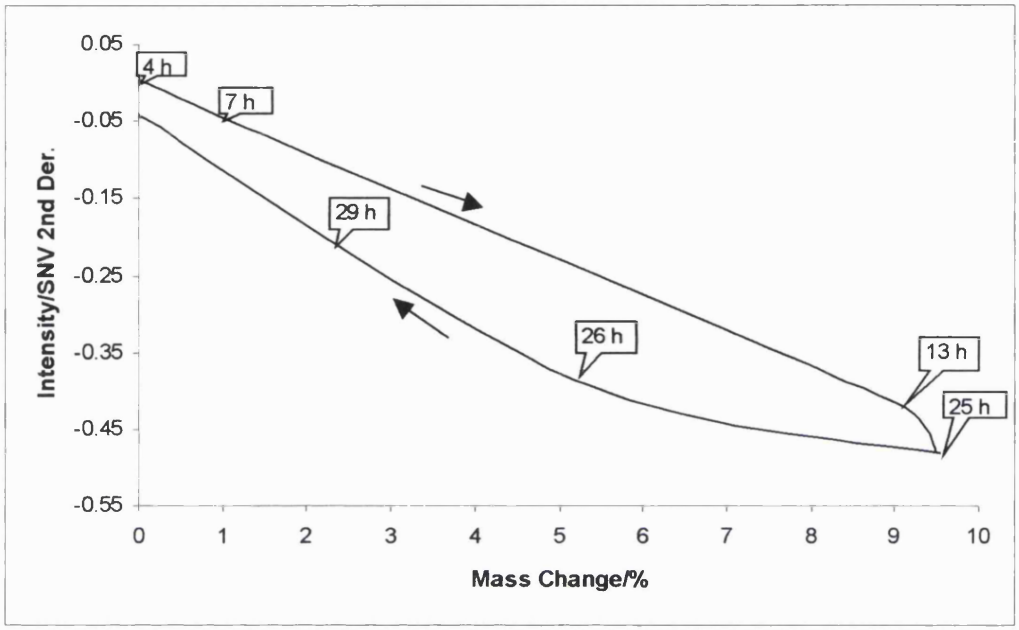

Fig. 4.8: Relationship between mass change and peak intensity at 1972 nm for the formation and loss of the hydrate (formation starts at 0 intensity).

Suihko *et al.* (1997) have argued that a doublet for the DSC dehydration peak demonstrates that theophylline dehydration is a two-step process. The data in Fig. 4.7 also indicated that a two rate processes occurred during dehydration, although these processes do not fit any simple kinetic equation the mass loss in the first hour of dehydration was 4.28% and the remainder (ca 50%) of the hydrate was lost over the following 7 hours. In Fig. 4.8 it is very clear that the rearrangement of the structure did follow a two stage process, there was relatively little change in structure over the first 3.5 h of the dehydration, despite losing ca 75% of the hydrate water during this period. The repacking of the structure from the hydrate form then became more rapid as the final 2% of water was lost. DVS-NIR is therefore able to show the nature of the transition *in situ*, without the need to remove the sample and subject it to a different test.

4.2.4 The Discovery Of A New Crystal Lattice Transition

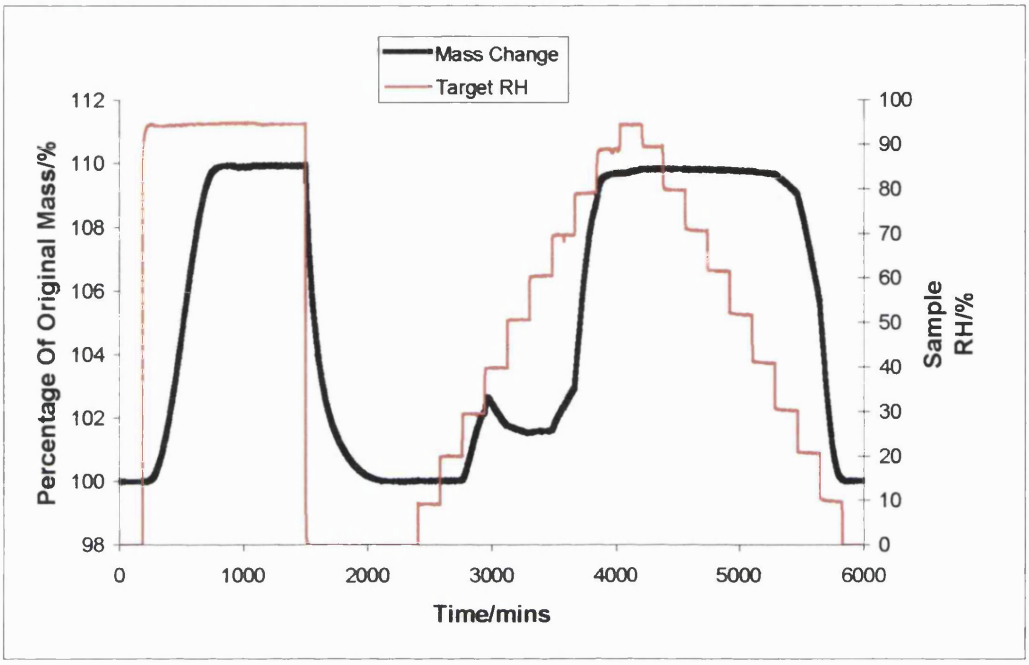

Fig. 4.9: **DVS plot showing the rehydration of dehydrated theophylline. (0% RH - 3 h, 95% RH - 22 h and 0% RH - 15 h to form the dehydrate. Thereafter 10% RH increases up to 90% RH, and then a further 5% RH increase to produce 95% RH conditions (RH decreases in same manner - each stage lasting for 3 h).**

The DVS data [Fig. 4.9] showed that during rehydration of the dehydrate there was a reproducible anomalous mass loss at 40% to 50% RH (this was not seen during the initial hydration of the original theophylline when a similar RH step increase experiment was conducted - results not shown). A mass loss with increasing RH would be characteristic of crystallisation of an amorphous material, however the sample was believed to already be crystalline. This raised the question about the nature of the dehydrate form. It was accepted that it shared characteristics of the anhydrate and the hydrate crystal forms, which presumably meant that it contained some stable anhydrate and some hydrate packing with spaces where the water molecules had departed (a "ghost hydrate structure"). These mixed crystals may therefore have amorphous content, as

disorder between the different packings and even within the "ghost hydrate structure".

NIR data had been obtained to follow the changes that occurred during the anomalous period. The peaks at and around 1660 nm [Fig. 4.10] were seen as a double peak for the anhydrous batch (1660 nm and 1682 nm) and as a single peak for the dehydrate (1678 nm) forms of theophylline (the hydrate had a peak at 1670 nm, but was omitted from the figure for clarity).

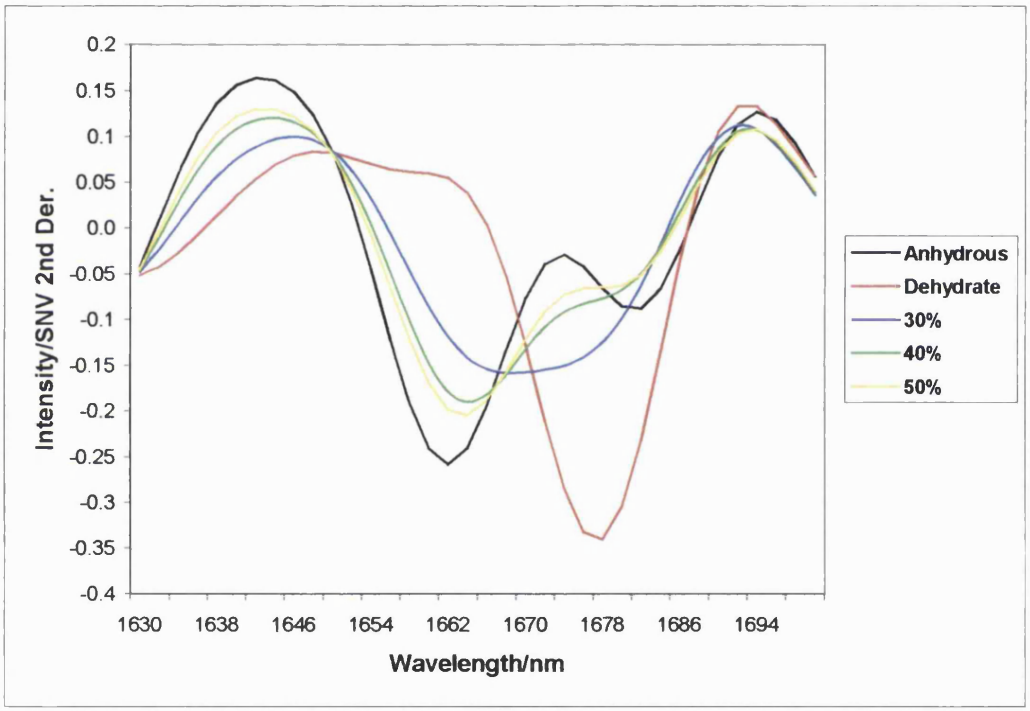

Fig. 4.10: NIR data of the peak at 1660 nm during rehydration at 30%, 40% and 50% RH compared with anhydrous and dehydrate spectra.

During rehydration, at the 30% RH stage, the peak (1670 nm) had become broader and had shifted from the position of the dehydrate towards that of the anhydrate. At 40% RH (where the mass loss began) the peak at 1664 nm had shifted further towards that seen with the anhydrous sample. The peak at 1682 nm developed at 40% RH and became more intense at 50% RH. Similar observations were made at other regions, for example the peak at 1710 nm (not

shown) was only present in the anhydrous spectra, whilst the peak at 1725 nm (not shown) was found on both the hydrate and dehydrate spectra. At 30% RH both peaks could be seen, but with lower intensities and a broader shape, showing that the peak at 1725 nm was beginning to disappear and the 1710 nm peak was appearing. At 40% and 50% RH the peak at 1710 nm strengthened further whilst the 1725 nm peak disappeared. In the region of 2260 nm [Fig. 4.11] a double peak was present for the anhydrous lattice and a single peak existed for the monohydrate and dehydrate lattice structures. As the RH was increased from 30-50% the intensity of the peak progressively decreased and the peak became broader. Spectra before 30% RH and after 50% RH followed the same pattern as that seen during initial hydration of the sample.

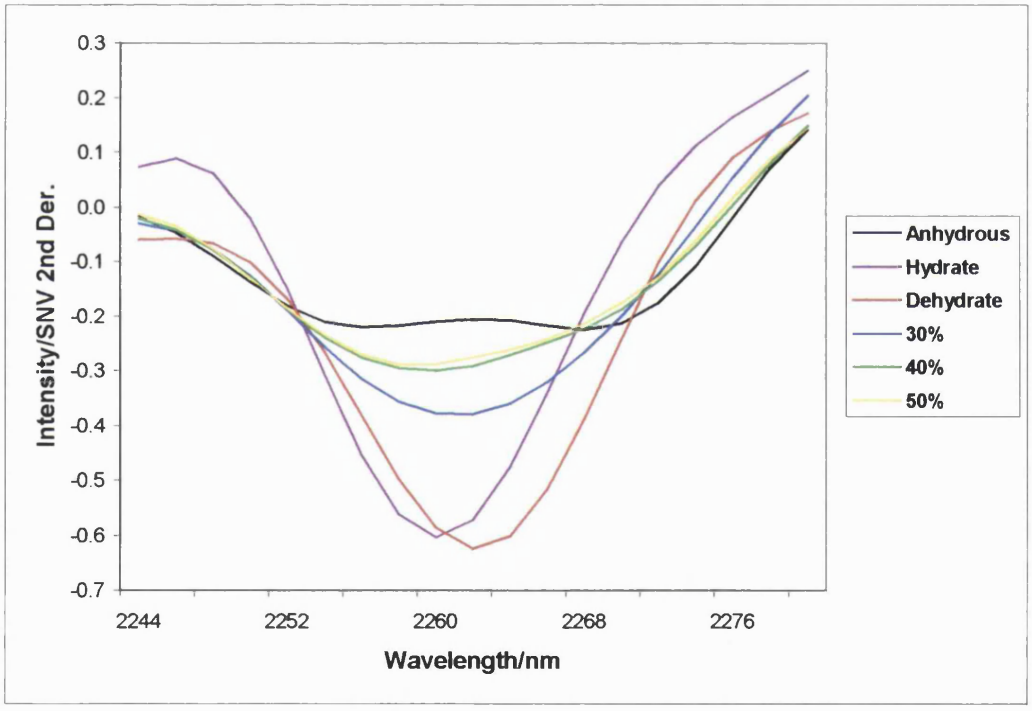

Fig. 4.11: NIR data of the peaks at 2260 nm during rehydration at 30%, 40% and 50% RH compared with anhydrous, hydrate and dehydrate spectra.

From the NIR data it was concluded that during the 30-50% RH rehydration stages the sample preferred to transform structures towards the anhydrous lattice from the dehydrate. Clearly the sorption of water allowed the structure to have

sufficient mobility to transform back into the anhydrous form. This was because the water content was too low to favour the hydrate formation. Experiments performed by missing out these low RH steps in the DVS-NIR, and going directly to 95% RH resulted in the immediate formation of the hydrate from the dehydrate (results not shown). Exposing the dehydrate structure to only 30% RH [Fig. 4.12] showed the gain and subsequent loss of water, after the crystallisation event, back to the original mass (XRPD results were similar to Fig. 4.6a).

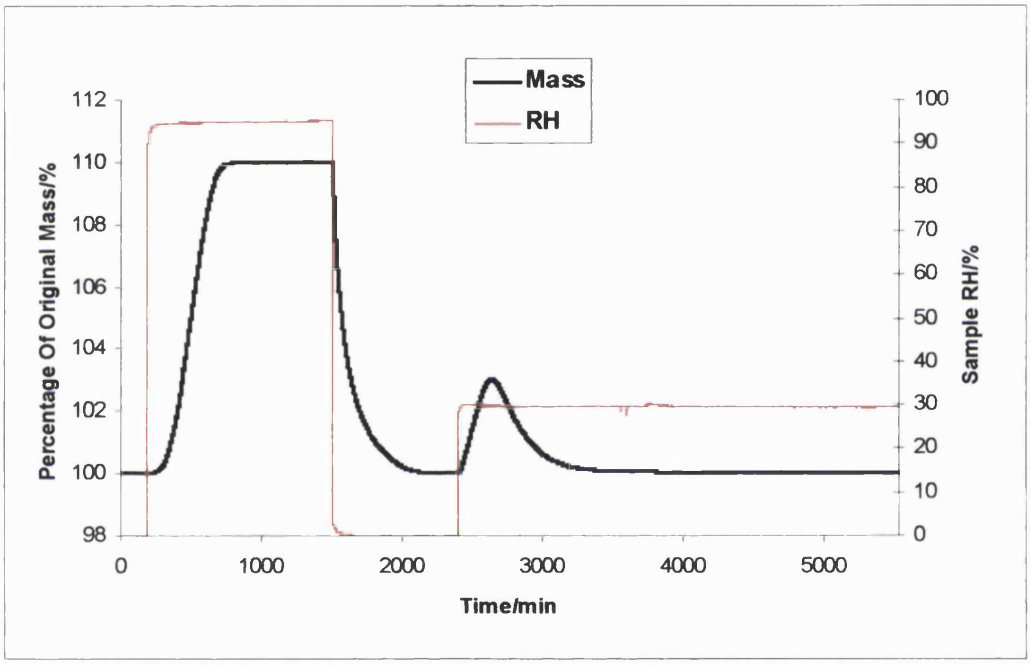

Fig. 4.12: DVS plot showing the effect of prolonged exposure at 30% RH on dehydrated theophylline.

4.2.5 Comparison Of Sigma & Fluka Batches Of Anhydrous Theophylline

The two batches of theophylline were compared because of some interesting DVS results [Fig. 4.13]. Although both batches of theophylline were meant to be the same, observations showed that the Sigma batch formed the monohydrate at a faster rate. Hydrate formation occurred within 820 min for Sigma theophylline compared to 2320 min for Fluka theophylline. The difference in time equated to 1500 min (25 h).

The results suggested that the difference was due to some variation in the manufacturing process of the batches of theophylline. This variation seen with moisture uptake is important because the end structural form of any drug in terms of its physical and chemical characteristics can be affected. For example if both batches of theophylline were converted from powder into tablet dosage forms at greater than 90% RH conditions and then stored at 50% RH, then the length of time this process would take would be important. It must be remembered that the hydrate is only lost below 20% RH (Fokkens & Blaey, 1984; Suihko *et al.*, 1997; Yoshihashi *et al.*, 1998), so if formed will remain in the hydrate form at 50% RH. Therefore if the process of converting the powder into a tablet took 1000 min, then the Sigma batch would be stored as a monohydrate whereas the Fluka batch will not have fully converted into a hydrate. If these forms were then delivered to a patient they would naturally act differently.

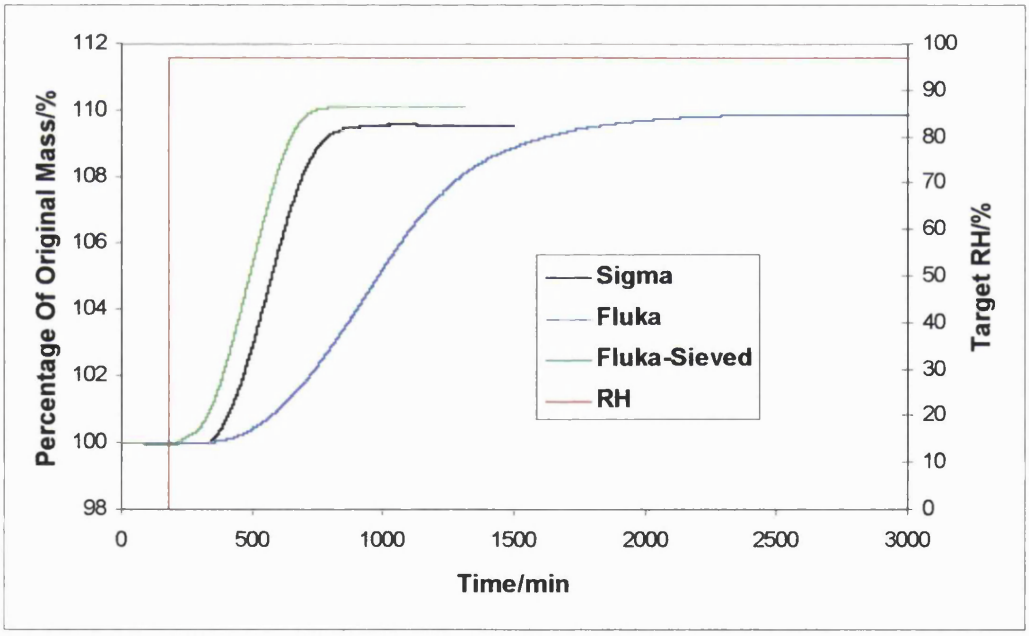

Fig. 4.13: DVS plot showing the hydrate formation of Sigma and Fluka batches of theophylline along with an air-jet sieved batch (Fluka).

SEM's of the two forms of theophylline [Fig. 4.14] were undertaken to investigate if the differences between the two batches was one purely of size.

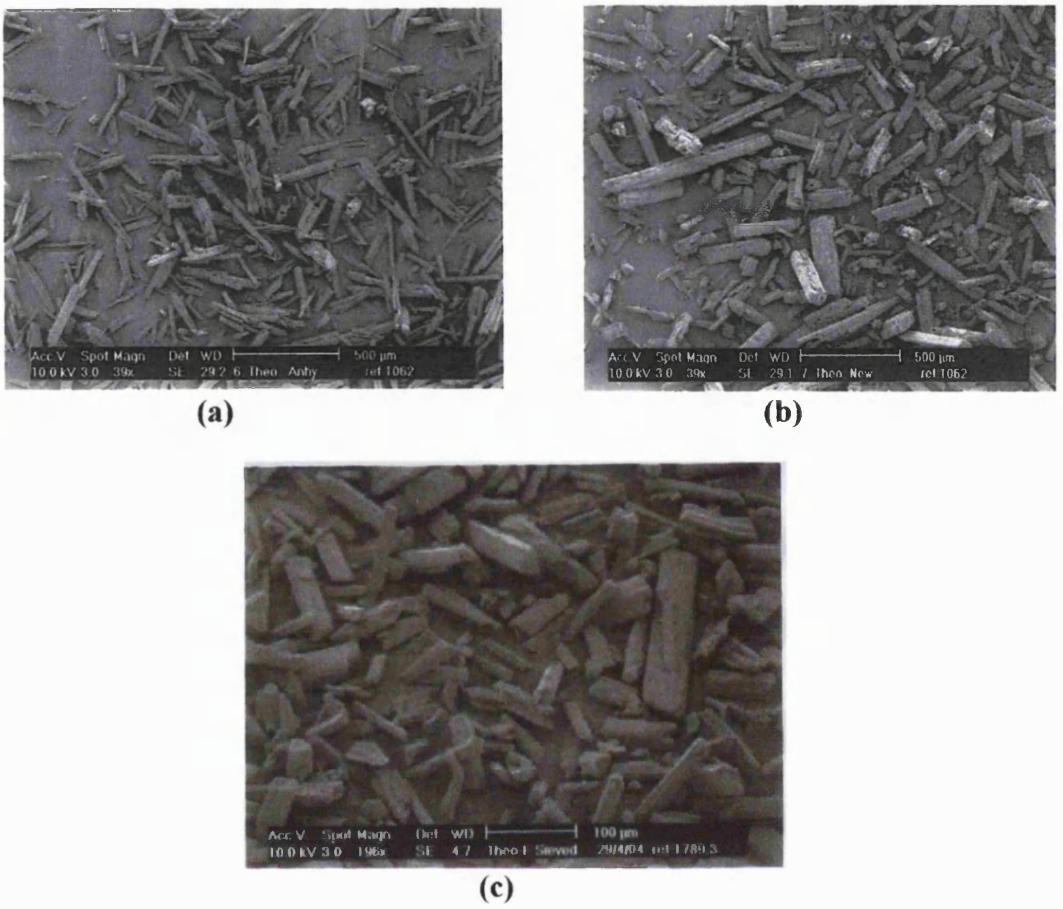

Fig. 4.14: SEM traces of anhydrous theophylline - (a) Sigma, (b) Fluka and (c) Fluka-air jet sieved.

The SEM's for anhydrous theophylline (Sigma batch) showed that the shape of the crystals were thin and needle-like in nature. However, the crystals from the Fluka sample were much bigger and some of the larger crystals had other particles aggregated to them. Also it was clear to see that there were a greater variety of sizes with the Fluka particles. The fact that the Sigma particles were thinner may account for the faster rate at which hydration occured. Unlike with the Fluka batch, water can incorporate into the crystal structure more easily and quickly with Sigma particles, as penetration is easier.

The batches were further characterised by specific surface area analysis. Assumptions made from the SEM's were corroborated by the surface area data. The average surface area for Sigma theophylline was 0.3210 m^2g^{-1} (S.D. 0.0118), for Fluka theophylline was 0.2231 m^2g^{-1} (S.D. 0.00446) and for sieved Fluka

theophylline was 0.3161 m^2g^{-1} (S.D. 0.00524). The Sigma batch had the greater surface area as expected because the crystals were thin and generally smaller than the abnormally shaped Fluka crystals. However the sieved Fluka crystals showed an overall increased average specific surface area (similar to Sigma batch) due to the removal of the larger crystals.

The Fluka crystals of theophylline were air-jet sieved through a 45 μm mesh. This would provide a result as to whether particle size was the only factor causing a slower rate of hydrate formation at 97% RH (within the DVS). It must be noted that the orientation of the particles interacting with the sieve would determine the final collection of theophylline crystals. This meant that particles that were too large to pass due to their length may filter through the sieve when orientated in terms of their width (as the width could be smaller than the mesh size). However, it was safe to assume that some large particles would not pass through the sieve. The SEM [Fig. 4.14c] of the air jet sieved batch showed that the size of the particles were generally within 100 μm (with a few exceptions). There was a smaller size distribution of particles than that seen in the SEM for the original Fluka theophylline [Fig. 4.14b]. Thus air-jet sieving the sample has had the desired effect of excluding larger particles.

The DVS plot [Fig. 4.13] showed that the sieved batch of theophylline Fluka formed the monohydrate at the quickest rate of all tested batches. The hydrate was formed within 640 min. This was a shorter length of time than lattice conversion for the Sigma batch probably because of a greater ratio of smaller crystals. The particle sizing results [Table 4.3] corroborated the surface area data and the assumptions made from the DVS results. Fluka particles showed a higher average particle size distribution than the Sigma batch. This further explains that the larger sized particles for the Fluka batch contributed to the slower rate of hydrate formation. However, the sieved Fluka particles showed the smallest size distribution. The hydration of the smallest sized particles, along with increased surface area, was easier than hydrating larger particles. This clarified the fact that the sieved sample formed a hydrate at the fastest rate. It must be noted that the sizing values can be used as a guide for comparison but not taken as absolute values for theophylline particles. The sizing technique

measures particles by assuming they are all spherical in shape. However, theophylline particles are actually rod shaped and thus the technique cannot provide accurate size distribution values for the particles.

Sample	x10/µm (S.D.)	x50/µm (S.D.)	x90/µm (S.D.)
Sigma	24.50 (0.364)	56.63 (0.741)	144.65 (5.128)
Fluka	15.03 (0.506)	91.95 (0.506)	297.29 (4.885)
Fluka-Sieved	18.89 (0.163)	38.29 (0.141)	80.22 (0.396)

Table 4.3: Table showing the average particle size distribution of the different batches of theophylline. (Dispersion pressure = 2.5 bar using the R5 lens).

4.2.6 Conclusions

DVS-NIR has proved a valuable tool in characterising the differences between the three forms of theophylline and providing kinetic data as both techniques simultaneously provide real time information. Also DVS has shown the discovery of a new crystal lattice transition and the NIR data produced alongside have helped to understand the apparent crystallisation process occurring during the anomalous period.

The importance of characterising the different batches of a drug have been highlighted with theophylline. Even though the same parent company (Sigma-Aldrich) manufactured both batches of theophylline they did not behave in the same manner in terms of hydrate formation.

The combination of DVS-NIR data therefore is valuable in aiding the characterisation of different crystal lattices of a powder, which should aid the understanding of how materials of pharmaceutical relevance may behave under environments they may meet during processing. Also the existence of batch-to-batch variation is a problem within the industry and thus characterisation to a high degree should be conducted at all times.

4.3 Calcium Mupirocin

4.3.1 Introduction

Calcium mupirocin is an antibacterial agent specifically used for the eradication of *Staphylococcus aureus*. It is the active ingredient found in the pharmaceutical products 'Bactroban' and 'Bactroban Nasal'. Its use is usually held in reserve for resistant cases (BNF 39).

Calcium mupirocin naturally exists as a dihydrate and is a hydrophilic compound. It can generate, what is believed to be, amorphous content at its surface when it is milled. This anneals in the presence of moisture vapour.

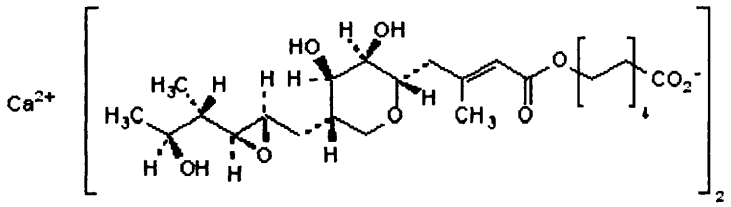

Fig. 4.15: Molecular diagram of calcium mupirocin.

The molecular weight of calcium mupirocin is 1075.3 and its melting point range is between 125-137 °C (GSK-Material Safety Data Sheet, 2002). The British Pharmacopeia (2003) states it is slightly soluble in water, sparingly in ethanol and Martindale (2004) states it is freely soluble in dehydrated alcohol, acetone and methyl alcohol.

4.3.2 Characterisation And Comparison Between Non-Micronised & Micronised Calcium Mupirocin

Calcium mupirocin is found to exist in the dihydrated state at standard room temperature and pressure. TGA was conducted to substantiate this fact. The results showed that approximately 3.335% (S.D. = 0.074) mass loss occurred.

This figure was close to the expected percentage moisture content (3.26%) of one molecule of calcium mupirocin dihydrate.

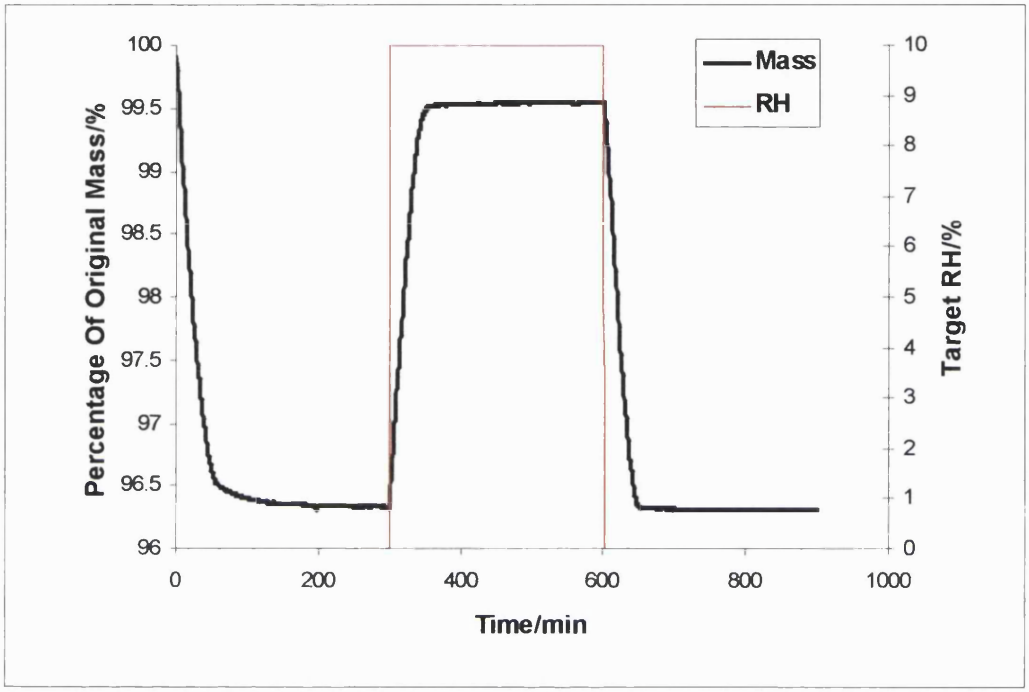

Fig. 4.16: DVS plot of calcium mupirocin dihydrate exposed to 0%, 10% and 0% RH's for 3 h each.

DVS studies showed the ease at which the hydrate could be lost and formed [Fig. 4.16]. The DVS plot showed that at the end of the initial 0% RH stage the sample had lost the dihydrate (3.67% mass loss) and then reformed it immediately when the RH was increased to 10% (3.22% mass rise). Thus DVS data have proved that calcium mupirocin will naturally exist in normal room temperature and pressure as a dihydrate.

A batch of calcium mupirocin was micronised, using the GEM-T microniser, for further studies with the DVS (chapter 5) and IGC (chapter 6) studies. It is a well known fact that processing-induced changes such as micronisation cause the development of amorphous regions within the compound, primarily on the surface (Mackin *et al.*, 2002b; Guinot & Leveiller, 1999; Ahmed *et al.*, 1996). Available techniques were utilised to attempt to determine any signs of amorphous content within the sample.

XRPD showed no differences in the crystal lattice structures of non-micronised [Fig. 4.17] and micronised calcium mupirocin. This was unsurprising as the detection limits of XRPD are about 10% amorphous content (Saleki-Gerhardt *et al.*, 1994). Therefore as micronisation would only produce small amounts of amorphous nature (mainly on the surface), it would be fair to assume that less than 10% would have been created.

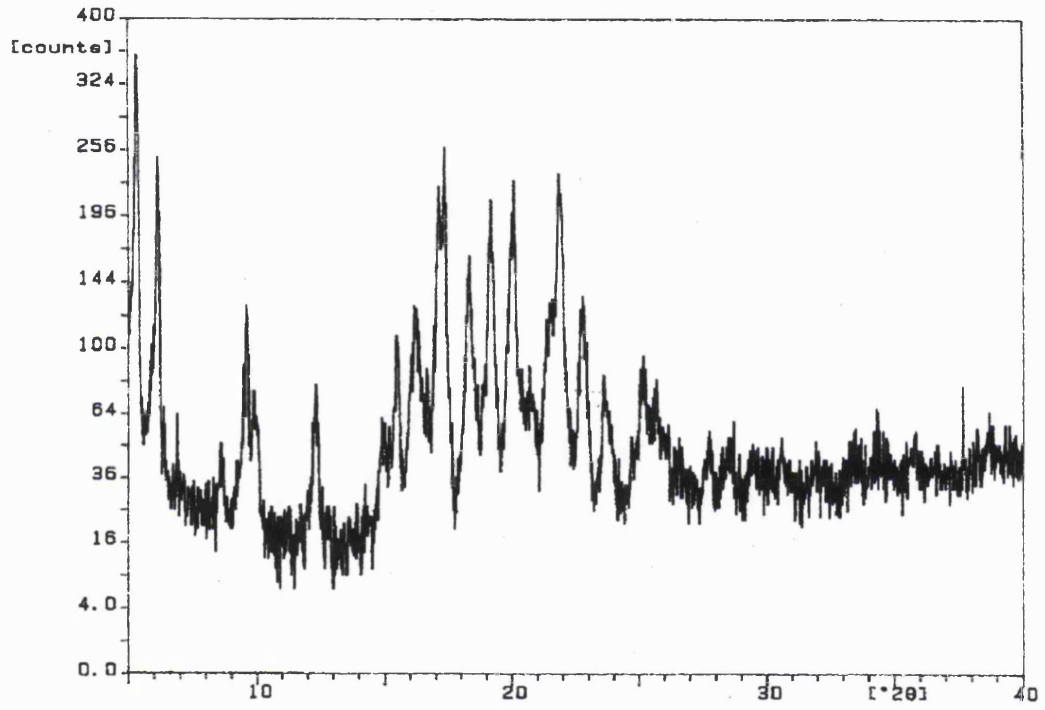

Fig. 4.17: XRPD pattern of calcium mupirocin dihydrate non-micronised. Exactly the same pattern observed for micronised sample.

Techniques such as SolCal and HDSC have been shown to detect levels of amorphousness below the capabilities of XRPD. Hogan and Buckton (2000) have found that they can measure amorphous content, using SolCal, to approximately 1% for lactose. However they have also stated that the quantification limits will not be the same for all materials. One reason was that this was believed to be dependent upon the difference in enthalpy of solution between the amorphous and crystalline forms (larger the difference, the greater the sensitivity).

HDSC is a development from conventional DSC. Standard DSC studies have only shown the measurable detection limits for amorphous content to be no less than 10% (Saklatvala *et al.*, 1999). However HDSC has recently been used to show that amorphous lactose can be detected to low levels of up to 1.5% amorphous content (Saunders *et al.*, 2004).

Both techniques were utilised to try and detect any amorphous nature created by micronisation.

	Non-micronised		**Micronised**	
Run	Pre-Calibration (J/g)	Post-Calibration (J/g)	Pre-Calibration (J/g)	Post-Calibration (J/g)
1	34.486	34.383	34.000	33.985
2	39.069	38.838	36.473	36.352
3	36.954	36.914	37.413	36.410
Average	36.836	36.712	35.962	35.582
S.D.	2.294	2.234	1.763	1.384

Table 4.4: Heats of solution for non-micronised and micronised calcium mupirocin.

The data obtained from the heats of solution [Table 4.4] for the two batches of calcium mupirocin did not show any statistical differences to suggest the detection of amorphous content within the micronised form. The *p* value obtained for the *t*-test was greater than 0.05, i.e. no statistical difference was shown when the pre-calibration data were analysed (no statistical difference also observed with the post-calibration data). HDSC also failed to establish any signs of amorphous nature. Scan rates of 100, 200 and 300 °C/min were unable to highlight any shifts in the baseline (representative of a T_g). Only endotherms for hydrate loss and melting of the compound were seen such as that shown in the example for a run conducted at 100 °C/min [Fig. 4.18].

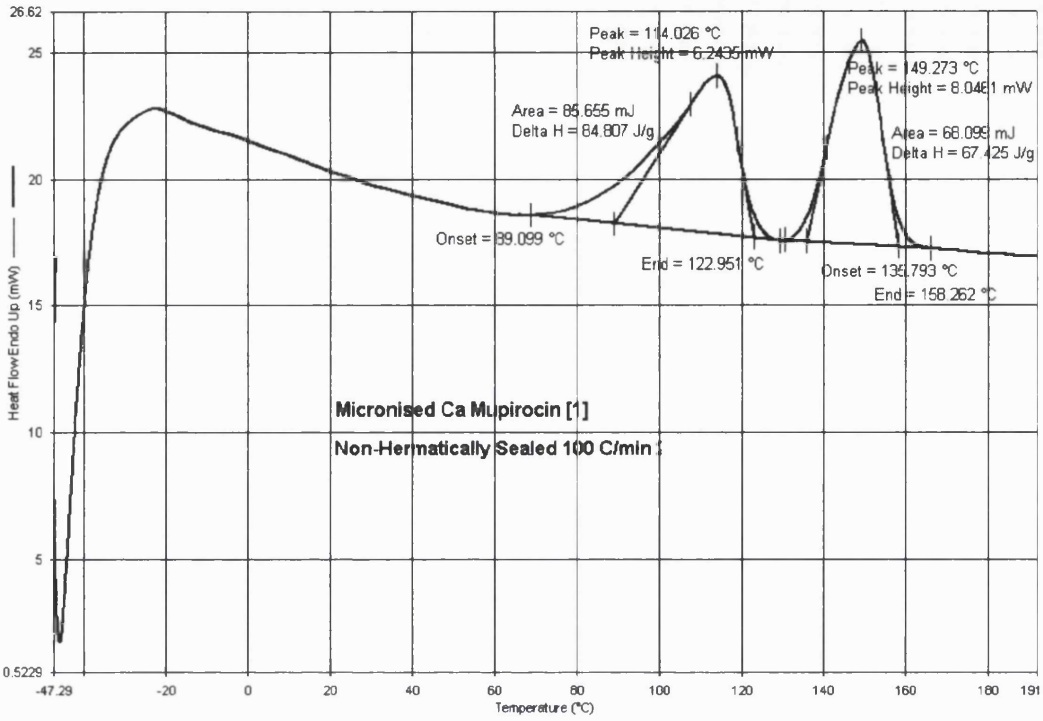

Fig. 4.18: HDSC trace of micronised calcium mupirocin at 100 °C/min.

A number of factors could account for the failure to establish any amorphous content in the micronised sample:

1. The time taken between initiation of micronisation and storage of the sample (approximately 2 h) could provide the sample enough time to crystallise using moisture from within the atmosphere. Also micronisation was not conducted in a 0% humidity chamber and so it was always reacting with the moisture within the atmosphere.

2. The sample that was micronised was the dihydrate form. As a result water molecules were already present within the compound. Thus, during micronisation, any amorphous content formed may have immediately been crystallised. Water within the compound could have reduced the T_g and accelerated the transition back to the stable crystalline form.

3. The time taken between setting up SolCal and HDSC may have allowed the sample to crystallise whilst being in contact with the room atmosphere.

4. The techniques utilised may not have been able to distinguish the low amounts of amorphous nature that would have been created during micronisation.

The effects of micronisation on the size of calcium mupirocin particles was investigated qualitatively (SEM) and quantitatively (Sympatec dry particle sizer). The SEM pictures [Fig. 4.19] showed that prior to micronisation the particles were fairly large in size (within 500 μm). However, after micronisation the size of the particles were considerably reduced (below 50 μm). Therefore it was clear to see that the size of the particles were reduced approximately 10 fold.

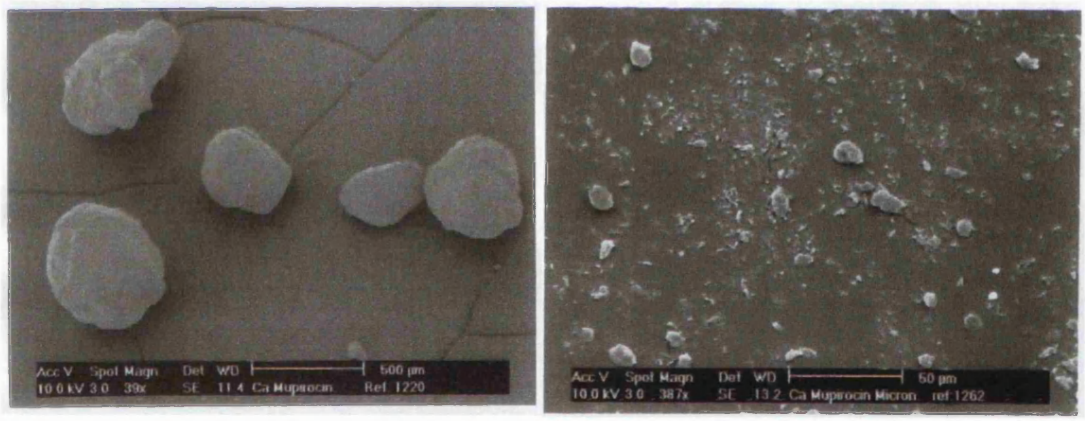

(a) **(b)**

Fig. 4.19: SEM pictures of calcium mupirocin (a) non-micronised & (b) micronised.

The particle sizing results [Table 4.5] showed that micronising greatly reduced the size of the particles. 90% of the particles for the non-micronised batch were within a size of 357 μm, whereas 90% of the particles were below 28 μm for the micronised sample. These data were consistent with the SEM pictures.

Sample	x10/µm (S.D.)	x50/µm (S.D.)	x90/µm (S.D.)
Non-Micronised	2.25 (0.007)	72.04 (0.912)	356.78 (5.883)
Micronised	0.72 (0.007)	2.29 (0.064)	27.07 (3.734)

Table 4.5: Table showing the average particle size distribution of non-micronised and micronised calcium mupirocin. (Dispersion pressure = 3.0 bar using the R6 lens).

Specific surface area determination, with the use of nitrogen BET, also provided information about the two batches of calcium mupirocin. As expected, micronisation (15.63 m^2/g, S.D. = 0.35) had caused the surface area of the particles to increase from that of the non-micronised sample (10.69 m^2/g, S.D. = 0.02). This was because smaller particles have a greater surface area to mass ratio.

4.3.3 Conclusions

Characterisation studies of calcium mupirocin have shown that the sample naturally exists in the dihydrated state. Conventional methods of amorphous content determination were unable to detect any levels of amorphous nature. This may have been due to the limitation of the machines or the rapid recovery of the sample to its stable crystalline form. However, expected differences were seen with SEM and particle sizing, showing smaller particles for the micronised batch. Also the average specific surface area of the non-micronised sample was lower due to the greater size distribution of particles.

4.4 Nabumetone

4.4.1 Introduction

Nabumetone is a non-steroidal anti-inflammatory drug (NSAID). It is primarily used for pain and inflammation in osteoarthritis and rheumatoid arthritis (BNF 39).

Nabumetone [Fig. 4.20] is a white, hydrophobic crystalline material (Martindale, 2004).

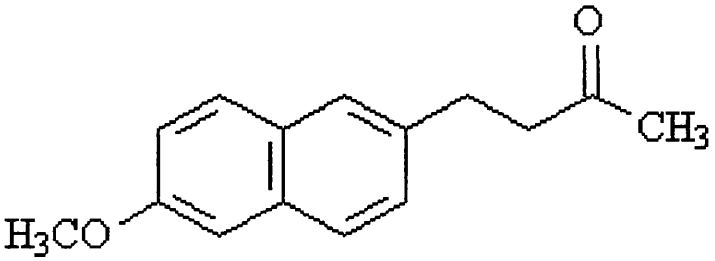

Fig. 4.20: Molecular diagram of nabumetone.

Its molecular formula is $C_{15}H_{16}O_2$ and a molecular weight of 228.29. Its melting point is found to be at 78-83 °C (GSK-Material Safety Data Sheet, 2002b). It is insoluble in water. However, it is freely soluble in acetone (Martindale, 2004).

4.4.2 Characterisation And Comparison Between Non-Micronised & Micronised Nabumetone

TGA studies were not conducted on nabumetone because the melting point of the compound was at approximately 80 °C, thus the melt and any loss of moisture would have been occurring simultaneously. DVS experiments showed no measurable mass loss at 0% RH for 3 h, suggesting that the sample was in its dry state (DVS data have been explained more thoroughly in chapter 5, section 5.4.6.2).

Similar to calcium mupirocin a batch of nabumetone was micronised for further studies in the DVS (chapter 5) and IGC (chapter 6). Once more it was important to attempt to differentiate between the non-micronised and micronised forms of nabumetone.

XRPD showed no difference in the crystal lattice structures of non-micronised [Fig. 4.21] and micronised nabumetone. As already stated by Saleki-Gerhardt *et al.* (1994), the limit of detection for XRPD is approximately 10% and therefore it was unlikely to establish any low levels of amorphous content created by micronisation.

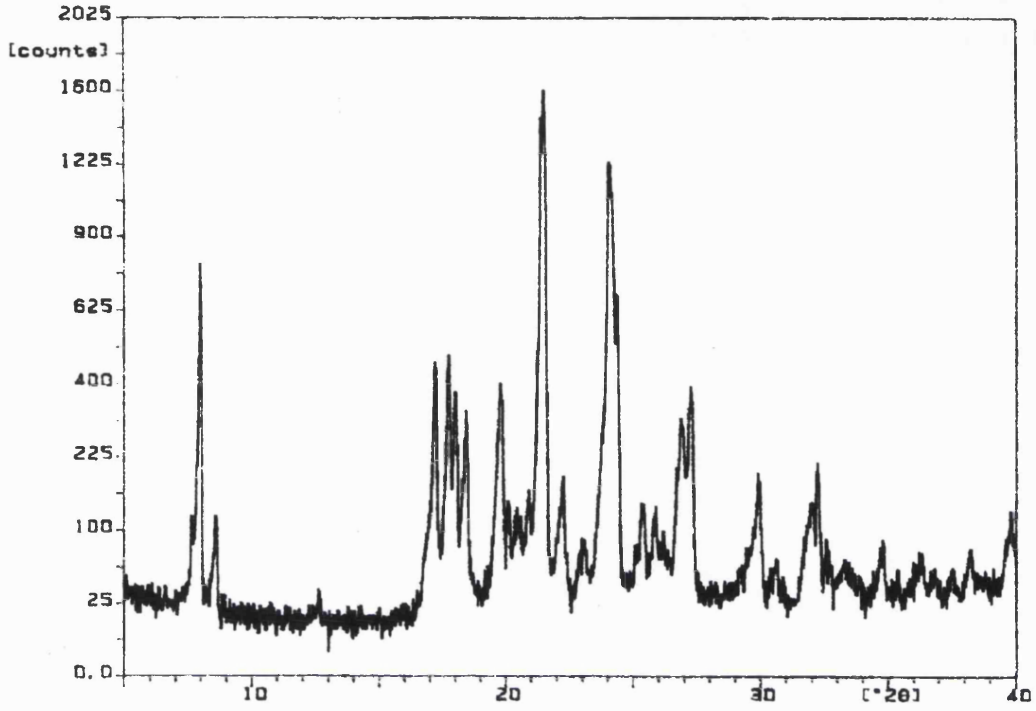

Fig. 4.21: **XRPD pattern of nabumetone non-micronised. Exactly the same pattern observed for micronised sample.**

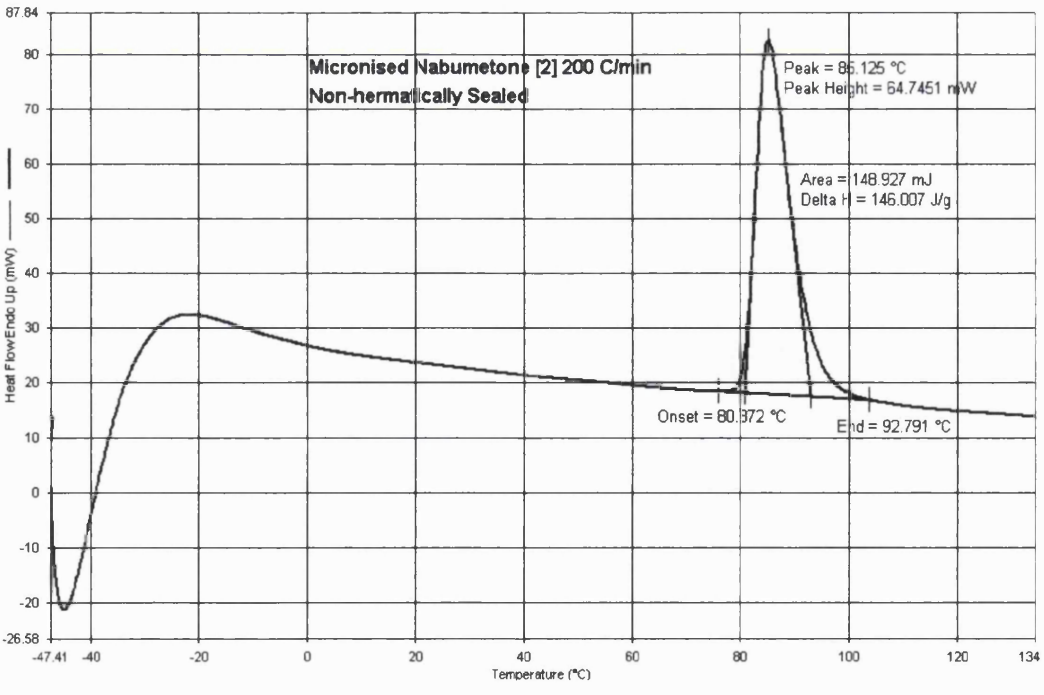

Fig. 4.22: **HDSC trace of micronised nabumetone at 200 °C/min.**

HDSC also proved to be inconclusive [Fig. 4.22 – example of HDSC trace]. The experiments at 100, 200 and 300 °C/min failed to show any signs of a T_g. Only a melt was observed at approximately 80 °C. Any amorphous content that was created by micronisation may have recovered within the time-span of setting up a DSC experiment or was not measurable by such a technique.

	Non-micronised		**Micronised**	
Run	Pre-Calibration (J/g)	Post-Calibration (J/g)	Pre-Calibration (J/g)	Post-Calibration (J/g)
1	153.112	152.994	154.469	153.474
2	153.213	153.146	152.873	152.732
3	153.367	153.215	153.064	152.821
Average	153.231	153.112	153.469	153.009
S.D.	0.128	0.113	0.872	0.405

Table 4.6: Heats of solution for non-micronised and micronised nabumetone.

The data obtained from the heats of solution [Table 4.6] for the two batches of nabumetone did not show any statistical differences to suggest the detection of amorphous content within the micronised form. Similar to the calcium mupirocin experiments, the *p* value obtained for the *t*-test was greater than 0.05 for both comparisons of pre-calibration and post-calibration data.

SEM pictures qualitatively showed the difference between non-micronised and micronised nabumetone [Fig. 4.23]. Both SEM scans showed that there was aggregation onto larger particles. The shape of the crystals varied, but were generally rod-shaped. There were naturally a greater variety of particle shapes with the micronised batch. The scans showed that many of the non-micronised particles were greater than 50 μm in size, whereas the micronised particles were generally below 50 μm in size.

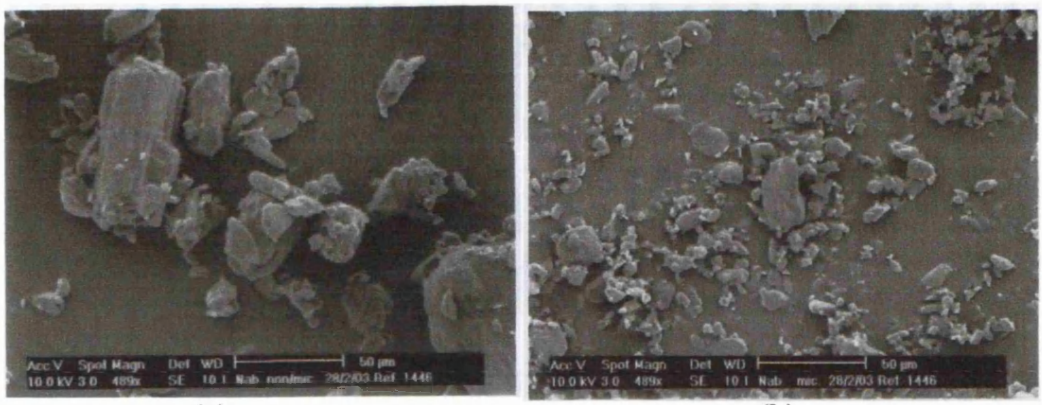

(a) (b)

Fig. 4.23: SEM pictures of nabumetone (a) non-micronised & (b) micronised.

The dry particle sizing data [Table 4.7] showed that the particle size of the micronised batch was lower than the non-micronised sample at each percentile. Micronisation had reduced the size distribution of particles by approximately 50%.

Sample	x10/µm (S.D.)	x50/µm (S.D.)	x90/µm (S.D.)
Non-Micronised	6.36 (0.007)	23.44 (0.014)	69.56 (0.962)
Micronised	3.48 (0.015)	9.32 (0.042)	22.30 (0.144)

Table 4.7: Table showing the average particle size distribution of non-micronised and micronised nabumetone. (Dispersion pressure = 0.5 bar using the R4 lens).

Specific surface area analysis was also conducted to further differentiate between the non-micronised and micronised batches of nabumetone. As expected, a greater specific surface area was found for micronised nabumetone (0.706 m^2/g, S.D. = 0.012). The specific surface area for the non-micronised batch was nearly 50% less (0.363 m^2/g, S.D. = 0.018), as larger particles have a smaller surface area to mass ratio.

4.4.3 Conclusions

Standard methods (XRPD, HDSC and SolCal) to detect amorphous nature created after micronisation proved unsuccessful. This may have been due to the limitation of the machines or the speedy recovery of the sample to its stable crystalline form. Positive results were obtained from SEM and particle sizing, showing that smaller particles were produced after micronisation. Also the average specific surface area for the micronised batch was nearly half of that obtained for the non-micronised form of nabumetone.

4.5 Magnesium Stearate

4.5.1 Introduction

Magnesium stearate is the most widely used lubricant in tabletting and capsule filling. It is the most efficient lubricant used in tablet formulations and belongs to the group of metallic salts of fatty acids commonly known as soaps. The molecular weight of pure magnesium stearate [Fig. 4.24] is 591.3 and its melting point varies due to the impurities and numerous polymorphic states. The melting point range quoted for commercial samples is 117-150 °C (Kibbe, 2000). It is a very fine, light powder that is practically insoluble in water and ethanol.

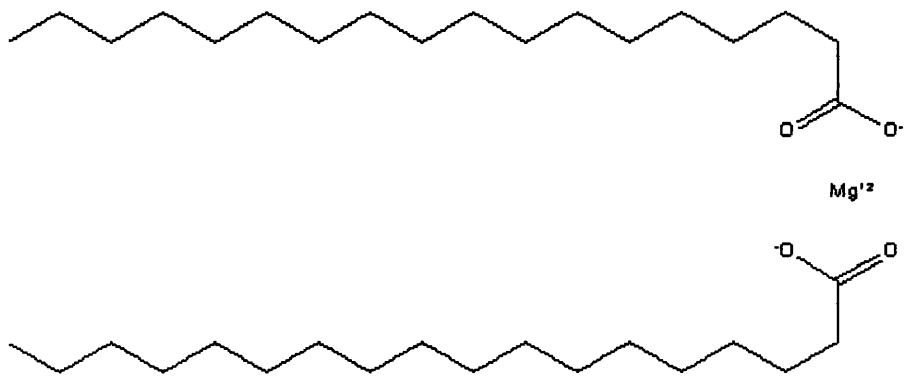

Fig. 4.24: Molecular diagram of pure magnesium stearate.

Magnesium stearate used within the pharmaceutical industry is not usually of the pure form. This is due to the fact that the unique lubricant properties obtained are in some part due to the impurities within the commercial forms. The British Pharmacopeia (2003), states that for magnesium stearate the fatty acid fraction should contain not less than 40% stearic acid and the sum of stearic acid and palmitic acid should not be less than 90%. The Sigma batch contained 65% magnesium stearate and 25% palimitate salt and the Fluka batch contained 50% magnesium stearate and 40% palmitate salt. The remainder of the commercial magnesium stearate contained impurities such as heavy metals, chloride, sulphur and moisture.

One of the problems in using magnesium stearate is that its lubricant properties vary from batch-to-batch, even when the material is obtained from the same manufacturer. Commercial magnesium stearate is a variable material with respect to chemical composition, often containing a large proportion of magnesium palmitate, but there may also be other fatty salts and variable amounts of moisture. Commercial magnesium stearate samples may also vary in its physical characteristics and hence may have unpredictable effects on formulations.

There is a large amount of literature in the public domain regarding this excipient. Physical parameters, such as crystal structure, particle size, specific surface area or moisture content affect the lubricity of magnesium stearate. Wade and Matsubara (1994) showed that the moisture content of magnesium stearate was an important factor for lubricity (reduced lubricating property due to a reduced moisture content). However, Dansereau & Peck (1987) contend that the specific surface area and the particle size are the major factors. Commercial magnesium stearate has also been shown to inhibit granule (Lerk *et al.*, 1977a) and tablet dissolution (Levy & Gumtow, 1963) and reduce tablet strength (De Boer *et al.*, 1978). According to Ertel and Carstensen (1988a), the lubrication properties of pure magnesium stearates depend on the moisture content and the crystal structure. When preparing the pure form of magnesium stearate the hydration state can be affected by the pH of the precipitation medium and the cooling rate (Muller, 1977). Miller *et al.* (1982) and Miller & York (1985) also

showed that the shape, surface area and moisture content of magnesium stearate are influenced by the pH of the manufacturing conditions. In contrast Ertel and Carstensen (1988b) found that neither the pH nor the cooling rate had an effect on crystal shape but only on the content of bound water within the crystals.

Magnesium stearate is a non-hygroscopic material. The compound will however sorb moisture when stored under high relative humidities. Although, magnesium stearate is insoluble in water, it forms hydrates (Muller, 1977; Swaminathan & Kildsig, 2001). Four forms of magnesium stearate have been identified – the mono-, di-, and trihydrates and an anhydrous form. The shape of the crystals are said to generally be needle-like or plate shaped.

Magnesium stearate is usually effective in low concentrations. However, care must be taken when preparing formulations with this compound due to the compound's hydrophobic nature, which has been shown to affect adversely tablet properties such as hardness (Strickland *et al.*, 1956; Shah & Mlodozeniec, 1977), disintegration time (Strickland *et al.*, 1956; Shah & Mlodozeniec, 1977), and dissolution rate (Levy & Gumtow, 1963; Lerk & Bolhus, 1977b; Shah & Mlodozeniec, 1977). Therefore, it is desirable to optimise the amount of magnesium stearate used in a formulation, for example to use an amount which adequately lubricates the formulation but minimises the adverse effects on the finished tablets. However, the optimisation process is difficult because commercial magnesium stearate exhibits significant batch-to-batch variations in the ability to function as lubricants (Muller, 1977).

4.5.2 DSC Investigations On Sigma And Fluka Magnesium Stearate

DSC studies were conducted on samples of Fluka and Sigma magnesium stearate. Tests were performed to study the effects of humidity on the two batches stored at 0%, 75% and 97% RH at periodic time intervals for two weeks [Table 4.9]. Data were also obtained for magnesium stearate 'straight from the pot' and dried samples [Table 4.8]. The values obtained were from the temperature at the maximum peak height, rather than the onset temperature. This

method of analysis was chosen due to the difficulty in always assessing the onset temperature because of superimposing of some endotherms.

Batch	Thermal Events (°C) (S.D.)		
Sigma As Received	109.8 (0.3)		
Fluka As Received	98.1 (0.4)	116.3 (0.9)	124.3 (2.3)
Sigma Dried 100 °C – 24 h	128.6 (0.4)		
Fluka Dried 100 °C – 24 h	116.4 (0.6)	129.0 (0.6)	

Table 4.8: Thermal events of the two batches of magnesium stearate as received and after 24 h drying in an oven at 100 °C.

The DSC traces obtained for the two batches of magnesium stearate [Fig. 4.25a & 4.26a], as received, were distinctly different. The commercial magnesium stearate from Fluka showed three thermal events when analysed by DSC. Endotherm peak temperatures were at 98.1 °C, 116.3 °C, and 124.3 °C. Scans of the Sigma batch showed one endotherm at 109.8 °C and a shoulder peak at approximately 119 °C. The difference in the DSC curves of the two batches may be due to differences in the fatty acid composition.

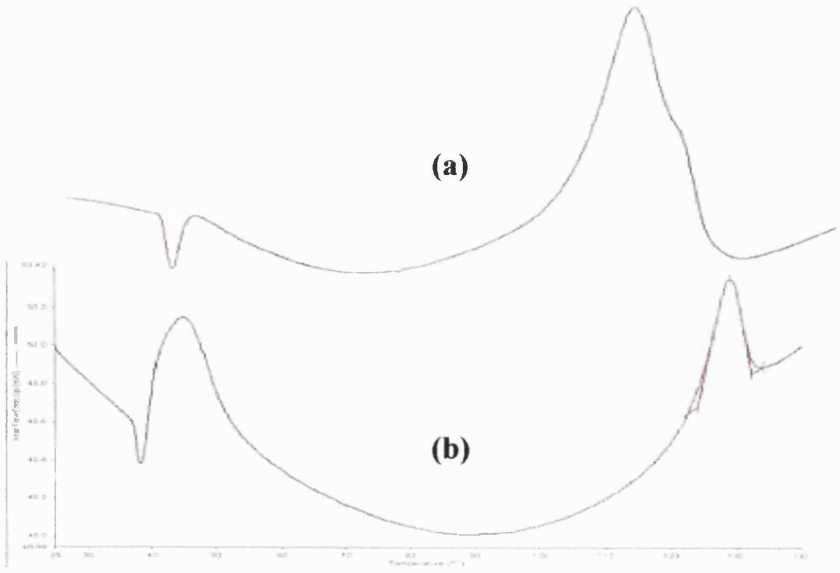

Fig. 4.25: DSC scans for the Sigma batch magnesium stearate (a) as received and (b) dried at 100 °C for 24 h.

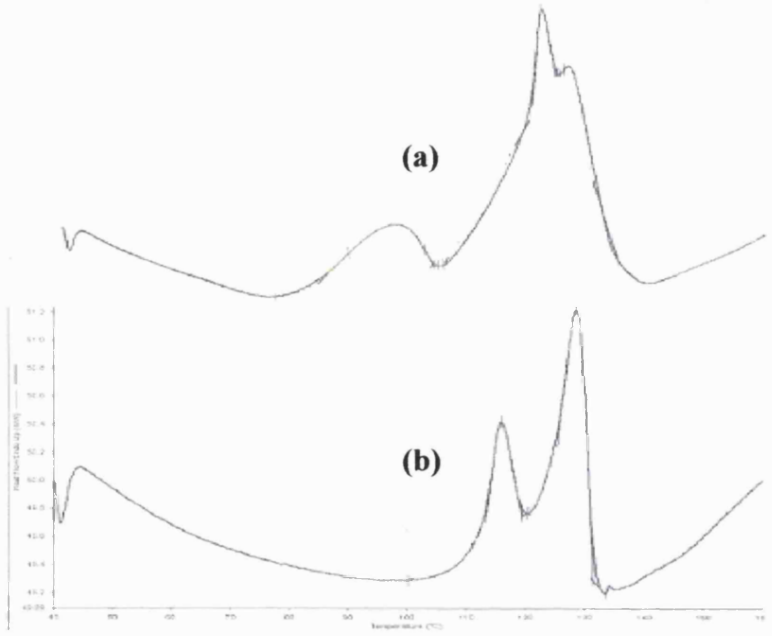

Fig. 4.26: DSC scans for the Fluka batch magnesium stearate (a) as received and (b) dried at 100 °C for 24 h.

Samples were placed in an oven at 100 °C for 24 hours to dry the batches of magnesium stearate. Fig. 4.25b shows the DSC scan for the Sigma sample when dehydrated. It was noted that a shift to a higher temperature occurred for the endotherm at 109.8 °C, which became evident at 128.6 °C. The lower temperature endotherm at 98.1 °C for the Fluka sample disappeared [Fig. 4.26b], indicating that this endotherm was associated with water within the sample. Thus it seems that only the Fluka batch was originally in the form of a hydrate.

As previously noted in Fig. 4.25a the original Sigma magnesium stearate sample exhibited one major endotherm at approximately 109.8 °C and a shoulder peak at about 119 °C. Fig. 4.27 showed the DSC scans obtained for Sigma magnesium stearate, as received which had been stored under different relative humidity conditions for one day, one week and two weeks. An additional endotherm at approximately 70-75 °C was visible for 75% and 97% RH. This endotherm became evident after one week at 75% RH. However, it was noticeable after one day in the 97% RH scan. The endotherm was more pronounced at the 97% RH

conditions. This additional endotherm could have been due to the presence of hydrate water occurring at the higher relative humidity conditions. The peak occurring at approximately 70-75 °C was associated with the loss of hydrate water whilst the peak at approximately 110 °C was associated with the melting of the magnesium stearate. However it must be noted that all the peaks at approximately 100 °C, when analysed using the 2nd derivative of the plot showed that two thermal events were in fact occurring. The peak at 110 °C was masking a second event taking place at approximately 117 °C.

	Thermal Events (°C) (S.D.)									
Sigma	***One Day***			***One Week***			***Two Weeks***			
0%	110.7 (0.3)			111.3 (1.6)			110.3 (0.6)			
75%	111.2 (0.4)			70.8 (0.6)	110.7 (0.2)		70.7 (0.5)	110.0 (0.7)		
97%	73.4 (0.5)	110.2 (0.4)		74.8 (0.9)	110.8 (0.2)		75.8 (0.2)	111.7 (0.4)		
Fluka										
0%	96.7 (0.5)	114.1 (0.1)	125.1 (0.2)	96.2 (1.8)	114.5 (0.3)	123.2 (2.5)	94.8 (0.5)	113.9 (0.5	122.1 (1.2)	
75%	96.2 (1.6)	114.3 (0.5)	123.2 (2.6)	94.3 (0.5)	114.3 (0.6)	124.2 (0.4)	98.6 (0.6)	114.4 (0.3)	124.3 (0.4)	
97%	100.0 (1.5)	114.5 (0.3)	124.5 (0.8)	96.9 (2.0)	114.6 (0.3)	124.8 (0.3)	71.4 (0.6)	99.4 (2.1)	114.6 (0.1)	124.5 (0.6)

Table 4.9: Thermal events of the two batches of magnesium stearate stored in varying RH desiccators over a period of 2 weeks.

The scans shown in Fig. 4.28 were acquired for Fluka magnesium stearate, as received stored under different relative humidity conditions, for the different lengths of time. These results were very similar to Fig. 4.26a (scan for Fluka as received) that the endotherms produced for all relative conditions were almost identical to those of the original untreated sample of magnesium stearate. The observable endotherm peak temperatures were at approximately 97 °C, 114 °C and 124 °C. The DSC scans for Fluka stored at 97% RH for two weeks, showed

an additional endotherm at approximately 71 °C. This would also relate to bound water within the sample. The lower temperature endotherm at 97 °C disappeared for the 0% RH sample (2 weeks storage). This indicated that this endotherm was associated with water within the sample. This was also seen in Fig. 4.26b when the samples were dried at 100 °C for 24 h.

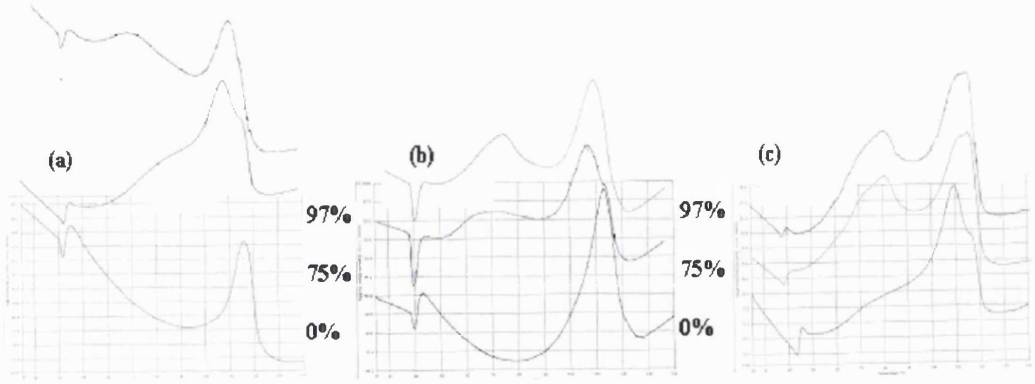

Fig. 4.27: DSC scans for the Sigma batch magnesium stearate stored under the different relative humidity conditions for (a) one day (b) one week and (c) two weeks.

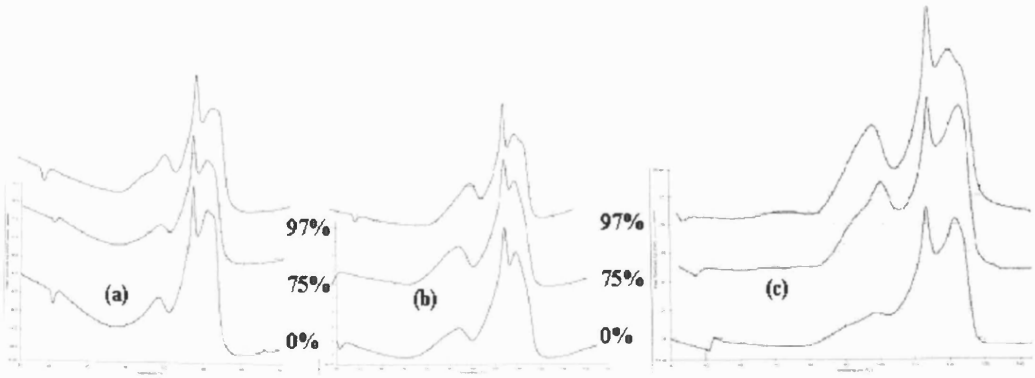

Fig. 4.28: DSC scans for the Fluka batch magnesium stearate stored under the different relative humidity conditions for (a) one day (b) one week and (c) two weeks.

The DSC traces on their own suggest that the original Sigma magnesium stearate was in the anhydrous form and the original Fluka batch was in one of the hydrated states – possibly a di- or trihydrate, given by the number of endotherms

present. However more conclusive evidence could be obtained by XRPD and TGA studies.

4.5.3 XRPD Investigations On Sigma And Fluka Magnesium Stearate

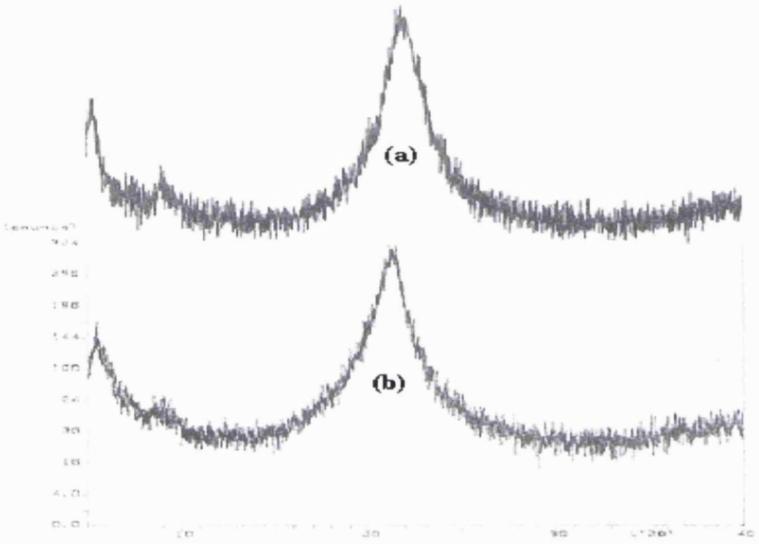

Fig. 4.29: XRPD patterns for the Sigma batch magnesium stearate (a) as received and (b) dried at 100 °C for 24 h.

In a similar manner to the DSC experiments XRPD was also conducted on the two batches of magnesium stearate under the varying humidity conditions used. Representative XRPD patterns of a sample from each commercial source, Sigma and Fluka are shown in Figs. 4.29a and 4.30a respectively. The diffraction pattern of the sample from Sigma showed a single broad peak within the 21° 2θ region. However 3 peaks were seen within the same region for the Fluka batch. None of the patterns matched the standard pattern in the Powder Diffraction File. This was expected because the commercial material has much lower purity than the sample used to generate the sample diffraction pattern.

Fig. 4.30b showed the XRPD spectra for Fluka when dried. Sample (a) [as received] had a triplet around 21° 2θ region; sample (b) [dried at 100 °C] produced a single broad band. This shows that drying the Fluka sample results in a loss of the hydrate structure. Only three peaks were noticeable in the dried Fluka sample and they were 5.5, 9.1 and 21.4° 2θ. Drying the magnesium stearate

from Fluka led to the loss of the bound moisture in the powder (loss of hydrates). There was no change in the XRPD pattern of the Sigma batch magnesium stearate [Fig. 4.29b] after it was heated to 100 °C. This indicated that the Sigma batch magnesium stearate had no bound moisture and so the powder as received, was in its dehydrated form.

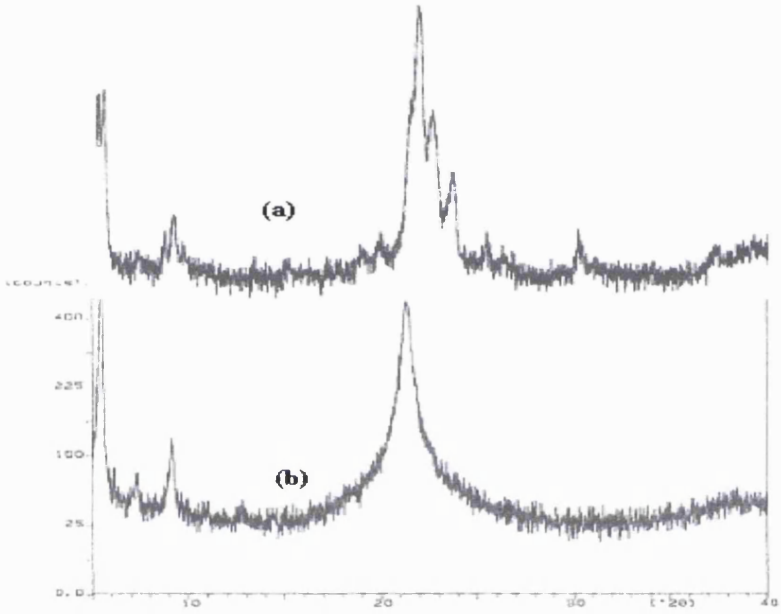

Fig. 4.30: XRPD patterns for the Fluka batch magnesium stearate (a) as received and (b) dried at 100 °C for 24 h.

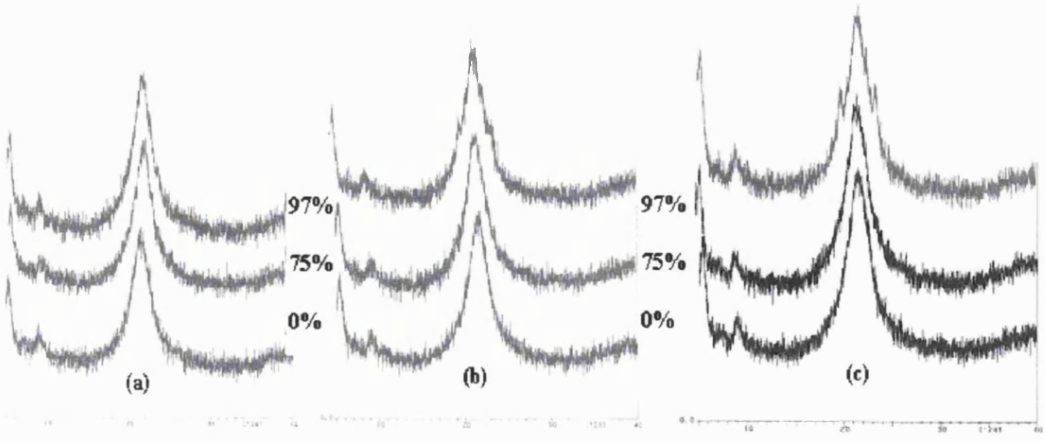

Fig. 4.31: XRPD patterns for the Sigma batch magnesium stearate stored under the different relative humidity conditions for (a) one day (b) one week and (c) two weeks.

The powder diffraction patterns of Sigma magnesium stearate samples that were exposed to a range of RH conditions are shown in Fig. 4.31. There was no change in the XRPD pattern of the Sigma material stored at 0% and 75% RH. The broad peak centred at 21.4° 2θ split up, and discrete peaks appeared at 19.8, 21.4 and 23.3° 2θ for samples stored at 97% RH (apart from the XRPD patterns of one day storage). An increase in the intensity of these peaks was observable in the diffraction patterns of samples stored at 97% RH for two weeks. The appearance of these additional peaks in the region near 19-23° 2θ, indicate the moisture uptake in the form of hydration.

The XRPD patterns of the Fluka batch magnesium stearate [Fig. 4.32] stored under the different relative humidity conditions were very similar to Fig. 4.30a in that the peaks produced for all the relative conditions were almost identical to those of the original untreated Fluka batch. However, there was an increase in the intensity of the peaks as the RH and time of storage was increased.

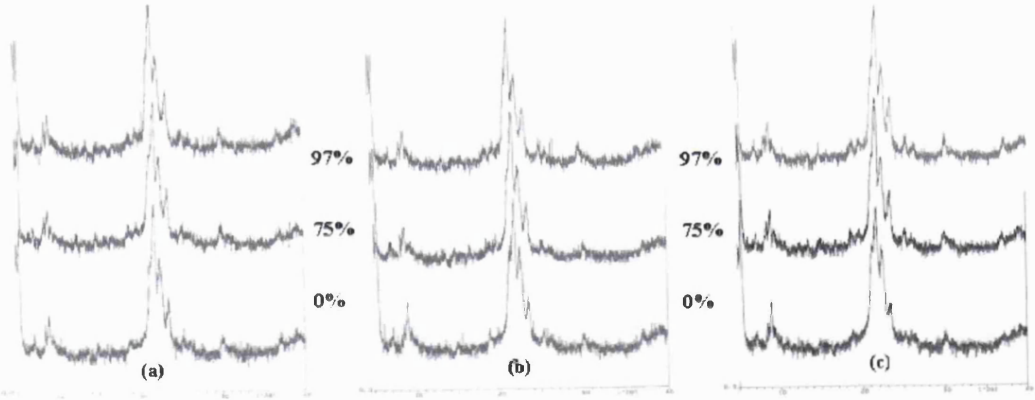

Fig. 4.32: XRPD patterns for the Fluka batch magnesium stearate stored under the different relative humidity conditions for (a) one day (b) one week and (c) two weeks.

The XRPD pattern obtained for the Sigma batch has been identified as the amorphous form by comparison with published patterns (Rajala & Laine, 1994; Swaminathan & Kildsig, 2001). However the sample is not believed to be amorphous. Other authors such as Leinonen *et al.* (1992) have suggested the x-

ray spectra of the Sigma batch to be anhydrous. This was in direct conflict with the TGA (section 4.5.4) data suggesting the batch was in a hydrate form originally. Furthermore it has proved difficult to distinguish between different hydrated forms using XRPD. Bracconi *et al.* (2003) have explained that a review of literature has found it difficult to isolate x-ray diffraction patterns of commercial magnesium stearate in anhydrous or hydrated forms due to the difficulty in preparing single phase samples. The mixture of hydrates produced x-ray spectra containing overlapping reflections from all the forms present. Such a problem is not encountered when differentiating between polymorphs of pure magnesium stearate (Ertel & Carstensen, 1988a; 1988b).

4.5.4 TGA Investigations On Sigma And Fluka Magnesium Stearate

TGA studies were also conducted to characterise further the two forms of magnesium stearate by similar humidity studies carried out using DSC and XRPD. All mass losses were measured prior to the melting point of the samples [Table 4.10 and Fig. 4.33].

Both samples as received showed a loss of mass that was perceived to be largely due to bound water. Sigma magnesium stearate showed a 3.2% mass loss and the Fluka batch showed a 4.2% mass loss. The reduction of these mass losses when stored under 0% RH conditions confirmed that they were related to bound moisture. The as received samples suggest that the Sigma and Fluka magnesium stearate batches were possibly a mixture of mono- and dihydrated forms. With pure magnesium stearate the equivalent mass due to moisture for the hydrates would equate to: mono- = 2.97%, di- = 5.77% and tri- = 8.41%).

The TGA data showed that even testing the samples after storage for 10 months in a 0% RH desiccator, approximately 1% mass loss was still seen on heating for both batches. The mass loss observed could be due to moisture that could have immediately interacted with the samples as they were removed from the desiccator prior to TGA analysis. Or it could be due to the fact that all of the water within the structure could not be removed purely by 0% humidity storage.

	Percentage Mass Loss (S.D.)				
Sigma	**0 Day**	**1 Day**	**1 Week**	**2 Weeks**	**10 Months**
0% RH	3.259 (0.027)	2.354 (0.36)	1.769 (0.15)	1.867 (0.14)	0.956 (0.074)
75% RH	3.259 (0.027)	3.365 (0.11)	3.477 (0.097)	3.552 (0.126)	3.878 (0.23)
97% RH	3.259 (0.027)	3.543 (0.29)	4.833 (0.13)	5.293 (0.14)	5.775 (0.38)
Fluka	**0 Day**	**1 Day**	**1 Week**	**2 Weeks**	**10 Months**
0% RH	4.225 (0.22)	4.05 (0.19)	3.428 (0.069)	3.699 (0.061)	1.157 (0.077)
75% RH	4.225 (0.22)	4.094 (0.37)	4.237 (0.042)	4.339 (0.17)	4.047 (0.051)
97% RH	4.225 (0.22)	4.452 (0.18)	4.437 (0.22)	4.385 (0.02)	4.383 (0.14)

Table 4.10: Mass losses of the two batches of magnesium stearate stored in varying RH desiccators over a period of 10 months.

The TGA data for magnesium stearate stored under 75% RH for 10 months showed a maximum of approximately 4% mass loss on heating for both batches. Once more the suggestions made from these data concur possibly towards the samples being present in a mixture of the hydrates. Also the analyses have shown that the Fluka batch did not incorporate any more moisture when stored at 75% RH (after 10 months) as the mass loss on drying was always approximately 4%. However the Sigma batch of magnesium stearate showed an approximate 0.6% mass increase during storage after 10 months from the original measured mass loss.

When the batches of magnesium stearate were stored at 97% RH, increases in mass loss occurred during TGA analysis. The Sigma batch incorporated approximately 2.5% additional moisture within the structure after 10 months of storage. This moisture uptake did not make it any clearer as to what hydrate structure had formed as comparable XRPD traces did not alter. It was likely that there was a mixture of hydrates present.

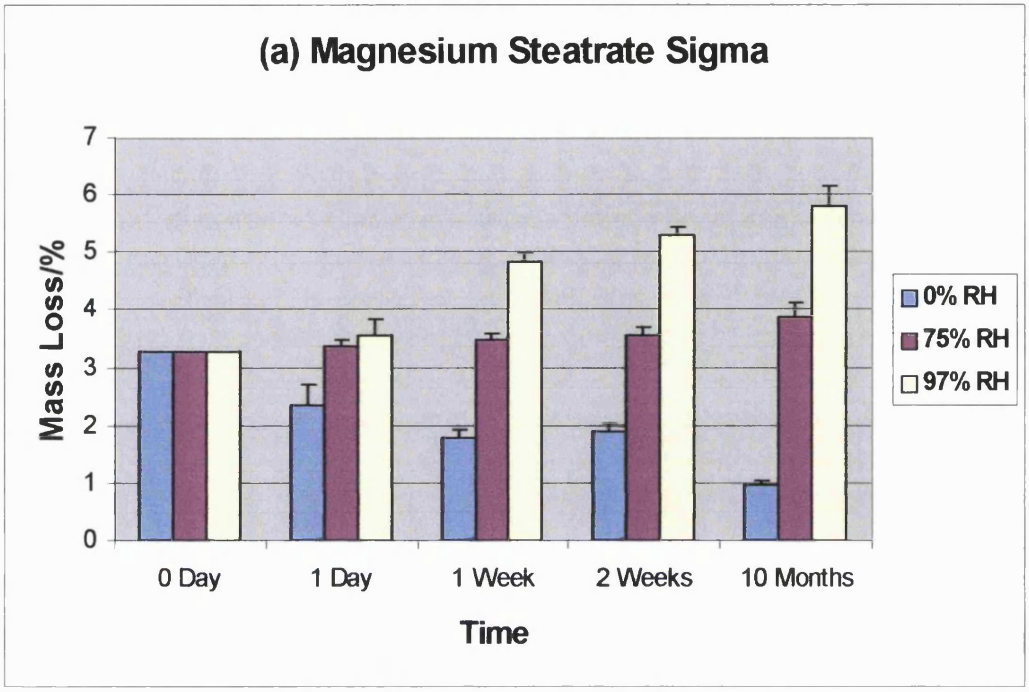

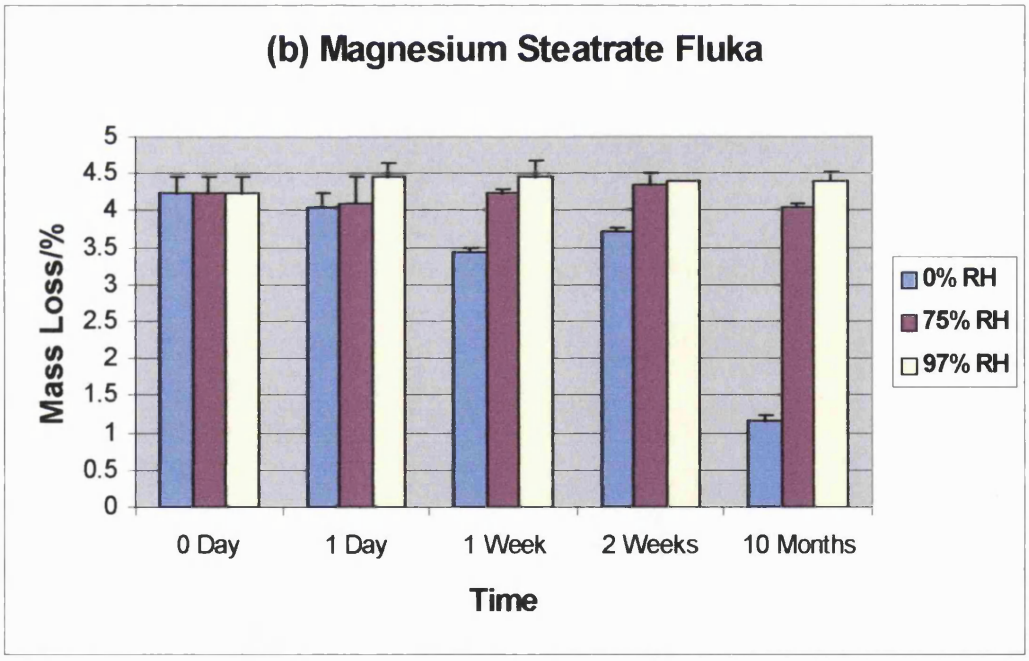

Fig. 4.33: Bar charts showing the change in mass loss over time for magnesium stearate (a) Sigma and (b) Fluka under different humidities.

The results for the Fluka batch (97% RH) did not show as large an increase in moisture uptake after 10 months storage as the Sigma batch. Only an

approximate 0.15% increase on mass loss was observed during storage. Once again magnesium stearate was probably present in a mixture of hydrate forms. TGA analysis suggested that the Fluka batch was unable to absorb any more moisture into the crystal lattice. A possible reason for this occurrence could be down to the tight packing that may be present in the original Fluka sample. The Sigma batch may have a more spacious lattice structure allowing greater freedom for the incorporation of water.

Also it must be noted that with all the TGA experiments the mass losses that were observed occurred in 2-3 steps suggesting that the batches were present in multiple hydrate states [Fig. 4.34 – example of a TGA trace]. Furthermore Bracconi *et al.*, (2003) have shown that the complete loss of moisture from commercial magnesium stearate is difficult and is a thermally activated process, usually under vacuum. However, dehydration by heating (especially at higher temperatures such as 100 °C) will alter the structure of magnesium stearate due to melting of the fatty acid chain. Therefore the problems of removing all moisture from commercial magnesium stearate samples are clearly highlighted.

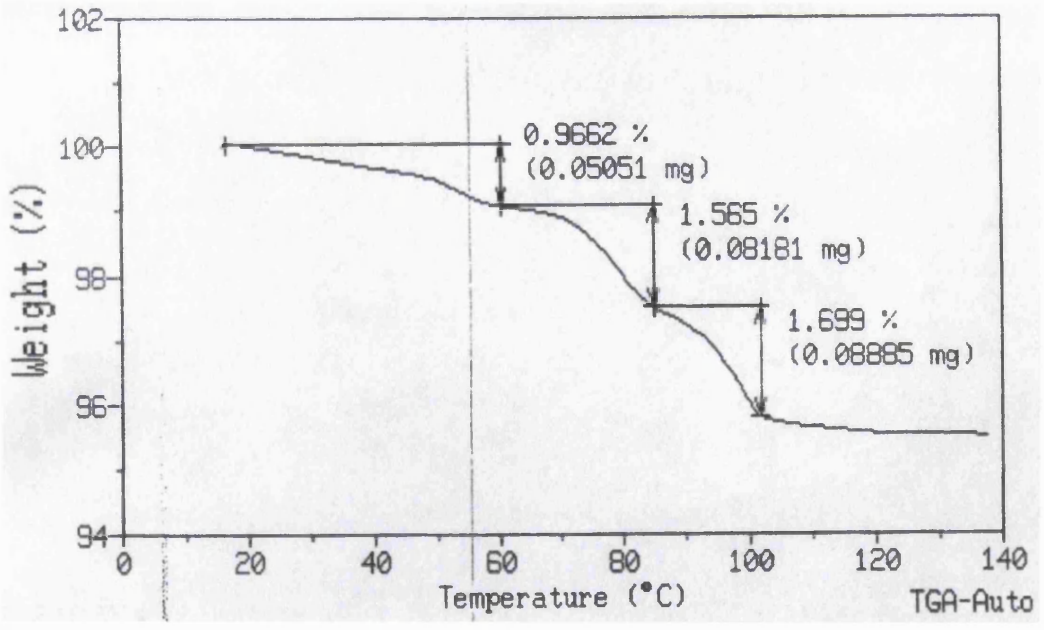

Fig. 4.34: TGA trace of magnesium stearate Fluka stored at 97% RH for 10 months.

4.5.5 Sizing And Specific Surface Area Analysis On Magnesium Stearate

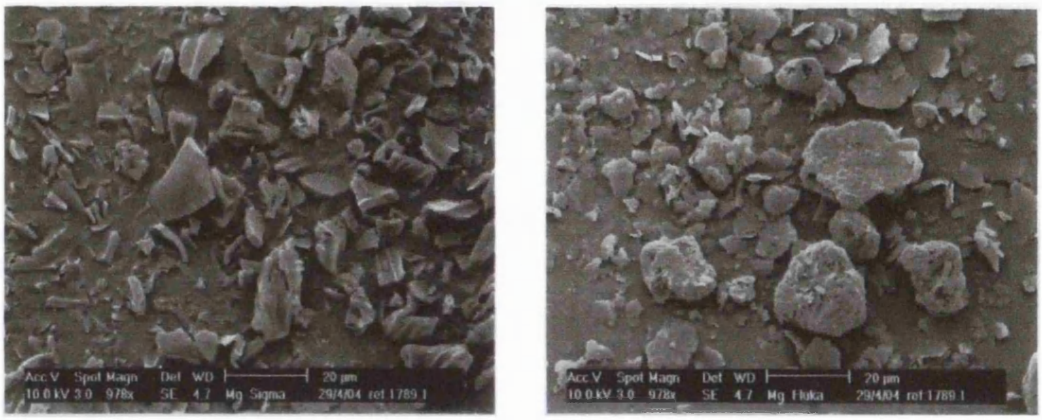

(a) (b)

Fig. 4.35: SEM pictures of magnesium stearate (a) Sigma and (b) Fluka.

The SEM traces [Fig. 4.35] for both batches of magnesium stearate showed great variation in particle size. The particles were also irregular in shape. Most of the particles for both batches suggested that the particle size was generally below 40 μm. However, no visual differences in size could be observed from the SEM scans.

Sample	x10/μm (S.D.)	x50/μm (S.D.)	x90/μm (S.D.)
Sigma	1.24 (0.006)	4.47 (0.032)	12.99 (0.142)
Fluka	1.36 (0.006)	5.11 (0.017)	17.69 (0.082)

Table 4.11: Table showing the average particle size distribution of Sigma and Fluka magnesium stearate. (Dispersion pressure = 2.0 bar [Sigma] & 1.5 bar [Fluka] using the R3 lens).

The particle sizing data [Table 4.11] corroborated the SEM pictures that most of the particles were below 40 μm. At each percentile the size distribution was lower for the Sigma batch compared to the Fluka batch of magnesium stearate. Specific surface area determination, with the use of nitrogen BET, also provided information about the two batches of magnesium stearate. The results for the Fluka batch showed the specific surface area as 19.91 m^2/g (S.D. = 1.14).

However, the Sigma batch produced a very low specific surface area value (3.12 m^2/g, S.D. = 0.028). The large difference observed may be due to the affinity of both batches to nitrogen represented by the obtained C value (adsorption energy constant – derived from the BET equation, section 1.5.5). The Fluka material showed a much lower affinity (highlighted by a low C value) to nitrogen than the Sigma sample leading possibly to erroneous results. Andres *et al.* (2001) have also found on experiments with magnesium stearate, low C values (below 5) were produced. They therefore concluded that the BET physical adsorption model was not appropriate for the 'accurate' determination of the specific surface area of such materials. Furthermore, experiments were conducted using a single-point determination due to the failure of the samples to form linear isotherms across a range of partial pressures. Andres *et al.* (2001) also found specific surface area values ranging from 8 to 45 m^2/g, thus showing the variability in data due to the inadequacies of the technique and probably also variations from batch-to-batch.

4.5.6 Conclusions

Characterisation studies of magnesium stearate Sigma and Fluka have showed that both batches are in the form of hydrates. However, it has proved difficult to say with any real confidence exactly which hydrate was present. The two batches were in fact likely to contain a mixture of hydrates. It has also proved very difficult to remove the moisture from within the two batches by storing the samples in a 0% RH desiccator over 10 months. The TGA studies have shown that the Sigma form is more likely to interact with water than Fluka magnesium stearate, possibly due to the tighter packing within magnesium stearate Fluka. SEM pictures have not highlighted any real differences in the morphology of the two samples and the specific surface area data cannot be greatly relied upon due to the difficulties in obtaining any useful information. However, the sizing data have shown that the Sigma particles are smaller than the Fluka particles. This could possibly provide another reason for the increased interaction with water by the Sigma batch.

5. RESULTS & DISCUSSION

Investigating The Interaction Of Powder Surfaces With Solvents Of Different Polarities Using Dynamic Vapour Sorption

5.1 Introduction

Dynamic vapour sorption has developed into a technique that has become utilised prominently within the last few years. The assessment of crystal changes and hygroscopicity can easily be measured using the DVS apparatus. Studies have been conducted to understand the interconversion of magnesium stearate hydrates (Swaminathan & Kildsig, 2001), the conversion of a di-sodium salt to a more stable hydrate form (Hodson *et al.*, 1996) and the application of a method to screen compounds for hygroscopicity and polymorphism when developing lead compounds within the pharmaceutical industry (Balbach & Korn, 2004). Also within chapter 4 the DVS has been used to show the conversion of anhydrous to hydrate forms of theophylline and calcium mupirocin.

Numerous research papers have highlighted the value of the technique at showing the recrystalisation of amorphous nature within compounds when exposed to water vapour. Lactose has proved to be a popular material of choice for such investigations. Buckton and Darcy (1995) have showed that a physical mixture containing as little as 0.05% amorphous content can be characterised by such a gravimetric approach. The crystallisation process of lactose has also been studied with an NIR probe linked to the DVS apparatus to follow the process in real time (Lane & Buckton, 2000), which is in contrast to a stand alone NIR technique (Buckton *et al.*, 1998) where structural changes cannot easily be followed as they occur. Others researchers have also used the combined technique of DVS-NIR to observe the crystallisation of salbutamol sulphate (Columbano *et al.*, 2002) and raffinose (Hogan & Buckton, 2001). DVS has

further been successfully employed to identify and quantify low levels of amorphous nature (Mackin *et al.*, 2002a; Mackin *et al.*, 2002b). Mackin *et al.* (2002b) have been able to characterise as low as 0.5% amorphous nature as long as the compound did not form hydrates or solvates. They also highlighted that with DVS experiments a fully homogenous mixture of amorphous/crystalline sample is not required. However, with for example XRPD, a homogenous mixture is essential as only a portion of the entire sample is analysed.

The effects on recrystallisation after milling and micronisation have been followed on salbutamol sulphate (Brodka-Pfeiffer *et al.*, 2003; Young & Price, 2004) and on revatropate hydrobromide (Ticehurst *et al.*, 2000). All these studies involved water vapour as the surface probe. The DVS apparatus has been used in many other aspects. These include temperature effects on water sorption of hydrogels (Kim *et al.*, 2003), study of water damage on cement based materials (Johannesson, 2002), plasticising effect of water on poly-DL-lactic acid (Steendam *et al.*, 2001) and investigating the effects of wet granulation on two forms of cellulose (Buckton *et al.*, 1999). Furthermore a methodology has been reported (Wilson & Beezer, 2003) to allow parameters such as equilibrium constants (K), van't Hoff enthalpy change ($\Delta H(v)$), Gibbs free energy for sorption (ΔG) and the entropy change for sorption (ΔS) to be calculated. This method could only be applied to samples that would not change i.e. no amorphous nature or polymorph change during experimentation.

All the above investigations have been dependent on using water vapour as the probe. There has been very limited work on the substitution of water for other organic probes within the DVS apparatus. This is quite surprising due to the valuable information that could be obtained about the wettability of powder surfaces if probed with different solvents. Most of the limited work on using organic solvents in the DVS has been conducted by the instrument manufacturers themselves, Surface Management Systems (SMS). SMS have shown the usefulness of the DVS to measure the BET surface area of lactose (Williams & Levoguer, application note 18). They provided an alternative method to the traditional means of measuring surface area; a volumetric technique using nitrogen and sometimes krypton or argon. However, they successfully used

octane vapour to determine the surface area of lactose gravimetrically. The advantages that were created included the undertaking of experiments at ambient temperature (300 K) as opposed to standard low temperatures (77 K - due to the need to be close to the boiling point of the probe), and smaller sample sizes could be used (100 mg as opposed to at least 1 g). The work conducted by SMS suggested that only alkane probes should be used as there would be a likelihood of adsorbate-adsorbate interactions with polar probes. SMS have also conducted experiments using methanol as the organic probe (Levoguer & Booth, application note 5). They showed the study of high concentrations of organic vapour on activated carbons, and concluded that such investigations are only possible/feasible if equilibration at each partial pressure step does not take too long.

5.2 Aims

The aims were to probe the powder surfaces of a hydrophilic (calcium mupirocin) and a hydrophobic drug (nabumetone) with solvents covering a full range of polarities to measure the degree of interaction with the probes, thus providing information on the nature and wettability of the compounds and their surfaces. The extent of interaction would be determined using the BET theory developed in 1938 by Brunauer, Emmett and Teller (Brunauer *et al.*, 1938). Furthermore the effects of the probes were to be investigated on micronised batches of the two drugs. This would allow the opportunity to assess whether the technique could show the effect of pharmaceutical processes that would be expected to change the nature of the surface, and would be representative of those that might take place during the development of a drug. It was important to understand the interaction of compounds with solvents for a number of reasons:

- The compounds often meet organic solvents during production and processing that may change their nature either at the surface (most likely) or in the bulk.
- Strong interactions with solvents can lead to changes in polymorphic form.

- An understanding of the nature and interactions of surfaces can aid development of the compound.

Two further compounds (theophylline and magnesium stearate) were also similarly investigated. In this case the aim was to evaluate the potential of the technique as a methodology for screening batch-to-batch variations in a model drug and excipient by highlighting any differences between the two batches of the compounds (Sigma and Fluka), both of which were supplied by Sigma-Aldrich, Poole, UK.

The goal was to create plots of BET interaction versus solvent polarity. It was hoped that this would provide a profile relating to the wettability of the compounds over the selected polarity range. Producing such a plot would then hopefully allow the opportunity to predict how probes of other polarities would interact with the drug in question. The overall aim, depending on the effectiveness of the technique, was to allow the rapid screening of 'New Chemical Entities (NCE's)' in industry to highlight any potential problems that could be faced during processing and possible undesirably strong interactions with certain probes, as well as offering a route to understanding issues that may arise during the development of assets.

Prior to conducting the studies it was hypothesised that hydrophilic compounds would interact greatly with the polar probes and less so with probes with reducing polarity [Fig. 5.1]. Consequently the opposite was expected for hydrophobic compounds. However, the strength of interaction with the probes would depend on the properties of the compound being investigated also. A strongly hydrophilic compound would naturally have greater interactions with polar probes than a weakly hydrophilic compound. However, a compound that does not wet easily would struggle to interact with any of the probes no matter what their polarity. Nevertheless, there would be a limited amount of wetting as it is not possible for a compound to not wet at all. The nature of the slope would also provide information about a compound. A steep slope would seem to suggest that the surface of a compound has a greater affinity to one polarity of vapours (more polar/non-polar) than another. However, a shallower slope would

suggest that the compound surface interacts more easily with both polar and non-polar sets of probes. A surface that does not wet would not show any adsorption to any polarity probe and a flat line would be observed.

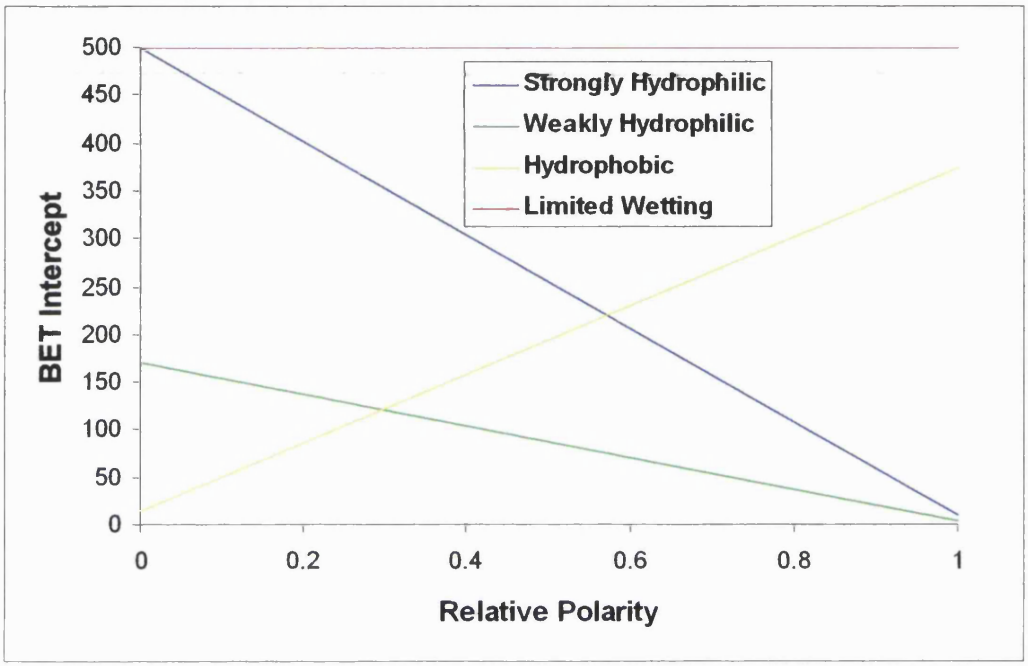

Fig. 5.1: Graph showing the predicted BET plots for compounds of different characteristics.

5.3 Methods

Name & Model: Dynamic Vapour Sorption Analyser 1
(Surface Measurement Systems, London, UK)

5.3.1 Introduction

Dynamic vapour sorption (DVS) was introduced in 1994 and is a powerful method to investigate properties of the surface of powders. It is a gravimetric technique that can also be used to detect changes in crystallinity (Buckton & Darcy, 1999). When water is added to an amorphous system, T_g can be lowered to allow rapid crystallisation due to sufficient stimulation of molecular mobility.

This can take place, with systems such as the DVS apparatus, by controlling the temperature and relative humidity (RH) that a sample is exposed to.

DVS allows the examination of the moisture/vapour sorption (absorption, adsorption and/or desorption) kinetics on powders over a range of humidities for any length of time. Measuring the mass changes that take place during water sorption and desorption at such varying relative humidities can produce sorption isotherms.

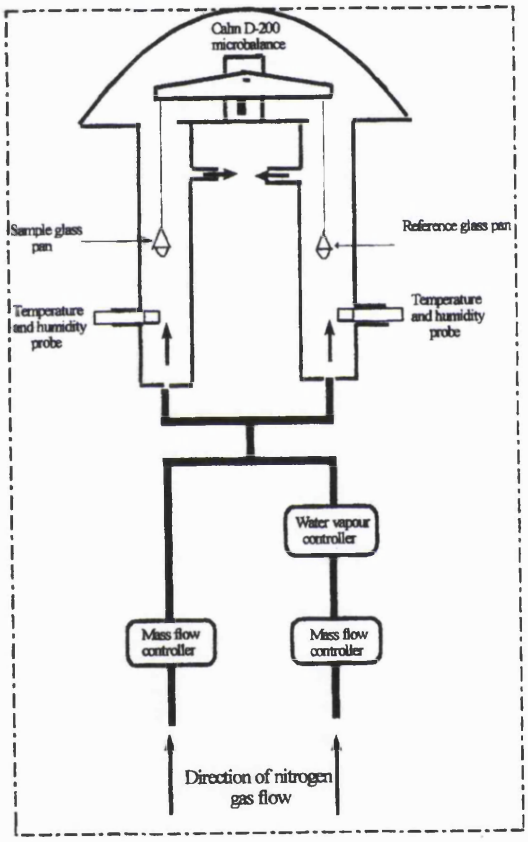

Fig. 5.2: Schematic diagram of the DVS apparatus (Dove, 1998).

Mass changes are detected by an ultra-sensitive Cahn microbalance, which is housed inside the DVS [Fig. 5.2]. The DVS analyser itself is held inside a thermal incubator to maintain the apparatus at a constant temperature throughout the experiment (25 °C – 80 °C). The sample and the reference (empty pan) are exposed to a continuous flow of specific relative humidity. This humidity is achieved by controlling the ratio of dry nitrogen and water saturated nitrogen

(saturated by passing through a water reservoir). The system can be set up to create relative humidities between 0% and 98%.

Experiments can be run in step mode, where the percentage RH remains constant until the next RH step begins. The steps can last for pre-determined time limits or can proceed to the next stage (dm/dt method) when the mass has remained constant for a set amount of time (5 min). Alternatively a ramp method can be selected to replace the steps, where the percentage RH is constantly changing.

5.3.2 Methodology

All experiments were conducted using a sample mass of 30 mg (+/- 10%). The mass of the sample should not have an effect on the overall results obtained, as the probe vapours should be able to interact with all of the molecules in given time. The total mass uptake would be affected but the percentage uptake should remain constant. The accuracy of the Cahn microbalance as stated by the manufacturer was +/- 10^{-4} mg.

In experiments where probes of varying polarity were used, the solvents had to continually be changed for different tests. The old solvent was removed, and the container washed with the new solvent. Then a fresh batch of the solvent was added. The DVS was run for 24 hours with no sample at 50% RH. (The desired humidity, for example 50%, was achieved by flowing a mix of 50% wet and 50% dry nitrogen over the sample.) This allowed the system to be completely washed from the old solvent before running an experiment. When solvents other than water were used the humidity probes were removed to avoid irreversible damage. The solvents used were distilled water, methanol, ethanol, propan-2-ol, butan-1-ol and hexane.

Most experiments were run for 180 or 240 min for each 0.05 P/Po (partial pressure) in/decrement up to 0.35 P/Po. It must be noted that the term relative humidity can only be applied when water was used as the solvent. The term partial pressure must be applied when other solvents are utilised. Also with all the DVS figures where water was not the probe used, RH stands for partial

pressure. Sample pans were washed using water, rinsed with absolute alcohol and dried prior to re-loading.

DVS experiments were also conducted on calcium mupirocin whilst attempting to maintain the hydrate, so as to have data that could be compared against the results produced from anhydrous calcium mupirocin. This was conducted in two ways:

1) DVS experiments were begun from 0.15 P/Po so that the hydrate was hopefully never removed.
2) A flow of lithium chloride salt solution (11.3 % RH at 25 °C - Nyqvist, 1983) was flowed through the sample side (where the RH probe would have been positioned). This would allow a constant flow of humidity to prevent hydrate loss at partial pressures below 0.1.

Finally experiments on theophylline were also conducted at higher partial pressures (0.3-0.65 P/Po) to investigate the wettability of the compound in comparison to the data that would be obtained at the standard experimental partial pressures (0-0.35 P/Po).

All experiments were run using the RH step method at 25 °C. The accuracy of the system was +/- 1.0% for the RH and +/- 0.2 °C for the temperature. All experiments were run in triplicate (unless otherwise stated).

5.3.3 Calibration

Calibration and maintenance of the DVS involved three procedures:

1. Defrosting of the incubator every month. This ensured the desired temperature of the incubator was maintained with greater accuracy. Defrosting took place by raising the temperature of the incubator to 50 °C.

2. Weight calibration was conducted every month, if the apparatus was switched off or when the operating temperature was changed. A 100 mg weight was used as the measure.

3. RH calibration was conducted every six months with the use of salt solutions. Magnesium chloride (provides 32.8% RH at 25 °C) and sodium chloride (provides 75.3% RH at 25 °C) salt solutions were used (values obtained from Nyqvist, 1983). The salt solutions were each placed in the sample pan and the RH elevated to over 5% of the deliquescence point for the solution. Then slowly the RH was brought down until no mass changes were observed. The RH values for this occurrence with each salt solution were noted and entered into the software's RH table. Finally using an empty pan the RH of the system was raised to 35% (adjustable setting in controller box). Readings for the sample and reference probes were observed and any differences were adjusted from the controller box to read the correct value. The same process was repeated for adjusting the 80% RH setting from the controller box.

Similarly flow rate and temperature settings can also be adjusted from the controller box (usually by a qualified engineer).

5.3.4 Probe Selection & BET Analysis

The probes were chosen on the basis to cover the full polarity range. Also it was important to try and select solvents that were within the same series. Unfortunately this was not possible, as each series of solvents would vary in polarity only within a specific range. Trying to obtain probes from each end of the polarity range would involve using solvents that would not be part of the same series. Also the probes had to be chosen to ensure they were safe to use with the machinery.

The probes selected for the DVS studies were (relative polarity values in brackets); Water (1), methanol (0.762), ethanol (0.654), propan-2-ol (0.546) and

hexane (0.009). Relative polarity of solvents has been derived from spectroscopic measurements. Solvent-sensitive standard compounds can absorb light in spectral ranges such as ultraviolet (UV) and visible light. One method derives values from the transition energy of the long wavelength absorption band (UV/visible) of the pyridinium-N-phenoxide betaine dye. The relative polarity is simply defined as the transition energy of the dissolved betaine dye. It is possible to make visual estimations of solvent polarity due to most spectral changes occurring within the visible region. For example, the solution colour of betaine dye is red in methanol and violet in ethanol. Due to the insolubility of the pyridinium-N-phenoxide betaine dye in non-polar solvents, the more lipophilic penta-tert-butylsubstituted betaine dye is used as a secondary reference probe. This method of deriving solvent polarity has been discussed in great detail by Reichardt (1988), and a table of the relative polarities of 271 organic solvents can be found in the text. Relative polarity is an arbitrary value that has no units. The extreme reference solvents are tetramethylsilane (0) and water (1).

It was decided to use 3 alcohols (methanol, ethanol and propan-2-ol) as the probes from within the same series. Water and hexane were also chosen as probes as their relative polarity values fell at the extremes of the range. Also structurally water contains an –OH bond similar to the alcohols, although it behaves very differently.

The results at the end of each partial pressure stage were treated to mathematical manipulation, producing BET plots (as described in the equation in section 1.5.5). The number of moles of vapour adsorbed was divided by the total dry mass of the sample, to ensure variability of sample size was not affected. Thus the plot consisted of:

X axis:- P/Po

Y axis:- (P/Po)/[Moles/G(1-P/Po)]

P/Po = Partial pressure of the solvent (analogue of RH).

Moles/G = Weight gain by the compound taking into account the molecular mass of the solvent.

Moles = Mass change due to uptake of solvent/RMM of the solvent.

G = Dry mass of the sample.

The Y-axis derivation is simply a mathematical rearrangement of the original equation for the Y-axis part [P/Vads (Po/P)]. The volume adsorbed (Vads) parameter was replaced by Moles/G. The idea here was that each of the probes has a defined molecular volume. Since this was so, measuring the number of moles adsorbed was a surrogate for measuring the volume adsorbed. However each of the probes has a different molecular volume so expressing them in terms of volume says nothing about the number of molecules adsorbed whereas expressing in terms of moles would directly be related to the number of molecules. This in turn allowed:

1) The different probes to be compared on the same basis independent of their size.
2) The interaction force per molecule to be isolated.

As the different probes are different sizes a monolayer will comprise of a different number of molecules of each probe. Expressing the adsorption in terms of moles means that there is a comparison of all the probes in terms of the same number of molecules, since by definition a mole comprises the same number of molecules.

5.4 Results & Discussion

5.4.1 Measuring The Wettability Of Calcium Mupirocin

Investigating the interaction of probes on compounds using the BET theory relies on the fact that predominantly adsorption takes place on the surface of interest. Any significant absorption into the material will cause the isotherm produced to deviate from that of a typical type II or IV isotherm (required for BET analysis). As stated in the introduction (section 1.5.5) the BET theory applies to the monolayer region of adsorption. This is expressed as a linear line and is commonly only observed over the partial pressure range of 0.05-0.35.

For the solvents methanol, ethanol, propan-2-ol and hexane, a standard DVS adsorption plot was seen such as that shown for ethanol [Fig. 5.3]. After the 0 P/Po drying stage (complete loss of dihydrate as shown by the approximate 3% mass loss), each 0.05 P/Po increment showed a step wise mass increase related solely to adsorption of the probe on to the powder surface. A similar mass loss was observed during gradual reduction of the partial pressure back down to zero.

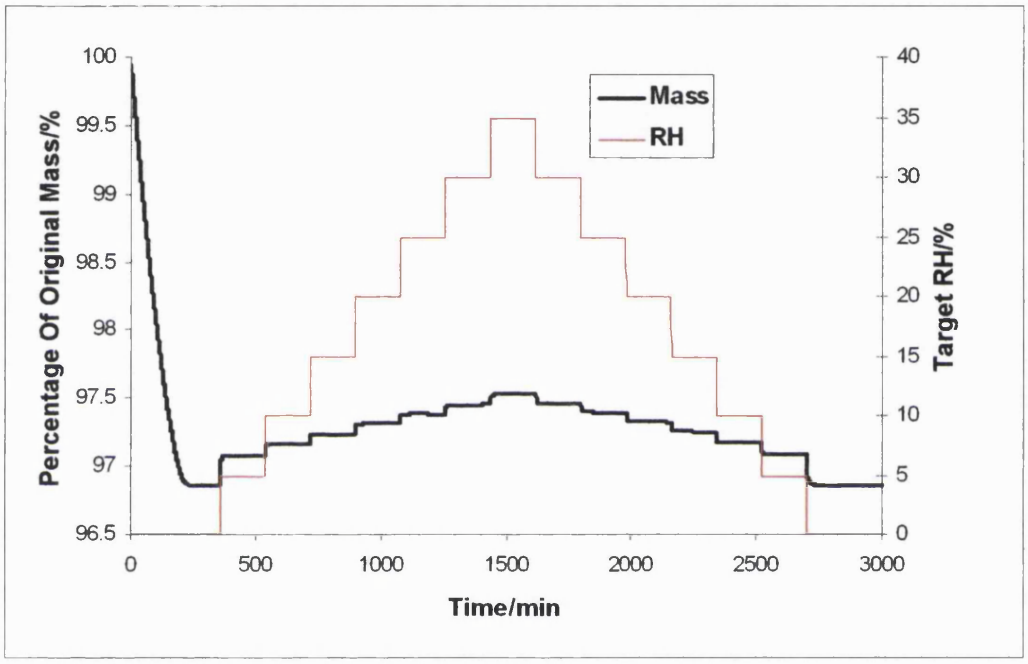

Fig. 5.3: DVS plot of calcium mupirocin probed with ethanol.

The only probe where results such as those seen for ethanol were not attainable was for experiments with water [Fig. 5.4]. As already reviewed in the last chapter (section 4.3.2), when calcium mupirocin was exposed to water it easily changed crystal structure from the anhydrous to dihydrated form. The DVS plot with water showed that initially at the 0% RH step the remaining water within the crystal was removed. With increasing humidity steps dihydrate formation inevitably proceeded. Dihydrate formation was complete by 15% RH, with the greatest moisture uptake transpiring at 10% RH. The remainder of the humidity steps up to 35% suggested that purely adsorption on to the surface was occurring. During reduction of the relative humidity within the system, the calcium mupirocin sample showed losses suggestive of desorption only from the powder

surface up to 5% RH. When the RH was finally reduced to 0%, the dihydrate rapidly vacated the crystal.

There would be a problem creating a BET plot for calcium mupirocin probed with water due to poor linearity as absorption has taken place within the compound as well as adsorption. Consequently there would be no value in comparing the BET data of water against the other solvents used. The only manner in which the water data could be analysed would be if a BET plot was created from 0.20 to 0.35 P/Po. However this plot would show the surface characteristics of the dihydrate and not the anhydrous form (which is how data from the other probes have been generated). All BET data from this point on will not include any data regarding the effects with water. Attempts of analysing calcium mupirocin as a dihydrate crystal, (as opposed to the anhydrous form), will be discussed later (section 5.4.5).

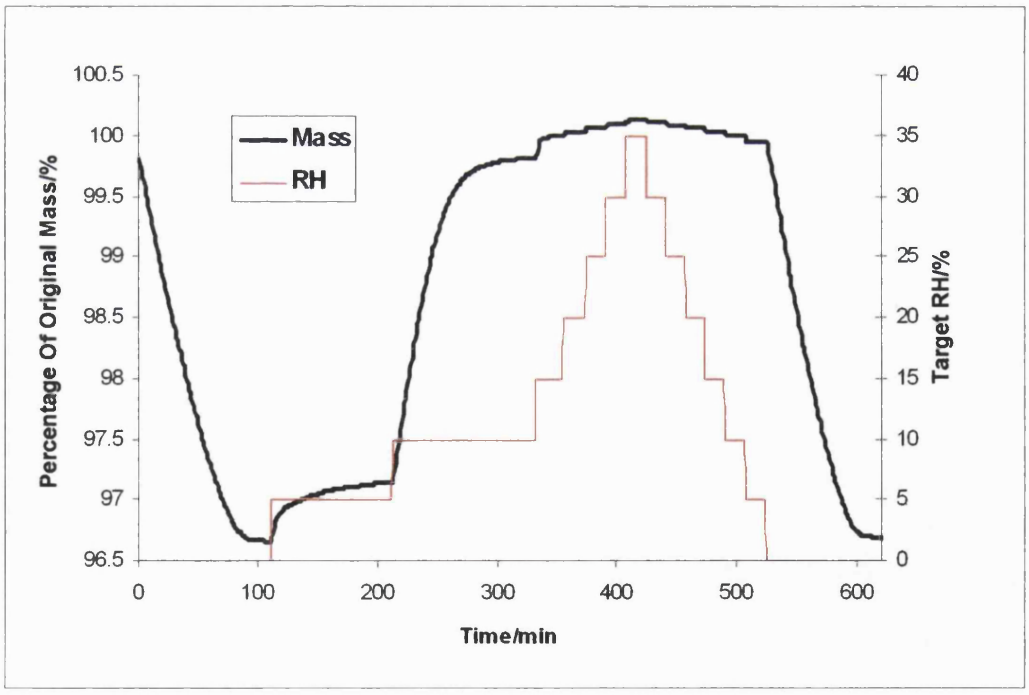

Fig. 5.4: DVS plot of calcium mupirocin probed with water.

The DVS results [Fig. 5.5] of calcium mupirocin probed with the chosen solvents showed an interesting trend. All the plots showed good linearity with the R^2 value always above 0.98. This suggested that the use of the BET model was

appropriate for this set of results. The least amount of adsorption took place when calcium mupirocin was probed with hexane and the greatest amount of adsorption was with methanol (Y-axis shows the inverse value of adsorption). Ethanol and propan-2-ol followed in a similar pattern, with the more polar probe (ethanol) adsorbing onto the surface with a greater affinity than propan-2-ol. Hexane, compared to the three alcohols, adsorbed onto the surface of calcium mupirocin much more poorly. Hence, such a high BET value was obtained with hexane as the probe. This could be due to one of two reasons or even more likely both. Firstly, as calcium mupirocin is a hydrophilic compound it would be natural to assume that there would be greater interaction with species that were also hydrophilic. Secondly, due to the surface of calcium mupirocin not being homogenous wetting by larger molecules may be more difficult. Therefore hexane may interact to a lesser extent than methanol.

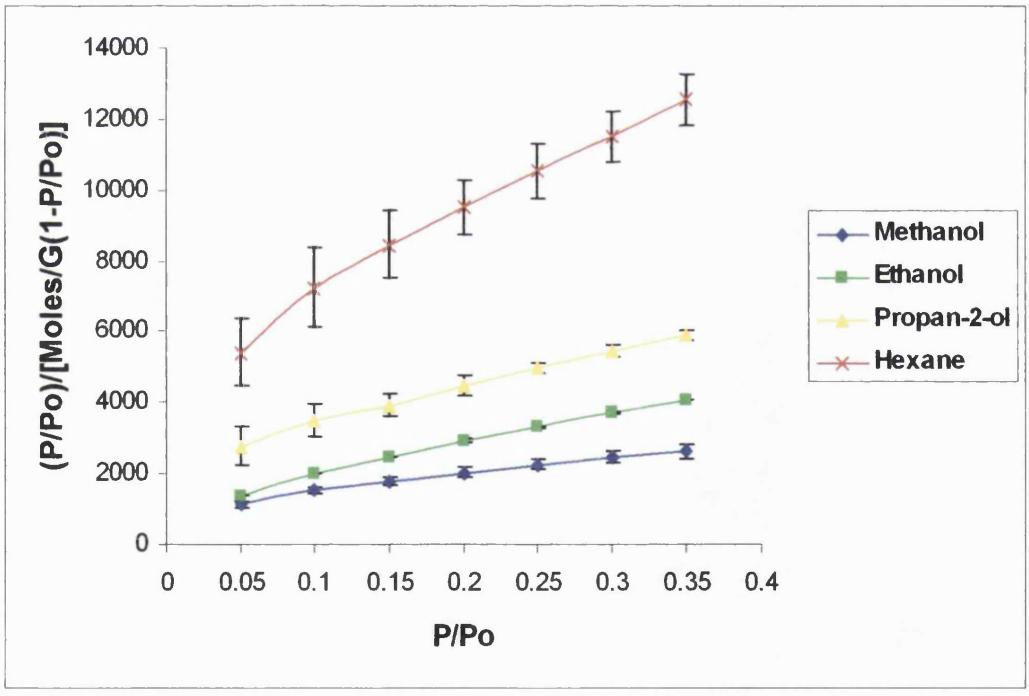

Fig. 5.5: Graph showing the BET plots for calcium mupirocin probed with the different solvents (water data has been excluded).

It must also be noted that there was a greater degree of standard deviation with the hexane results than the other probes. This could probably be accounted for by the fact that lower amounts of the probe were being adsorbed and thus the

sensitivity of the machine was playing a greater role. Overall, the BET plots showed that as the polarity of the probe used decreased, its subsequent BET value increased. This was due to the fact that with less polar solvents the increase in mass caused by adsorption to the powder surface was smaller (Y-axis shows the inverse value of adsorption). Therefore, there was a greater interaction between calcium mupirocin and methanol than that with hexane.

The graph [Fig. 5.6] showed that as the polarity of the probe was increased, the value for the BET intercept decreased. This again suggested that calcium mupirocin wetted with greater ease with more polar solvents such as methanol than with hexane (very low polarity). The R^2 value for the set of data points was very high, although not as high as the desirable confidence level of 0.99. Using this graph as a guide the BET intercept value could be estimated for any polarity probe, assuming there was no absorption between the solvent and calcium mupirocin.

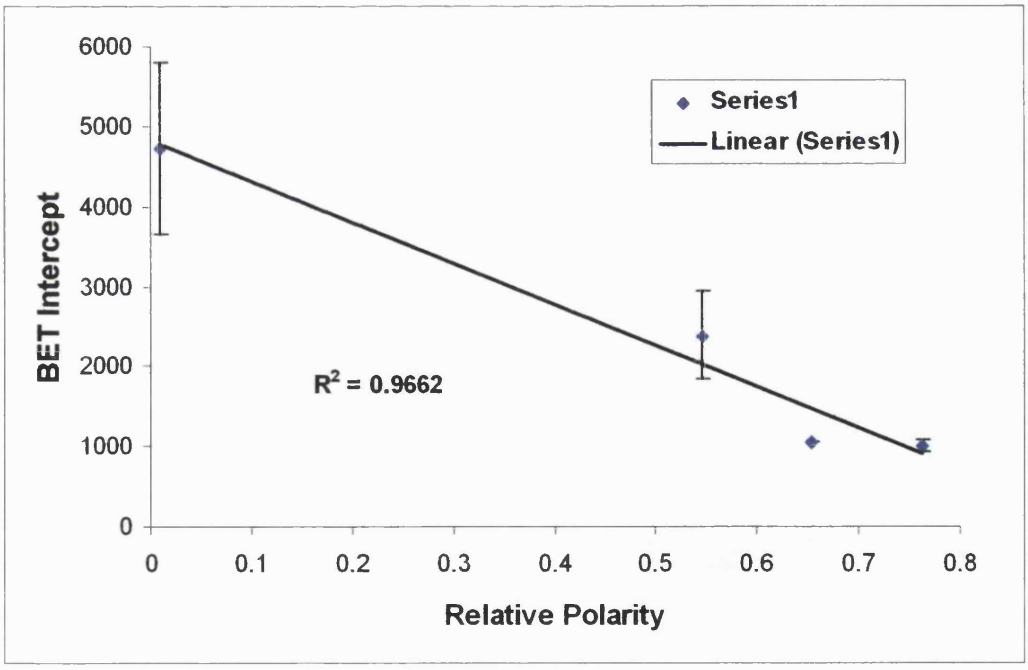

Fig. 5.6: Graph showing the plot of BET intercept versus the solvent polarity.

5.4.2 The Wettability Of The Probes On Micronised Calcium Mupirocin

Investigations into the measurement of amorphous nature in micronised calcium mupirocin proved inconclusive with the techniques employed (XRPD, HDSC and SolCal – Section 4.3.2). It was interesting to observe whether any changes in surface nature could be detected by DVS and how the data may differ when analysed using the BET equation.

The results [Table 5.1 & Fig. 5.7] showed that the micronised batch interacted more greatly than the non-micronised form with all the selected solvents. This would be as expected due to the increased specific surface area of the particles during micronisation and possibly any amorphous nature that may have been created. Water data have been included to show that even though hydrate formation took place there was still a difference in the uptake of moisture for all three sets of data.

	Probe Uptake (mol/g) (S.D.)		
Probe	**Non-Micronised**	**Micronised**	**Micronised 1 Year**
Water	1.97×10^{-3} (7.07×10^{-6})	2.01×10^{-3} (8.62×10^{-6})	1.98×10^{-3} (1.41×10^{-5})
Methanol	2.06×10^{-4} (1.39×10^{-5})	3.22×10^{-4} (2.08×10^{-6})	3.05×10^{-4} (3.22×10^{-6})
Ethanol	1.33×10^{-4} (7.07×10^{-7})	1.65×10^{-4} (1.16×10^{-6})	1.55×10^{-4} (2.65×10^{-6})
Propan-2-ol	9.15×10^{-5} (2.26×10^{-6})	1.17×10^{-4} (4.04×10^{-6})	1.07×10^{-4} (5.77×10^{-7})
Hexane	4.30×10^{-5} (2.55×10^{-6})	4.60×10^{-5} (5.66×10^{-7})	4.71×10^{-5} (6.27×10^{-6})

Table 5.1: Table showing the quantity of probe uptake by calcium mupirocin (the final column shows the results of a batch tested after it was micronised a year ago).

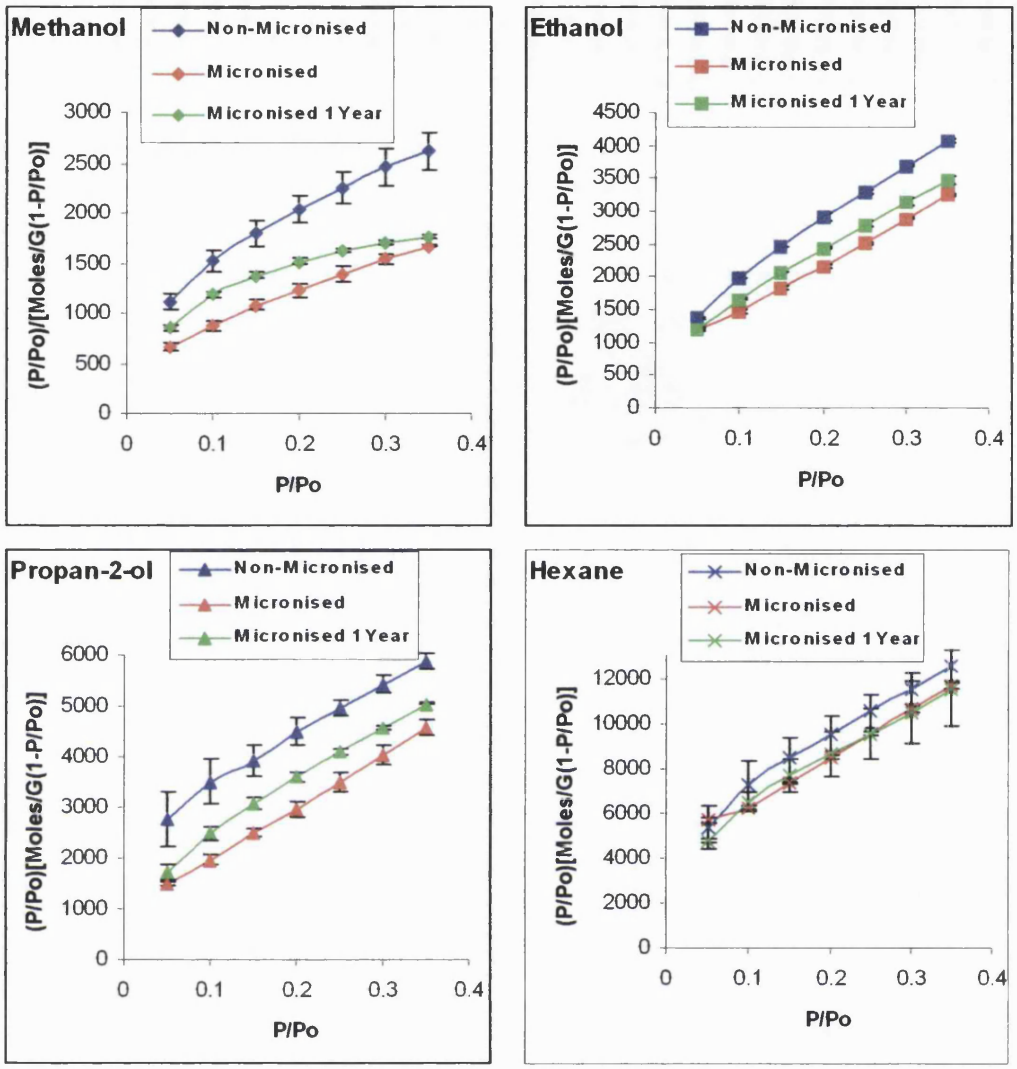

Fig. 5.7: BET plots showing the surface interaction of non-micronised and micronised calcium mupirocin with all the probes (except water).

When similar DVS experiments were conducted on the micronised sample one year later, the wettability of the compound had decreased, although not as low as that seen for the original calcium mupirocin (non-micronised). This was important as it tended to suggest that the reason for increased probe uptake was not solely due to the increased specific surface area of the particles. The difference between the two micronised sets of data suggested that the compound was recovering over time. This must be linked to the surface energy of the two batches. The activity of the surface must have decreased over time such that the interactions with the probes also decreased towards that seen for the non-

micronised sample. Therefore although techniques such as SolCal and HDSC (section 4.3.2) were unable to detect any amorphous nature within the compound, the DVS data suggested there was some difference in surface characteristics that had changed over time.

All the BET plots for the two micronised batches of calcium mupirocin showed very good linearity, usually a R^2 value of above 0.98. As a result, once more the use of the BET equation was found to be suitable for these data. Statistical analysis (ANOVA) was conducted on the data [from Table 5.1] to corroborate the visual interpretations made. ANOVA showed that there were significant differences between the three sets of data (non-micronised, micronised and micronised 1 year) for each probe. The *p*-value obtained was below 0.05 for water (0.014), methanol (<0.001), ethanol (<0.001) and propan-2-ol (<0.001), confirming a significant difference at the 5% significance level. However, for hexane (0.646) the *p*-value was above 0.05 and thus as suggested there was no measurable difference between the three groups. Also ANOVA was utilised to show statistically if differences were present between the adsorption values for each probe. A value of below 0.05 confirmed that there were significant differences in adsorption of all the probes.

The graph [Fig. 5.8] showing the BET intercept against the relative polarity of all three batches of calcium mupirocin showed interesting data. It was clear that higher BET values were obtained for the non-micronised samples than the micronised batches, as there was less interaction with all the probes (Y-axis shows the inverse value of adsorption). This was as expected due to the reduction in particle size and probable formation of amorphous nature on the surface of micronised calcium mupirocin. Apart from the hexane results it was also observable that the micronised batch had recovered when the DVS experiments were repeated a year later. This was characterised by the reduced wettability of the 1 year old micronised batch as opposed to the freshly micronised batch.

The linearity of the plots provided a very good R^2 value of above 0.95. This suggested that such a plot could be used to help predict the behaviour of solvents

of other polarities if their relative polarity was known. However, at closer inspection it seemed as if the hexane data were distorting the line of best fit that was produced for all three calcium mupirocin batches. The standard deviation values for the hexane plots were high and were in fact overlapping between the three sets of data. This was possibly due to the fact that with the very low quantities of adsorption seen with this probe, there was a greater degree of error due to the sensitivity of the machine itself.

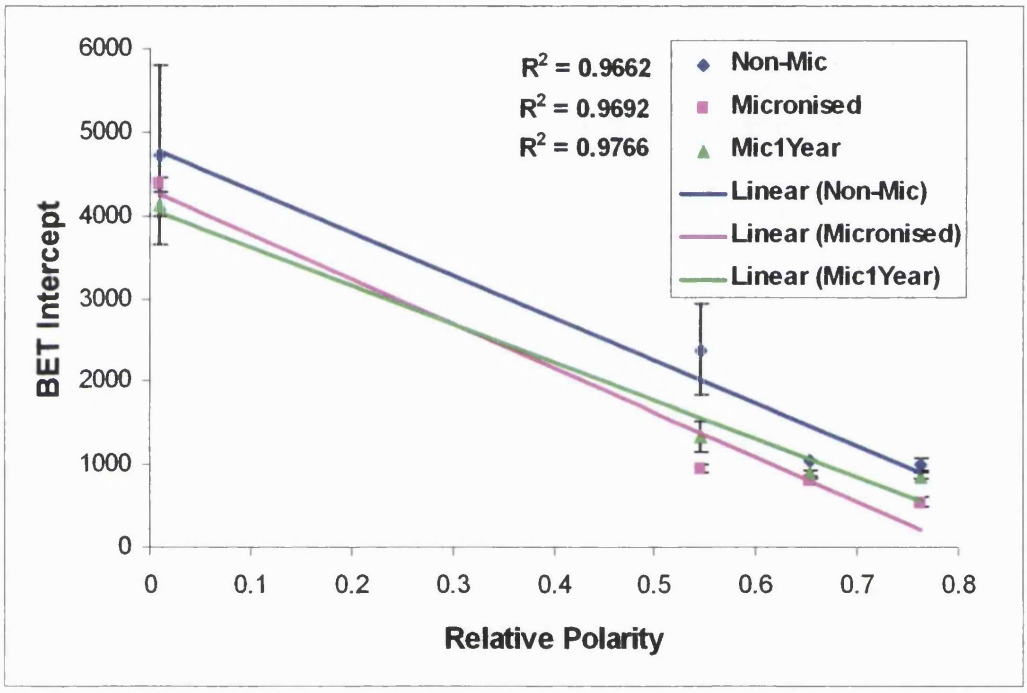

Fig. 5.8: Graph showing the plot of BET intercept versus the solvent polarity for all three batches of calcium mupirocin.

A plot of only the alcohol data [Fig. 5.9] removed the uncertainties caused by the hexane results. Only the R^2 value for the freshly micronised batch improved. The R^2 values for non-micronised and 1 year old micronised calcium mupirocin decreased. This may partially be explained by the fact that only three data points were used for each plot. Thus an odd set of results accounting for just one data point could change the R^2 value drastically. However, analysis of the data in this manner was important as information was obtained on a true homologous series of solvents. This should provide the most accurate set of data that could be used for prediction of the behaviour of interaction of other alcohols. The largest

difference highlighted was for the propan-2-ol data between the micronised plots and the non-micronised plot. This suggested that micronisation must have changed the surface character of the material in terms of the polarity of the functional groups residing on the surface.

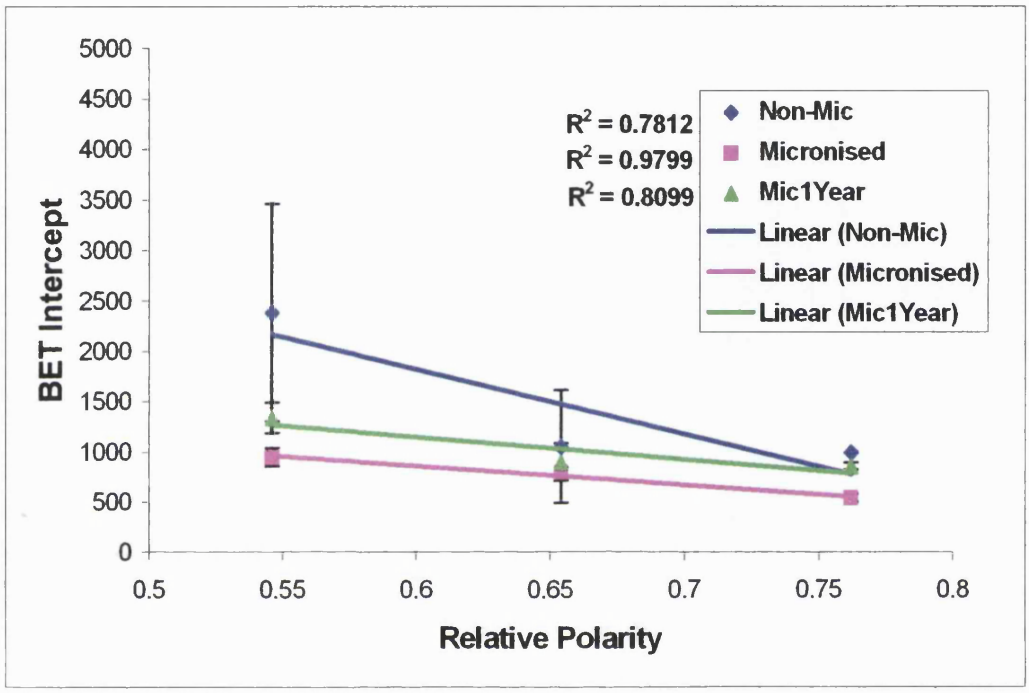

Fig. 5.9: Graph showing the plot of BET intercept versus the solvent polarity of calcium mupirocin probed with only the alcohols.

5.4.3 Use Of The BET Plots To Predict The Interaction Of Butan-1-ol

Having created BET plots for calcium mupirocin with the set of alcohols it was important to test the efficiency of the technique in predicting the BET intercept value with another alcohol. Butan-1-ol was selected as it was not extremely volatile and was obtainable in the form of a liquid at normal room temperature. The relative polarity value for butan-1-ol was 0.602 (Reichardt, 1988). Experiments were conducted with non-micronised and 1 year old micronised samples of calcium mupirocin. A freshly micronised sample was not tested because conditions during micronisation of a new batch may be different to the original micronised sample. As a result the properties of the sample, such as amorphous content and specific surface area, may vary. As there was a

measurable difference between non-micronised and 1 year old micronised batches of the drug, a comparison between the aforementioned samples would be sufficient for such a test.

It was hypothesised that both forms of calcium mupirocin would show a reduced interaction at the surface with butan-1-ol than ethanol or methanol. However, there would be greater interaction than that observed with propan-2-ol. This was predicted as butan-1-ol had a higher relative polarity value than propan-2-ol even though it was a longer chained alcohol. Propan-2-ol was less polar than butan-1-ol due to the increased stabilisation of the $-CH_3$ groups surrounding the –OH group. This was in contrast to the stabilisation effect by the $-CH_3$ groups in butan-1-ol as they were all acting from one direction.

	BET Intercept (S.D.)		
Sample	***Predicted***	***Actual***	***Difference***
Non-Micronised	1800	1681.15 (123.11)	118.85
Micronised 1 Year	1120	1090.25 (6.58)	29.75

Table 5.2: Results showing the predicted and actual BET intercept values for calcium mupirocin probed with butan-1-ol (n = 2).

The results showing the interaction between calcium mupirocin and butan-1-ol [Table 5.2] have corroborated the predictions made prior to investigations. The non-micronised batch did produce a higher BET value and consequently lower amount of adsorption to the surface than the micronised sample. Also the predicted values of the intercept did closely agree with the actual values. The correlation was very high with the 1 year old micronised calcium mupirocin. There was a larger difference between the predicted and actual values for the non-micronised batch. However, this difference was still within the standard deviation value obtained for the actual reading, thus emphasising the usefulness of the technique.

The graph [Fig. 5.10] showed that with the butan-1-ol data added, the linearity of the set of points reduced. The methanol data was now out of place in the plot. Although there was a large difference (nearly 0.1) in the relative polarity of methanol and ethanol, methanol did not interact as strongly with the surface of calcium mupirocin as expected. This suggested that there might possibly be a larger influence, than first expected, of probe size rather than just relative polarity. A threshold limit may be reached where the –OH group does not have as great an effect, in terms of interacting with the surface of calcium mupirocin. This, as discussed earlier, may be due to the greater effect of the carbon chain within the probe structure as well as the increased size of the solvent molecule. The effect of one carbon or two carbons (as in methanol and ethanol respectively) may not exert a great difference in wettability onto the surface. Also the largest differences observed between the non-micronised and micronised data were with the butan-1-ol and propan-2-ol results. Therefore micronisation must have changed the surface character of calcium mupirocin to allow greater wetting by less polar probes.

The orientation of the probe molecule when it adsorbs onto the surface and the nature of the adsorbent surface (including porosity) could also help answer the trends observed in Fig. 5.10. Methanol, ethanol and butan-1-ol could interact with the surface in two directions; vertically or horizontally. However propan-2-ol could only interact in one position as the –OH group is shielded from all other directions. Therefore it was not unsurprising that propan-2-ol showed the least interaction with calcium mupirocin than the other alcohol probes. With the remainder of the alcoholic solvents, the ability to wet the surface vertically as well as horizontally allowed greater interaction to take place. However, butan-1-ol did not show as strong an interaction as ethanol and methanol. If methanol, ethanol and butan-1-ol only interacted in a vertical orientation then it would be expected that the interaction of all three probes would only be affected by its relative polarity. However, butan-1-ol may not be able to interact with the pores of calcium mupirocin (as well as methanol and ethanol) as it may not be able to reach certain pores due to the larger size of the probe molecule. The effect of pore sizes may not exert as great a difference between methanol and ethanol interaction due to the smaller size of the aforementioned particles.

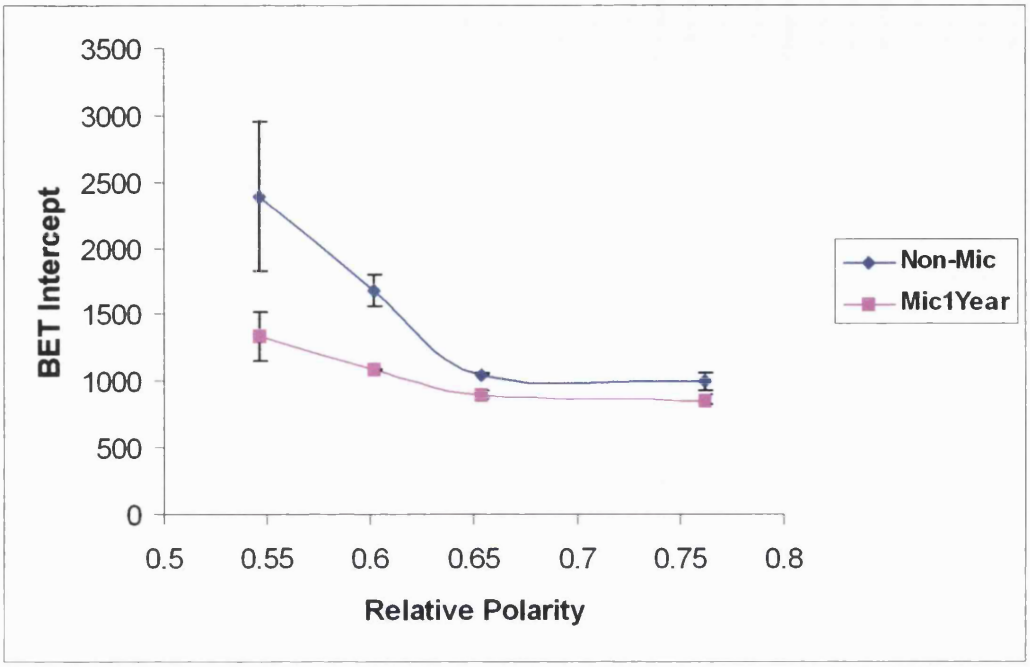

Fig. 5.10: **Graph showing the plot of BET intercept versus the solvent polarity of calcium mupirocin probed with the original alcohols and butan-1-ol.**

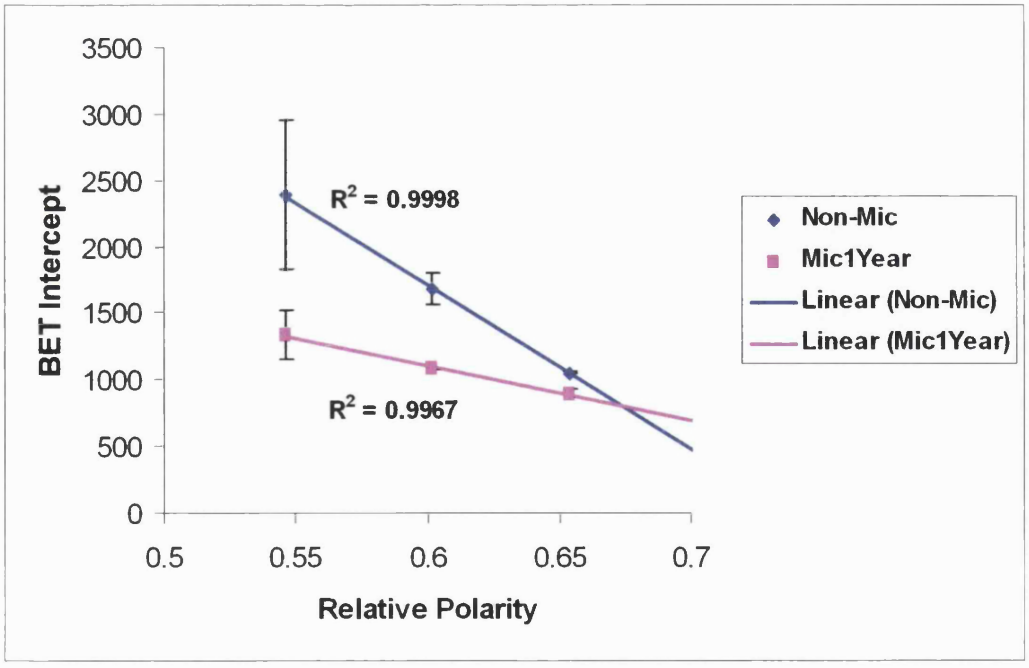

Fig. 5.11: **Graph showing the plot of BET intercept versus the solvent polarity of calcium mupirocin probed with all the alcohols except methanol.**

Removal of the methanol data points [Fig. 5.11] showed extremely good correlation between the sets of data. In fact the highest R^2 values were obtained for any set of data analysed using the DVS to understand the surface characteristics of calcium mupirocin. This highlighted the fact that the methanol data may interact in a different manner to the remainder of the alcohols employed for the experiments.

5.4.4 Comparison Of Perfusion Calorimetry Data With DVS Results

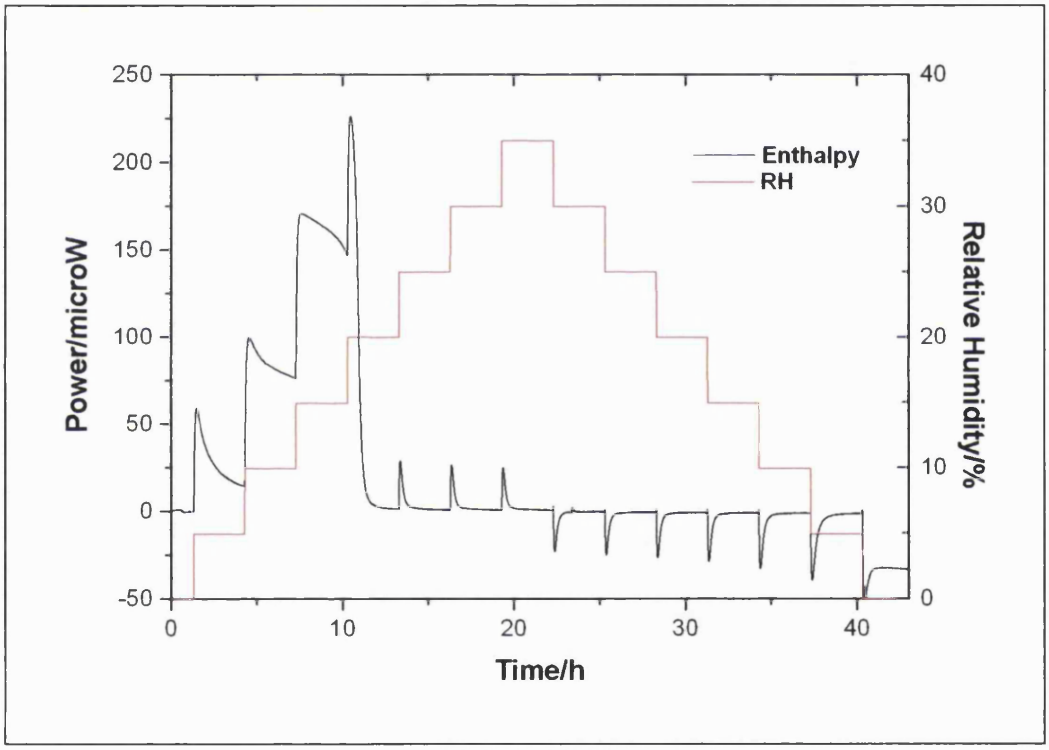

Fig. 5.12: Graph showing the enthalpic responses of calcium mupirocin when probed with water.

Perfusion calorimetry was conducted in the TAM to explore whether a link could be established with the DVS data already discussed. A few points must be noted prior to discussion of the results obtained. Firstly, the micronised data could not be directly compared to the micronised or 1 year old micronised data from the DVS. This was because the micronised form of calcium mupirocin was tested, using perfusion calorimetry, over the course of 16 months. Such a length of time was taken to obtain the data because of the large experimental time (3-4 days) for

a single experiment; due to calibration for each run, the slower kinetics as compared to the DVS tests and the availability of the instrument. Secondly, experiments were not conducted using hexane and water as probes. Hexane was omitted as it could corrode the seals within the perfusion unit. Water [Fig. 5.12] was also excluded due to the inability of the enthalpic reactions returning to baseline within a feasible amount of time, during hydration/dehydration at the specific relative humidities.

As can be seen from Fig. 5.12, the exothermic responses from the initial 5-15% RH stages did not return to baseline within the three hours step time. Also the endothermic response during the final 0% RH stage failed to reach baseline. It was clear that these responses would take a great length of time to return to baseline. This was not investigated further as hydrate formation data was not required.

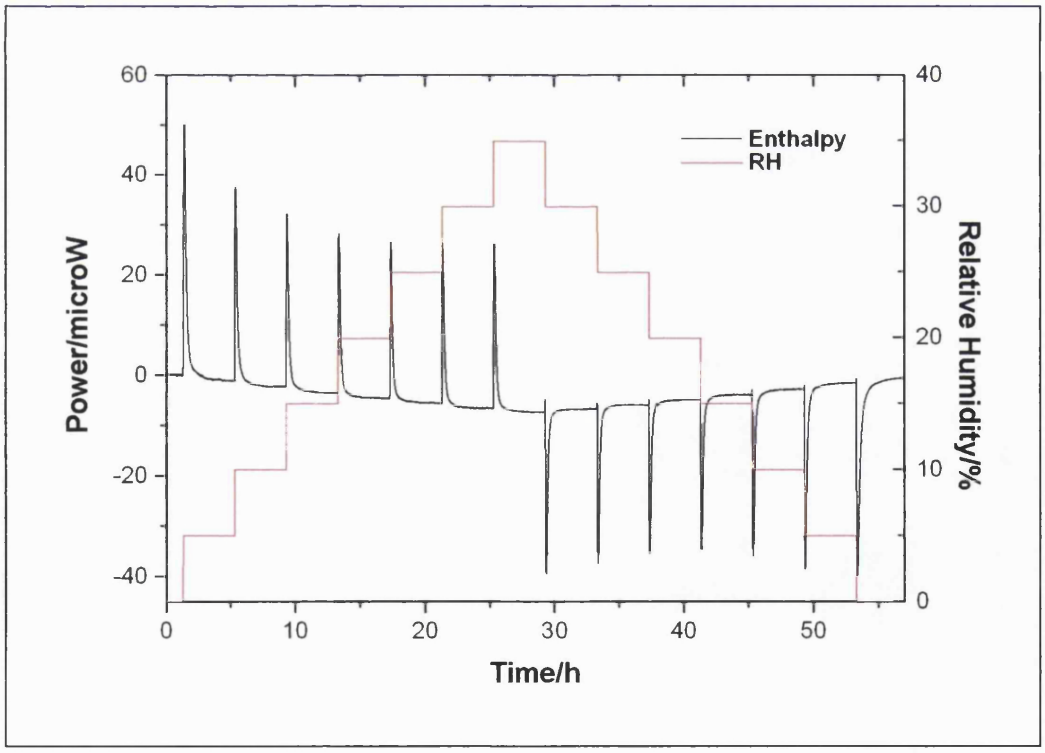

Fig. 5.13: Graph showing the enthalpic responses of calcium mupirocin when probed with propan-2-ol (methanol and ethanol interacted similarly).

The three alcohol probes provided responses within each of the three hour stages. The responses were small due to only adsorption taking place on the powder surface, as shown by one example [Fig. 5.13].

The results obtained from perfusion calorimetry [Table 5.3 & Fig. 5.14] did show some trends similar to that observed from the DVS tests. Methanol interacted with the surface of the drug the greatest, out of the three alcohols, for both micronised and non-micronised batches. This was as expected due to the polarity of the probes, with the lower polarity probes wetting the surface of the particles the least.

	Adsorption Enthalpy Response (J/g) (S.D.)		
Probe	**Non-Micronised**	**Micronised**	**Blanks (mJ)**
Methanol	11.77 (1.75)	10.85 (0.36)	29.06 (0.45)
Ethanol	7.84 (1.33)	8.18 (0.10)	24.08 (0.23)
Propan-2-ol	5.08 (0.71)	5.88 (0.48)	6.19 (0.15)

Table 5.3: Table showing the total adsorption enthalpy associated with non-micronised and micronised calcium mupirocin, and blank runs.

It was expected (similar to the DVS data) that the enthalpies associated with adsorption onto the powder surface would be greater for the micronised sample than the non-micronised form. This was definitely the case with the data for propan-2-ol as the probe used. The *p* value obtained for the *t*-test was less than 0.05, i.e. a statistical difference was observed between the two batches. However, the methanol and ethanol data did not show the same trend. The plots for non-micronised and micronised forms of ethanol were very similar and a change was only seen at 0.35 P/Po. With the methanol data a change was observed from 0.25 P/Po. The non-micronised batch showed a higher enthalpy of adsorption than the micronised form. There is no rationale behind such data, as even if there was no amorphous nature remaining on the surface of the micronised sample, the reduced particle size should still have resulted in a

greater enthalpy response due to the increased surface area. Also statistically there were no significant differences between the batches of calcium mupirocin when probed with methanol and ethanol (p value greater than 0.05 for the t-test).

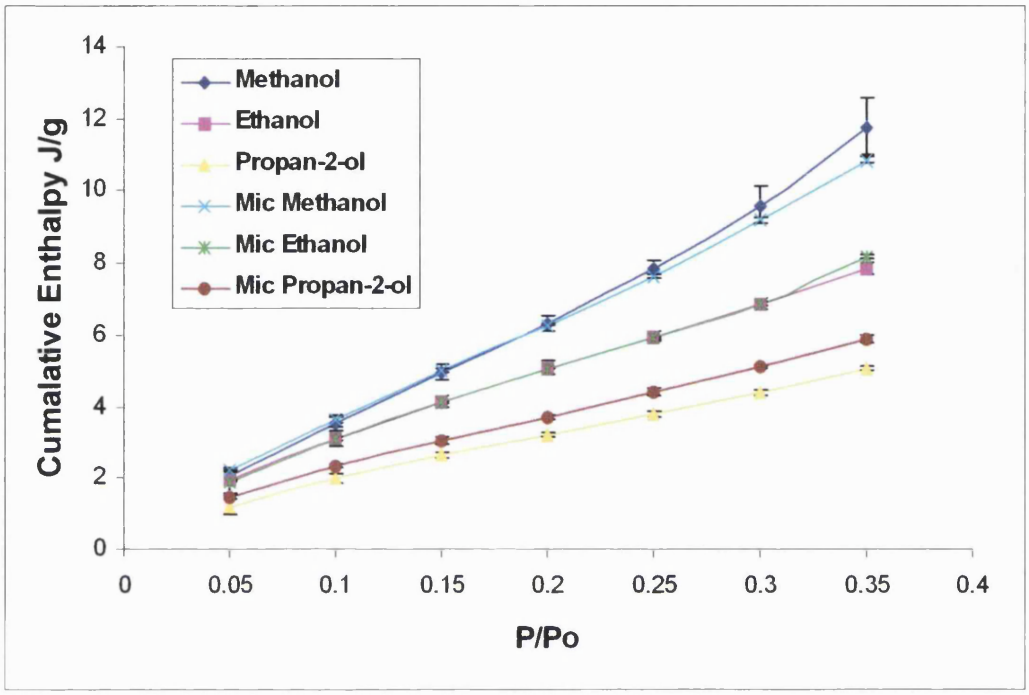

Fig. 5.14: Graph showing the cumulative enthalpy of adsorption for calcium mupirocin probed with methanol, ethanol and propan-2-ol.

Attention must also be drawn to sources of error that would affect the results obtained. These errors would be magnified especially when differences between sets of data were small (such as those shown on Table 5.3). Calculations of the enthalpic responses were subjective as the area to be measured was dependent upon the start and end of where the events were thought to occur from. Therefore the results obtained would vary each time the response was measured. This could have led to smaller or larger differences between the two sets of data. The enthalpy responses from the blank runs would also have an influence, in terms of experimental error, on the final values obtained. Overall, unlike DVS experiments, the calorimetry work did not show clear differences between the non-micronised and micronised forms of calcium mupirocin.

A plot of the perfusion data against the relative polarity of methanol, ethanol and propan-2-ol [Fig. 5.15] provided very strong linear correlation. Although the methanol data point for the non-micronised batch may not be accurate, the set of points still produced great correlation. Tests on other alcohols would have helped ascertain whether the lines of best fit could aid in predicting how alcohols of varying polarity would behave. However, due to the limitations and possible sources of error already discussed with this technique, it seems as if the DVS results in this instance would provide better results to make predictions from. Also the DVS instrument has highlighted differences between the batches of calcium mupirocin with all the probes except hexane, whereas TAM data have only shown a significant difference between the propan-2-ol results.

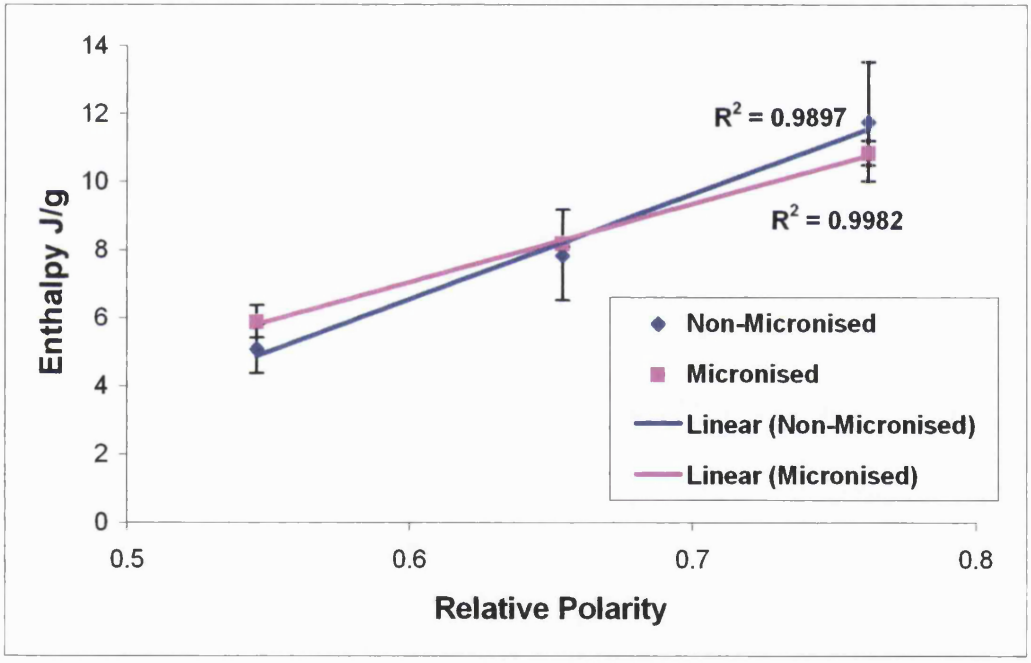

Fig. 5.15: Graph showing the plot of adsorption enthalpy against the relative polarity of calcium mupirocin probed with the alcohols (methanol, ethanol and propan-2-ol).

5.4.5 Exploration Of DVS Technique On Calcium Mupirocin Dihydrate

Studies using the DVS technique have so far showed the wetting characteristics of calcium mupirocin in the anhydrous state. However, calcium mupirocin exists as a dihydrate at ambient humidity. Therefore, it was important to attempt to

investigate how the surface of the hydrated form interacted with the probes using the same technique. With the standard DVS experiments the hydrate was automatically stripped from the compound as soon as the humidity/partial pressure was reduced to zero. Two methods, detailed in section 5.3.2, were employed to attempt to prevent hydrate loss.

The first method was to start the experiments from 0.15 P/Po. The reasoning behind this method was that it was hoped that by not exposing the sample to lower partial pressures the hydrate would not be removed. However, this method was not expected to provide much success as it was thought that when probed with solvents other than water, the hydrate would still detach due to the actual humidity in the chamber equating to 0%.

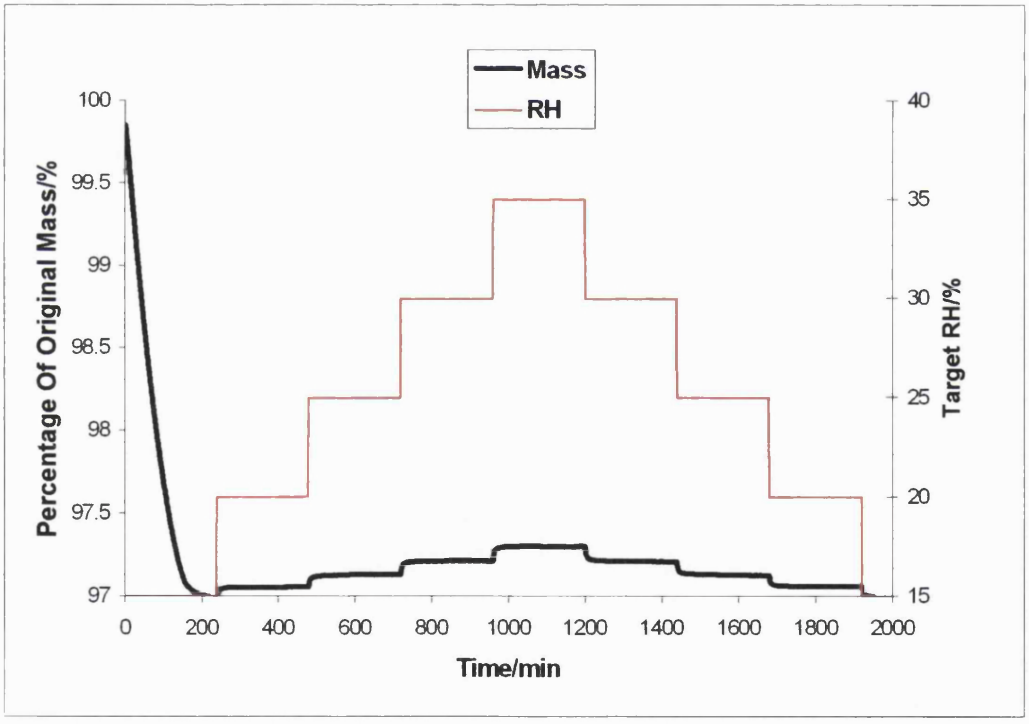

Fig. 5.16: DVS plot of calcium mupirocin dihydrate probed with butan-1-ol at higher partial pressures.

The graph [Fig. 5.16] of calcium mupirocin probed with butan-1-ol showed the immediate loss of hydrate (approximate 3% mass loss). As already discussed, the loss of bound water proceeded because of the 0% RH conditions within the

chamber. Thus the removal of moisture from the compound was the more favourable process in such an environment.

The second method involved passing a flow of lithium chloride salt solution (11.3% at 25 °C) over the sample. It was hoped that this action would prevent the loss of the dihydrate by maintaining at least 10% RH within the system (the hydrate has been shown to form easily at 10% RH with previous DVS experiments – Fig. 4.16). If the hydrate could be retained the sample could be probed by the vapours over the partial pressure range of 0-0.35, and the measure of wettability of the dihydrate could be investigated. This would provide valuable information as calcium mupirocin exists as a dihydrate under standard temperature and pressure.

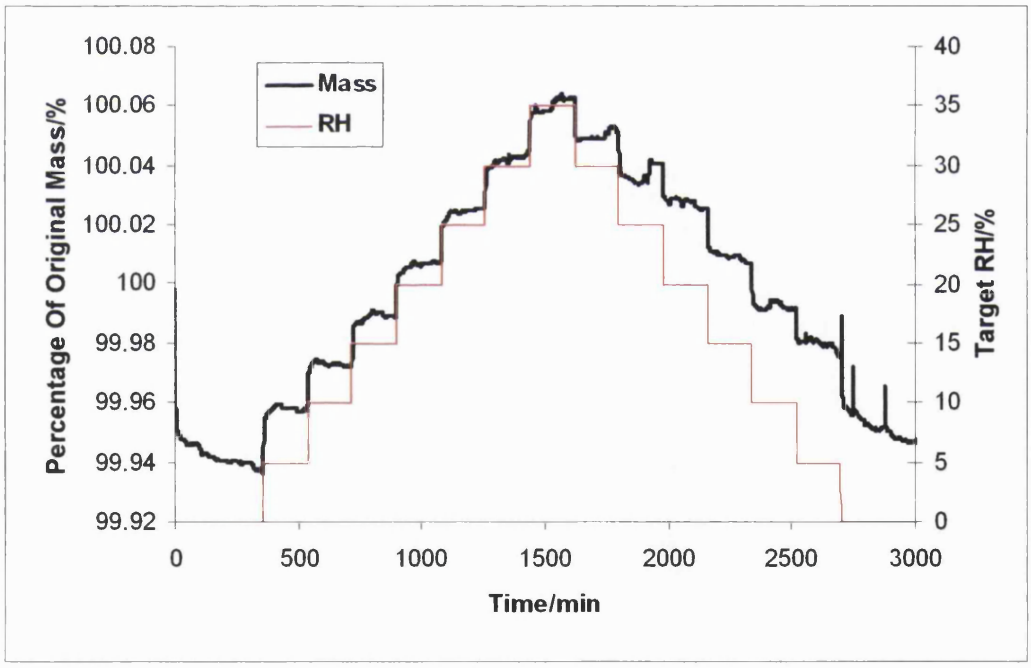

Fig. 5.17: DVS plot of calcium mupirocin dihydrate probed with butan-1-ol whilst providing a constant flow of lithium chloride salt solution over the sample.

An example of the results [Fig. 5.17] showed that the trace was not very smooth. Although the dihydrate did not seem to be stripped off from the compound, a lot of noise was seen in the traces. This made it very difficult to analyse along with

the fact that many of the traces produced were of a poorer quality than that presented here. Some of the noise created may have been due to the fact that the air was bubbling through the lithium chloride salt solution thus creating pulses. This could have been minimised by introducing a smoothing coil of some sort between the sample pan and the flow of humidity created by the salt solution. Another factor that must be considered is that of the water vapour from the salt solution itself. Although the hydrate may be retained on the calcium mupirocin particles, other water vapour molecules could further interact with the sample in the form of adsorption onto the surface. This would result in competition between the water and butan-1-ol vapour molecules, creating an environment where it would be difficult to know with certainty whether adsorption on the surface was purely due to butan-1-ol molecules or a percentage of those molecules. Bearing in mind the difficulties associated with these experiments in terms of analysis and interpretation the work was not pursued any further.

5.4.6 Exploration Of The DVS Technique With Other Compounds

Other compounds were probed with polar and non-polar vapours to investigate the effectiveness of the technique in terms of the wettability of their surfaces. Similar experiments to that seen for anhydrous calcium mupirocin were conducted on theophylline, nabumetone and magnesium stearate.

5.4.6.1 DVS Studies With Theophylline

On exposure to the pre-selected probes (0-0.35 P/Po) theophylline did not show any signs of adsorption even with water [Fig. 5.18]. Such small amounts of changes were occurring that the data were not possible to analyse. The changes observed were a combination of baseline variation and static events. Other difficulties appeared from the traces (with all the probes) such that when the partial pressure was increased a representative mass loss would be seen and during reduction of partial pressure a mass increase could be observed.

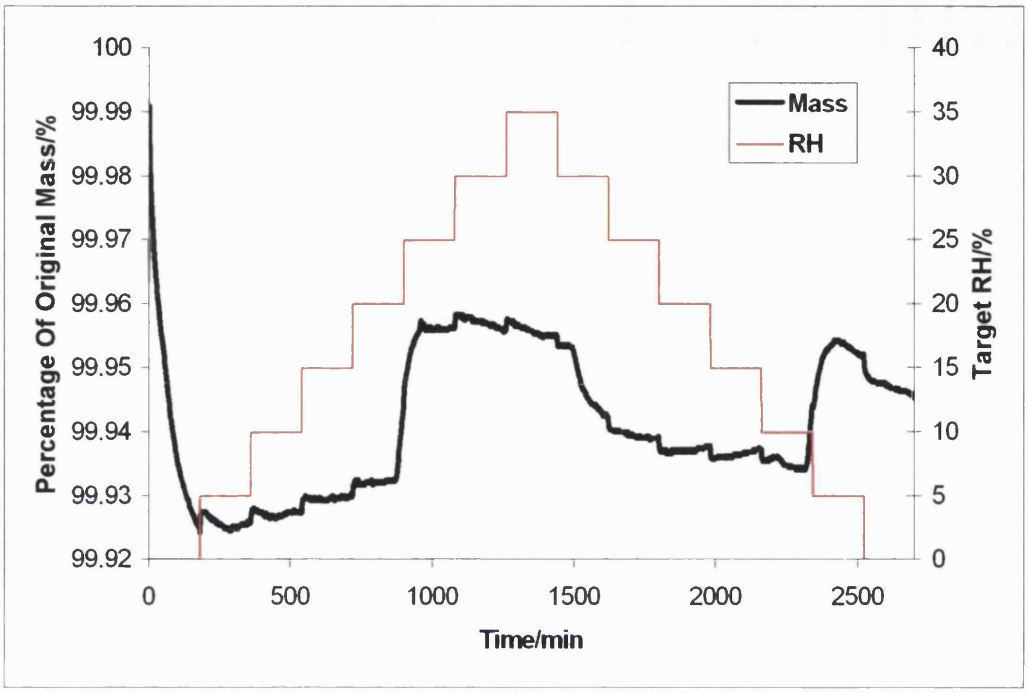

Fig. 5.18: **DVS plot of theophylline probed with water (traces for the other solvents were found to be a lot more difficult to analyse).**

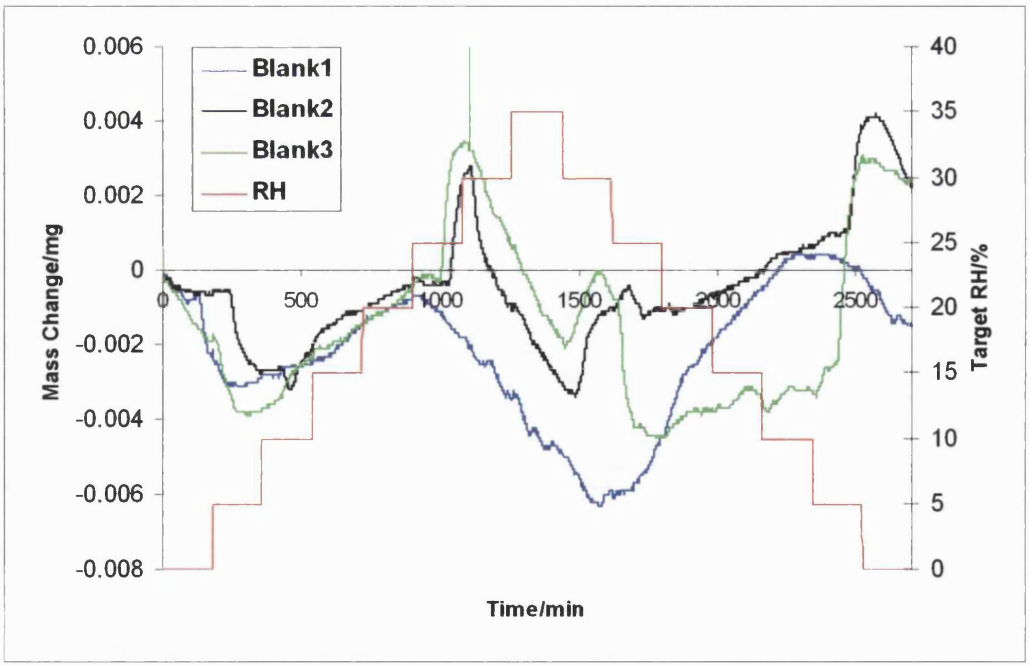

Fig. 5.19: **Blank DVS experiments probed with water to analyse the variability of the baseline.**

These events are not theoretically possible for example a mass increase or no mass change should be observed during partial pressure increases, except during crystallisation. Similarly when the partial pressure of the vapour was reduced only a mass loss or no mass change should have taken place. Blank DVS experiments [Fig. 5.19] highlighted the variability of the baseline for three runs. With each run the baseline followed a different path showing the difficulties in assessing a trace when there was a limited mass change (below 10^{-3} mg). The lack of interaction with the probes suggested that theophylline was showing signs of being poorly wettable at low partial pressures. Even trial experiments run at higher partial pressures (from 0.3-0.65 P/Po – not presented) showed no change in behaviour of the material.

5.4.6.2 DVS Studies With Nabumetone

The studies with nabumetone followed the same patterns as theophylline. It was expected that nabumetone, being hydrophobic, would interact greater with the least polar probes (such as hexane) than the highly polar probes (such as water). However, the material did not appear to wet with any of the solvents it was exposed to.

DVS plots were never repeatable and unexpected events would regularly and randomly be observed. This led to difficulties in analysing the data and therefore being able to determine any suitable conclusions about the material apart from the fact that it was poorly wettable. The DVS plot for ethanol [Fig. 5.20] highlighted some of the problems with the data produced. The changes in mass that were taking place initially were very small and fluctuating up and down. Towards 0.3 and 0.35 P/Po definite probe uptake could be seen. However, during reduction of the partial pressure the trace still suggested adsorption was taking place on the powder surface. This was impossible as the concentration of the probe was being reduced and therefore there should be no mass change or a loss of mass. It must be re-iterated that there was no reproducibility with any of the solvents probing nabumetone. It could be concluded that such a DVS technique was not suitable to investigate the surface wetting properties of nabumetone.

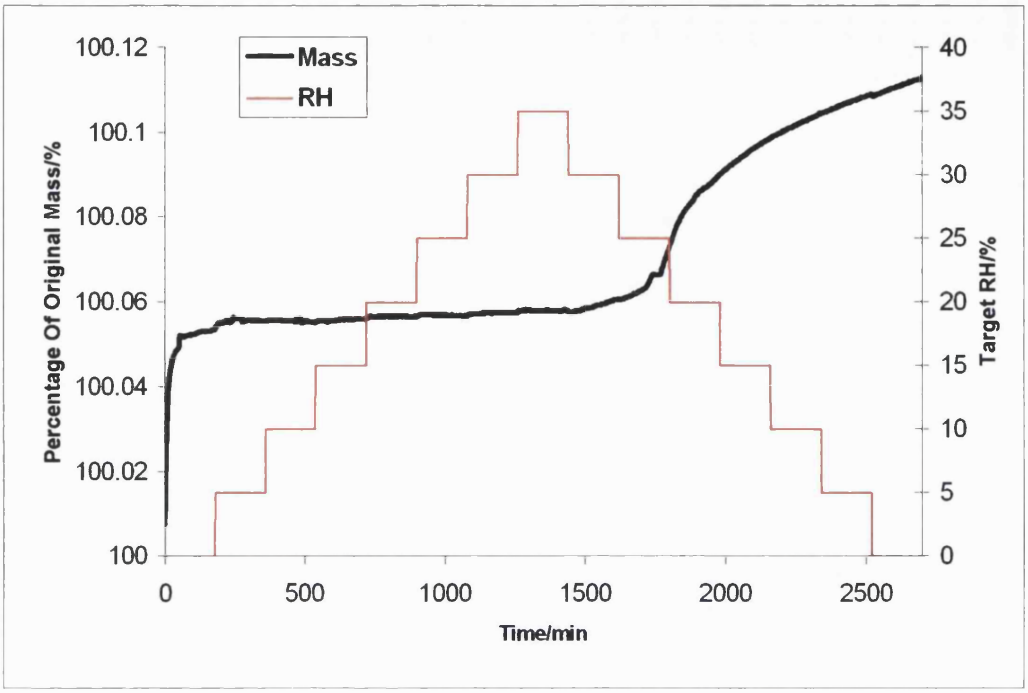

Fig. 5.20: DVS plot of nabumetone probed with ethanol (no reproducibility with the data).

5.4.6.3 DVS Studies With Magnesium Stearate

The poor wetting problems experienced with theophylline and nabumetone were not present for magnesium stearate. The DVS plots (not presented) showed clear adsorption/desorption during the different partial pressure stages. However, problems still remained in attempting to analyse the data. For accurate BET interpretations to be conducted each stage must reach equilibrium. Unfortunately due to the very slow drying rate of the compound, the initial 0% stage never obtained equilibrium within the time spans of the experiment (maximum 6 hours at 0 P/Po stage). This drying (loss of moisture) from the compound was undoubtedly related to hydrate loss. Even storing the sample in a 0% RH desiccator for 14 months before transferring to the DVS [Fig. 5.21] showed a gradual mass loss over 2000 minutes (greater than 33 hours). It may be that moisture from the environment could have interacted with the compound immediately as it was being transferred from the desiccator to the DVS apparatus, thus explaining the moisture loss observed during the DVS run. This was similar to the data obtained from DSC and TGA studies discussed in

sections 4.5.2 and 4.5.4 respectively. As already stated the complete loss of moisture from commercial magnesium stearate has been shown to be a thermally activated process, usually under vacuum (Bracconi *et al.*, 2003). However, this was not undertaken because the dehydration process by heat can change the fatty acid structure and therefore the structure of magnesium stearate would have been altered.

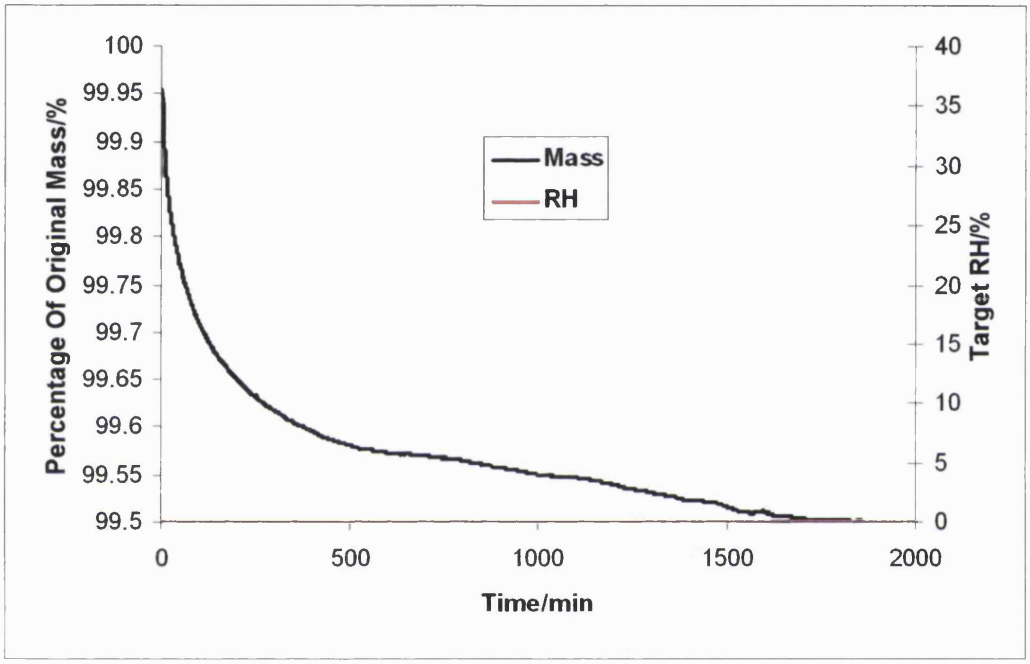

Fig. 5.21: DVS plot of magnesium stearate probed with 0% RH (water vapour).

Due to the sample never being in the dry state during the partial pressure stages, equilibration was also difficult to reach. Initially the sample would gain mass when the partial pressure was increased. After the primary adsorption, mass loss was routinely observed due to moisture still escaping from the compound, thus again preventing many steps from reaching equilibration. Also, as described in section 4.5, the DSC, TGA and XRPD studies could not differentiate between hydrate forms probably due to the presence of a mixture of hydrate states. This made it impossible to understand what form of magnesium stearate was being dealt with during the DVS experiments. Although magnesium stearate showed adsorption and desorption processes, the length of time that would be required to

reach equilibration of each partial pressure step limited the feasibility of the continuation of tests.

5.5 Conclusions

The BET equation was successfully used to measure the extent of interaction with anhydrous calcium mupirocin using probes of varying polarity, to provide important surface wetting characteristics. The isotherms produced obeyed the conditions of the BET equation that a linear plot should be produced between 0.05 and 0.35 P/Po. This allowed the manipulation of the data to produce solvent polarity versus BET intercept plots. Data obtained from water vapour was rejected due to the subsequent hydrate formation between 0.05-0.15 P/Po. The linear plot produced beyond 0.15-0.35 P/Po was not utilised due to the data then relating to the surface of the hydrate and not the anhydrous form of calcium mupirocin. Calcium mupirocin interacted greater with the more polar probes, with decreasing interaction as the polarity of the solvent reduced. Thus the surface was wetted the most with water (bearing in mind the addition of absorption due to hydration) and least with hexane. The linearity of the solvent polarity versus BET intercept plot was great, showing the potential of the technique and the appropriate usefulness of the selected solvents in terms of attempting to cover the full polarity range.

Standard techniques such as XRPD, solution calorimetry and HDSC (section 4.3.2) were unable to highlight any small amounts of amorphous nature that would have been created during micronisation. Prior to DVS studies it was assumed that the recovery of calcium mupirocin, after micronisation, was so quick that any amorphous nature produced was rapidly lost and therefore not detected by any of the aforementioned techniques. Repeating the experiments on freshly micronised material showed that there was a greater degree of adsorption with every solvent used. This was as expected due to the increased specific surface area available of the particles and the increased surface energy as a result of the production of any amorphous nature. The importance of the technique was revealed when the experiments were re-conducted on the micronised batch of

calcium mupirocin after one year. The material still showed greater surface adsorption of the solvents than that of the non-micronised batch but importantly less than the freshly micronised batch. These results confirmed that the sample was recovering over time. Therefore suggesting that the increased adsorption observed was not purely to do with the change in specific surface area but also a change in the energy of the surface.

The relative polarity versus BET intercept plots for the three batches of calcium mupirocin showed great linearity. However, on closer inspection it seemed as if the hexane data was distorting the line of best fit produced by the remaining alcohol points. It must be noted that the results, when the batches of calcium mupirocin were probed with hexane, did not show any statistical difference at the 5% significance level and there was a large standard deviation between the sets of data. The lack of adsorption difference could be attributed to the poor wetting of the surface by hexane. Consequently a new plot was created removing the hexane data. The plot produced showed purely the alcohol data. This was a more realistic plot as probes from within the same group of solvents were being compared. However, a subsequent reduction in linearity was observed for the non-micronised and micronised 1 year plots.

The strength of such a technique was highlighted when using the results to predict the likely BET intercept of butan-1-ol for the non-micronised and 1 year old micronised batches. The actual experimental values obtained were extremely close to that predicted. Although the linearity of the now four alcohol points for both batches was not great a pattern was definitely seen. The methanol data seemed out of place possibly due to the greater effect of the –OH group than for the other alcohol probes. The polarity of the –OH group may have been reduced by the longer carbon chains for ethanol, butan-1-ol and propan-2-ol, and thus the size of the interacting probe also has to be taken into consideration. Removal of the methanol data produced the best linearity seen of all the relative polarity versus BET intercept plots.

Similar studies as with the DVS were conducted using the perfusion calorimeter and proved not as successful as the data obtained from the DVS. Apart from the

methanol data the micronised sample showed a higher enthalpy of adsorption than the non-micronised batch due to the increased surface coverage of the probe. However the technique did have its limitations. The analysis was user subjective and thus if an experiment was re-analysed a slightly different answer would be obtained. The major drawback of the technique was that it took at least four days to run an experiment. This was problematic as the length of time to complete all the experiments was much greater than with the DVS, and thus there was greater recovery of the micronised batch.

Bearing in mind the advantages and usefulness of the DVS technique, certain factors must be taken into consideration when employing such a technique. The sample must not change form (hydration/solvation and crystallisation) during the test as the results obtained would include absorption and not purely be related to the adsorption of the surface. This would prevent the suitable application of the BET theory as the isotherm would deviate from a type II or IV plot. The material of interest must wet to a degree that could be measured by the DVS apparatus. If the material does not wet sufficiently (as in the case of theophylline and nabumetone) adequate data analysis cannot be conducted. The compound under investigation also has to reach equilibrium at each partial pressure to ensure completion of each stage and correct adsorption values to be obtained at each step.

Other limitations also exist with the technique. The linearity of the isotherm over the BET region needs to be very good for accurate information to be obtained from the plot. If linearity is not high, then it is impossible to assume simple monolayer coverage occurred. The recovery rate of a micronised sample must also be taken into account. For example a fast recovery rate would involve rapid testing of the sample in the DVS. Also a micronised sample that is tested in triplicate with a probe will be changing (recovering) over time, thus increasing the standard deviation of the results further. The choice of solvents will play a part in predicting the accuracy of how other solvents will interact when exposed to the compound. Solvents from a similar family will provide greater linearity for the polarity versus BET intercept plots, and thus more accurate predictions of how another solvent of the same/similar family may behave.

In summary, a plot of BET intercept versus solvent polarity can be created for certain compounds. This can be used to predict interaction of additional solvents of known polarity with the drug in question. Knowing this information can allow the selection of the appropriate solvent during processing in order to prevent certain undesirable changes to the original compound.

6. RESULTS & DISCUSSION

The Use Of Inverse Gas Chromatography To Investigate The Surface Energetics Of Powder Surfaces

6.1 Introduction

Inverse Gas Chromatography (IGC) is a gas phase technique for characterising surface and bulk properties of solid materials. A statement by Papirer *et al.* (1988) highlights the differences between conventional chromatography and IGC; "Chromatographic methods are usually applied for the separation of the individual components of a mixture; generally only limited attention is paid to the chromatographic support as long as it works satisfactorily. In inverse chromatography, on the contrary, the main interest is focused on the support so as to give better understanding of its surface properties." The earliest thoughts of gas chromatography suggested that adsorption isotherms could be determined from the breakthrough curves of gas-solid chromatography. However, the first such experiments were conducted by James and Phillips in 1954. From these initial beginnings the technique has developed to provide surface chemical characterisation of the solid surface of materials. Unlike conventional gas chromatography, IGC involves the passing of known vapours and liquids (mobile phase) through the solid material of interest (stationary phase). Williams (1991) has provided a short review and basic understanding of IGC of solid surfaces. Also Voelkel (2004) has discussed some of the most important parameters used for the description of dispersive and acid-base properties of examined materials. The principles and calculations involved with the IGC technique have been described in section 6.3.

Traditionally, surface properties of powders had been studied by gas or vapour adsorption. Adsorption was measured gravimetrically or volumetrically as a function of vapour pressure. One of the earliest methods was to place a sample

in different humidity desiccators and periodically measure the mass changes that took place to produce isotherms. These isotherms were then utilised to obtain surface area, porosity, thermodynamics and kinetics of adsorption. However, such a method was time consuming and labour intensive. IGC is a method where rapid measurements can be taken. Other advantages include the studies of varying temperature and humidity, accurate measurements at surface concentrations and the ability to obtain physisorption and chemisorption data.

Research utilising the IGC technique has grown rapidly within the last ten years, especially since advantages of the method and understanding of the data obtainable has increased. The use of IGC has spread to many areas of research. One of the first studies of pharmaceutical systems using IGC involved measuring the adsorption of water at zero and infinite surface coverage of a form of cyclosporin (Djordjevic *et al.*, 1992). Batch-to-batch variability of powders has become an important application of IGC that has developed within the last ten years. Two batches of salbutamol sulphate have been investigated (Ticehurst *et al.*, 1994) using IGC. Ticehurst *et al.* (1994) have shown one batch to have a more energetic surface than the other regarding both its dispersive and specific components. Equivalent batches of the excipient α-lactose were also investigated (Ticehurst *et al.*, 1996) and showed variation in polar probe interaction between the batches, but no significant change exhibited for the non-polar interactions. IGC, in conjunction with isothermal microcalorimetry, conducted on saquinavir samples (Buckton *et al.*, 1999) also highlighted the usefulness of such a technique to differentiate between batches.

Numerous authors have also showed the effects on the surface of a material after processing. The milling of cefditoren pivoxil powder has been investigated along with the effects of different humidities (Ohta & Buckton, 2004a). The surface properties of salbutamol sulphate, before and after micronisation have been explored (Feeley *et al.*, 1998) to show an increase in the dispersive component of the micronised batches as well as differences in their acid/base nature. The effects of milling on lactose (Newell *et al.*, 2001a & 2001b), dl-propranolol hydrochloride (York *et al.*, 1998) and calcium oxide powder (Fu & Wei, 1996) are other pharmaceutical compounds that have been studied in such a

manner. The acid/base contributions have been utilised to evaluate the incompatibility between drug and excipient at the interface between solids (Ohta & Buckton, 2004b).

The use of IGC to study surface characteristics has a much broader appeal than just pharmaceutical systems. Industrial carbon fibres have been tested to characterise their surfaces (van Asten *et al.*, 2000). It is important to ensure there is almost no variation in carbon fibre batches as they are used in composite materials for aeroplane construction and thus safety issues are of paramount concern. The dispersive and acid-base properties of polymers have also been ascertained as well as their effects of annealing at elevated temperatures (Fafard *et al.*, 1994; Voelkel *et al.*, 1996; Andrzejewska *et al.*, 1996).

Other interesting areas of IGC research include the study of printing ink pigments and ink fillers (Belgacem *et al.*, 1996) where contact angle was unable to provide surface energy data, characterisation of cotton fabrics and their interactions with fragrance molecules (Cantergiani & Benczedi, 2002), the study of interactions between aroma compounds and corn starch under varying humidities (Boutboul *et al.*, 2000) and the influence of air humidity on the retention of hydrocarbons on soil (Garcia-Herruzo *et al.*, 2000).

IGC papers into the four chosen compounds (calcium mupirocin, nabumetone, theophylline and magnesium stearate) were very limited. Theophylline had been studied to compare contact angle methods with IGC (Dove *et al.*, 1996) and showed good agreement for the apolar component with both techniques. There is also a lack of research in the public domain regarding the use of IGC to study polymorphs and hydrates. The dispersive component of xemilofiban has been characterised (Butler & Mackin, application note 207) to show the difference in surface non-polar values of the two polymorphs. The more stable of the two polymorphs attributed to the lower non-polar value.

6.2 Aims

The aims were to probe the surfaces of the four test powders (calcium mupirocin, nabumetone, theophylline and magnesium stearate) to obtain information regarding the energetics of such surfaces during batch-to-batch comparisons. The compounds were to be probed with the conventional solvents (as listed in Table 6.1). This selection of solvents would provide an insight into the dispersive (non-polar) and specific acid-base (polar) interactions of the compounds. It was hoped that this information could be linked to the data obtained from the DVS experiments to provide a more complete conclusion or to highlight advantages and disadvantages of the technique compared to DVS.

Investigations would be conducted on non-micronised and micronised batches (calcium mupirocin and nabumetone) to show the effects of processing. Tests would be performed on the micronised samples over time to ascertain if any changes in surface energetics occurred relating to possible recovery of the material or further change of the surface structure.

Experiments would also be run to help determine any batch-to-batch differences between Sigma and Fluka compounds (theophylline and magnesium stearate) from the same supplier (Sigma-Aldrich, Poole, UK). This would hopefully highlight the difficulties presented due to batch variability and promote the need to re-assess new batches prior to further processing.

Finally, tests would also be completed to help distinguish the differences in surface properties of anhydrous and hydrate forms of the materials (calcium mupirocin, theophylline and magnesium stearate). The variations in surface energetics of hydrates would help to highlight the need to be aware of the form of the compound and how it interacts differently with the probes during manufacture of pharmaceutical products.

6.3 Methods

Name & Model: Inverse Gas Chromatograph Analyser
(Surface Measurement Systems, London, UK)

6.3.1 Introduction

Various probes are passed through the stationary phase (drug under observation). Each probe will bind to the solid phase with varying degrees. This interaction with the probe results in differing speeds at which the probe is eluted – referred to as the retention time (t_r).

The carrier gas for the probes is either helium or nitrogen. A period of time is required for the flow of these gases, (delay period). Using an inert probe such as methane, a reference elution time can be calculated to account for the delay (t_o). Therefore the net retention time (t_n) can be defined as:

$$t_n = t_r - t_o \qquad \text{[Equation 6.1]}$$

To normalise variants such as column packing and flow rate, equation 6.1 is converted to the net retention volume (V_N), by applying a correction factor for the pressure drop experienced over the column:

$$V_N = JF\,(t_r - t_o) \qquad \text{[Equation 6.2]}$$

- F is the flow rate (mL/min) of the carrier gas.
- *J* is the compression factor for the pressure drop due to the compressibility of the gas over the column:

$$J = \frac{3}{2}\,\frac{[(P_i/P_o)^2-1]}{[(P_i/P_o)^3-1]} \qquad \text{[Equation 6.3]}$$

- P_i/P_o is the ratio of the inlet to outlet pressures.

The free energy of adsorption (ΔG_A^0) for a gaseous probe (De Boer, 1953) can be linked to V_N by series of complex calculations to provide the equation below:

$$\Delta G_A^0 = -RT \ln (V_N P_{sg}/\pi w Sa) \qquad \text{[Equation 6.4]}$$

- R is the gas constant.
- T is the temperature of the column (K)
- P_{sg} is the adsorbate vapour pressure in the gaseous standard state (1.013×10^5 Pa) – (arbitrary standard from De Boer, 1953).
- π is the standard surface pressure (3.37×10^{-4} N/m^2) – (De Boer, 1953).
- w is the weight of the adsorbent in the column (g).
- Sa is the surface area of the adsorbent (m^2/g).

Since Sa, P_{sg}, π and w are all constant, these terms can be reduced to the constant, *K'* (Schultz *et al.*, 1987). Therefore equation 6.4 can now read as:

$$\Delta G_A^0 = -RT \ln V_N + K' \qquad \text{[Equation 6.5]}$$

6.3.2 Dispersive Surface Energy

The dispersive energy component of the surface of a compound can be calculated by the interaction of non-polar probes (alkanes), with regards to their free energy of adsorption. ΔG_A^0 is related to the work of adhesion (W_{adh}) per unit surface area between an adsorbate and adsorbent:

$$\Delta G_A^0 = -N a W_{adh} \qquad \text{[Equation 6.6]}$$

- N is Avogadro's number.
- a is the surface area of one probe molecule.

The interaction with a non-polar probe is primarily due to dispersive Van der Waal's forces. The dispersive components of the solid surface energy (γ^D_S) and the surface energy of the non-polar liquid (γ^D_L) can be utilised to determine the W_{adh} (Fowkes, 1964):

$$W_{adh} = 2 (\gamma^D_S \gamma^D_L)^{0.5} \qquad \text{[Equation 6.7]}$$

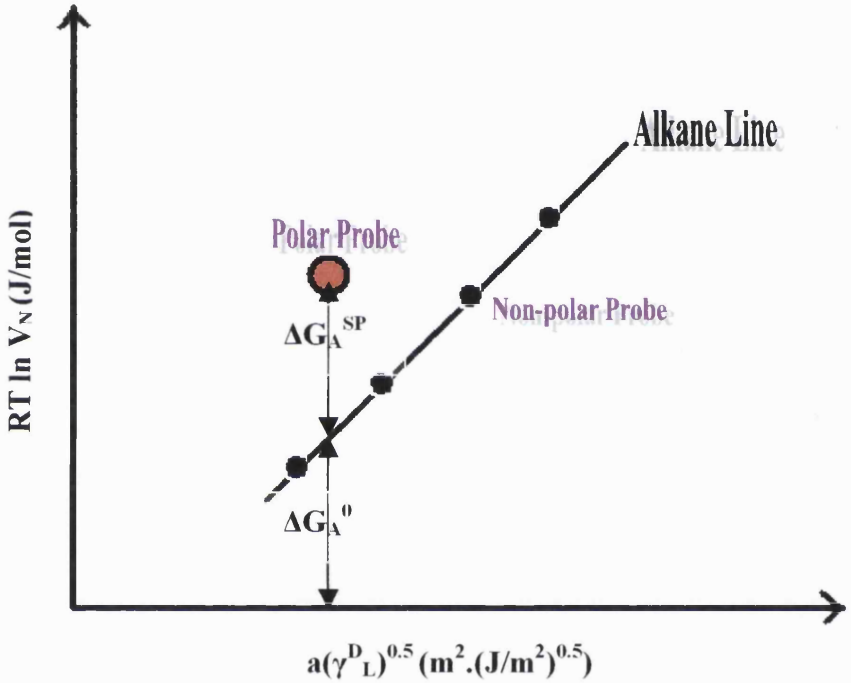

Fig. 6.1: Illustration of the free energy of adsorption of alkane and polar probes.

By combining equations 6.5, 6.6 and 6.7 we obtain the following y = mx + c formula:

$$RT \ln V_N = 2N(\gamma^D_S)^{0.5}.a(\gamma^D_L)^{0.5} + K' \qquad \text{[Equation 6.8]}$$

A plot of the free energy of adsorption versus the dispersion component of the alkanes should provide a straight line [Fig. 6.1]. From the slope of the line the dispersive component of the solid can be calculated, $2N(\gamma^D_S)^{0.5}$. To create such a plot values of 'a' and 'γ^D_L' of the n-alkanes are required. These were obtained from literature (Schultz *et al.*, 1987; Nardin & Papirer, 1990).

6.3.3 Specific (Acid/Base) Interactions

Interactions of polar probes with a solid involve both Van der Waals forces (dispersive component) and polar interactions (specific or acid-base interactions). As a result the interactions of a polar probe would be expected to provide higher energies of adsorption than non-polar probes. The distance between the polar probe and the alkane line [Fig. 6.1] is the specific free energy of adsorption (ΔG_A^{SP}), and the distance to the X-axis is termed the total free energy of adsorption (ΔG_A^0).

Vapour Probe	Molecular Area (m^2 x10^{-19})	γ^D_L (mJ/m^2)	AN* (kcal/mol)	DN (kcal/mol)
Decane	7.5	23.4	0	0
Nonane	6.9	22.7	0	0
Octane	6.3	21.3	0	0
Heptane	5.7	20.3	0	0
Hexane	5.2	18.4	0	0
Acetone	3.4	16.5	2.5	17.0
Chloroform	4.4	25.0	5.4	0
Ethanol	3.5	21.1	10.3	19.6
Ethyl Acetate	3.3	19.6	1.6	17.1
Propan-2-ol	4.3	21.2	9.1	----------

Table 6.1: Properties of the probes used in IGC analysis - (γ^D_L being representative of the surface tension of the probes as liquids).

Having determined ΔG_A^{SP}, the acid-base properties of the surface can be calculated from each probe. Gutmann (1978) suggested that the heat of the acid-base interaction of each probe is related to a Gutmann acceptor and donor number; the acceptor number (AN) being the acid component and the donor number (DN) related to the basic component as essentially they are Lewis acid-base interactions. Also the Gutmann approach allows the amphoteric nature of liquids such as acetone to be accounted for. Gutmann suggested that strong

interactions only develop between an acid and a base. Therefore materials of a similar nature will create an almost zero specific interaction. Some probes possess high AN values due to contributions from Van der Waals forces, thus AN* was created (Riddle & Fowkes, 1990). This value only takes account of the polar interactions. The values and other properties of the solvents have been listed in Table 6.1.

The acid-base parameters (K^A and K^D) can then be used to describe the specific free energy of adsorption:

$$-\Delta G_A^{SP} = K^A DN + K^D AN^* \qquad \text{[Equation 6.9]}$$

A plot of $\Delta G_A^{SP}/AN^*$ against DN/AN* for various probes will provide values for the K^A and K^D nature for the surface of the compound.

The acid-base characteristics can also be calculated using other physical properties of the injected probes. Alternate properties can be plotted against $RTlnV_N$ to determine the free energy of adsorption values. The conventional method plots the molecular area of each probe '$a(\gamma^D_L)^{0.5}$ ($m^2.(J/m^2)^{0.5}$)' against $RTlnV_N$ (Schultz *et al.*, 1987; Nardin & Papirer, 1990). Two other methods include:

- The dispersive component of the heat of vaporisation of the probes, ΔH^D_{VAP}/ kJ mol^{-1} (Chehimi & Pigois-Landureau, 1994).
- Boiling point temperatures (T_b/°C) of the probes (Sawyer & Brookman, 1968).

Using the heat of vaporisation of the probes allowed the opportunity to take into account the effect of self-association of each probe. The advantage of plotting boiling points against $RTlnV_N$ is that the values of the test probes are well known and documented. The disadvantage of both these methods of analysis is that the dispersive component of the solid cannot be calculated. This can only be achieved by plotting $a(\gamma^D_L)^{0.5}$ against $RTlnV_N$. However, by using boiling point and heat of vaporisation values the specific free energy of adsorption can be

calculated and thus the acid-base contribution of the material under investigation to be determined. Table 6.2 shows the values of the different physical properties that can be plotted against $RTlnV_N$.

It must be noted that the heat of vaporisation values for ethanol and propan-2ol were not available in literature and therefore acid-base calculations using such a method was not possible.

Vapour Probe	γ^D_L (mJ/m^2)	ΔH^D_{VAP} (kJ/mol)	T_b (°C)
Decane	23.4	51.4	174.15
Nonane	22.7	46.4	150.82
Octane	21.3	41.5	125.67
Heptane	20.3	36.5	98.5
Hexane	18.4	31.5	68.73
Acetone	16.5	22.4	56.05
Chloroform	25.0	30.4	61.17
Ethanol	21.1	----------	78.29
Ethyl Acetate	19.6	29.3	77.11
Propan-2-ol	21.2	----------	82.50

Table 6.2: Physical properties of the probes used in IGC analysis that can be plotted against $RTlnV_N$ to determine the free energy of adsorption values.

6.3.4 Methodology

The IGC instrument contains mass flow controllers to control accurately the flow of gas within the system. Helium is the carrier gas. It powers the thermal conductivity detector (TCD), which detects the alkanes and the humidity. The flame ionisation detector (FID – measures all the probes) is powered by the hydrogen and air gases.

Glass columns of 6 mm (4 mm internal diameter) and 30 mm length were prepared. All columns were silanated with a solution of 'repelcote' (solution of dimethyldichlorosilane in octamethylcyclotetra-siloxane), to ensure the surface of the columns would not interact with any gaseous probe. The column was then washed with ethanol and rinsed with distilled water before being allowed to dry. Silanated glass wool was placed into one end of the column to create a loose plug. The sample was then introduced and carefully packed. Tapping of the column allowed the particles to pack more uniformly. It was important to ensure there were no cracks or channels within the packed columns, as these may have altered during the course of gaseous probes travelling through the column.

The columns were equilibrated in the oven for 2 hours before starting the experiment at the desired temperature and RH. This allowed the removal of any weakly adsorbed surface contaminants such as adsorbed moisture. Then once the experiment began the column was injected with the probes at infinite dilution (0.04% v/v). At infinite dilution, the probe molecules will have minimal lateral interactions with each other, thus maximising the interaction of the probe with the material surface.

The probes used were the same as those listed in Table 6.1. They were of HPLC grade (greater than 99% purity). Methane gas (BOC grade) was used for the reference probe. The probes were held at an oven temperature of 303 K and the columns at 298 K. The relative humidity was maintained at 0% RH unless where stated (experiments where the hydrate was retained). The helium gas flow rate was varied to provide a good balance between elution speed, shape of solute peak and pressure drop along the column. Results were obtained from an average of three runs. Calcium mupirocin dihydrate experiments were run at 10% RH and theophylline monohydrate tests at 30% RH.

6.3.5 Calibration

There was no reference material to calibrate the system with. However checks with poly methyl methacrylate (PMMA) were conducted to ensure the dispersive surface energy component measured was within that stated by the manufacturer

(35-40 mJ/m^2). Also the IGC was periodically serviced to maintain high standards.

6.4 Results & Discussion

6.4.1 Surface Energetics Of Calcium Mupirocin

Investigations on calcium mupirocin were conducted to determine the surface characteristics of a non-micronised batch compared to a micronised form of the drug over a period of time. Also a hydrated form of non-micronised calcium mupirocin was analysed to determine the surface differences caused by a change in hydrated state (against the anhydrous non-micronised batch).

6.4.1.1 Determination Of The Dispersive Surface Energies Of Calcium Mupirocin

The injecting of all five non-polar probes, into the calcium mupirocin columns, showed elution of every solvent except decane. The decane peak did not elute within the maximum experimental time possible (100 min) with the SMS software. However, the remaining four probes that did produce elution peaks were used to sufficiently calculate the dispersive component of the samples.

Fig. 6.2 shows the non-polar surface energies of calcium mupirocin for the different batches. It was clear that the non-micronised sample exhibited the largest non-polar value (66.7 mJ/m^2). Micronisation of the sample had reduced the dispersive component at the surface of the drug. The values did not change measurably over time. This suggested that no change (recovery) in possible amorphous nature could be detected by the non-polar probes, and that the difference in values between the non-micronised and micronised forms were probably due to the change in particle morphology. Statistical analysis (ANOVA) showed that micronised batches were significantly different (p-value <0.05) to the non-micronised form, and that there were no significant differences (p-value >0.05) between all the micronised results compared with each other.

Characterisation studies (XRPD, HDSC and SolCal - section 4.3.2) were also unable to determine any amorphous nature within the micronised sample. Only DVS experiments (section 5.4.2) were able to follow a change in the amorphous character of the material. All the micronised samples showed a dispersive component of at least 2-3 mJ/m^2 lower than the non-micronised batch. The batch tested 1.5 months after micronisation did show a higher than expected non-polar value but could be explained by the high standard deviation obtained (in comparison with all the other runs).

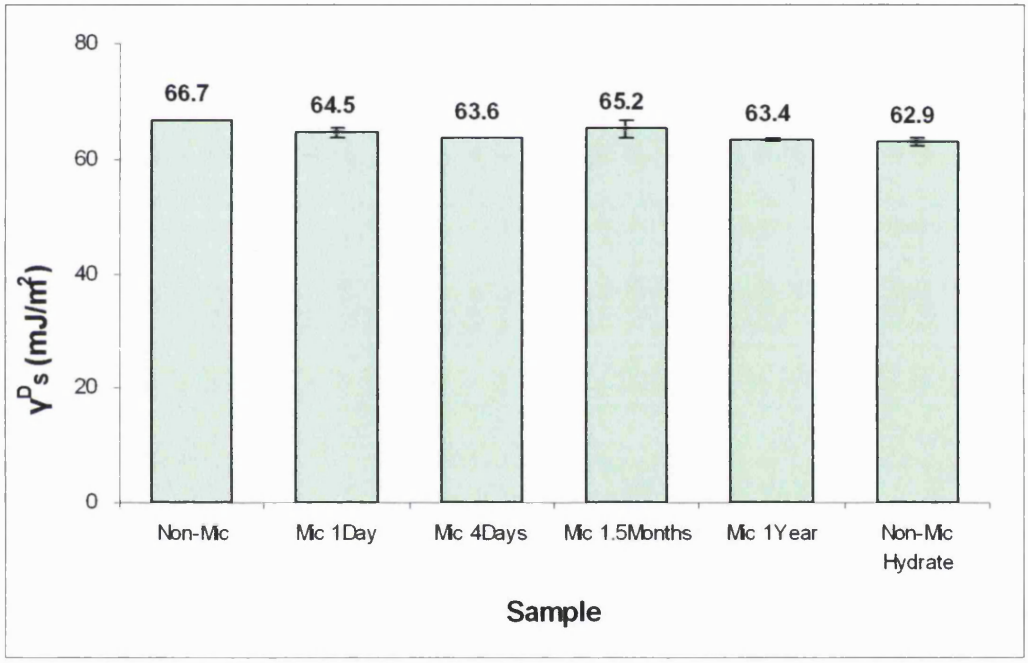

Fig. 6.2: Bar chart showing the variation in dispersive component of the investigated calcium mupirocin batches. (N.B. Mic = Micronised. Non-micronised hydrate run at 10% RH and all other columns run at 0% RH).

Micronisation and subsequent reduction in particle size would induce the surface of the material to become more energetic. In fact increased surface area alone should provide a greater area for all probes to interact with and thus an increased retention time. However, as the data showed, this was not the case. The decrease in dispersive component after micronisation could be postulated to be a result of a number of factors. Firstly aggregation of the particles within the

column would lead to a reduced surface area available for probe interaction and hence a subsequent lower dispersive value. Aggregation would be more of a factor with IGC than with the DVS technique, because of packing of the material and follow up 'tapping' of the column to ensure no particle movement during IGC runs. Secondly, micronisation of the drug could have led to the appearance of more polar groups onto the surface and hence reducing the interaction with the non-polar probes.

It has been reported (Newell *et al.*, 2001a & 2001b) that the apolar component of a partially amorphous material has been found to be higher than its respective fully crystalline form. This would be as expected as the amorphous state would be in a higher energy state, but has not been the case for calcium mupirocin. However, interestingly other authors (York *et al.*, 1998; Ohta & Buckton, 2004a) have shown that as the particle size of D,L-propranolol and cefditoren pivoxil respectively decreased during milling, the dispersive component increased until a critical point was reached after which the dispersive values decreased. At this point the material is said to change from a predominantly brittle to a predominantly ductile form. Size reduction below the critical point is associated with attrition rather than fracture of specific crystal planes. As a result new surfaces would contain the same functional groups at the surface, and therefore the dispersive component may remain constant or decrease. This could help explain the non-polar component values observed for micronised calcium mupirocin. Although such a study had not been undertaken, the size of the particles could be beyond such a critical point that the dispersive component would be lower than that of intact calcium mupirocin.

Analysis of the non-micronised dihydrated form of calcium mupirocin (run at 10% RH) showed a dispersive value of 62.9 mJ/m^2 [Fig. 6.2]. This value was measurably lower (nearly 4 mJ/m^2) than that for the non-micronised anhydrous sample. It was also slightly lower than the non-polar values observed for the micronised batches. The hydrate value was found to be significantly different (ANOVA) to all the other forms of calcium mupirocin. A plot of the interaction of each of the non-polar probes [Fig. 6.3] showed some interesting data. The interaction of the solvents as they passed through the columns did not vary

greatly between the non-micronised and micronised batches. However, with the dihydrated form it was clear to observe that all the probes interacted with the drug to a lesser extent as highlighted by the reduced interaction on the material surface. The water in the system (at 10% RH) could have had a two-fold effect on the compound. Firstly, the formation of the dihydrate itself could have changed the surface of the material. The water molecules could have attached themselves and orientated in a manner where they were positioned at the surface. Secondly, excess moisture could have created an adsorbed layer onto the material surface. Both of these possibilities would naturally reduce the ability of the non-polar solvents to interact with the drug's surface. The newfound polar attributes located on the surface, as a cause of the water molecules, hence can have a marked effect on the surface energetics of a compound.

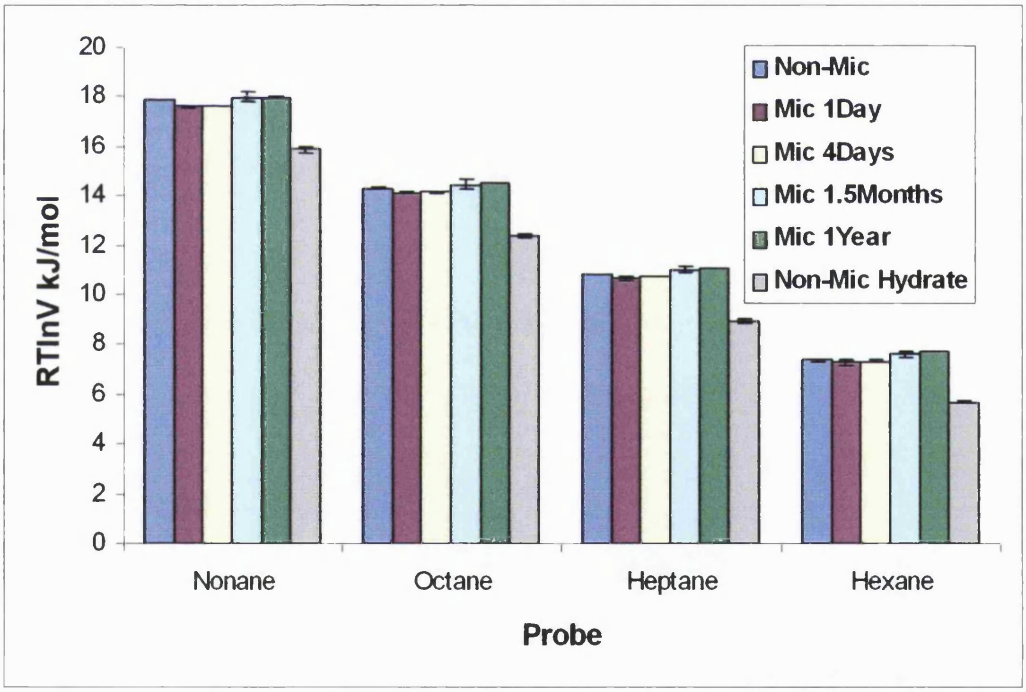

Fig. 6.3: **Bar chart showing the variation in interaction of the non-polar probes on the different batches of calcium mupirocin. (N.B. no decane peak eluted, Mic = Micronised, Non-micronised hydrate run at 10% RH and all other columns run at 0% RH).**

Humidity having a lowering effect on the dispersive component has been shown in the past (Cantergiani & Benczedi, 2002). Tests were conducted on cotton fabrics and increasing relative humidity caused the cotton to swell, changing the structure and lowering the subsequent dispersive surface energy of the material. These changes were shown to occur at high relative humidities. Contrastingly, differences were seen with calcium mupirocin at 10% RH and structural changes that occurred were due to hydration and possible adsorption onto the surface by water molecules.

6.4.1.2 Determination Of The Acid/Base Character Of Calcium Mupirocin

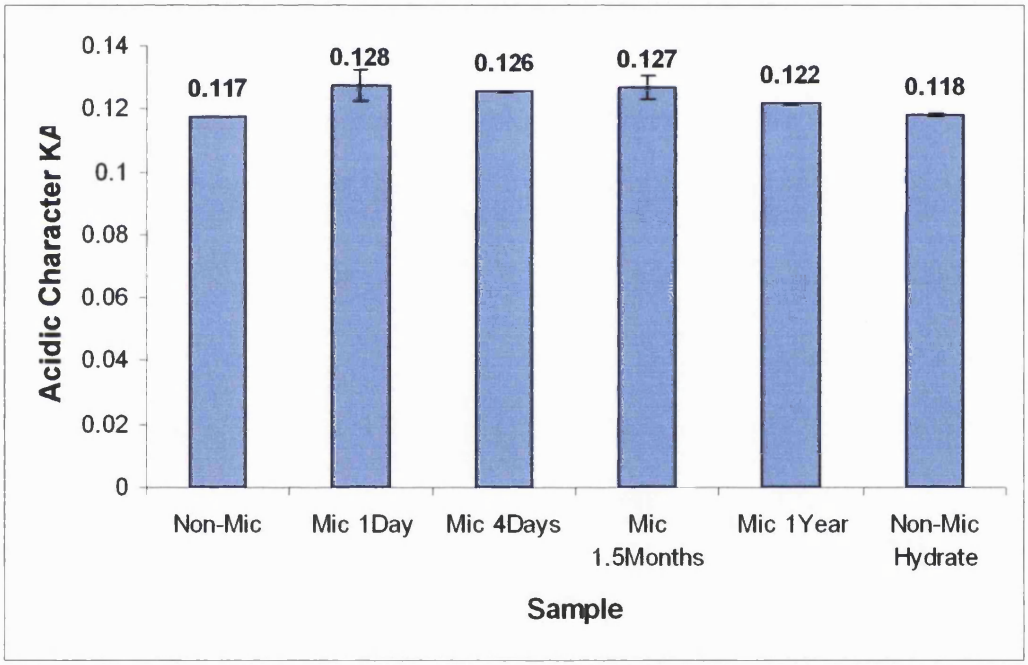

Fig. 6.4: Acid character of calcium mupirocin batches. (N.B. Mic = Micronised. Non-micronised hydrate run at 10% RH and all other columns run at 0% RH).

The acid/base character of calcium mupirocin was also investigated. Unfortunately of the four chosen polar probes, ethanol did not elute within the maximum experimental time possible (100 min). The only explanation for such an occurrence would possibly be due to the strong interactions between ethanol and the powder surface (also suggested by Ticehurst *et al.*, 1996). The acidic

and basic character of the batches of calcium mupirocin could be used to further understand the surface properties of calcium mupirocin.

From the data [Fig. 6.4 & Fig. 6.5] it was clear to see that the sample once micronised had a greater K^A value and lower K^D value. ANOVA statistically showed that the K^A and K^D values for micronised samples were significantly different when compared to the non-micronised batch. The K^A value increased due to a rise in the gradient of the line of best fit of the polar probes (DN/AN^* versus $-\Delta G_A^{SP}/AN^*$). This suggested that the powder surface, after micronisation, became more acidic in nature (electron accepting) as a result of the greater polar acidic components of the compound being available for interaction.

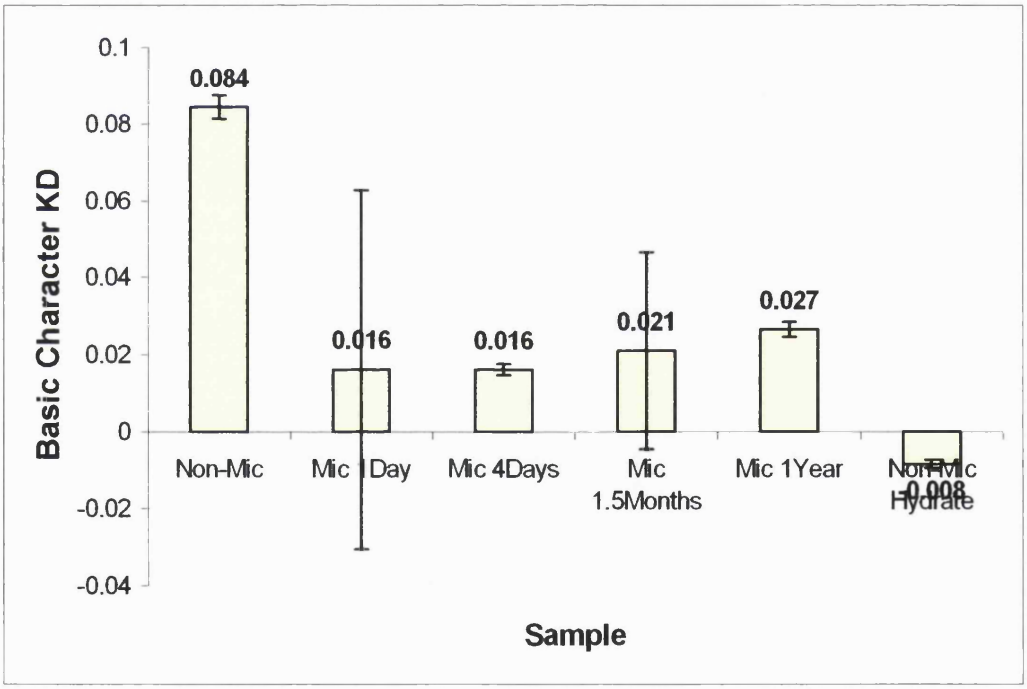

Fig. 6.5: Basic character of calcium mupirocin batches. (N.B. Mic = Micronised. Non-micronised hydrate run at 10% RH and all other columns run at 0% RH).

The data showed that when measuring the K^A value, on the sample micronised 1 year ago, the calculated result was significantly lower (ANOVA) than the other micronised samples. A possible explanation of this could be that the surface of

the freshly micronised batch may have been in a more excited (higher energy state), which then showed recovery over time to the more energetically stable configuration. Thus the acidic components of the compound could have become less available over time. These observations could have been further strengthened if experiments had also been conducted periodically between the data obtained for 1.5 months and 1 year after micronisation.

Not surprisingly, the K^D values (extrapolated from the Y-axis intercept) decreased once the micronised material was tested when compared to the non-micronised results. This was the opposite to the K^A data obtained as the sample surface character was transforming to that of a more acidic nature. The K^D value changed from 0.084 to very low figures varying from 0.016-0.021 (micronised sample up to 1.5 months). Micronisation of the material probably rearranged basic components of the compound so that they were present to a lower degree on the surface. It must also be noted that the standard deviation for two results (1 day and 1.5 month samples) was large and could have distorted the actual values. From the results for 1.5 months (0.021) and 1 year (0.027) after micronisation, there was a suggestion that the sample was recovering slowly towards the original K^D value of non-micronised calcium mupirocin. ANOVA showed that the K^D result for sample tested one year after micronisation was significantly different to the other micronised results. This was in corroboration with the K^A results (for 1 year after micronisation sample), which also suggested signs of recovery of the sample.

Looking at the retention of the polar probes [Fig. 6.6] onto the surface of calcium mupirocin provided a greater insight into the K^A and K^D values observed for the different batches. The acidic probe, chloroform, showed the highest variation in interaction compared to the other polar probes. Chloroform interacted with the non-micronised calcium mupirocin (anhydrous) the greatest. Being an acidic probe the strongest interaction with the non-micronised material showed that the surface was more basic than any other of the batches (as acid interacts with base). After micronisation the interaction of the probe reduced confirming a more predominantly acidic surface than before. Also it was important to observe the large standard deviations for chloroform (tests after 1 day and 1.5 months

after micronisation), which directly correlated to the large standard deviations seen on the K^D values for the respective samples. The basic probes, acetone and ethyl acetate, showed an initial small increase in interaction (after micronising – 1 day, 4 days and 1.5 months) which then subsequently decreased (1 year after micronisation). This was in line with the observed change in nature of the surface, such that the surface became more acidic leading to greater interaction for basic probes. With the recovery of the sample the basic probe interactions decreased with a similar drop in K^A value (increase in K^D value). The changes observed in retention of the basic probes were not as large as that seen for the acidic probe, thus suggesting that the changes in surface properties affected acidic probes to a greater extent.

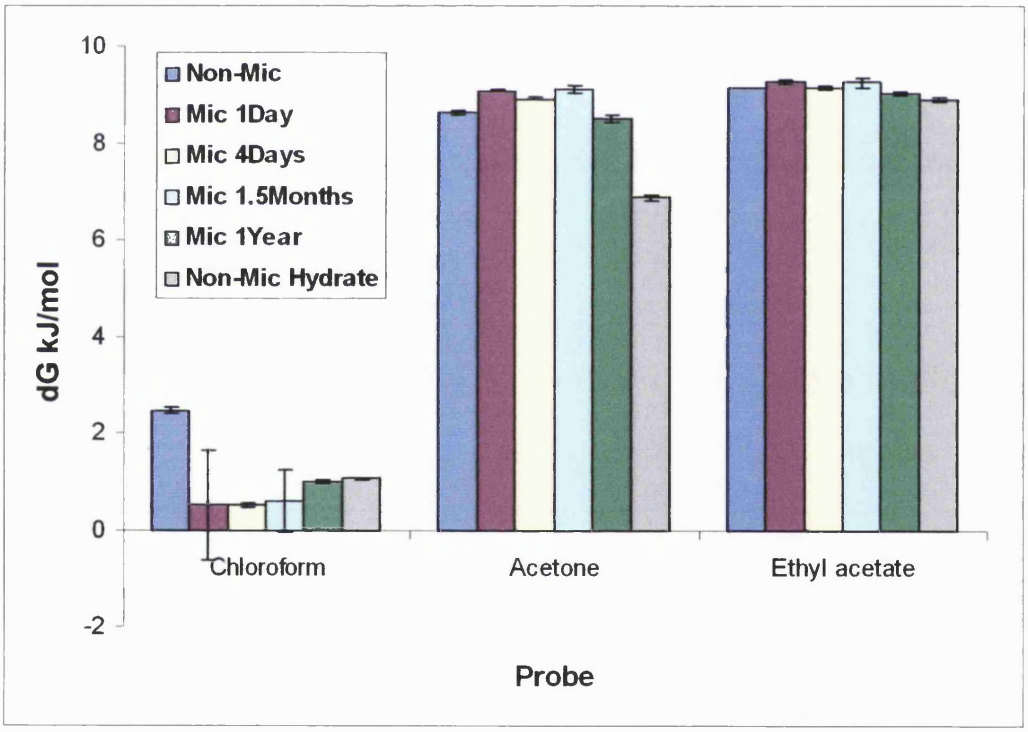

Fig. 6.6: Bar chart showing the variation in interaction of the polar probes on the different batches of calcium mupirocin. (N.B. no ethanol peak eluted, Mic = Micronised).

Comparing the K^A values [Fig. 6.4] for the non-micronised original calcium mupirocin (anhydrous form) and the non-micronised hydrated form (dihydrate), there was no significant difference (ANOVA). This suggested that the

incorporation of water into and/or onto the compound did not alter the polarity of the surface in terms of its acid character. However, actual probe retention on the surface of calcium mupirocin [Fig. 6.6] showed a decreased interaction for all the polar probes. Therefore, the sorption of water into and/or onto the material had reduced the interaction between the polar probes and the compound surface, but the K^A value had remained constant due to the gradient of the DN/AN* versus - ΔG_A^{SP} plot remaining the same. Paracetamol and carbamazepine have been studied (Sunkersett *et al.*, 2001) at 0% and 47% RH. They have shown that two different drugs can interact with probes in varying manner when pre-subjected to humidity changes. Neither the dispersive surface energy nor the acid/base components altered when changing the RH from 0 % to 47% for carbamazepine. However for paracetamol, the aforementioned humidity change caused the specific energies of adsorption for the polar probes to either remain constant or decrease. This was similar to what was seen for calcium mupirocin anhydrous and hydrated forms (non-micronised batches). The chloroform and acetone surface interaction decreased noticeably, whereas the interaction for ethyl acetate was not very different between both batches (although marginally lower). The decrease in interaction observed could be a result of the water molecules adsorbing onto the same sites as the polar probes.

Unlike the K^A value, the K^D value was significantly different (ANOVA) [Fig. 6.5] for the hydrated form of calcium mupirocin (at 10% RH) when compared to the anhydrous non-micronised sample. The K^D value for the hydrate was almost zero, implying that the surface contained limited basic properties. This could be due to the shielding effect of water on groups that may have an electron donating nature (i.e. carbonyl groups). This effect has been previously seen (Sunkersett *et al.*, 2001; Ohta & Buckton, 2004a), where a dramatic fall in the K^D value was observed between 0% and 10% RH.

As ethanol did not elute from the column, propan-2-ol was also injected [Fig. 6.7] to attempt to review some of the similar solvents that were used for the DVS experiments. There was no significant difference (ANOVA), at the 5% significance level, observed between the specific energy of adsorption for the non-micronised and micronised after 1 year batches. However, a significant

difference (ANOVA, p-value <0.05) was once again observed between the non-micronised anhydrous and non-micronised hydrate samples. The hydrate showed a decreased interaction of the polar probe, similar to that seen with chloroform. Thus the sorption of water into the structure and onto the surface had reduced the interaction of the polar probe and the compound surface as previously reported for paracetamol (Sunkersett *et al.*, 2001). DVS studies showed (section 5.4.2) that propan-2-ol interacted to a greater degree with the micronised sample than the non-micronised sample. This was not clear to see with IGC. A possible explanation could be due to the very low concentrations of probe being injected, that interactions at such low concentrations are similar and only change when greater concentrations are delivered. Another probe that was used with IGC and DVS was hexane. Just as with DVS experiments (section 5.4.2) no real difference in interaction was observed between the different batches (except when hydrated for IGC experiments).

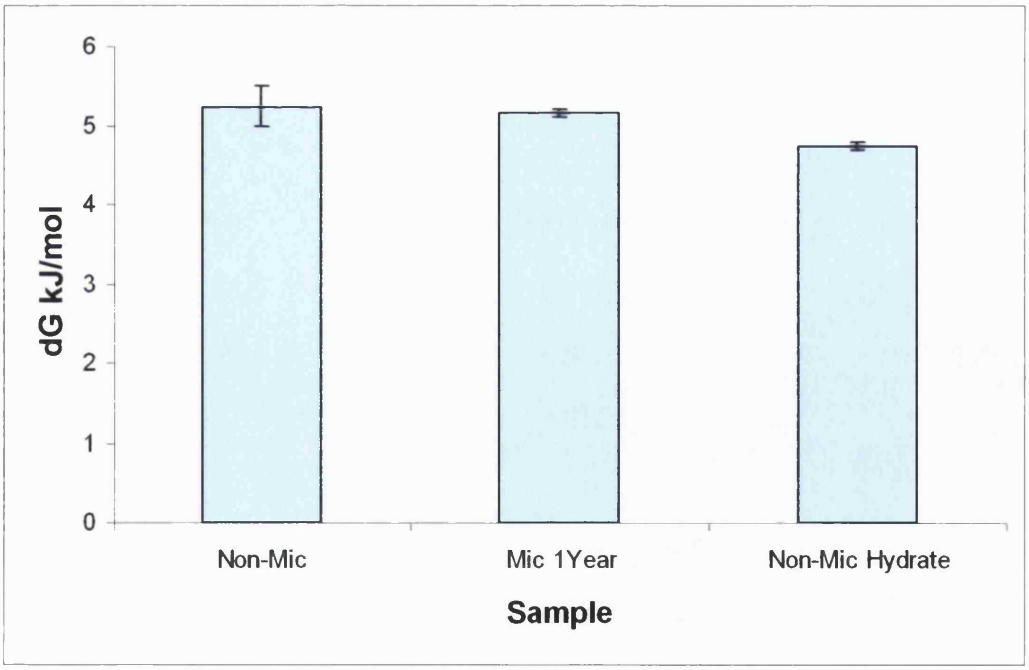

Fig. 6.7: Bar chart showing the variation in interaction of the polar probe propan-2-ol on three batches of calcium mupirocin. (N.B. Mic = Micronised. Non-micronised hydrate run at 10% RH and all other columns run at 0% RH).

6.4.1.3 Conclusions Of The Surface Energetics Of Calcium Mupirocin

It must be noted that only 0.04% vapour of the solvents was being injected for IGC (infinite dilution) compared to finite concentrations (0.05-0.35 P/Po) that were used during the DVS experiments. Thus the solvents in IGC experiments preferentially acted upon the higher energy sites on the surface, whereas with the DVS tests they acted on the higher energy sites first but also upon the remainder of the surface thereafter. As a result both instruments showed interesting and different surface characteristics data but some direct correlation between the sets of data were possible. The IGC results have been summarised in Table 6.3. The non-polar component showed a small measurable change (statistically significant) between non-micronised (anhydrous) and micronised batches of calcium mupirocin. However, from the results obtained with the DVS there was no observed difference in adsorption of hexane for the three batches of the material (non-micronised, freshly micronised and micronised after 1 year – section 5.4.2).

Sample	γ^D_S (mJ/m^2) (S.D.)	K^A (S.D.)	K^D (S.D.)
Non-Micronised	66.7 (0.16)	0.117 (0)	0.084 (0.0031)
Micronised 1 Day	64.5 (0.72)	0.128 (0.0051)	0.016 (0.0467)
Micronised 4 Days	63.6 (0.08)	0.126 (0.0003)	0.016 (0.0015)
Micronised 1.5 Months	65.2 (1.57)	0.127 (0.0037)	0.021 (0.0256)
Micronised 1 Year	63.4 (0.32)	0.122 (0.0005)	0.027 (0.0019)
Non-Micronised Hydrate	62.9 (0.71)	0.118 (0.0007)	-0.008 (0.0011)

Table 6.3: Summary of the non-polar surface energy and acid/base character of the different batches of calcium mupirocin. (Non-micronised hydrate column run at 10% RH. All other columns run at 0% RH).

However, observations of the K^A and K^D values showed that possible recovery over time of the micronised sample did take place. Variations in the interaction of chloroform, acetone and ethyl acetate were observed due to changes on the surface of calcium mupirocin caused by comminution. With the DVS

experiments, changes were also seen after micronisation (increased sorption of all the polar probes) and subsequent recovery after testing the micronised sample one year later. Furthermore, studies using the IGC made it possible to investigate the effects of hydration on calcium mupirocin and comparing the data with the representative anhydrous form. DVS experiments (section 5.4.5) were unsuccessful in performing hydrate studies with all probes (except water), due to the immediate loss of the dihydrate on initiation of the tests.

6.4.2 Surface Energetics Of Nabumetone

Surface characteristics of nabumetone were studied using IGC for the non-micronised and micronised batches. It was hoped that IGC would help highlight differences between the two batches after processing using the air-jet microniser. Unfortunately DVS studies (section 5.4.6.2) were unable to provide any information about the compound, except that it did not wet easily with any of the probes used during the DVS experiments.

6.4.2.1 Determination Of The Dispersive Surface Energies Of Nabumetone

Elution peaks were obtained for all five non-polar probes injected into the nabumetone columns. Fig. 6.8 showed the non-polar surface energy of nabumetone for the different batches. There was a significant difference (ANOVA, p-value <0.05) between the dispersive surface energies of the non-micronised and micronised forms of the material. The non-micronised sample exhibited the lowest value (35.0 mJ/m^2). Micronisation of the sample had increased the dispersive component at the surface of the drug. Testing micronised nabumetone after 1 day showed an approximate 17% increase in the non-polar value (40.9 mJ/m^2). Further tests after 2 months showed a decrease (38.6 mJ/m^2) from the original micronised value and the non-polar component did not vary significantly (ANOVA, p-value >0.05) when tested again at 5 months and 1 year after micronisation. The results suggested that initially the micronisation of the particles caused higher energy sites on the surface of the material, which then recovered over time as there was a decrease in interaction with the probes. The micronised batch may have recovered further if the samples

were measured over a greater length of time. Alternatively the material may have reached the new low energy state caused by the increased surface area of the particles to allow probe interaction.

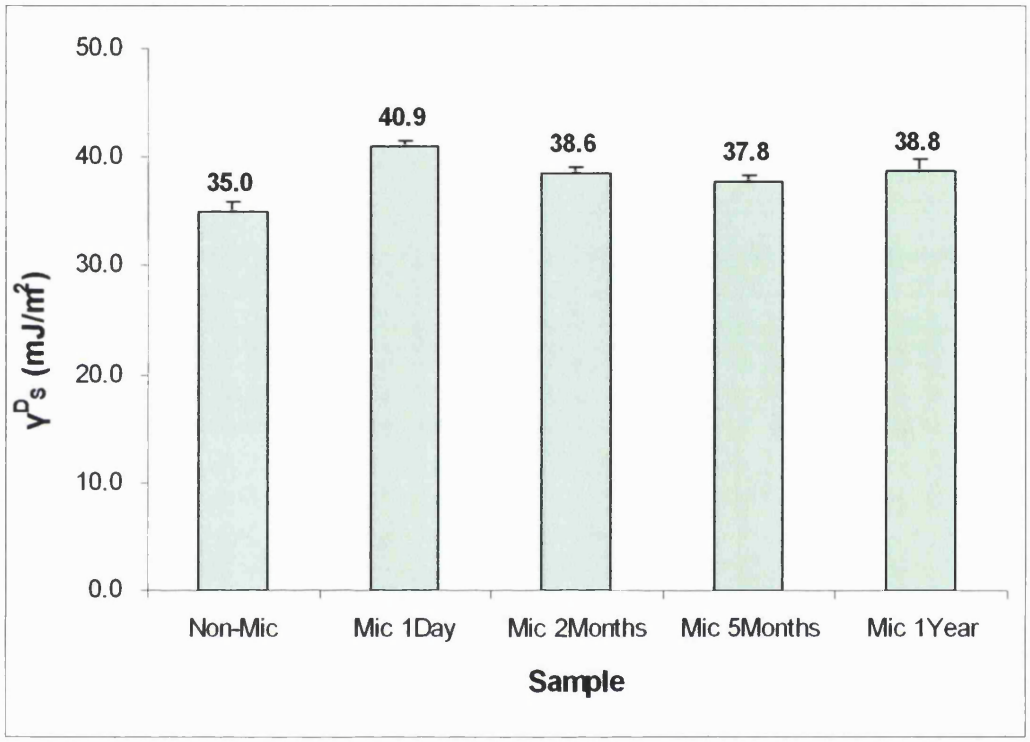

Fig. 6.8: Bar chart showing the variation in dispersive component of the tested nabumetone batches. (N.B. Mic = Micronised).

Micronisation, and therefore particle size reduction, had induced the surface of the material to become more energetic. Experiments on lactose (Newell *et al.*, 2001a & 2001b) have also shown that the apolar component of partially amorphous lactose to be higher than the respective crystalline form. The comminution of the particles could have caused the production of higher energy sites and also the appearance of more non-polar components onto the surface of the material. Both of these events would thus lead to a greater interaction of the non-polar probes with the drug surface.

Interpreting the data of individual non-polar probes interaction with the surface of the material [Fig. 6.9] showed data that corroborated the discussions proposed for the dispersive values seen for all the batches. The probes interacted least

with the non-micronised form of nabumetone. After micronisation (1 day), the degree of interaction increased due to the higher energy state of the surface and greater surface area of the smaller particles. However, the subsequent recovery (towards that seen for the non-micronised batch) of the columns tested 1 month, 5 months and 1 year later proved that increased surface area was not the only factor towards the higher dispersive values obtained. The micronisation of the material must have created areas of disorder (excited energy states or 'reactive hot spots') that led to this increase in interaction between probe and surface. Within a short time the disorder of the surface had re-stabilised to produce a lower apolar component, where possibly only an increased surface area played a part in the subsequent differences seen between the non-micronised and micronised samples.

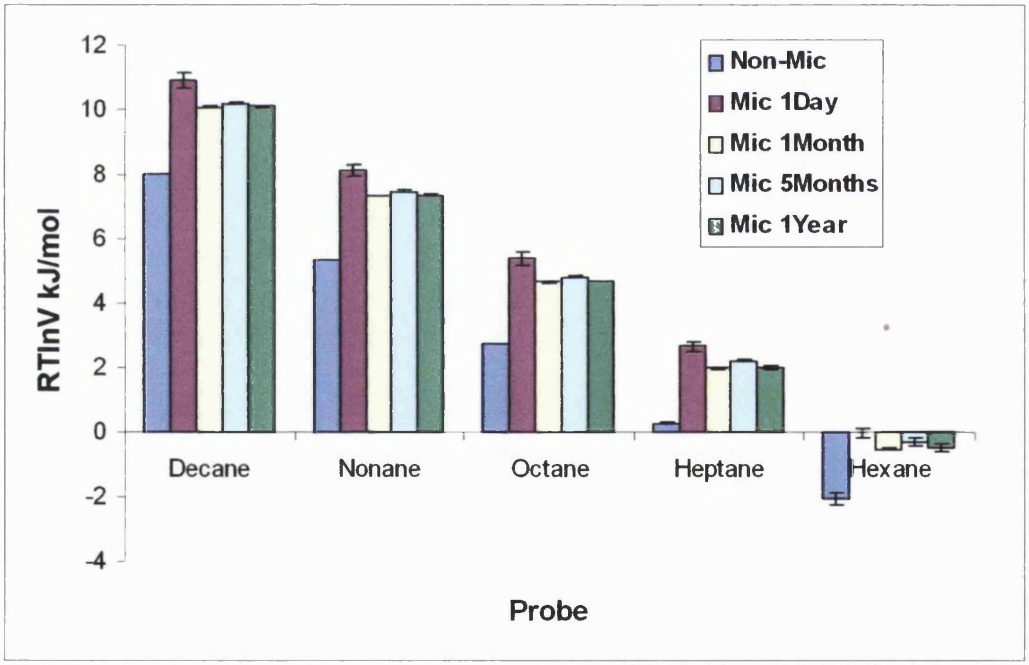

Fig. 6.9: **Bar chart showing the variation in interaction of the non-polar probes on the different batches of nabumetone. (N.B. Mic = Micronised).**

6.4.2.2 Determination Of The Acid/Base Character Of Nabumetone

The acid/base character of nabumetone was obtained using the polar probes. All four polar probes (chloroform, acetone, ethyl acetate and ethanol), produced guassian peaks when eluted from the columns. The acidic and basic nature of the batches of nabumetone may help further understand the surface properties of the material after processing.

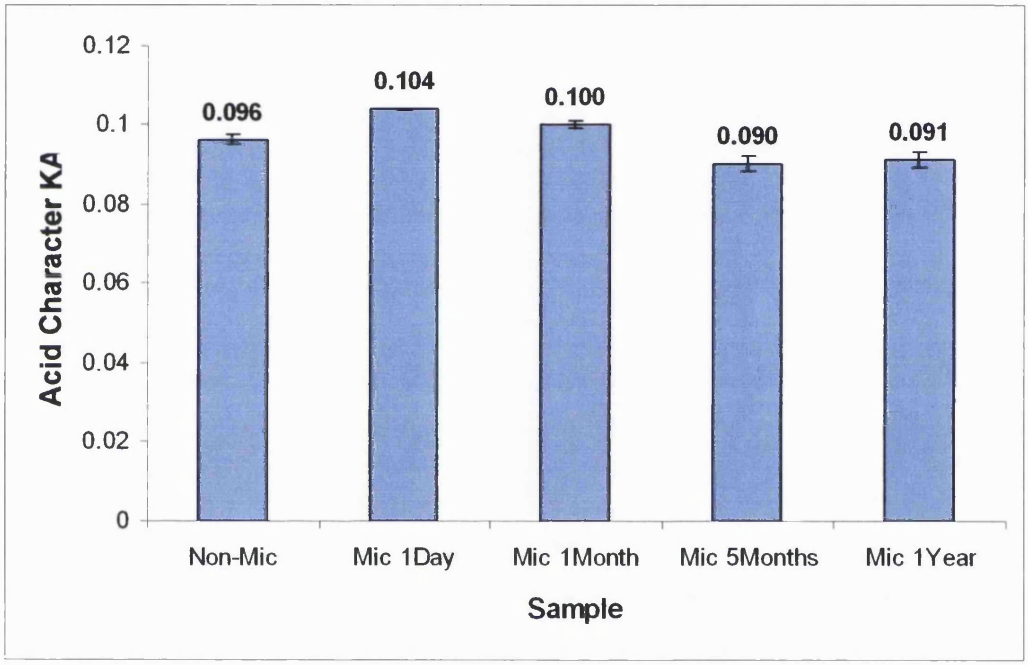

Fig. 6.10: Acid character of nabumetone batches. (N.B. Mic = Micronised).

The data [Fig. 6.10 & Fig. 6.11] showed the changes in K^A and K^D values of the batches of nabumetone. All the samples showed a greater K^A value than K^D value, suggesting the material surface was more acidic in nature (electron accepting). After the sample had been micronised the acid character of nabumetone increased from 0.096 to 0.104 (1 day after micronising). Subsequent tests showed a decrease in the K^A value. However from the experiments conducted on the micronised sample after 5 months and a year, the acid character had decreased (0.09) to below the value originally obtained for the non-micronised sample. This suggested that immediately after micronisation the

surface was altered in a manner where a greater number of polar acidic components of the compound were available for interaction. However, with the recovery of the sample (as also seen by the apolar measurements) to a more energetically stable state, a reduced quantity of acidic sites became available for interaction with the probes. The K^A values of the samples tested 5 months and 1 year after micronisation showed a value below that for the non-micronised sample, possibly because the micronised sample may now have possessed a different energetically stable state to the original compound. Statistically, ANOVA corroborated the interpretations made. It showed that all the micronised samples were significantly different to the non-micronised batch (p-value <0.05), but there were no significant differences (p-value >0.05) between (a) micronised one day and one month batches and (b) micronised five months and one year batches.

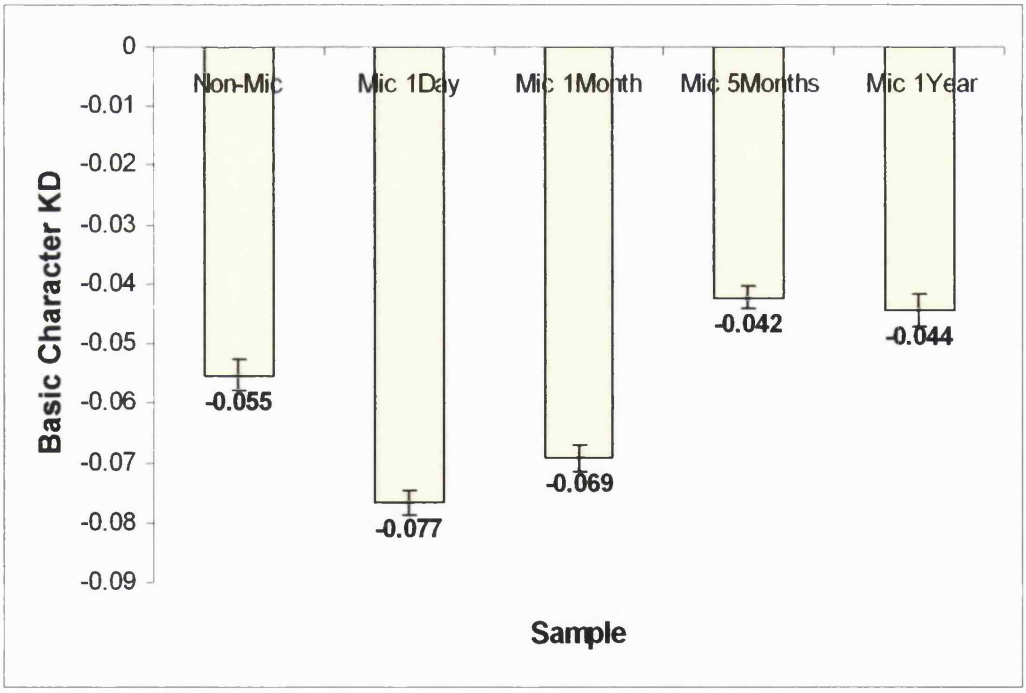

Fig. 6.11: Basic character of nabumetone batches. (N.B. Mic = Micronised).

The basic component (K^D) of nabumetone changed in a manner relative to the changes in K^A observed. Statistical observations (ANOVA) followed the same patterns as that discussed for the K^A values too. Thus the K^D values decreased

when K^A increased and the opposite took place when K^A decreased. As the acidic nature of the surface increased immediately after micronisation the subsequent basic character decreased. All tests from one month onwards after micronising showed a steady increase in the basic nature of the surface, as the acidic components of the material were available at a lesser extent for interaction with the polar probes. This change was exhibited due to the recovery of the surface to probably a more energetically stable state. However, although these changes were seen all the results for K^D were of a negative value. Theoretically it should be impossible for a compound to show a negative value for the basic character (or even the acidic character). The interaction of polar probes should be expected to provide higher energies of adsorption than non-polar probes. Such is the case, as polar probes should involve both Van der Waals forces (only seen for the dispersive, non-polar component) and polar interactions (acid-base interactions).

Observations of the interactions of the polar probes [Fig. 6.12] with the nabumetone surface concurred with the discussions already formed for the acid/base character. Chloroform, being an acidic probe, interacted greatest with the surface of the 5 months and 1 year after micronisation batches. Thus the acid character of the sample reduced and the subsequent basic character increased (although still below zero). However, immediately after micronisation chloroform interacted the weakest of all the runs and hence coincided with the greatest K^A value. The other acidic probe, ethanol, showed an increase over time of the interaction with the surface after the sample had been micronised. However, the interaction was never as strong as that for the non-micronised batch. Ethyl acetate (basic probe) showed greater interaction with the surface after the sample was micronised, which subsequently reduced as the surface became less acidic in nature. Finally acetone (basic probe) showed greater interaction after micronisation too but this interaction decreased below that seen for the non-micronised sample over time. The stronger interactions coincided with the increase in K^A values and thereafter the weaker interactions represented the drop in K^A values. The greatest effect on the K^A and K^D components were represented by the changes seen in the chloroform and acetone probes with the different batches of nabumetone.

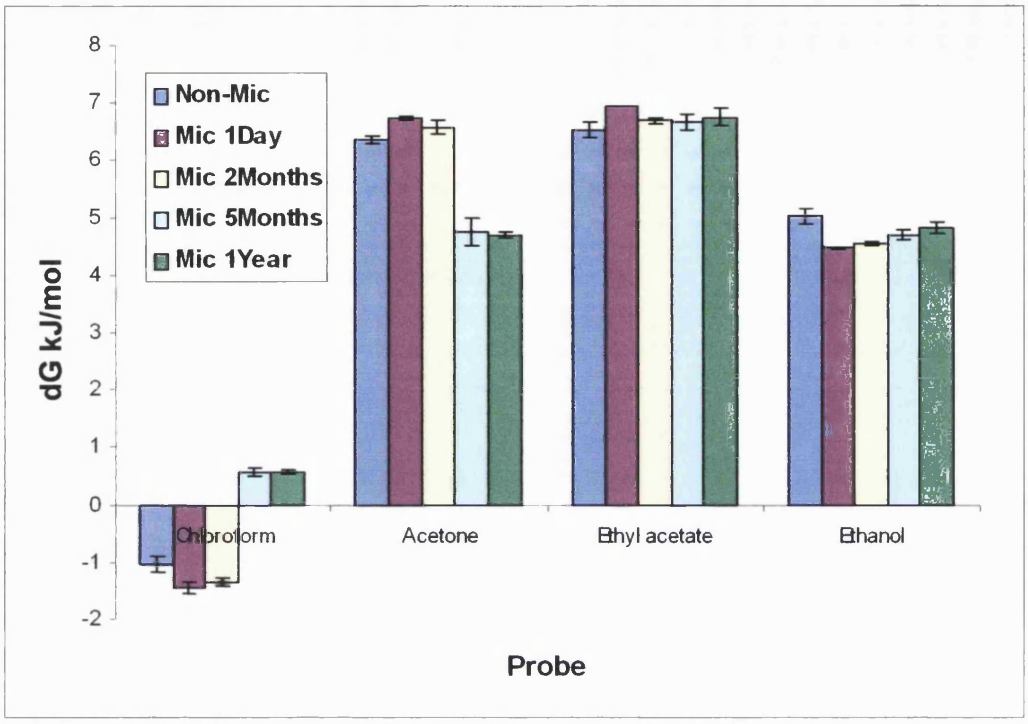

Fig. 6.12: Bar chart showing the variation in interaction of the polar probes on the different batches of nabumetone. (N.B. Mic = Micronised).

The heats of vaporisation (ΔH^{D}_{VAP}) and boiling point values (T_b) have been used, instead of the molecular area as a function of the dispersive component of the liquid probes ($a(\gamma^{D}_{L})^{0.5}$), to determine the free energy of adsorption values (section 6.3.3). From these values the acid-base character could also be established and hopefully the re-plotting of the graph could help remove the negative values seen for the basic component (K^D value). The plot of all three methods of measurement for the non-micronised nabumetone batch [Fig. 6.13] showed that the R^2 value of the line of best fit for the acid/base plot was poor for the heat of vaporisation and boiling point analysis methods. With such a correlation there was no justification in using the K^A and K^D values that such a plot produced. Also re-plotting in such a manner did not necessarily remove the negative K^D values that have been seen with the molecular area approach for all the batches. The use of boiling points as an alternative method has been shown to provide negative acid-base interaction energies by other authors too (van Asten *et al.*, 2000). Correlation could have been improved if a greater number of

polar probes had been injected. This would also have been able to show whether one of the probes was causing distortion of the lines of best fit.

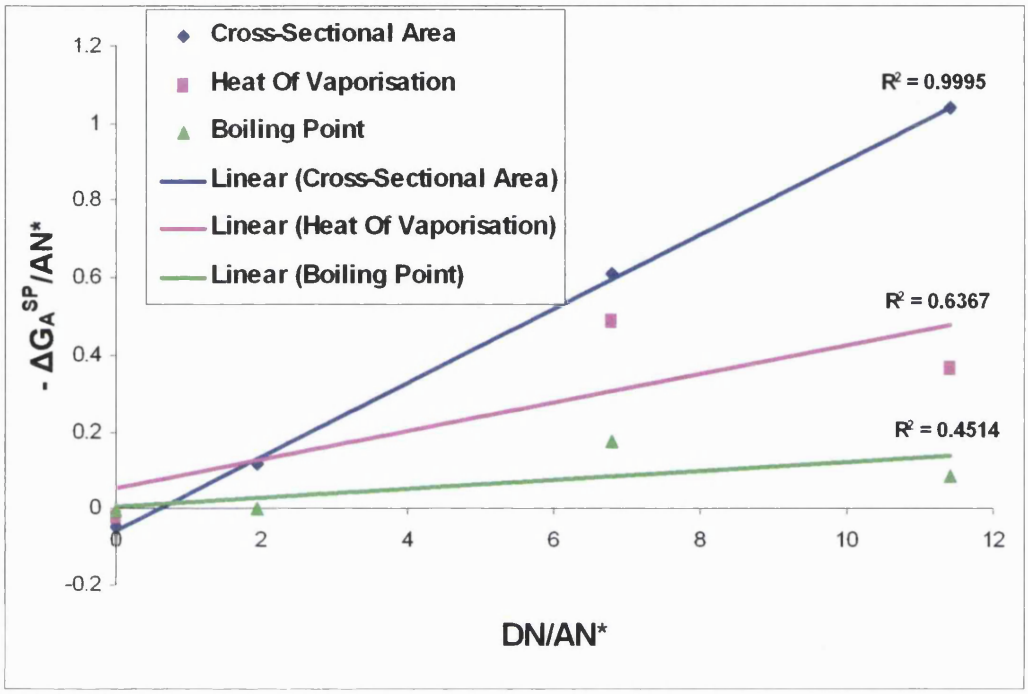

Fig. 6.13: Acid/base plot for the non-micronised batch of nabumetone as an example to show the correlation of the polar probes using 'cross-sectional area', 'heat of vaporisation' and 'boiling point' data of the probes. (No ethanol data for heat of vaporisation plot).

6.4.2.3 Conclusions Of The Surface Energetics Of Nabumetone

The results from the IGC analysis of nabumetone [summary of results – Table 6.4] showed that after micronisation the surface of the material sufficiently changed to record a difference in the dispersive component when compared to the non-micronised form. Thus micronisation led to a greater degree of non-polar interactions. Interestingly over time the micronised material showed recovery, which later stabilised to a non-polar component still higher than the value obtained for the non-micronised form. Thus the higher energy state of the surface after micronisation recovered to a more energetically stable form whose surface still differed from the original non-micronised batch.

Sample	γ^D_S (mJ/m^2) (S.D.)	K^A (S.D.)	K^D (S.D.)
Non-Micronised	35.0 (0.96)	0.096 (0.0012)	-0.055 (0.0026)
Micronised 1 Day	40.9 (0.66)	0.104 (0.0003)	-0.077 (0.0021)
Micronised 1 Month	38.6 (0.46)	0.100 (0.0009)	-0.069 (0.0021)
Micronised 5 Months	37.8 (0.58)	0.090 (0.0020)	-0.042 (0.0018)
Micronised 1 Year	38.8 (0.99)	0.091 (0.0019)	-0.044 (0.0029)

Table 6.4: Summary of the non-polar surface energy and acid/base character of the different batches of nabumetone.

The acid/base character of the surface also exhibited changes after micronisation of the non-micronised nabumetone. The acidic nature of the samples increased immediately post-micronising (greater acidic components protruding out on the surface). With time, this character reduced towards that observed for the non-micronised form. However, after 5 months post-micronisation, the K^A value was lower than the original value for non-micronised nabumetone. This suggested that the recovery of the sample produced a surface that would interact with basic probes to a lesser extent. Therefore the micronised sample may now have possessed a different energetically stable state to the original compound. The K^D values obtained were all negative and attempts at re-plotting the data using heats of vaporisation and boiling points of the probes against $RTlnV_N$ instead of molecular area proved unsuccessful. In fact the correlation of the polar probes for the DN/AN* versus $-\Delta G_A^{SP}$/AN* plot decreased for these alternative methods of analysis.

Importantly, the IGC technique proved successful where the DVS technique failed. Data were obtained from IGC to help follow changes that occurred after micronisation for nabumetone. However, no data from the DVS were produced to follow such changes as the adsorption of the probes onto the surface of the material was too small to differentiate between.

6.4.3 Surface Energetics Of Theophylline

Investigations with DVS-NIR and XRPD (section 4.2.2) have highlighted the differences between the three crystal lattice structures of theophylline. Anhydrous theophylline converts to the monohydrate above 80% RH (Fokkens & Blaey, 1984; Rodriguez-Hernando *et al.*, 1992; Serajuddin, 1986; Lehto & Laine, 2000; Zhu *et al.*, 1996). This hydrate is lost below 20% RH (Fokkens & Blaey, 1984; Suihko *et al.*, 1997; Yoshihashi *et al.*, 1998). However, the subsequent anhydrous lattice structure (dehydrate) is different to the original anhydrous form. Over time and under appropriate conditions, dehydrated theophylline will revert back to the energetically stable original anhydrous form. IGC was utilised to explore whether the three lattice structures could be differentiated between. Also measurements were taken to compare two batches of theophylline (Sigma and Fluka) that were supposedly comparable.

6.4.3.1 Determination Of The Dispersive Surface Energies Of Theophylline

The dispersive component for each form of theophylline was calculated [Fig. 6.14]. The anhydrous form was maintained by setting the column to run at 0% RH. The monohydrate was prepared in a 97% RH desiccator and the dehydrate was subsequently formed from the hydrate in a 0% RH desiccator (described in section 3.12). The monohydrate columns were run at 30% RH and the dehydrate columns at 0% RH to maintain the respective forms of theophylline throughout the experiments. All five of the non-polar probes were eluted. Statistically (ANOVA), all the dispersive component values were significantly different (p-value <0.05) from each other. The anhydrous forms of both batches showed very different non-polar values. The Fluka batch presented a much higher dispersive component (48.1 mJ/m^2) than the equivalent Sigma batch (39.3 mJ/m^2). Such a high difference in values must suggest a greater non-polar surface for the Fluka batch. This would most likely have been created during processing of the product into the powder form. The results seen point out the problems faced by the pharmaceutical industry. Large differences between the same powdered compound manufactured by two divisions of the same company (Sigma-Aldrich,

Poole, UK), will undoubtedly interact with excipients differently when formulated into other dosage forms such as tablets.

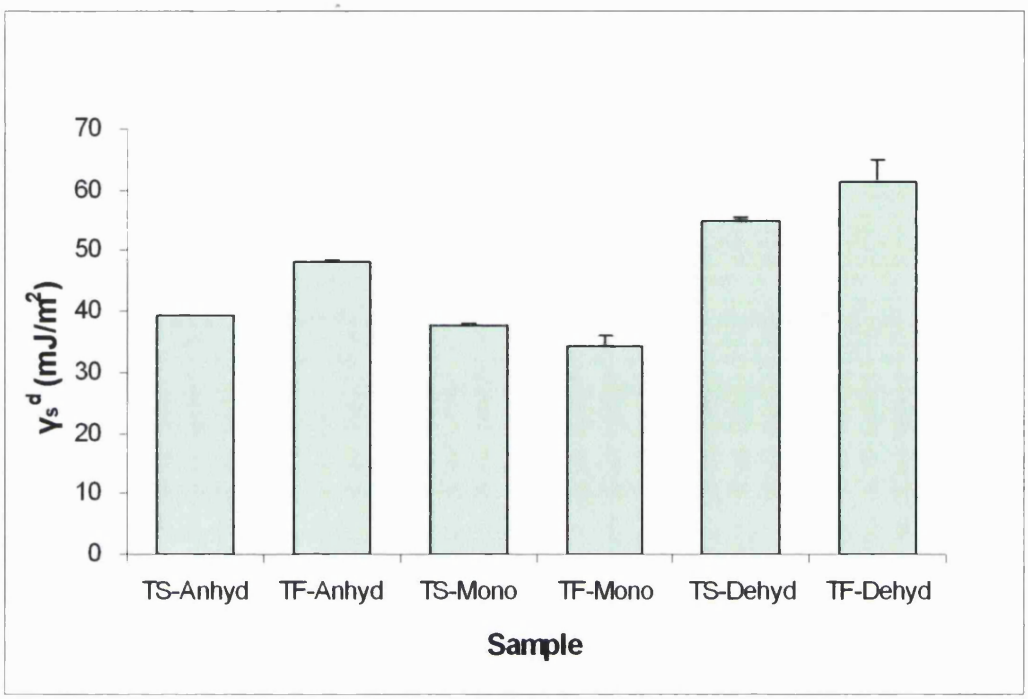

Fig. 6.14: Bar chart showing the variation in dispersive component of the tested theophylline batches. (N.B. T = Theophylline, S = Sigma & F = Fluka).

IGC measurements taken after hydration of theophylline showed a decrease in the dispersive component compared to the values obtained for the anhydrous crystal lattices. Incorporation of water in the structure (to form the monohydrate) and some probable adsorption on the surface had reduced the availability of non-polar sites for the probes to interact with. The lowering effect of the dispersive component by high humidity has been shown in the past (Cantergiani & Benczedi, 2002). The difference in the dispersive component between the anhydrous (39.3 mJ/m^2) and the monohydrate (37.8 mJ/m^2) Sigma batches was small but statistically significant (ANOVA, p-value <0.05). However, when comparing the Fluka batch the hydrate showed a value (34.4 mJ/m^2) that was 14 mJ/m^2 lower. These data showed that the incorporation of water changed the surface of the Fluka batch greatly. Contrastingly monohydrate conversion of Sigma anhydrous theophylline showed only a small change in dispersive

component, suggesting the interaction with water was different to that seen with the Fluka batch. Therefore the hydrate state of a compound can have a marked effect on the surface energetics of the material.

Finally investigations of the dehydrated batches of theophylline were analysed. As already shown, DVS-NIR and XRPD (section 4.2.2) have proven that the dehydrated form of theophylline was structurally different to the original anhydrous form. The data from IGC showed that both batches exhibited significantly higher dispersive component values (Sigma = 54.8 mJ/m^2 and Fluka 61.2 mJ/m^2) than the original anhydrous forms. The higher values observed represented the fact that the dehydrated form was energetically unstable (at the higher energy state) and therefore a greater interaction with the non-polar probes was observed. Once again the Fluka batch exhibited the higher dispersive value than the Sigma batch, as the standard anhydrous value for the Fluka batch was also higher.

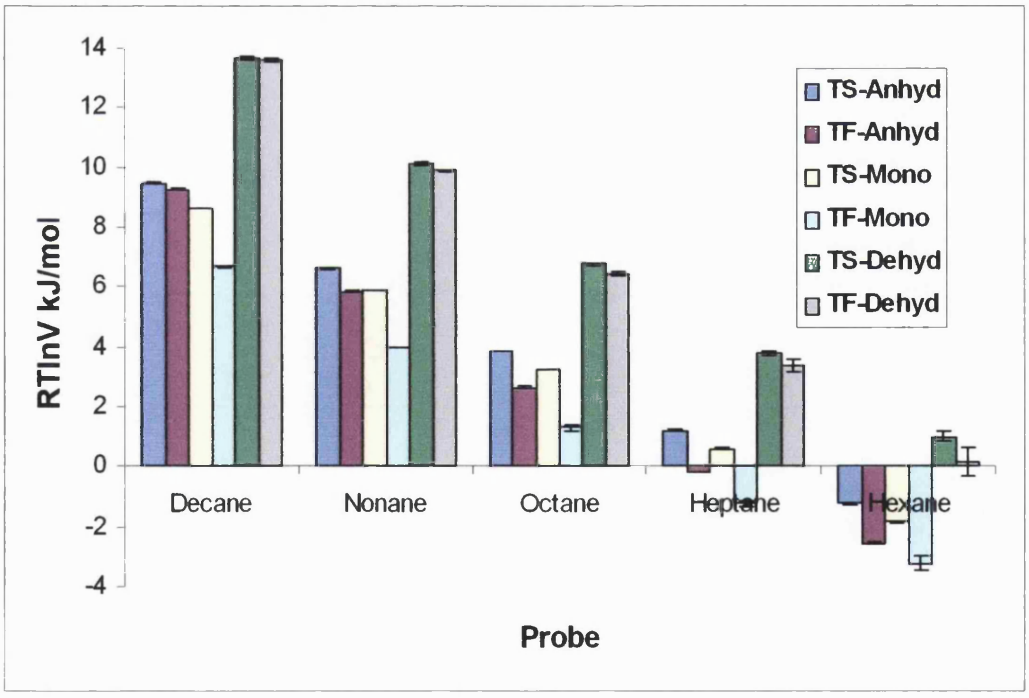

Fig. 6.15: Bar chart showing the variation in interaction of the non-polar probes on the different batches of theophylline. (N.B. T = Theophylline, S = Sigma & F = Fluka).

The interaction of the individual non-polar probes [Fig. 6.15] also provided similar discussion to that already presented for the dispersive values of theophylline. The interaction of the non-polar probes with the material surface was found to be the weakest for the monohydrate batches and the strongest with the dehydrated forms. Therefore the incorporation of water into and/or onto the monohydrate form provided less non-polar components at the surface for the apolar probes to interact with. Also the dehydrated form, being unstable, provided a surface that was found to be highly interactive with the probes. Interestingly all the probes interacted to a lesser degree with the Fluka batch than its equivalent Sigma batch, but produced a higher dispersive component for the Fluka samples. This occurrence was explained by the fact that the gradient of the linear plot (from where the dispersive value is obtained) of the non-polar probes was greater for the Fluka batches compared to their respective Sigma forms of theophylline.

6.4.3.2 Determination Of The Acid/Base Character Of Theophylline

Investigations into the acid/base nature of theophylline were also conducted to provide a greater understanding of the surface changes of the different forms and batches of theophylline. All four of the polar probes were eluted within the maximum experimental time.

The acid/base character [Fig. 6.16 & Fig. 6.17] showed a similar trend to the results discussed for the dispersive component. Comparisons of the K^A values for the lattices of each batch separately were found to be significantly different (ANOVA, p-value <0.05). The K^A value for the Fluka batch of the equivalent lattice structure was always higher than the Sigma batch and also significantly different. Thus the Fluka sample possessed a more acidic surface (electron accepting). After conversion to the monohydrate form the respective acidic components decreased when compared to the original anhydrous form. This suggested that the incorporation of water into the lattice structure and some possible adsorption onto the surface reduced the availability of acidic sites for interaction.

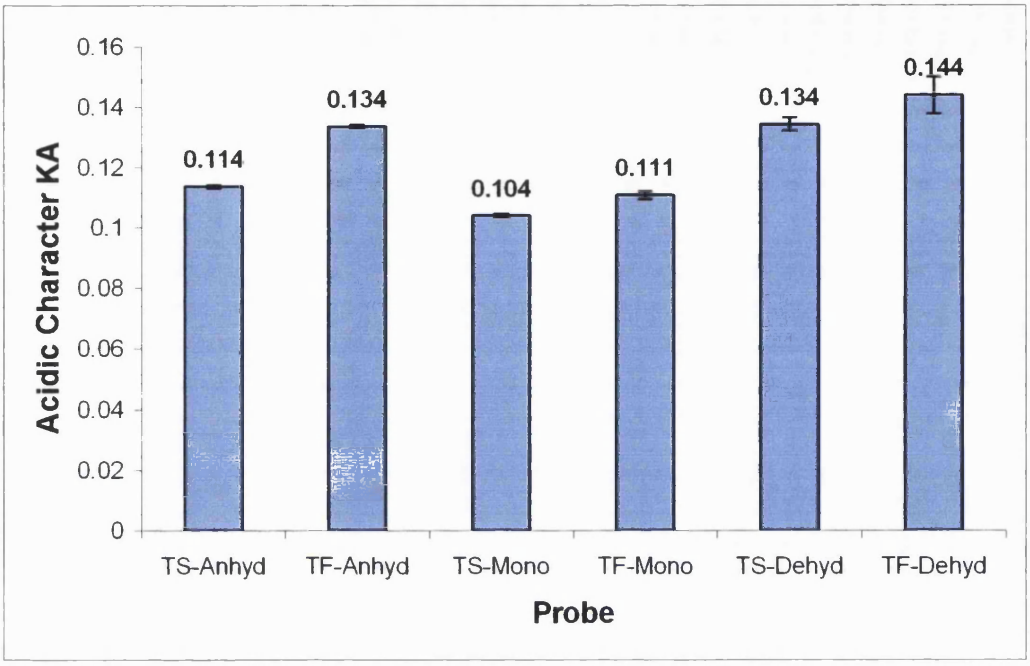

Fig. 6.16: **Acid character of theophylline batches. (N.B. T = Theophylline, S = Sigma & F = Fluka).**

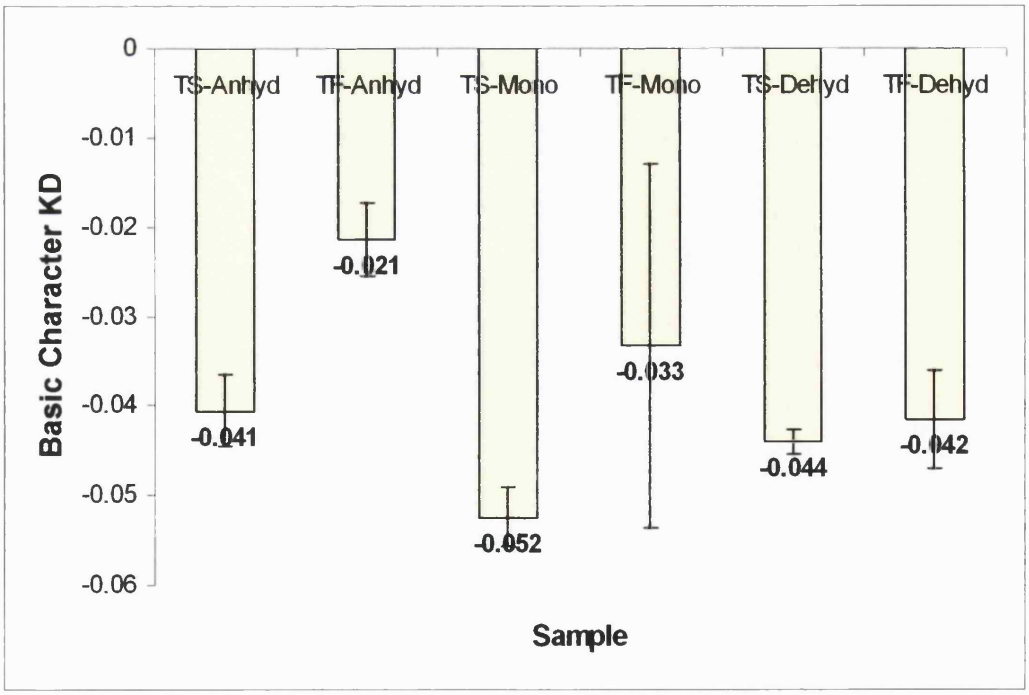

Fig. 6.17: **Basic character of theophylline batches. (N.B. T = Theophylline, S = Sigma & F = Fluka).**

In two ways, the hydrate formation could have re-orientated the acidic groups of the drug away from the surface and secondly any adsorbed water could have blocked acidic sites on the surface. The removal of water, to produce the dehydrated crystal lattice, showed the highest K^A values of all the three polymorphs. Therefore after hydrate loss the lattice changed to provide the largest number of polar acidic sites for interaction on the surface of the material. Such large differences in the K^A values of the different lattices and batches highlight the importance of batch reproducibility, and understanding the properties of the material can change under varying conditions.

Similar to the nabumetone data the K^D values were all negative. Theoretically it should be impossible for a compound to show a negative value for the basic character (or even the acidic character). The interaction of polar probes should be expected to provide higher energies of adsorption than non-polar probes. Such is the case, as polar probes should involve both Van der Waals forces (only seen for the dispersive, non-polar component) and polar interactions (acid-base interactions). As a result no relevant information could be obtained from such data.

With calcium mupirocin and nabumetone investigations it had been shown that an increase in the K^A value was accompanied by a decrease in the interaction of the acidic probes with the surface. Similarly, an increase in the K^D value was associated with a decrease in the basic probe interactions. These comparisons have justifiably been made for samples that have changed to a small degree due to micronisation and have shown recovery over a period of time. However, with theophylline different batches and different crystal lattice structures were being investigated [Fig. 6.18]. As a result comparisons of the actual probe interactions may not necessarily follow the same patterns as that seen for calcium mupirocin and nabumetone.

An increase in K^A value from the anhydrous to dehydrate form did not correlate with a respective decrease in surface interaction with ethanol and chloroform. The hydrated structure having the lowest acidic component did not however show the greatest interaction with the acidic probes (ethanol and chloroform).

Conversely, interpreting the results of the basic probes (acetone and ethyl acetate) did show trends as expected. The hydrated forms of theophylline interacted with the basic probes the least as they had the lowest K^A values (least acidic components on the surface for interaction with the probes). Also the dehydrated crystal lattice surfaces interacted with the basic probes the greatest as the most acidic components (of all three lattices) were available.

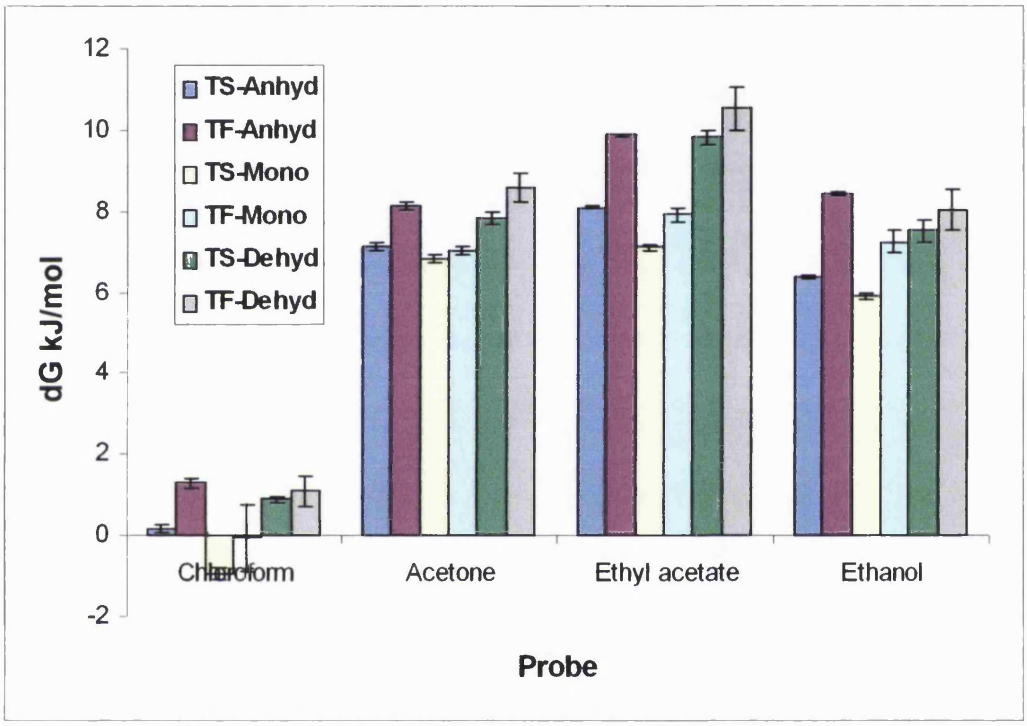

Fig. 6.18: Bar chart showing the variation in interaction of the polar probes on the different batches of theophylline. (N.B. T = Theophylline, S = Sigma & F = Fluka).

It must be remembered that the K^A value is dependent on the gradient of the line of best fit of the polar probes (DN/AN* versus $-\Delta G_A^{SP}/AN^*$). Therefore the combined interaction of the polar probes (and not the direct comparison of the probes) in this case provided a better explanation of the results observed. In every plot [Fig. 6.19] the Fluka batch showed a steeper slope for the line of best fit, and hence a larger gradient relating to the higher K^A value.

Attempts were made to quantify the acid/base character of the batches using data plotting the heats of vaporisation (ΔH^{D}_{VAP}) and boiling point values (T_b) that determined the free energy of adsorption (section 6.3.3). This was instead of the molecular area as a function of the dispersive component of the liquid probes ($a(\gamma^{D}_{L})^{0.5}$). Hopefully the re-plotting of the graph (from the new specific free energy of adsorption of the polar probes) could help to eliminate the negative K^{D} values for the basic component.

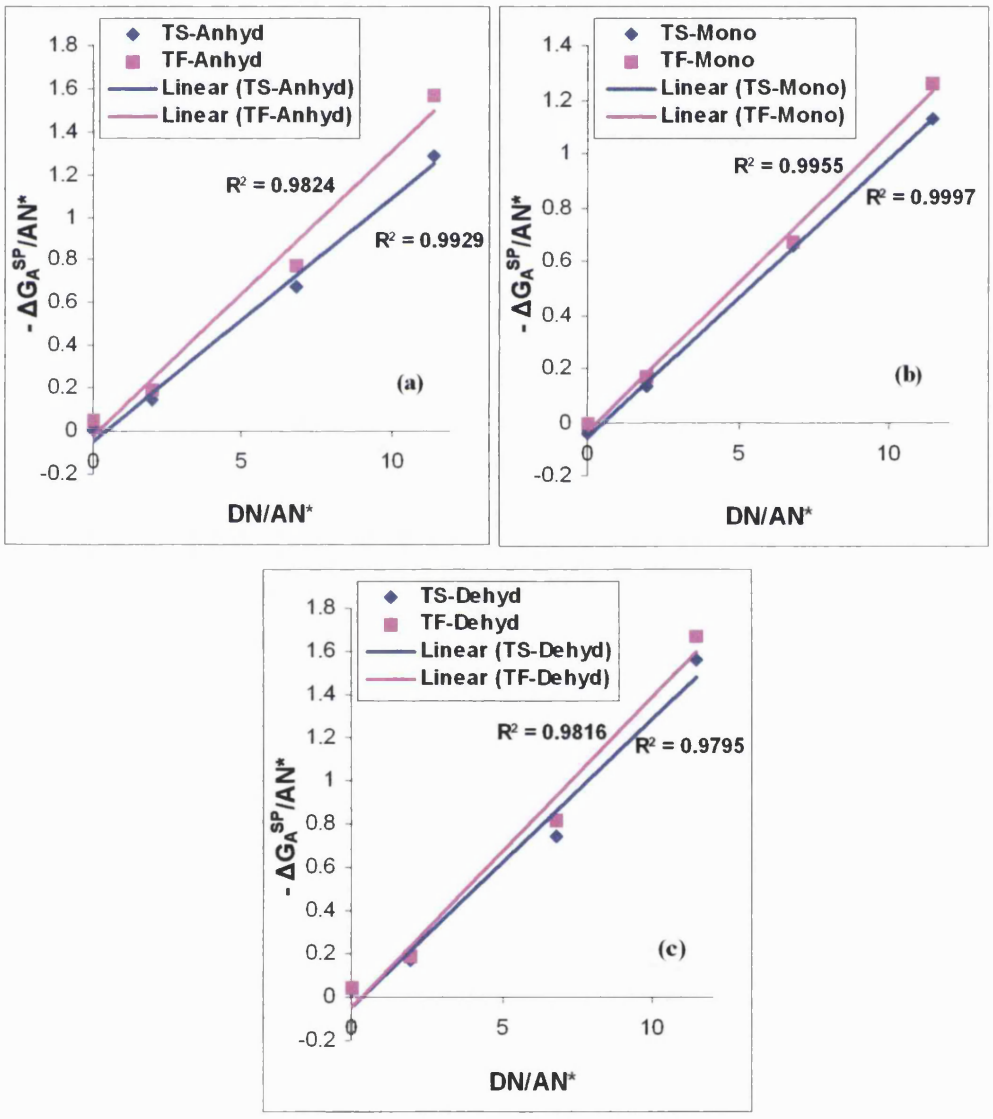

Fig. 6.19: **Plots of DN/AN* versus $-\Delta G_A^{SP}/AN^*$ to show the variation in gradient of the lines of best fit for Sigma and Fluka batches of theophylline (a) anhydrous, (b) monohydrate and (c) dehydrate. (N.B. T = Theophylline, S = Sigma & F = Fluka).**

A comparison of all three methods [Fig. 6.20], for anhydrous theophylline Sigma batch, showed that the R^2 value of the lines of best fit were poor for both the heat of vaporisation and boiling point methods of analysis. The poor correlation prevented justifiable use of these methods to obtain K^A and K^D values and further analyse the remaining data. Re-plotting in such a manner did not always remove the negative values, however the approach may have been better suited if a greater number of probes were used. The use of boiling points as an alternative method has also been shown to provide negative acid-base interaction energies by other authors (van Asten *et al.*, 2000).

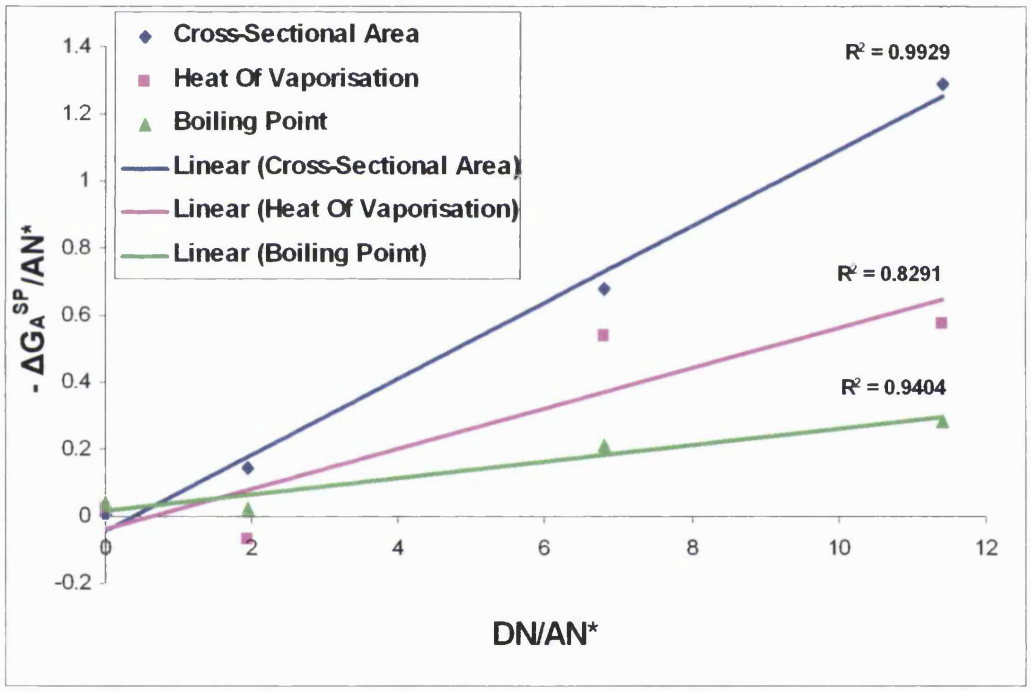

Fig. 6.20: Acid/base plot for the Sigma batch of anhydrous theophylline as an example to show the correlation of the polar probes using 'cross-sectional area', 'heat of vaporisation' and 'boiling point' data of the probes. (No ethanol data for heat of vaporisation plot).

6.4.3.3 Conclusions Of The Surface Energetics Of Theophylline

The results of the IGC experiments [summary – Table 6.5] on the three crystal lattice structures of theophylline clearly highlighted differences between the

forms. The Fluka batch always presented a higher dispersive and K^A value than the equivalent lattice form of the Sigma batch. This emphasised the problem of batch-to-batch variation from two branches of the same company. The incorporation of water to form the monohydrate changed the structure of the drug to reduce the interactions with both the non-polar and polar probes, resulting in lower dispersive and K^A values. Thus the water in the system reduced the available non-polar and acidic sites on the surface of the theophylline batches.

Sample (Column RH)	γ^D_S (mJ/m^2) (S.D.)	K^A (S.D.)	K^D (S.D.)
Sigma Anhydrous (0%)	39.3 (0.16)	0.114 (0.0005)	-0.041 (0.0040)
Fluka Anhydrous (0%)	48.1 (0.34)	0.134 (0.0005)	-0.021 (0.0042)
Sigma Monohydrate (30%)	37.8 (0.39)	0.104 (0.0008)	-0.052 (0.0034)
Fluka Monohydrate (30%)	34.4 (1.67)	0.111 (0.0014)	-0.033 (0.0202)
Sigma Dehydrate (0%)	54.8 (0.84)	0.134 (0.0022)	-0.044 (0.0014)
Fluka Dehydrate (0%)	61.2 (3.78)	0.144 (0.0061)	-0.042 (0.0055)

Table 6.5: Summary of the non-polar surface energy and acid/base character of the different batches of theophylline.

The dehydrated form of theophylline produced the highest dispersive and K^A values of the three lattices. The dehydrated form is a polymorph of the original anhydrous theophylline. The higher values observed represented the fact that the dehydrated form was energetically unstable (at the higher energy state) and therefore a greater interaction with the non-polar and polar probes was observed. The K^D values measured were all negative and other methods of interpreting the data were not successful in removing the negative values. These differences between the three forms of theophylline may affect their interaction with excipients during manufacture. Therefore it is very important to be aware of the properties of the batch of theophylline being dealt with. Also it must be remembered that an unstable form, such as dehydrated theophylline, will over time and appropriate conditions revert back to the stable anhydrous form and so its surface character would accordingly alter.

6.4.4 Surface Energetics Of Magnesium Stearate

Previous studies (DSC section 4.5.2; XRPD section 4.5.3; TGA section 4.5.4; DVS section 5.4.6.3) have highlighted the problems associated with identifying the exact hydrate state of magnesium stearate and isolation of each hydrate form. The tests have shown the batches of excipient to exist in a multi-hydrate component system. With the impurities always found in commercial forms of magnesium stearate, it has proved difficult to manufacture batches of the same standard. This is an important problem faced by the pharmaceutical industry as the lubricant properties of the compound vary from batch-to-batch and rely on the impurities present. IGC would help provide another means of assessing and differentiating between different batches of magnesium stearate. Hopefully this would allow the appropriate selection of a batch of magnesium stearate that would be comparable to a favourable sample in the past.

It was hoped to run tests on different hydrate forms of magnesium stearate similar to the studies conducted on calcium mupirocin dihydrate and theophylline monohydrate. This was not deemed possible due to the presence of a multi-hydrate system. Also the problems faced by the DVS results (section 5.4.6.3) showed continual mass loss of water at 0% RH. This would change the structure and probable surface properties of the material as the experiment was running. However, tests were conducted to observe if this technique could be used to highlight any differences in the surface properties of the Sigma and Fluka batches of magnesium stearate.

6.4.4.1 Determination Of The Dispersive Surface Energies Of Magnesium Stearate

Of the five non-polar probes injected, decane did not elute within the maximum experimental time for each injection. The dispersive component of the excipient was suitably determined from the gradient produced by the remaining four non-polar probes [Fig. 6.21].

The experimentally obtained dispersive value for the Sigma batch (46.7 mJ/m^2) was much higher than the Fluka value (35.6 mJ/m^2). This was found to be significantly different (p-value <0.05) from the t-test. Thus, the surface of the Sigma batch protruded a greater degree of non-polar components than the Fluka sample. Also it must be noted that although the sample was expected to change over time whilst held at 0% RH (due to the loss of water from the lattice), the standard deviation values did not suggest any large changes in the characteristics of the surface.

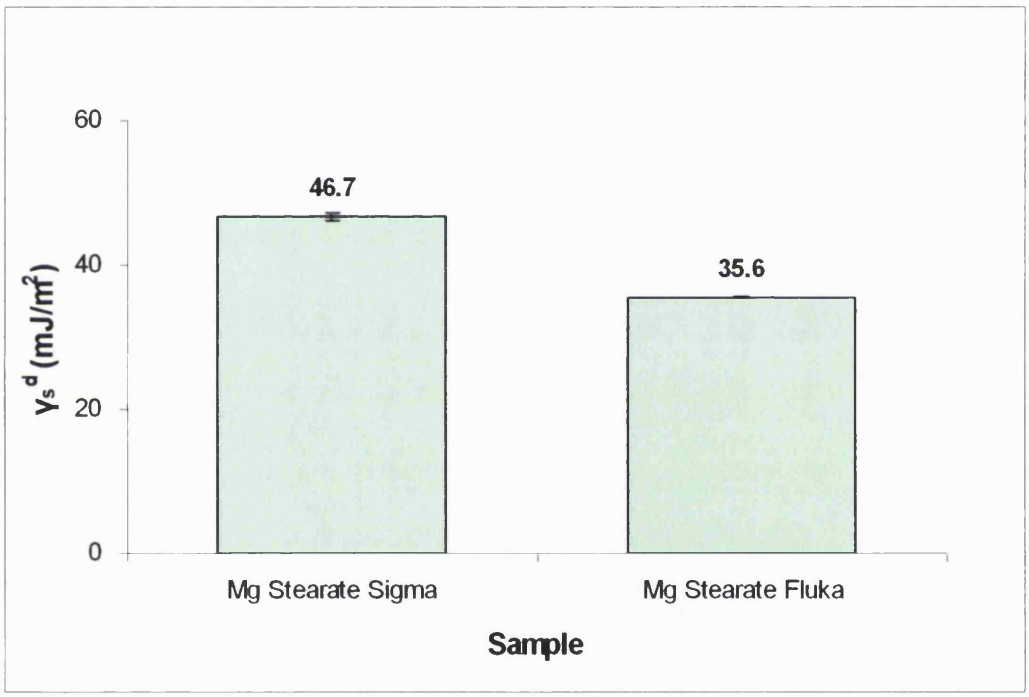

Fig. 6.21: Bar chart showing the variation in dispersive component of the tested magnesium stearate batches. (N.B. Mg = Magnesium stearate).

A comparison of the individual probes [Fig. 6.22] also highlighted the stronger interactions with the surface of the Sigma batch. This correlates well with the conclusion that the Sigma batch surface contains more non-polar components for interaction with the non-polar probes.

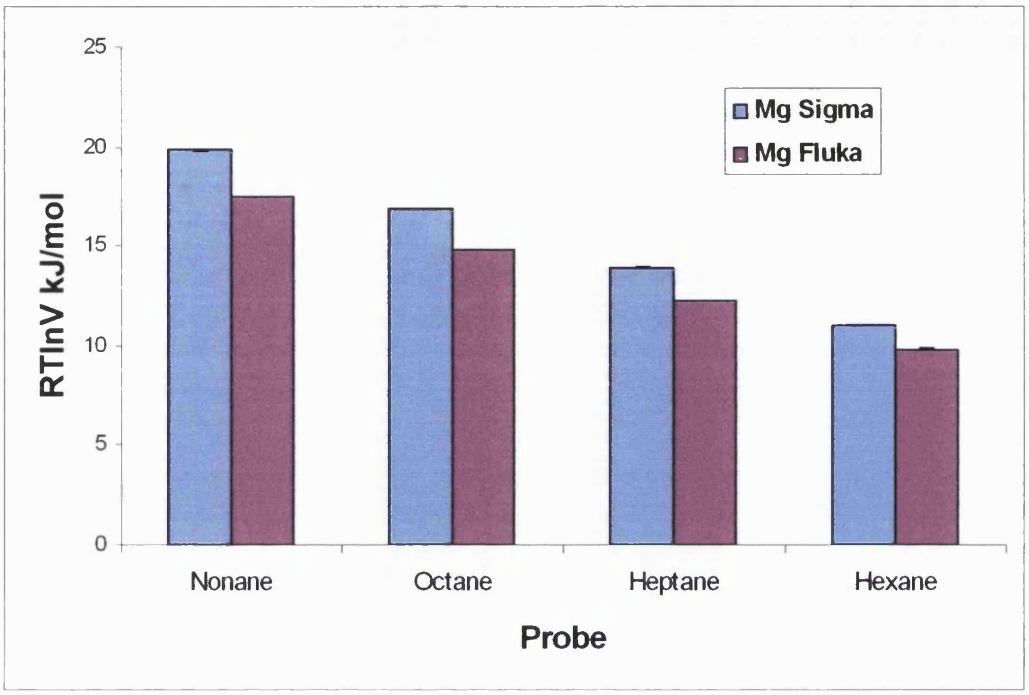

Fig. 6.22: Bar chart showing the variation in interaction of the non-polar probes on the different batches of magnesium stearate. (N.B. no decane peak eluted, Mg = Magnesium stearate).

6.4.4.2 Determination Of The Acid/Base Character Of Magnesium Stearate

The polar probes were used to determine the acid/base character of the surface of the magnesium stearate batches [Fig. 6.23 and Fig. 6.24]. The Sigma batch exhibited a significantly higher (*t*-test, *p*-value <0.05) acidic character on its surface (0.11) compared to the Fluka batch (0.072). This suggested that the surface of the Sigma batch was composed of more acidic components and/or the acidic parts of the compound were available for interaction on the surface to a greater extent.

Regarding the basic character of the two batches, as expected, the Fluka batch showed the higher K^D value (significantly different – *t*-test, *p*-value <0.05) due to its respective K^A value being lower than that observed for the Sigma batch. Thus, it would suggest that there was a greater basic surface for the Fluka batch.

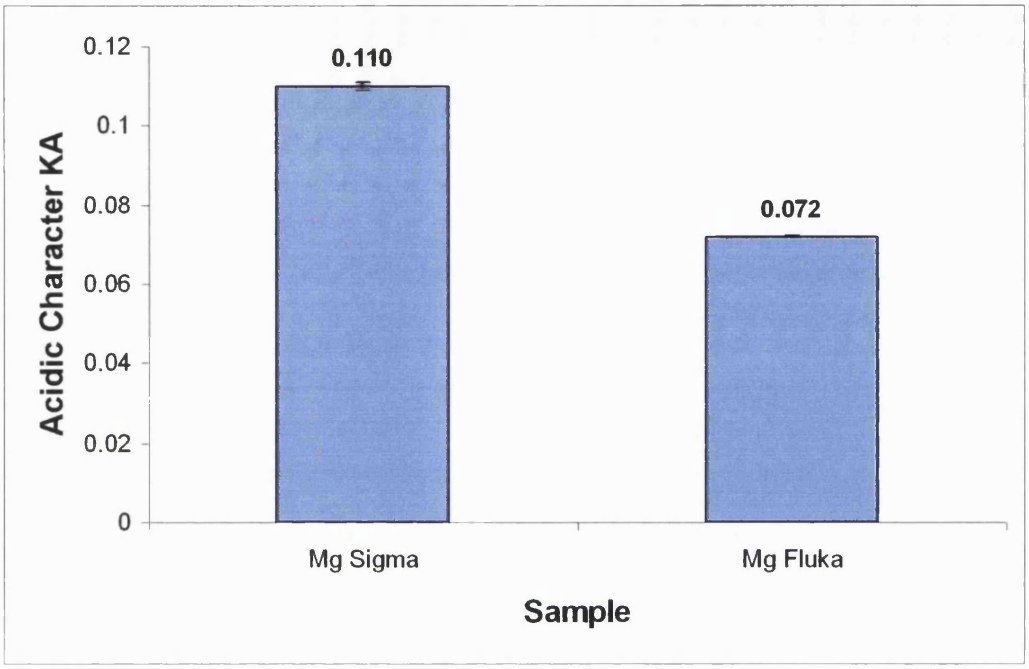

Fig. 6.23: **Acid character of magnesium stearate batches. (N.B. Mg = Magnesium stearate).**

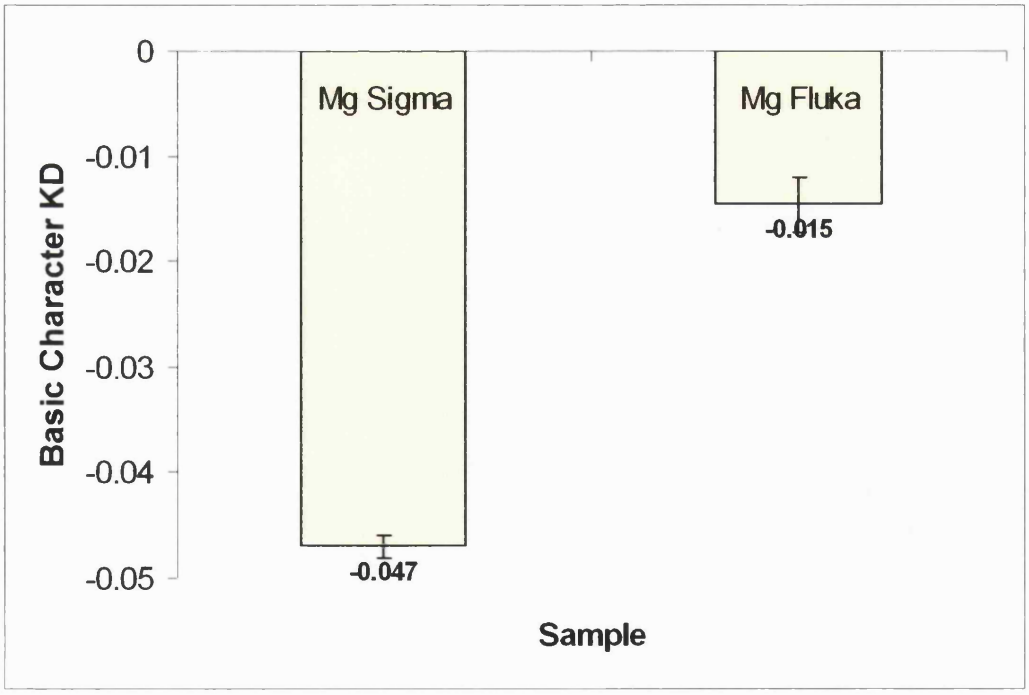

Fig. 6.24: **Basic character of magnesium stearate batches. (N.B. Mg = Magnesium stearate).**

However, all the results for K^D were of a negative value. Theoretically it is impossible for a compound to show a negative basic value (or even an acidic value). The interaction of polar probes should be expected to provide higher energies of adsorption than non-polar probes. Such is the case, as polar probes should involve both Van der Waals forces (only seen for the dispersive, non-polar component) and polar interactions (acid-base interactions).

The graph comparing the interaction of the polar probes [Fig. 6.25] correlates with the acid/base discussions already provided. The interaction of the basic probes (acetone and ethyl acetate) was strongest for the Sigma batch. This was hardly surprising as the basic probes interacted with the greater acidic components on the surface of the Sigma material.

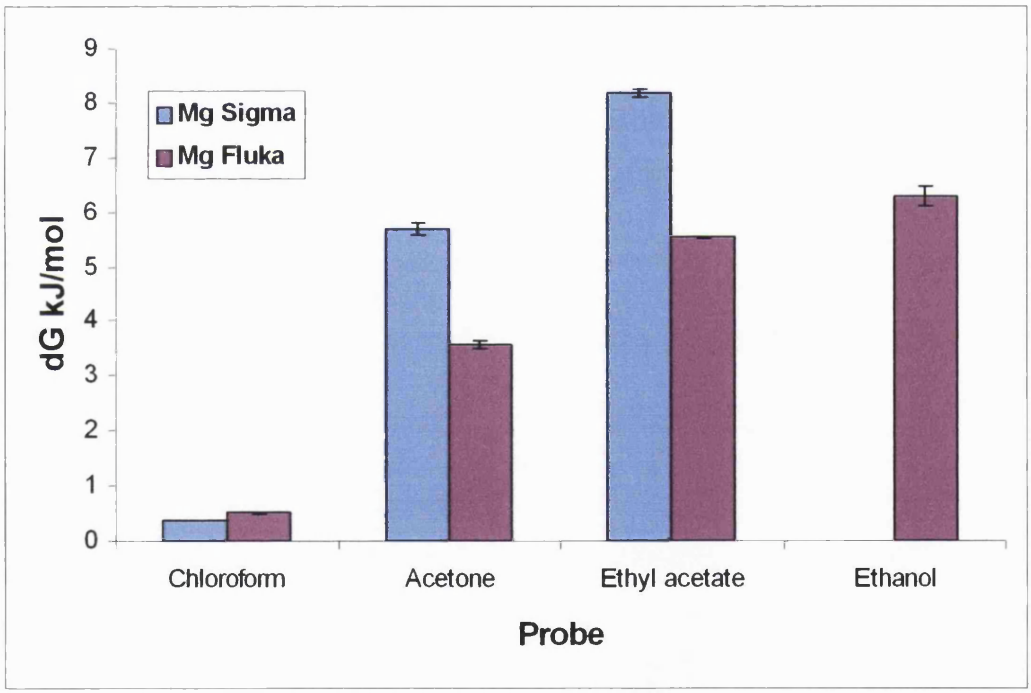

Fig. 6.25: Bar chart showing the variation in interaction of the polar probes on the different batches of magnesium stearate. (N.B. no ethanol peak eluted for the Sigma batch, Mg = Magnesium stearate).

The heats of vaporisation (ΔH^D_{VAP}) and boiling point values (T_b) have been used, instead of the molecular area as a function of the dispersive component of the

liquid probes ($a(\gamma^D_L)^{0.5}$), to determine the free energy of adsorption values (section 6.3.3). From these values the acid-base character could also be established and hopefully the re-plotting of the graph could help remove the negative values seen for the basic component (K^D value). The plot of all three methods of measurement for the Sigma magnesium stearate batch [Fig. 6.26] showed that the R^2 value of the line of best fit for the acid/base plot was poorer for the heat of vaporisation and boiling point analysis methods. With such a correlation there was no justification in using the K^A and K^D values that such a plot produced. Correlation could have been improved if a greater number of polar probes had been injected. This would also have been able to show whether one of the probes was causing distortion of the lines of best fit.

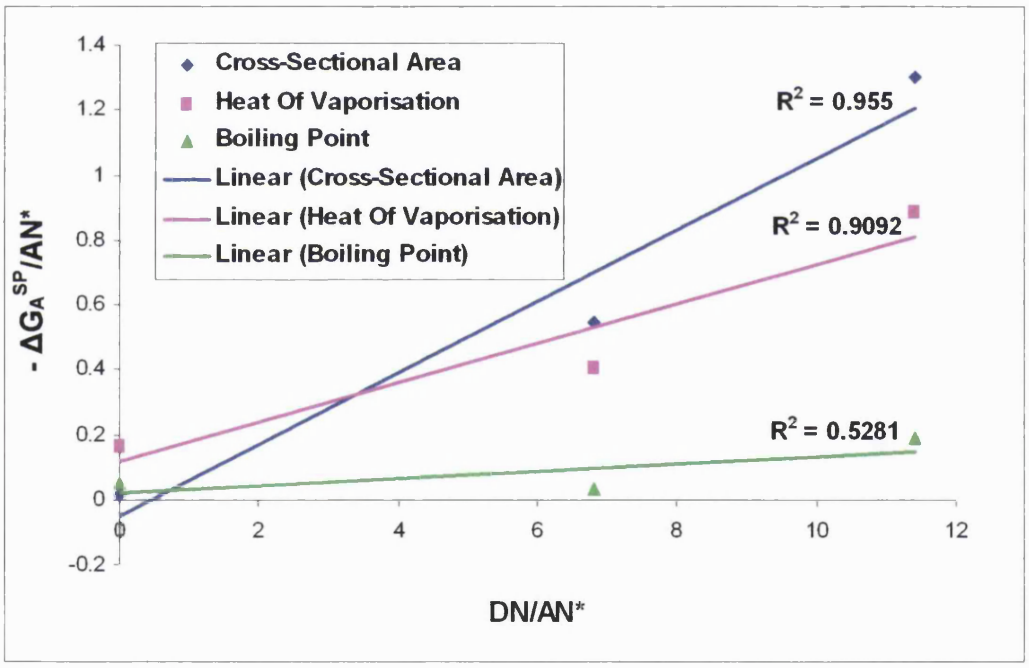

Fig. 6.26: **Acid/base plot for the Sigma batch of magnesium stearate as an example to show the correlation of the polar probes using 'cross-sectional area', 'heat of vaporisation' and 'boiling point' data of the probes. (No ethanol data for any plot).**

6.4.4.3 Conclusions Of The Surface Energetics Of Magnesium Stearate

The IGC studies on magnesium stearate [summary – Table 6.6] showed that the surface of the Sigma batch was more non-polar and acidic compared to the Fluka batch. This showed that although the samples were manufactured by two divisions of the same company (Sigma-Aldrich), there was a large difference between the surface properties of the materials. This difference must have been produced during some stage of the processing. Unfortunately it was not possible to analyse the different hydrates of these commercial batches of magnesium stearate. This was due to the multi-hydrate system that the excipients existed in. Such experiments would have been possible to perform on pure magnesium stearate as isolation of the different hydrate forms is manageable. Thus IGC will only be useful in the pharmaceutical industry to purely compare batches of magnesium stearate, and to find a suitable candidate that provides the most ideal lubricant properties.

Sample	γ^{D}_{S} (mJ/m^2) (S.D.)	K^{A} (S.D.)	K^{D} (S.D.)
Mg Stearate Sigma	46.7 (0.56)	0.110 (0.0010)	-0.047 (0.0011)
Mg Stearate Fluka	35.6 (0.20)	0.072 (0.0002)	-0.015 (0.0026)

Table 6.6: Summary of the non-polar surface energy and acid/base character of the different batches of magnesium stearate.

6.5 Comparison Of DVS & IGC Techniques

Having investigated the four compounds with both DVS and IGC techniques to understand their surface characteristics, it was important to review the techniques and evaluate the advantages and disadvantages of both methods. The DVS was used to probe the powder surfaces of the materials with solvents covering a full range of polarities to measure the degree of interaction with the probes, thus providing information on the nature and wettability of the compounds and their surfaces. The extent of interaction was determined using the BET theory. IGC was utilised to provide surface characteristics of the materials in terms of their

energetics. This was obtained by calculating the dispersive component and acid/base character of each surface. Both techniques were used to identify differences between batches after micronising or directly from suppliers.

Although both instruments were providing results regarding the surface of the materials, different types of information were obtained. The compounds in the DVS were subjected to finite concentrations of probe vapour to progressively obtain full surface coverage (monolayer). This interaction with the probes gave an indication of the wetting properties of the sample. On the other hand, very low concentrations (infinite) of probes were injected onto the materials in the IGC. This allowed the higher energy sites on the surface to preferentially interact with the probes.

Compound	DVS	IGC
Calcium Mupirocin	YES	YES
Nabumetone	NO	YES
Theophylline	YES*	YES
Magnesium Stearate	NO	YES

Table 6.7: A table showing the applicability of the DVS and IGC techniques to the four compounds under investigation. (*Applicable only for the study of different crystal lattices).

The DVS technique only proved successful in providing data for calcium mupirocin (adsorption studies only) [Table 6.7]. It showed that with all the selected probes (except hexane) a greater degree of wetting was observed with the freshly micronised sample compared to the non-micronised batch. This interaction reduced over time when the micronised sample was re-tested after one year, suggesting recovery of the material. It was found that after manipulation with the BET equation the strongest interaction was found to occur with the more polar probes and reduced as the polarity decreased. This pattern remained constant regardless of the batch investigated. Using a plot of solvent

polarity versus BET intercept, successful prediction of the wettability of butan-1-ol was performed on the drug. With IGC calcium mupirocin also provided interesting surface data. With the non-polar components very little change was seen after micronisation (although statistically significantly different). This was similar to the DVS results where no measurable change in adsorption occurred with hexane. However with the polar probes (K^A and K^D values), the acidic character of the material increased after micronisation and subsequently reduced over time. Thus IGC was able to show changes to the surface of the material after processing which recovered over time (in the same manner as the DVS).

With the three other materials no meaningful surface data could be obtained with the DVS method. However, the DVS technique (along with NIR – section 4.2) did allow the characterisation of the three crystal lattices of theophylline along with the crystallisation of the 'ghost hydrate structure'. Nabumetone, being a strong hydrophobic drug, was unable to show any adsorption with all five solvents that could be recorded by the DVS. Similar problems were observed with theophylline too. Although not strictly hydrophobic, at low partial pressures (0.05 – 0.35) no measurable adsorption onto the surface of the material took place. However it must be remembered that differences in the two batches of theophylline have been highlighted using DVS during conversion of the anhydrous form into the monohydrate (section 4.2.5). Unfortunately though the technique of applying the BET equation was not possible. Finally, with magnesium stearate difficulties occurred due to the inability to equilibrate each partial pressure step (within 3-4 h) due to the loss of water from the excipient. The BET theory could only be applied if equilibration at each partial pressure had been reached.

Where the DVS technique failed the IGC technique prospered [Table 6.7]. The ability to interact with the higher energy sites showed that IGC could provide valuable data to show differences between different batches. With nabumetone changes in surface character were exposed after micronisation and subsequent recovery with both the dispersive and acid/base components were followed. With theophylline and magnesium stearate differences in the Sigma and Fluka batches were easily determined.

One area where the DVS studies did not provide successful results for calcium mupirocin was on the hydrate form of the drug (section 5.4.5). Each time the hydrate would be stripped off when probed with the solvents. The only solvent where the loss of hydrate would not occur was when probed with water. With the other solvents the hydrate was lost due to the inability to provide a constant flow of water vapour sufficient enough to retain the hydrate. The IGC apparatus already had a system that allowed the flow of water vapour through the column whilst injecting with the probes. This allowed the study of the surface of calcium mupirocin dihydrate and theophylline monohydrate. Both materials showed the lowest dispersive values and acidic character. This suggested that the incorporation of water reduced the interaction of the probes with the material surface.

6.5.1 DVS versus IGC – Advantages & Disadvantages

The advantages and disadvantages of both techniques have been listed in relation to using the BET theory for wettability data (DVS) and the IGC used for surface energetics information. There are many other uses of both techniques, some of which are common to both methods such as isotherm formation, but they have not been discussed with regards to their advantages and disadvantages. Tables 6.8 and 6.9 detail the positives and negatives of both techniques.

No other techniques were able to show any differences between non-micronised and micronised data except for DVS (calcium mupirocin alone) and IGC (calcium mupirocin and nabumetone). XRPD, HDSC and solution calorimetry all failed to highlight any variation in non-micronised and micronised forms of calcium mupirocin (section 4.3.2) and nabumetone (section 4.4.2). The DVS and IGC techniques have provided another means of detecting variations in batches that may not have otherwise been identified, and shown characteristics of material surfaces as to their interaction with probes. Knowing this information, in industry, can allow the selection of the appropriate solvent during processing in order to prevent certain undesirable changes to the original compound.

Advantages Of DVS	*Disadvantages Of DVS*
▪ No sample preparation. The sample can be placed directly into the measuring pan. ▪ Fast data production. ▪ Samples can be re-used for other techniques. ▪ The technique is very easy to learn and use. ▪ Very small quantities of powder are required. ▪ Can use organic vapours. ▪ Rapid construction of isotherms and kinetic data compared to the old fashioned method of using many desiccators of salt solutions covering the range of relative humidities. ▪ High reproducibility. ▪ Excellent humidity and temperature control.	▪ Does not work well with strong hydrophobic compounds. ▪ Is not as sensitive as IGC where all four compounds produce valuable data. ▪ Surface characteristics of hydrates as yet cannot be studied due to the loss of the hydrate when solvents other than water are used. ▪ Cleaning system to change probes can take 1-2 days (longer than IGC). ▪ Only valid for samples that produce a linear isotherm over the BET region. ▪ Equilibration times of each partial pressure could be too long and reduce the feasibility of such a study. ▪ BET theory is based on a number of assumptions that are unlikely to be achieved in the real world. ▪ Difficult to find a family of solvents that cover the full range of polarities.

Table 6.8: The advantages and disadvantages of the DVS technique.

Advantages Of IGC	*Disadvantages Of IGC*
▪ Speed of analysis. ▪ Accuracy of the concentration of probe being injected. ▪ Can get surface data for high energy sites (infinite dilution) and all surface coverage (finite dilution). ▪ Data can be obtained for hydrophilic and hydrophobic compounds. ▪ Hydrates can easily be studied due to a controlled humidity line passing through the column. ▪ Able to detect changes in the surface of micronised nabumetone and the recovery over a period of time. ▪ More sensitive technique than DVS as results for all four compounds were obtained. ▪ Changing of solvent and cleaning the system (purging) can be completed within 3-4 hours (faster than DVS). ▪ High reproducibility. ▪ Excellent humidity and temperature control.	▪ Column packing has to be performed carefully so that there is uniformity. Any re-organisation of particles can affect reproducibility of results. ▪ Difficult to pack a column using a wet and sticky material. ▪ Not as easy a technique to use as the DVS apparatus. ▪ More powder required to pack a column than with the DVS. ▪ Pre-packing of column required before beginning an experiment. ▪ With the IGC apparatus available it is not possible to use any solvents other than water in the humidifying bottles. ▪ Columns need to be silanised prior to packing. ▪ There is a maximum time limit for analysis of an injected probe. It must be ensured that the probe fully elutes within such a time. ▪ When passing humidity through a column it is difficult to know the extent at which the water molecules are competing with the injected probe for interaction with the surface. ▪ Negative acid/base values equates to poor theories.

Table 6.9: The advantages and disadvantages of the IGC technique.

7. FINAL CONCLUSIONS & FUTURE WORK

Aim – To characterise the compounds in terms of their crystal lattice structures (anhydrous and hydrate forms).

Accurate understanding of the characterisation of the lattice structure of compounds is important, as the form can have a bearing on its physicochemical properties.

The different crystal lattices of theophylline (section 4.2.2) were characterised by numerous techniques (DVS-NIR, XRPD, TGA and KF). The use of DVS-NIR provided simultaneous real time information to observe the changes of the lattice structure from anhydrous-hydrate-dehydrate. The technique highlighted the differences in the structures of the two polymorphs (anhydrous and dehydrated forms). The NIR spectra showed that the dehydrated form of theophylline, after water loss, maintained some spectral peaks characteristic of the hydrate and formed some peaks prevalent in the anhydrous lattice. The DVS-NIR technique also provided kinetic data (section 4.2.3) of peak changes to follow the conversion of the crystal lattices and highlighted the two-step dehydration process.

The conversion of the dehydrate back to the hydrate was also followed by DVS-NIR (section 4.2.4). The technique allowed the discovery of a new crystal lattice transition. During rehydration an anomalous mass loss, similar to crystallisation of an amorphous material, at 40-50% RH was observed. It was accepted that the dehydrate shared some stable anhydrate and some hydrate packing with spaces where the water molecules had departed. This has been termed a "ghost hydrate structure". These mixed crystals may therefore have amorphous content, as disorder between the different packing and even within the "ghost hydrate structure". NIR data helped follow the anomalous period. It showed that the sorption of water, during rehydration, allowed the structure to have sufficient mobility to transform back into the anhydrous form prior to hydrate formation. The combination of DVS-NIR data therefore is valuable in aiding the

characterisation of different crystal lattices of a powder, which should aid the understanding of how materials of pharmaceutical relevance may behave under environments they may meet during processing.

Calcium mupirocin existed as a dihydrate at ambient humidity and temperature. DVS studies [Fig. 4.16] showed the ease at which the hydrate could be lost at 0% RH. Nabumetone, a hydrophobic crystalline material, was not known to exist in any hydrated forms. Commercial magnesium stearate was understood to exist in multiple hydrate states. It did not prove possible to isolate any of the hydrate forms when stored under extreme relative humidities and analysed using DSC (section 4.5.2), XRPD (section 4.5.3) and TGA (section 4.5.4). It was concluded that the magnesium stearate was likely to consist of a mixture of hydrates at any one time. It also proved impossible to strip the magnesium stearate of moisture under 0% RH conditions. The complete loss of moisture is known to be a thermally activated process (Bracconi *et al.*, 2003). However, dehydration by heating would alter the structure of magnesium stearate due to melting of the fatty acid chain.

Future work could involve the use of DVS-NIR to follow the changes in structure of commercial magnesium stearate under varying humidity and temperature. This may help identify the changes in hydrate states.

Aim – To investigate the materials in terms of their batch-to-batch variability as regards to the effects of micronisation and direct batch comparisons from supplier products obtained from Sigma-Aldrich, Poole, UK (Sigma and Fluka batches).

XRPD, HDSC and solution calorimetry techniques were unable to determine any amorphous nature within non-micronised and micronised forms of calcium mupirocin (section 4.3.2) and nabumetone (section 4.4.2). Either the instruments were not sensitive enough to detect such low amounts of amorphous nature, or the samples recovered rapidly after micronisation that no amorphous character remained when tested. SEMs, dry particle sizing and specific surface area

measurements for both drugs confirmed that the size of the micronised particles was significantly reduced and the surface area increased.

Sigma and Fluka batch comparisons for theophylline (section 4.2.5) clearly showed differences between two supposedly equal batches, supplied from the same company. Hydrate formation with the Sigma batch took place at a faster rate than the Fluka batch. This was shown to be a cause of the differences in particle size and shape between the two batches. SEM pictures showed that the shape of the crystals were thin and needle-like in nature (Sigma batch). However, the crystals from the Fluka sample were much bigger and some of the larger crystals had other particles aggregated to them. Also there were a greater variety of sizes with the Fluka particles. Dry particle sizing corroborated the observations made from the SEMs, that there was a larger particle size distribution for the Fluka batch. Also surface area analysis showed that the Sigma batch had a greater surface area and therefore explained the ease at which hydrate formation would occur. Sieving of the Fluka batch successfully reduced the time taken to hydrate the anhydrous sample, due to the smaller size distribution of the particles.

All studies conducted on the Sigma and Fluka batches of commercial magnesium stearate have shown the samples to be different. DSC studies (section 4.5.2) have shown the Fluka sample to produce three thermal events as opposed to one (with a shoulder peak) by the Sigma sample. This suggested possible differences in the fatty acid composition and hydrate forms. XRPD patterns (section 4.5.3) showed three distinct peaks for the Fluka batch and just one broad peak for the Sigma sample at approximately 21° 2θ region. It proved difficult to ascertain the exact state of each sample due to the x-ray spectra probably producing overlapping reflections from all the hydrates present. TGA investigations (section 4.5.4) showed that the Fluka batch contained approximately 1% more moisture than the Sigma batch. However, it was not possible to distinguish the hydrate state of each batch due to the mixture of hydrate forms present.

Future work could involve micronising calcium mupirocin and nabumetone under 0% RH conditions. This would provide the opportunity to minimise the

recovery of any amorphous nature created during micronisation by moisture within the air. The techniques already employed to characterise any amorphous nature could then be re-utilised to establish the degree of amorphousness created after micronisation.

Aim – To study the nature and wettability of compounds and their surfaces when probed with polar and non-polar solvents to compare:

a) Effects of micronisation.

The degree of wetting (adsorption) by a series of solvents (varying polarity) was measured on micronised forms of calcium mupirocin and nabumetone by DVS. With the application of the BET equation it was successfully shown (sections 5.4.1 and 5.4.2) that there was a greater surface interaction with all the probes after micronisation for anhydrous calcium mupirocin than for the non-micronised batch. The material interacted greater with the more polar probes, with decreasing interaction as the polarity of the solvent reduced. In fact there was no change seen with the least polar probe (hexane). The greater degree of adsorption observed for the freshly micronised material was expected due to the increased specific surface area and/or the increased surface energy as a result of the production of any amorphous nature. The importance of the technique was emphasised when experiments were re-conducted on the micronised batch after one year of storage under standard room temperature and humidity. The results showed greater adsorption of the solvents than the non-micronised batch but surprisingly statistically significantly less than the freshly micronised batch. This confirmed that the sample was recovering over time, and suggested that the increased adsorption was not purely due to the change in specific surface area but also a change in the energy of the surface.

The relative polarity versus BET intercept plots for the three batches of calcium mupirocin showed the extent of wetting of each batch. Water data were not plotted due to absorption into the compound taking place during hydrate formation, and thus producing an isotherm that did not conform to the BET

principles. Also hexane data were omitted due to distortion of the lines of best fit and to leave a homologous series of probes (just the alcohols). The plots produced were used to predict the likely BET intercept of butan-1-ol to establish the usefulness of the technique (section 5.4.3). The actual experimental values agreed extremely closely to those predicted. Unfortunately all analyses of data with nabumetone (section 5.4.6.2) proved unsuccessful due to the inability of the material to sufficiently wet.

In summary, a plot of BET intercept versus solvent polarity can be created for compounds that can be wet by a series of probes. This can be used to predict interaction of additional solvents of known polarity with the drug in question. Knowing this information can allow the selection of the appropriate solvent during processing in order to prevent certain undesirable changes to the original compound.

Unlike DVS investigations, experiments using IGC have proven successful for both calcium mupirocin (section 6.4.1) and nabumetone (section 6.4.2) to study the surface energetics of non-micronised and micronised batches. The dispersive component (section 6.4.1.1) showed a small measurable change between non-micronised and micronised batches of calcium mupirocin. This was similar to the DVS data where no change was observed when the surfaces were probed with the non-polar solvent (hexane). However, observations of the acid/base character (section 6.4.1.2) showed that possible recovery over time of the micronised sample did take place. The K^A values increased after micronisation, suggesting that the surface became more acidic in nature (electron accepting) as a result of the availability of more polar acidic components. Testing of the same micronised sample after 1.5 months and a year showed a reduction in the K^A values. This suggested recovery of the sample surface over time to a more energetically stable configuration.

The dispersive component for nabumetone (section 6.4.2.1) increased after micronisation. Re-testing after 2 months showed that the sample recovered from a higher energy state to a lower and more stable energy state. This was represented by a reduction in the non-polar surface energy values. The acid/base

character (section 6.4.2.2) of the material surface also changed after micronisation. The surface of nabumetone was shown to be predominantly acidic. The K^A values increased immediately after micronisation but then over time decreased to below the original K^A value obtained for the non-micronised sample. Initial micronisation provided a greater number of polar acidic components for interaction at the surface. However, with the recovery of the sample to a more energetically stable state (even lower than the original non-micronised value), a reduced number of acidic sites became available. Thus, the measurement of process-induced surface changes can be effectively detected by the IGC technique.

b) Hydrate forms of the compounds.

Comparisons, by IGC, between the surface characteristics of non-micronised hydrate and anhydrous lattices of the compounds were investigated. Calcium mupirocin dihydrate showed a lower dispersive value (section 6.4.1.1) than the anhydrous form. All the non-polar probes interacted with the drug surface to a lesser extent. The incorporation of water into the crystal structure could have changed the surface of the material, where the water molecules attached themselves and orientated in a manner where they were positioned at the surface. Also excess water molecules could have adsorbed onto the surface to reduce the ability of the non-polar solvents to interact with the drug's surface. The K^A values for anhydrous and hydrated calcium mupirocin (section 6.4.1.2) were not different. However, a decreased interaction with individual probes was shown to occur with the dihydrate. Therefore, the sorption of water into and/or onto the material had reduced the interaction between the polar probes and the compound surface, but the K^A value had remained constant due to the gradient of the DN/AN* versus $-\Delta G_A^{SP}$ plot remaining the same. After hydration the K^D value (section 6.4.1.2) significantly reduced when compared to the value for the anhydrous sample. The K^D value reduced to almost zero probably due to the shielding effect of water on groups that may have an electron donating nature. Similar DVS studies (section 5.4.5) were unsuccessful, as the hydrate could not be retained when solvents other than water were utilised.

IGC studies (sections 6.4.3.1 and 6.4.3.2) on the three crystal lattices of theophylline have shown some interesting data. The non-polar components of the hydrate were lower than the respective anhydrous form. Incorporation of water in the structure (to form the monohydrate) and some probable adsorption on the surface had reduced the availability of non-polar sites for the probes to interact with. The dehydrated form of theophylline showed the highest dispersive values. They were significantly higher than that observed for the respective anhydrous form. The higher values represented the fact that the dehydrated form was energetically unstable and therefore a greater interaction with the non-polar probes was seen. The acid/base character of the lattices also produced a similar set of results as that found for the dispersive components. The K^A values decreased on hydrate formation (compared to anhydrous form) due to less acidic components being available for interaction at the surface. However, the subsequent removal of water to form the dehydrate corresponded to the highest K^A values. This was once more due to the reduced stability of the lattice structure, and subsequent increased polar acidic sites available for interaction. DVS studies with theophylline, to probe only the surface (section 5.4.6.1), proved unsuccessful due to the difficulties in wetting the surface of the drug with any of the solvents at partial pressures up to 0.65.

Hydrate studies were not possible with commercial magnesium stearate due to the inability to isolate any of the hydrate forms and the anhydrous form. This was due to the difficulty of removing all moisture from the material and because the sample existed in a multi-hydrate state. Also no studies were conducted with nabumetone because the drug is hydrophobic and is not known to form hydrates. Overall the IGC technique has shown the ability to measure the surface changes of crystal lattices. This can provide information relating to the stability of the lattices and how they may react to excipients during manufacture.

c) Batch variability from supplier.

Differences in the batches of theophylline were evident with the IGC data (section 6.4.3). The Fluka batch showed higher dispersive and acid character values compared to the Sigma batch for all three crystal lattices. This suggested

that the surface of the Fluka batch contained greater non-polar and polar acidic components. A comparison of the individual probe interactions for both batches did not necessarily equate to the appropriate higher/lower energetics values. This was because different batches were being investigated and not an effect on the same batch. However, the combined interaction of all the non-polar probes (for the dispersive component) and polar probes (for the acid/base character) provided gradients for the lines of best fit for the appropriate values. DVS studies on both batches (section 5.4.6.1) failed to show wetting of the surfaces to obtain any meaningful batch variability data. On the other hand, hydration of the batches (section 4.2.5) did show that the Sigma batch was different to the Fluka batch characterised by the faster rate of hydrate formation.

IGC studies with commercial magnesium stearate (section 6.4.4) also showed differences between the surfaces of the Sigma and Fluka batches. The dispersive component and the K^A value for the Sigma batch was significantly greater than the Fluka batch. This suggested that the surface of the Sigma batch had a greater degree of non-polar and polar acidic functional groups than the Fluka batch. DVS studies were not possible to study both batches of magnesium stearate (section 5.4.6.3). For accurate BET interpretations to be conducted each stage must reach equilibrium. Unfortunately due to the very slow drying rate of the compound, the initial 0% stage never obtained equilibrium within the time spans of the experiments.

The IGC studies have highlighted the problems of batch-to-batch variation from two branches of the same company (Sigma-Aldrich). These differences in surface characteristics can cause varying interaction with excipients during manufacture. Therefore it is very important to be aware of the properties of the batch being dealt with, and to have some idea as to what the ideal properties may be.

Future work could involve testing other compounds using the DVS and IGC techniques to review if the methods are successful outside the four test materials (possibly pure magnesium stearate). Investigations with different series' of solvents will show how robust the application of the BET theory is with regards

to measuring the wettability of compounds. Finite concentrations of solvents could be used to probe samples in the IGC instrument to directly compare results with DVS data. Attempt to create generic profiles of how compounds of certain characteristics would react to surface wetting by different types of solvents.

Aim – To evaluate two vapour adsorption techniques for assessing the wettability of compounds:

The IGC instrument helped provide surface characteristics data for all four compounds investigated. Calcium mupirocin and nabumetone were differentiated between their non-micronised and micronised forms, and batch-to-batch variability were successfully measured for theophylline and commercial magnesium stearate. Contrastingly, the DVS apparatus provided results only for calcium mupirocin during the surface wetting studies. Surface changes due to micronisation were detectable as well as the recovery of the sample after one year. It must be noted that the DVS technique did also prove useful for the hydrate studies on theophylline, when probed with water (using DVS-NIR). It clearly showed differences in the three crystal lattices and the discovery of a new transition.

Unlike the DVS instrument, IGC experiments were able to probe the surface and provide energetics data related to the characteristics of the hydrates of calcium mupirocin and theophylline. Also surface data from IGC were able to differentiate between Sigma and Fluka batches of theophylline and magnesium stearate.

The advantages and disadvantages of DVS and IGC have clearly been described in Tables 6.8 and 6.9 (chapter 6). DVS and IGC techniques have provided another means of detecting variations in batches that may not have otherwise been identified, and shown characteristics of material surfaces as to their interaction with probes. In industry, prior knowledge of batch variability can allow the selection of the appropriate solvent during processing in order to prevent any undesirable changes to the original compound.

8. REFERENCES

Agbada C.O. & York P. Dehydration of theophylline monohydrate powder – effects of particle size and sample weight. Int. J. Pharm. 106 **(1994)** 33-40.

Ahlneck C. & Zografi G. The molecular basis of moisture effects on the physical and chemical stability of drugs in the solid state. Int. J. Pharm. 62 **(1990)** 87-95.

Ahmed H., Buckton G. & Rawlins D.A. The use of isothermal microcalorimetry in the study of small degrees of amorphous content of a hydrophobic powder. Int. J. Pharm. 130[2] **(1996)** 195-201.

Andres C., Bracconi P. & Pourcelot Y. On the difficulty of assessing the specific surface area of magnesium stearate. Int. J. Pharm. 218 **(2001)** 153-163.

Andrzejewska E., Voelkel A., Andrzejewski M. & Maga R. Examination of surfaces of solid polymers by inverse gas chromatography: 2. Acid-base properties. Polymer. 37[19] **(1996)** 4333-4344.

Antila R. & Yliruusi J. Measurement of specific surface area of pharmaceutical powders by the BET method: effect of drying time and temperature. Acta. Pharm. Nord. 3[1] **(1991)** 15-18.

Author Anon. The Concise Oxford Dictionary 8th Ed. Clarendon Press, Oxford, UK **(1990)**.

Author Anon. BNF 39. Bemrose Security Printing, Derby **(2000)**.

Author Anon. British Pharmacopeia 2003. The Stationary Office, London, UK **(2003)**.

Balbach S. & Korn C. Pharmaceutical evaluation of early development candidates "the 100 mg-approach". Int. J. Pharm. 275[1-2] **(2004)** 1-12.

Barton T., Bull L., Klemperer W., Loy D., McEnaney B., Misono M., Monson P., Pez G., Scherer G., Vartuli J. & Yaghi O. Tailored porous materials. Chem. Mater. 11 **(1999)** 2633-2656.

Belgacem M.N., Blayo A. & Gandini A. Surface characterization of polysaccharides, lignins, printing ink pigments, and ink fillers by inverse gas chromatography. J. Coll. Inter. Sci. 182[2] **(1996)** 431-436.

Blanco M., Coello H., Iturriaga S., Maspoch S. & de la Pezuela C. Near-infrared spectroscopy in the pharmaceutical industry – Critical Review. Analyst. 123 **(1998)** 135R-150R.

Boutboul A., Giampaoli P., Feigenbaum A. & Ducruet V. Use of inverse gas chromatography with humidity control of the carrier gas to characterise aroma–starch interactions. Food Chemistry. 71[3] **(2000)** 387-392.

Braconni P., Andres C. & Ndiaye A. Structural properties of magnesium stearate psuedopolymorphs: effect of temperature. Int. J. Pharm. 262 **(2003)** 109-124.

Brittain H.G. Raw materials. Drug Dev. Ind. Pharm. 15[3] **(1989)** 2083-2103.

Brodka-Pfeiffer K, Langguth P., Graß P. & Häusler H. Influence of mechanical activation on the physical stability of salbutamol sulphate. Eur. J. Pharm. Biopharm. 56[3] **(2003)** 393-400.

Brunauer S., Emmett P. & Teller E. Adsorption of gases in multimolecular layers. J. Am. Chem. Soc. 60 **(1938)** 309-319.

Buckton G. Assessment of the wettability of pharmaceutical powders. In K.L. Mittal (ed.), Contact angle, Wettability and Adhesion. VSP, Utrecht, Germany **(1993)** 437-451.

Buckton G. Interfacial phenomena in drug delivery and targeting. Harwood Academic Publishers, Chur, Switzerland **(1995)**.

Buckton G., Choularton A., Beezer A.E. & Chatham S.M. The effect of the comminution technique on the surface energy of a powder. Int. J. Pharm. 47 **(1988)** 121-128.

Buckton G. & Darcy P. The use of gravimetric studies to assess the degree of crystallinity of predominantly crystalline powders. Int. J. Pharm. 123 **(1995)** 265-271.

Buckton G & Darcy P. Assessment of disorder in crystalline powders – a review of analytical techniques and their application. Int. J. Pharm. 179 **(1999)** 141-158.

Buckton G., Dove J.W. & Davies P. Isothermal microcalorimetry and inverse phase gas chromatography to study small changes in powder surface properties. Int. J. Pharm. 193[1] **(1999)** 13-19.

Buckton G. & Lane R. The novel combination of dynamic vapour sorption, gravimetric analysis and near infra-red spectroscopy as a hyphenated technique. Int. J. Pharm. 207 **(2000)** 49-56.

Buckton G., Yonemochi E., Hammond J. & Moffat A. The use of near infra-red spectroscopy to detect changes in the form of amorphous and crystalline lactose. Int. J. Pharm. 168 **(1998)** 231-241.

Buckton G., Yonemochi E., Yoon W.L. & Moffat A.C. Water sorption and near IR spectroscopy to study the differences between microcrystalline cellulose

and silicified microcrystalline cellulose before and after wet granulation. Int. J. Pharm. 181[1] **(1999)** 41-47.

Butler D. & Mackin L.A. Characterisation of drug polymorphs by inverse gas chromatography. Surface Management Systems. Application Note 207 **(No Year)** 1-6.

Byrn S.R., Pfeiffer R.R & Stowell, J.G. Solid-state chemistry of drugs 2nd Ed. SSCI Inc, Indianna, US **(1999)**.

Cantergiani E. & Benczédi D. Use of inverse gas chromatography to characterize cotton fabrics and their interactions with fragrance molecules at controlled relative humidity. J. Chromatography A. 969[1-2] **(2002)** 103-110.

Chaubal M.V. Application of formulation technologies in lead candidate selection and optimisation. Drug Disc. Today. 9[14] **(2004)** 603-609.

Chehimi M.M. & Pigois-Landureau E. Determination of acid-base properties of solid materials by inverse gas chromatography at infinite dilution. J. Material Chem. 4[5] **(1994)** 741-745.

Ciurczak E. & Drennen J. Pharmaceutical and medical applications of near-infrared spectroscopy. Marcel Dekker, New York, US **(2002)**.

Columbano A., Buckton G. & Wikeley P. A study of the crystallisation of amorphous salbutamol sulphate using water vapour sorption and near infrared spectroscopy. Int. J. Pharm. 237[1-2] **(2002)** 171-178.

Craig D., Royall P., Kett V. & Hopton M. The relevance of the amorphous state to pharmaceutical dosage forms: glassy drugs and freeze dried systems. Int. J. Pharm. 179 **(1999)** 179-207.

Dansereau R. & Peck G.E. The effect of the variability in the physical and chemical properties of magnesium stearate on the properties of compressed tablets. Drug Dev. Ind. Pharm. 22[11] **(1987)** 1105-1120.

De Boer J.J. The dynamic character of adsorption. Clarendon Press, Oxford, UK **(1953)**.

De Boer A.H., Bolhuis G.K. & Lerk C.F. Bonding characteristics by scanning electron microscopy of powders mixed with magnesium stearate. Powder Technol. 20 **(1978)** 75-82.

Dewar J. The absorption and thermal evolution of gasses occluded in charcoal at low temperatures. Proc. R. Soc. A74 **(1904)** 122-127.

DiMasi J.A., Hansen R.W. & Grabowski H.G. The price of innovation: new estimates of drug development costs. J. Health Economics. 22[2] **(2003)** 151-185.

Djordjevic N.M., Rohr G., Hinterleitner M. & Schreiber B. Adsorption of water on cyclosporin A, from zero to finite surface coverage. Int. J. Pharm. 81[1] **(1992)** 21-29.

Dabrowski A. Adsorption — from theory to practice. Adv. Coll. Inter. Sci. 93[1-3] **(2001)** 135-224.

Dove J. PhD Thesis. University of London, School of Pharmacy. **(1998)**.

Dove J.W., Buckton G. & Doherty C. A comparison of two contact angle measurement methods and inverse gas chromatography to assess the surface energies of theophylline and caffeine. Int. J. Pharm. 138[2] **(1996)** 199-206.

Duddu S.P., Das N.G., Kelly T.P. & Sokoloski, T.D. Microcalorimetric investigation of phase transition: I – Is water desorption from theophylline • HOH a single step process? Int. J. Pharm. 114 **(1995)** 247-256.

Ertel K.D. & Carstensen J.T. Chemical, physical and lubricant properties of magnesium stearate. J. Pharm. Sci. 77[7] **(1988a)** 625-629.

Ertel K.D. & Carstensen J.T. An examination of the physical properties of pure magnesium stearate. Int. J. Pharm. 42 **(1988b)** 171-180.

Fafard M., El-Kindi M., Schreiber H.P., Dipaola-Baranyi G. & Hor A.M. Estimating surface energy variations of solids by inverse gas chromatography. J. Adhesion Sci. Technol. 8[12] **(1994)** 1383-1394.

Feeley J.C., York P., Sumby B.C. & Dicks H. Determination of surface properties and flow characteristics of salbutamol sulphate, before and after micronisation. Int. J. Pharm. 172[1-2] **(1998)** 89-96.

Fokkens J.G. & Blaey C.J. Drug release from non-aqueous suspensions. II – The release of methylxanthines from paraffin suspensions. Int. J. Pharm. 18 **(1984)** 127-138.

Fowkes F.M. Attractive forces at interfaces. Ind. Eng. Chem. 56[12] **(1964)** 40-52.

Fu Z.Y. & Wei S.L. Mechanochemical activation of calcium oxide powder. Powder Tech. 87[3] **(1996)** 249-254.

García-Herruzo F., Rodríguez-Maroto J.M., García-Delgado R.A., Gómez-Lahoz C. & Vereda-Alonso C. Column study of the influence of air humidity on the retention of hydrocarbons on soil. Chemosphere. 41[8] **(2000)** 1167-1172.

Gardner C.R., Almarsson Ö., Chen H., Morissette S.L., Peterson M., Zhang Z., Wang S., Lemmo A., Gonzalez-Zugasti J., Monagle J., Marchionna J., Ellis S., McNulty C., Johnson A., Levinson D. & Cima M. Application of

high throughput technologies to drug substance and drug product development. Comp. Chem. Eng. 28[6-7] **(2004)** 943-953.

GlaxoSmithKline. Material Safety Data Sheet – Calcium Mupirocin Dihydrate. **(2002)** 1-6.

GlaxoSmithKline. Material Safety Data Sheet – Nabumetone. **(2002)** 1-11.

Guinot S. & Leveiller F. The use of MTDSC to assess the amorphous phase content of a micronised drug substance. Int. J. Pharm. 192[1] **(1999)** 63-75.

Guo J., Skinner G., Harcum W., Malone J. & Weyer L. Application of near-infrared spectroscopy in the pharmaceutical solid dosage form. Drug Dev. Indus. Pharmacy. 25[12] **(1990)** 1267-1270.

Gutman V. The donor-acceptor approach to molecular interactions. Plenum Press, New York, US **(1978)**.

Hahn T. (Ed.). International Tables for Crystallography. International Union of Crystallography, Boston, US **(1987)**.

Haleblian J. & McCrone W. Pharmaceutical applications of polymorphism. J. Pharm. Sci. 58[8] **(1969)** 911-929.

Hancock B. & Parks M. What is the true solubility advantage for amorphous pharmaceuticals? Pharm. Res. 17 **(2000)** 397-404.

Hancock B., Shamblin S. & Zografi G. Molecular mobility of amorphous pharmaceutical solids below their glass transition temperatures. Pharm. Res. 12[6] **(1995)** 799-806.

Hancock B. & Zografi G. Characteristics and significance of the amorphous state in pharmaceutical systems. J. Pharm. Sci. 86 **(1997)** 1-12.

Herman J., Visavarungroj N. & Remon J.P. Instability of drug release from anhydrous theophylline-microcrystalline cellulose formulations. Int. J. Pharm. 55 **(1989)** 143-146.

Hodson A.C., Peter G Ferrie P.G. & Dennis A.B. Identification of a hydrate using the complementary techniques of dynamic vapour sorption (DVS), DSC, TGA and hot stage microscopy. Eur. J. Pharm. Sci. 4[Supplement 1] **(1996)** S181.

Hogan S.E. & Buckton G. The quantification of small degrees of disorder in lactose using solution calorimetry. Int. J. Pharm. 207 **(2000)** 57-64.

Hogan S.E. & Buckton G. Water sorption/desorption - near IR and calorimetric study of crystalline and amorphous raffinose. Int. J. Pharm. 227[1-2] **(2001)** 57-69.

James D.H. & Phillips C.S.G. The chromatography of gases and vapours: Part III - the determination of adsorption isotherms. J. Chem. Soc. **(1954)** 1066-1070.

Johannesson B.F. Pre-study on diffusion and transient condensation of water vapour in cement mortar. Cement Concrete Res. 32[6] **(2002)** 955-962.

Kibbe A. Handbook of pharmaceutical excipients 3rd Ed. Pharmacetical Press, London, UK **(2000)**.

Kim S.J., Lee K.J. & Kim S.I. Water sorption of poly(propylene glycol)/poly(acrylic acid) interpenetrating polymer network hydrogels. Reactive Funct. Poly. 55[1] **(2003)** 69-73.

Koh H., Yau W., Ong P. & Hegde A. Current trends in modern pharmaceutical analysis for drug discovery. Drug Disc. Today. 8[19] **(2003)** 889-897.

Lane R & Buckton G. The novel combination of dynamic vapour sorption, gravimetric analysis and near infra-red spectroscopy as a hyphenated technique. Int. J. Pharm. 207 **(2000)** 49-56.

Langmuir I. Constitution and fundamental properties of solids and liquids – Part I Solids. J. Am. Chem. Soc. 38 **(1916)** 2221-2295.

Langmuir I. The adsorption of gases on plane surfaces of glass, mica and platinum. J. Am. Chem. Soc. 40 **(1918)** 1361-1404.

Ledwidge M.T. & Corrigan O.I. Effects of environmental factors on the dehydration of diclofenac HEP dihydrate and theophylline monohydrate. Int. J. Pharm. 147 **(1997)** 41-49.

Lehto V. & Laine E. Simultaneous determination of the heat and the quantity of vapour sorption using a novel microcalorimetric method. Pharm. Res. 17 **(2000)** 701-706.

Leinonen U.I., Jalonen H.U., Vihervaara P.A. & Laine E.S. Physical and lubrication properties of magnesium stearate. J. Pharm. Sci. 81[12] **(1992)** 1194-1198.

Lerk C.F., Bolhus G.K. & Smedema S.S. Interactions of lubricants and colloidal silica during mixing with excipients. Pharm. Acta Helv. 52 **(1977a)** 33-39.

Lerk C.F & Bolhus G.K. Interactions of lubricants and colloidal silica during mixing with excipients. Pharm. Acta. Helv. 52 **(1977b)** 39-44.

Levoguer C.L. & Booth J. Adsorption of high concentrations of organic vapour on activated carbon. Surface Management Systems. Application Note 5 **(No Year)** 1-3.

Levy G. & Gumtow R.H. Effect of certain formulation factors on dissolution rate of the active ingredient III - Tablet lubricants. J. Pharm. Sci. 52 **(1963)** 1139-1144.

Mackin L., Sartnurak S., Thomas I. & Moore S. The impact of low levels of amorphous material (<5%) on the blending characteristics of a direct compression formulation. Int. J. Pharm. 231[2] **(2002a)** 213-226.

Mackin L., Zanon R., Park J.M., Foster K., Opalenik H. & Demonte M. Quantification of low levels (<10%) of amorphous content in micronised active batches using dynamic vapour sorption and isothermal microcalorimetry. Int. J. Pharm. 231[2] **(2002b)** 227-236.

Martindale W. Martindale: the complete drug reference 34th ed. Pharmaceutical Press, London, UK **(2004)**.

Miller T.A., York P. & Jones T.M. Manufacture and characterisation of magnesium stearate and palmitate powders of high purity. J. Pharm. Pharmacol. 34 **(1982)** 8P.

Miller T.A. & York P. Physical and chemical characteristics of some high purity magnesium stearate and palmitate powders. Int. J. Pharm. 23 **(1985)** 55-67.

Morris K.R., Griesser U.J., Eckhardt C.J. & Stowell J.G. Theoretical approaches to physical transformations of active pharmaceutical ingredients during manufacturing processes. Adv. Drug Del. Rev. 48[1] **(2001)** 91-114.

Morissette S.L., Almarsson Ö., Peterson M.L., Remenar J.F., Read M.J., Lemmo A.V., Ellis S., Cima M.J. & Gardner C.R. High-throughput crystallization: polymorphs, salts, co-crystals and solvates of pharmaceutical solids. Adv. Drug Del. Rev. 56[3] **(2004)** 275-300.

Muller B.W. The pseudo-polymorphism of magnesium stearate. In: First International Conference on Pharmacy Technology, Paris **(1977)** 134-141.

Nardin M. & Papirer E. Relationship between vapour pressure and surface energy of liquids: Applications to inverse gas chromatography. J. Coll. Inter. Sci. 137[2] **(1990)** 534-545.

Newell H.E., Buckton G., Butler D.A., Thielmann F. & Williams D.R. The use of inverse phase gas chromatography to study the change of surface energy of amorphous lactose as a function of relative humidity and the processes of collapse and crystallisation. Int. J. Pharm. 217[1-2] **(2001a)** 45-56.

Newell H.E., Buckton G., Butler D.A., Thielmann F. & Williams D.R. The use of inverse phase gas chromatography to measure the surface energy of crystalline, amorphous, and recently milled lactose. Pharm. Res. 18 **(2001b)** 662-666.

Nyqvist H. Saturated salt solutions for maintaining specified relative humidities. Int. J. Pharm. Tech. & Prod. Mfr. 4[2] **(1983)** 47-48.

Ohta M. & Buckton G. Determination of the changes in surface energetics of cefditoren pivoxil as a consequence of processing induced disorder and equilibration to different relative humidities. Int. J. Pharm. 269[1] **(2004a)** 81-88.

Ohta M. & Buckton G. The use of inverse gas chromatography to assess the acid–base contributions to surface energies of cefditoren pivoxil and methacrylate copolymers and possible links to instability. Int. J. Pharm. 272[1-2] **(2004b)** 121-128.

Otsuka M., Teraoka R. & Matsuda Y. Physicochemical stability of nitrofurantoin anhydrate and monohydrate under various temperature and humidity conditions. Pharm. Res. 8 **(1991)** 1066-1068.

Papirer E., Balard H. & Vidal A. Inverse gas chromatography: a valuable method for the surface characterisation of fillers for polymers (glass fibres and silicas). Eur. Polymer J. 24[8] **(1988)** 783-790.

Phadnis N.V. & Suryanarayanan R. Polymorphism in anhydrous theophylline – Implications on the dissolution rate of theophylline tablets. J. Pharm. Sci. 86 **(1997)** 1256-1263.

Pijpers T.F.J., Mathot V.B.F., Goderis B., Scherrenberg R.L. & Van der Vegte E.W. High-speed calorimetry for the study of the kinetics of (de)vitrification, crystallisation, and melting of macromolecules. Macro. 35 **(2002)** 3601-3613.

Rajala R. & Laine E. The effect of moisture on the structure of magnesium stearate. Thermo. Acta. 248 **(1994)** 177-188.

Rasanen E., Rantanen J., Jorgensen A., Karjalainen M., Paakkari T. & Yliruusi J. Novel identification of pseudopolymorphic changes of theophylline during wet granulation using near infrared spectroscopy. J. Pharm. Sci. 90[3] **(2001)** 389-396.

Reichardt C. Solvents and solvent effects in organic chemistry 2nd Ed. VCH Publishers, Cambridge, UK **(1988)**.

Riddle F.L. & Fowkes F.M. Spectral shifts in acid-base chemistry: 1 – Van der Waals contributions to acceptor numbers. J. Am. Chem. Soc. 112[9] **(1990)** 3259-3264.

Rillosi M. & Buckton G. Modelling mucoadhesion by use of surface energy terms obtained by the Lewis acid-Lewis base approach. Int. J. Pharm. 117[1] **(1995)** 75-84.

Rodriguez-Hernando N., Lechuga-Ballesteros D. & Wu H. Phase transition and heterogeneous/epitaxial nucleation of hydrated and anhydrous theophylline crystals. Int. J. Pharm. 85 **(1992)** 149-162.

Rudzinski W. & Everett D.H. Adsorption of gases on heterogenous. Academic Press, Boston, US **(1992)**.

Ruthven D.M. Principles of adsorption and adsorption processes. John Wiley & Sons Inc., New York, US **(1984)**.

Saklatvala R., Royall P.G. & Craig D.Q.M. The detection of amorphous material in a normally crystalline drug using modulated temperature DSC – a case study. Int. J. Pharm. 192 **(1999)** 55-62.

Saleki-Gerhardt A., Ahlneck C. & Zografi G. Assessment of disorder in crystalline solids. Int. J. Pharm. 101 **(1994)** 237-247.

Saunders M., Podluii K., Shergill S., Buckton G. & Royall P. The potential of high speed DSC (Hyper-DSC) for the detection and quantification of small amounts of amorphous content in predominantly crystalline samples. 274 **(2004)** 35-40.

Sawyer D.T. & Brookman D.J. Thermodynamically based gas chromatographic retention index for organic molecules using salt-modified aluminas and porous silica beads. Analytical Chem. 40[12] **(1968)** 1847-1853.

Schultz J., Lavielle L. & Martin C. The role of the interface in carbon fibre-epoxy composites. J. Adhesion. 23 **(1987)** 45-60.

Serajuddin A.T.M. Comparative thermal properties of the monohydrates of sodium theophylline and theophylline. J. Pharm. Pharmacol. 38 **(1986)** 93-96.

Shah A.C. & Mlodozeniec A.R. Mechanism of surface lubrication: influence of lubricant-excipient mixing on processing characteristics of powders and properties of compressed tablets. J. Pharm. Sci. 66 **(1977)** 1377-1382.

Shefter E. & Kmack G. Phase Transitions I – Preliminary study of theophylline hydrate-anhydrate system. J. Pharm. Sci. 56[8] **(1967)** 1028-1029.

Sing K. The use of nitrogen adsorption for the characterisation of porous materials. Coll. & Surf. A: Physicochem. Eng. Aspects. 187-188 **(2001)** 3-9.

Smith E.B. Basic chemical thermodynamics 3rd Ed. Oxford University Press, Oxford, UK **(1982)**.

Sing K., Everett D., Haul R., Moscou L., Pierotti R., Rouquerol J. & Siemieniewska T. Reporting physisorption data for gas/solid systems with special reference to the determination of surface area and porosity. Pure Appl. Chem. 57 **(1985)** 603-609.

Steendam R., van Steenbergen M.J., Hennink W.E., Frijlink H.W. & Lerk C.F. Effect of molecular weight and glass transition on relaxation and release behaviour of poly(DL-lactic acid) tablets. J. Controlled Release. 70[1-2] **(2001)** 71-82.

Strickland Jr. W.A., Nelson E., Busse L.W. & Higuchi T. Physics of tablet compression IX. Fundamental aspects of tablet lubrication. J. Am. Pharm. Assoc. Sci. Ed. 45 **(1956)** 51-55.

Suihko E., Ketolainen J., Poso A., Ahlgren M., Gynther J. & Paronen P. Dehydration of theophylline monohydrate – a two step process. Int. J. Pharm. 158, **(1997)** 47-55.

Sunkersett M.R., Grimsey I.M., Doughty S.W., Osborn J.C., York P. & Rowe R.C. The changes in surface energetics with relative humidity of

carbamazepine and paracetamol as measured by inverse gas chromatography. Eur. J. Pharm. Sci. 13[2] **(2001)** 219-225.

Suzuki E., Shimomura K. & Sekiguchi K. Thermochemical study of theophylline and its hydrate. Chem. Pharm. Bull. 37[2] **(1989)** 493-497.

Swaminathan V. & Kildsig D.O. An examination of the moisture sorption characteristics of commercial magnesium stearate. AAPS Pharm. Sci. Tech. 2[4] **(2001)** article 28.

Ticehurst M.D., Basford P.A., Dallman C.I., Lukas T.M., Marshall P.V., Nichols G. & Smith D. Characterisation of the influence of micronisation on the crystallinity and physical stability of revatropate hydrobromide. Int. J. Pharm. 193[2] **(2000)** 247-259.

Ticehurst M.D., Rowe R.C. & York P. Determination of the surface properties of two batches of salbutamol sulphate by inverse gas chromatography. Int. J. Pharm. 111 **(1994)** 241-249.

Ticehurst M.D., York P., Rowe R.C. & Dwivedi S.K. Characterisation of the surface properties of α-lactose monohydrate with inverse gas chromatography, used to detect batch variation. Int. J. Pharm. 141[1-2] **(1996)** 93-99.

Toth J., Berger F. & Dekany I. Calculation of the BET compatible surface area from any type I isotherms measured below the critical temperature. J. Coll. Inter. Sci. 212 **(1999)** 402-410.

van Asten A., van Veenendaal N. & Koster S. Surface characterization of industrial fibers with inverse gas chromatography. J. Chromatography A. 888[1-2] **(2000)** 175-196.

Vippagunta S.R., Brittain H.G. & Grant D.J.W. Crystalline Solids. Adv. Drug Del. Rev. 48 **(2001)** 3-26.

Voelkel A. Inverse gas chromatography in characterization of surface. Chemometrics Intelligent Lab. Sys. 72[2] **(2004)** 205-207.

Voelkel A., Andrzejewska E., Maga R. & Andrzejewski M. Examination of surfaces of solid polymers by inverse gas chromatography: 1. Dispersive properties. Polymer. 37[3] **(1996)** 455-462.

Vora K., Buckton G. & Clapham D. The use of dynamic vapour sorption and near infra-red spectroscopy (DVS-NIR) to study the crystal transitions of theophylline and the report of a new solid-state transition. Eur. J. Pharm. Sci. 22[2-3] **(2004)** 97-105.

Wade Y. & Matsubara T. Pseudopolymorphism and lubricating properties of magnesium stearate. Powder Tech. 78 **(1994)** 109-114.

Willard H., Merritt Jr, L., Dean J. & Settle Jr, F. Instrumental methods of analysis. 7th Ed. Wadsworth Inc., California, US **(1988).**

Williams D.R. Inverse gas chromatography of solid surfaces. Chromatography & Analysis. Feb **(1991)** 9-11.

Williams D.R. & Levoguer C.L. Measuring BET surface areas using organic probe molecules. Surface Management Systems. Application Note 18 **(No Year)** 1-5.

Wilson R.J. & Beezer A.E. The determination of equilibrium constants, ΔG, ΔH and ΔS for vapour interaction with a pharmaceutical drug, using gravimetric vapour sorption. Int. J. Pharm. 258[1-2] **(2003)** 77-83.

York P., Ticehurst M.D., Osborn J.C., Roberts J.R. & Rowe R.C. Characterisation of the surface energetics of milled dl-propranolol hydrochloride using inverse gas chromatography and molecular modelling. Int. J. Pharm. 174[1-2] **(1998)** 179-186.

Yoshihashi Y., Makita M., Yamamura S., Fukuoka E. & Terada K. Determination of heat of hydration and hydration kinetics of theophylline by thermal analysis. Chem. Pharm. Bull. 46 **(1998)** 1148-1152.

Young P.M. & Price R. The influence of humidity on the aerosolisation of micronised and SEDS produced salbutamol sulphate. Eur. J. Pharm. Sci. 22[4] **(2004)** 235-240.

Yu L. Amorphous pharmaceutical solids: preparation, characterisation and stabilisation. Adv. Drug Del. Rev. 48 **(2001)** 27-42.

Yu L.X., Lionberger R.A., Raw A.S., D'Costa R., Wu H. & Hussain A.S. Applications of process analytical technology to crystallization processes. Adv. Drug Del. Rev. 56[3] **(2004)** 349-369.

Zhang G.G.Z., Law D., Schmitt E.A. & Qiu Y. Phase transformation considerations during process development and manufacture of solid oral dosage forms. Adv. Drug Del. Rev. 56[3] **(2004)** 371-390.

Zhu H., Yeun C. & Grant D.J.W. Influence of water activity in organic solvent + water mixtures on the nature of the crystallising drug phase. 1. Theophylline. Int. J. Pharm. 135 **(1996)** 151-160.